ENERGY ABSORBED IN IMPACT EXTRUSION

BY

PETER JOSEPH LEAVESLEY

A thesis submitted in fulfilment of

the requirement for the

degree

of

Master of Philosophy

THE UNIVERSITY OF ASTON IN BIRMINGHAM

FACULTY OF ENGINEERING

DEPARTMENT OF PRODUCTION TECHNOLOGY AND

MANAGEMENT

MAY 1978

THE UNIVERSITY OF ASTON IN BIRMINGHAM

DEPARTMENT OF PRODUCTION TECHNOLOGY AND MANAGEMENT

ENERGY ABSORPTION IN IMPACT EXTRUSION

PETER JOSEPH LEAVESLEY

Master of Philosophy May 1978

Summary

A survey of the literature showed that little had been published on using the extrusion process to absorb the energy of an impact. For the investigation a rig was designed and manufactured and tests were carried out to assess the energy absorption characteristics of various materials when extruded at various reductions of area and at various impact speeds.

Some design problems arose from the presence of high transient elastic stress waves. These elastic stress waves also had some effect on the instrumentation.

A theory, modified from a standard theory, makes allowances for the kinetic forces present in the various components at any instant during the extrusion. The theory always predicted a lower extrusion pressure than that measured experimentally.

Energy absorption; extrusion; stress waves; kinetic forces; impact.

CONTENTS

CHAPTER ONE

INTRODUCTION

Injuries to man caused by colliding with another object, have occurred ever since man first moved on this planet. Collision or impact injuries are directly affected by the amount of kinetic energy transferred to the human frame and by the level of acceleration or deceleration experienced by the body. Man has always been searching for ways to reduce or completely eliminate the injuries from collisions or impacts, whether the cause be accidental or deliberate. Since it is virtually impossible to eliminate all collisions or impacts, any device or system that reduces the amount of injuries resulting from the collisions or impacts is very desirable. The first step in designing such a device or system is to know how much impact, acceleration or deceleration the human body can withstand.

1.1 Human Tolerance to Impact

A considerable amount of work has been carried out into the resistance of the human body to impact and to the prevention of accidents. If protective devices, such as safety belts or padding in motor vehicles, are to provide optimum protection for vehicle occupants on impact, it is desirable that they should absorb as much energy as possible, in the space available for their operation, to reduce damage. To do this in severe impacts the restraining load exerted on the occupant by the device should rise as quickly as possible to a load which is just below that which would cause serious injury to the occupant and should remain constant at this level until the occupant is brought to rest.

The serious injury threshold level and hence the limiting load which should be exerted by the device will depend on the part of the occupant on which the device acts. Some parts of the human body may also require a limit on the deceleration level (forces), the rate of rise of the load or on the duration.

Knowledge of the tolerance to impact loadings of various parts of the human body is thus essential for the optimum design of crash protection devices. Such knowledge cannot be obtained from tests using volounteers because the level of tolerance which is being defined is the serious injury threshold level.

In vehicle accidents (this type of accident is the principal consideration of this thesis), it has been seen that injuries to certain specific parts of the human body are often associated with a particular pattern of damage to the vehicle interior. By measuring the dynamic load required to reproduce the damage associated with a particular accident injury it is possible to determine the load which acted on the injured part of the person during the impact.

The human tolerance level is defined as the level of load and or acceleration below which the chances of receiving a serious injury is one in a thousand. The point at which an injury becomes a serious injury is difficult to define; usually if the person requires any more than a few hours of medical treatment, the injury is said to be serious. The human tolerance level for most impact injuries is now readily available. From the analysis of data of vehicle accidents, it has been shown that, for an occupant correctly wearing a seat belt, the human tolerance level for any

serious injury is about 29.5kN. The deceleration necessary to produce this force on a man weighing 75kg (12 stone) is 40g. Thus external protective devices, such as crash barriers or bumpers, should limit the vehicle's deceleration to 30g while absorbing as much energy as possible in the space available for their operation. See Fig.1.1. The 30g deceleration limit has been adopted by most vehicle manufacturers as the 40g limit, while producing no serious injuries, produces a large number of minor injuries, while the 30g limit reduces the number of minor injuries by half. This new level of minor injuries was felt by most manufacturers, after careful market research, to be acceptable to the general public. It might be argued that the only level acceptable is that which produces no injuries, but to guarantee this even a deceleration level of 1g might be too high. Clearly to design for this level of deceleration is impracticable and impossible in crash situations.

The important factor correlating with voluntary tolerance and beginning of injury impact is the 'rate of onset'; this is defined as the ratio of maximum deceleration divided by the time in seconds in which it is attained. Subjectively, the effect is perceived as a jolt. The higher the rate of onset, the more severe is the sensation of jolt for a given deceleration peak. Tolerance varies with the axis of deceleration and is optimum in front-to-back or back-to-front orientation with respect to force, with the body adequately restrained and supported.

The effect of jolt, or rate of change of deceleration is evident from the diagram of onset slopes from human experiments. See Fig.1.1. The highly damped, visco-elastic structure of the body compresses and deforms as a function of the rate of applicat-

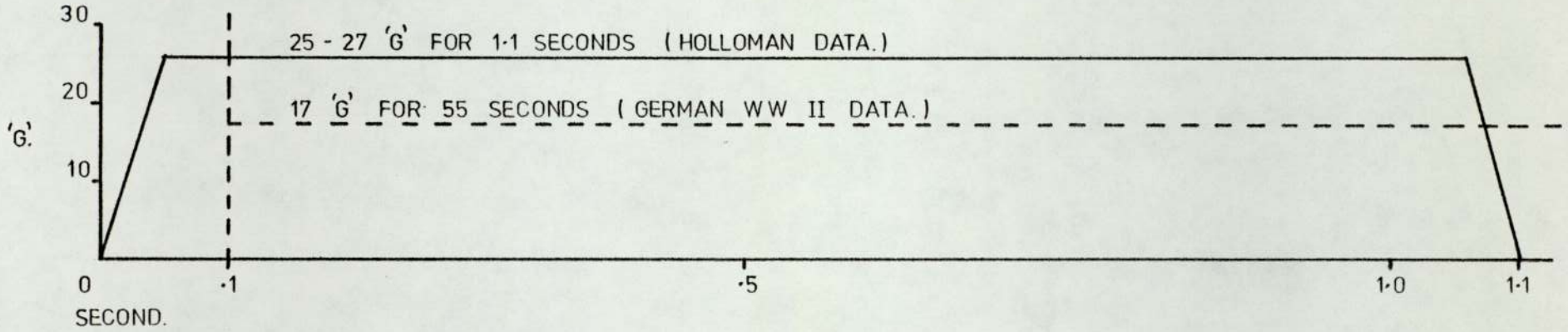

A. TOLERANCE FOR DURATION OF 'G' HUMAN SEATED FACING FORWARD.

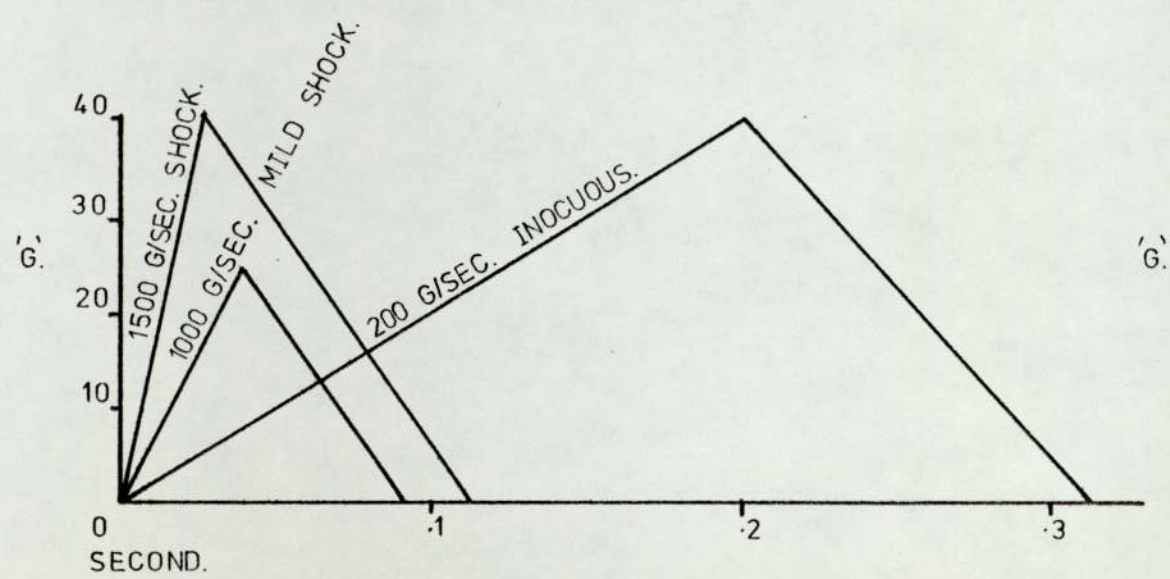

B. TOLERANCE FOR JOLT.

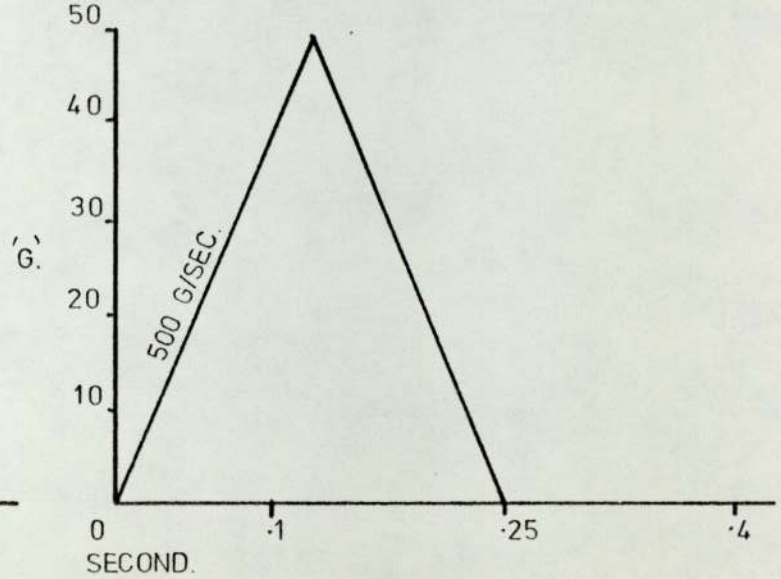

C. TOLERANCE FOR PEAK 'G'

FIG. 1.1. HUMAN TOLERANCE : THE LIMITS FOR REVERSIBLE INCAPACITATION.

ion of mechanical force, storing and releasing energy as a spring does. For the masses and springs of the human body, there is resonance to single impacts manifested by amplitude and acceleration of the human trunk when repetitively shaken reaches a maximum at 5 cycles per second, for the shoulder at 8 to 10 cycles per second, and the head and neck displace fore and aft maximally at 18 to 21 cycles per second.

In the case of a single impact, the dashpot effect of viscous body structures and fluids quickly damp out the resonant response after an initial overshooting response. The magnitude of first overshooting acceleration of the body relative to the acceleration of the rigid seat or platform is a function of the rate of onset of impact, and becomes a maximum as the rise time becomes equal to or shorter than the rise time for resonant frequency of the body. Considering the human physiological responses to rates of onset in a series of experiments where the peak deceleration was between 38 to 40g, a rise time of 130 milliseconds to 40g, or 331g per second, was easily tolerated with no more reaction than would be produced by heavy exercise and excitement. Only mild reddening occurred in areas impinged against by webbing straps. The 130 millisecond rise time corresponds to about 2.5 cycles per second, compared with 5 cycles per second for whole body resonance. A rise time of 29 milliseconds to 38g, corresponding to about 9 cycles per second, resulted in circulatory shock with fainting, deep purple bruises where straps struck the shoulders and thighs, severe pain, lassitude and fatigue

for three days after this experience.

"Buying" time with distance and absorbing energy by deformation of resistant structures in order to delay onset and attenuate the jolt can make the difference between tolerance and injury resulting from the impact. It is better to let surrounding structures fail than to excite resonant amplifications and resultant damaging distortion in the human occupant of a crashing vehicle.

1.2 Development of Energy Absorbing Systems.

From early history man has always worn a helmet into battle. This was one of man's first attempts to reduce injuries from impacts, ie, by reducing the energy transmitted to the head. The helmet either deflected the attacker's blow away from the head or the energy of the blow was absorbed in physically deforming the helmet. The energy absorbing properties of the helmet depend greatly on the material used, shape and method of construction. Some of the more popular materials used were leather, copper, bronze and steel. The success of the helmet can still be seen today, as the basic design of modern helmets has changed very little from the basic design of early helmets. The major differences are to be seen in the use of modern materials like glass fibre and plastics. Helmets can still play an important part in protecting the head; some modern uses are:- policeman's helmet, motor cycle crash helmets, horse riding helmets, crash helmets for sports and steel helmets for the armed forces.

Another early successful energy absorbing system was body armour, which is still used in some sports and in "flack" jackets.

Again the major differences from earlier designs occur in the materials used and means for fastening to the body. The early suits of armour were usually made of copper, bronze or iron. Leather armour was produced in European countries, Bamboo and leather were popular protection materials in the Eastern countries and bones and leather were used in the American and African continents. Body armour performed in the same way as the helmets by either deflecting the attacker's blow, or by the energy of the blow being absorbed in physically deforming the armour.

The next important development of energy absorbing systems was the spring. A spring is not a true energy absorber, since it stores energy and releases it in the same form at a later time, but it merits a mention. In the early days of horse drawn vehicles, springs were used to make the ride of the vehicle more acceptable to its human passengers. The springs which were situated either between the axle and the carriage or between the carriage and seat, converted the short sharp movements of the wheels from the road into longer movements of the seat. Because of the nature of springs a single bump on the road would cause several oscillations of the seat. Although the total energy transmitted through the springs to the seat and hence the human body is the same as the energy of the initiating bump, it is more acceptable as several slight jolts are preferred to one severe jolt.

The addition of viscous damping, sometimes called a dashpot, to springs produced the first commercially used energy converter type of energy absorber. When an object impinges on a spring,

without viscous damping, the kinetic energy of the object is stored by the compression of the spring until the object is brought to rest. From being at rest the spring releases an equal amount of stored energy which is converted to the kinetic energy of the object. Now if the object were firmly attached to the spring, this reversal of direction of the object would stretch the spring and again the kinetic energy of the object would be stored as elastic strain energy but this time by the tension of the spring. Once the object was brought to rest again, the spring on releasing it's stored energy would impart the original kinetic energy back to the object. This cycle would continue indefinitely were it not for the hysteresis loss in the spring which slowly dissipated the energy as heat. When viscous damping is added to the spring system, a different picture emerges as the object does work against the viscous damping when compressing the spring. The kinetic energy of the object is converted, by the viscous damping, into heat. The number of oscillations that the object and spring depends on the amount of viscous damping. The higher the viscous damping the smaller the number of oscillations. Also the consecutive amplitudes of the oscillations reduce in size as the energy of the system is absorbed by the damping media. Two good examples of this type of system can be seen frequently, namely, railway buffers and vehicle shock absorbers. The railway buffers are capable of absorbing considerable amounts of kinetic energy and hence are physically large with very high viscous damping levels. They operate in one direction only, with a light spring which just stores enough energy to return the buffer to its original position slowly after it has been used. The buffers generally have long strokes, from one foot

on the train itself to about six feet at the end of a line. Vehicle shock absorbers are used to improve the ride of the vehicle by reducing the number of oscillations of the passenger compartment. As before in the horse drawn vehicles, the springs of the vehicle converted the short sharp movements of the road wheels into many oscillations of the vehicle. The viscous damping in the shock absorber absorbs the energy in the system and reduces the number of oscillations of the vehicle. A vehicle correctly damped, fitted with the correct shock absorbers, should overshoot only once before returning to its original position.

Early motor vehicles did not employ crash protection devices either for the vehicle or for its occupants. Most manufacturers were satisfied with fitting a fairly robust bumper at either end of the vehicle to take the impact of the crash. This gave little protection to either the vehicle or its occupants, as the full force and hence the energy of the crash was transferred, sometimes with disastrous results, to both.

As the vehicle performance improved, so the speed and hence the amount of kinetic energy of the crash increased. This development caused a considerable increase in the seriousness of damage to both the vehicle and its occupants. The first action taken by vehicle manufacturers was to increase the strength of the vehicles; this reduced the damage to vehicles. But this, in turn, made the injuries to the occupants more serious as the deceleration or jolt felt by the occupants increased. These injuries were caused by the occupants striking the interior of the vehicle. To try to reduce the seriousness of these injuries, padding and later deformable panels were added to the interior of the vehicles. Various materials were employed including plastic covered foams

which were bonded to pressed metal panels. The energy absorbing characteristics of the mild steel panels, overall, was superior to the other materials. Some of the plastics, while having a superior energy absorbing capability at slow impact speed, tended to rupture at higher impact speeds thus losing their energy absorbing capability. Another undesirable characteristic of some of the plastics, is that upon rupture they produce sharp edges, thus causing puncture type injuries to the occupants; whereas mild steel panels rarely tear and therefore do not produce sharp edges to cause puncture type injuries.

While the padding and deformable panels were partially successful, it was felt that if the occupants could be prevented from coming into contact with the dash panel or steering wheel during a crash, the seriousness of the injuries would be greatly reduced. A harness, like an aircraft pilot's harness, worked extremely well, but the design of the harness was costly and awkward to use. A full pilot's harness consisted of two shoulder straps, two leg straps and a waist strap. After much testing with dummies and following enlightened public opinion, the modern seat belt configuration emerged, which consists of a single diagonal shoulder strap and a waist strap. This design needs only three anchor points and one fastening by comparison with the five anchor points and two fastenings needed for the full harness. Such a seat belt has to be capable of being fitted and unfitted, in a few seconds, by any user, so instead of the sudden deceleration which the occupant experiences when striking the interior of the vehicle, he feels the usually less severe deceleration of the crashing vehicle to which he is attached.

While the seat belt on its own is not an energy absorbing system, - apart from slight plastic stretching of the straps, - it prevents large numbers of serious injuries during some high speed accidents, the restraining force exerted by the seat belt on the occupant is sufficient to cause injury. There are some devices, which when fitted between the seat belt and its anchor points, limit the load exerted by the seat belt on its occupant. These devices are usually an energy absorbing device, rather than just a load limiter. The energy absorbing device can only be used once normally, since the principles of deformation are employed to absorb the energy. Commonly devices absorb energy in bending, cutting, drawing or extrusion of metals or plastics.

About twenty or twenty five years ago, following recommendations by several government bodies, vehicle manufacturers started to look for methods of vehicle protection that would enable vehicles to withstand slow speed collisions without structural damage. At the same time, recommendations for high speed collisions to the front and rear of a vehicle were that the structure should crumple in a controlled manner absorbing most of kinetic energy of the collision, leaving the stiffened passenger compartment virtually undamaged. Later requirements insisted on vehicles being able to withstand repeated collisions to the front and rear of the vehicle without damage. The first collision requirement was at $2\frac{1}{2}$ miles per hour, but this figure was soon amended to 5 miles per hour - the trend is still upwards.

To meet these requirements manufacturers have carried out tests on a wide range of energy absorbing systems and devices.

Energy absorbing systems can usually be divided into two main groups, the groups being; "energy converters" and "energy absorbers". The main difference between the two groups is that the "energy absorbers" can only be used once, while the "energy converters" can be used repeatedly. The process involved in energy dissipation for both systems must be non-elastic. hence a spring is not a true energy absorber, it merely stores energy and releases it in the same form. A vehicle shock absorber however, is a true energy absorber as the applied kinetic energy is degenerated to heat and dissipated.

There are numerous energy absorbing systems which exhibit the desired non-elastic properties. The choice of a system generally lies in the amount of kinetic energy to be absorbed, the rate at which it can be absorbed, how this rate varies with time, and the physical limitations to the size of the device. The desirable deceleration pulse is usually square-shaped, this allows constant deceleration with respect to time and thus enables the "Safest" arrest to take place without high transient decelerations which are damaging.

Some of the more common energy converter type of energy absorbing systems are: - hydraulic buffers; shock absorbers; recoverable rubbers; plastic and foams; certain types of friction devices. Another system usually classed as an energy converter is the "pneumatic piston", but unless carefully designed it exhibits some elastic properties.

The main advantages of the energy converter type of energy absorbing systems are:- capable of multiple impacts; capacity for large energy absorption. While the main disadvantages are:- expensive to manufacture; physically large; unsuitable for high deceleration rates.

Some of the more common energy absorber type of energy absorbing systems are:- physical deformation (many sub-groups, Invertube, crumpling of tubes, bending of bars, drawing of bars, extrusion of bars etc); metal foams, tear-webbing.

The main advantages of this group are:- cheap to produce; physically small; suitable for both high and low deceleration rates. While the main disadvantages are:- inability to automatically reset; more suited to large and medium absorption requirements.

At the present state of development of energy absorbing systems and devices, the "physical deformation" type of system seems to be the more practicable for motor vehicle protection. Although perhaps not as attractive as the energy converter, the energy absorbers are more easily controllable and have greater predictability.

Some energy absorbing systems combine two or more basic devices together to obtain the advantages of both devices. They may be devices from either of the two main groups, one example being the coupling in series of a recoverable rubber buffer with a crumple tube. The reason for this design is that for impacts of low kinetic energy the recoverable rubber buffer absorbs all the energy. When the kinetic energy is high but the recoverable rubber

buffer still absorbs its maximum amount of energy and the crumple tube is brought into action to absorb the remaining kinetic energy. Overall the system has a low level multiple absorption characteristic with a "one off" high level energy absorption reserve. Either device on it's own cannot match the performance of the two together.

1.3 Extrusion used in Energy Absorbing Systems

Most of the systems in use today for motor vehicle collision protection, employ recoverable rubbers and plastics to absorb the energy of the slow speed collision and they meet today's standard, without being obtrusive to the design of the vehicle. Any further amendments to the collision level requirements would require the recoverable rubber bumper to increase in size to accommodate the higher energy levels involved. The larger bumper would be obtrusive in most behicle designs. The requirements for vehicle collision protection in the near future are unlikely to call for an increase in the ability to withstand repeated collisions but it is probable that the vehicle must withstand a single collision of 10 miles per hour without damage to the vehicle - apart from the collision protection device which should be easily replaceable. Energy absorbing systems employing physical deformation of metals and plastics appear to meet these requirements. Some systems are well documented (crumple tube, Invertube, metal cutting), but there appears to have been very little work carried out in the use of the metal forming process, known as "Extrusion", for energy absorbing systems. Imperial Metal Industries Ltd., of Birmingham, a company

with long experience in the shaping, deformation, and extrusion of metals, developed an energy absorbing bumper system for road vehicles employing the extrusion principle. The system contains a recovery and extrusion phase, which operate in sequence. (See appendix L.). This system appears to be the only one in commercial use at the moment which contains an extrusion device.

In the extrusion manufacturing process, very large amounts of energy are needed to force the metal billet through the extrusion die. In the same way, if a metal or plastic billet is squeezed by collision impact through a suitable die, large amounts of kinetic energy can be dissipated in a controlled manner.

Since little work has been carried out into the use of the extrusion process as an energy absorbing device, reference must be made to the enormous amount of information available in the closely related fields of; impact extrusion, conventional extrusion, wire drawing and general plastic deformation of metals.

Wire-drawing, one of the oldest known metal-forming processes, has inevitably received considerable attention over a long period of time. An extensive experimental and theoretical investigation and review of it's mechanics was reported by Wistreich.[1] [2] [3] The latter is principally concerned, as is Wistreich's own work, with the equilibrium type of analysis, but it also takes into account Shield's[4] theory of flow through a converging channel.

More recently the theoretical analyses of Avitzur,[5] [6] [7] have been published employing an upper-bound approach in the study of the mechanics of wire drawing.

Redundancy effects, apparent in the cold drawing of rod, have been specifically examined from both theoretical and experimental points of view by among others Johnson and Rowe [8] and Caddell and Atkins, [9] [10] using the equilibrium approach.

Earlier developments in conventional extrusion were summarised by Johnson and Kudo [11] in their detailed survey of the mechanics of the operation, and discussed in some detail by, among others Rowe [12]. An approximate, force-equilibrium method of treating cold rod extrusion was proposed by Sachs [13], whereas a semi-empirical estimate of extrusion pressure, based on the slip-line approach and applied to lead, aluminium and tin, was suggested by Johnson [14] [15] for the general case of axisymmetric extrusion. The treatment of the flow through a conical die, including the incidence of the dead metal zone and central burst, was analysed by Avitzur [6] [7] in conjunction with the upper-bound approach to rod and wire drawing.

The visioplasticity method is particularly well adapted to the needs of extrusion and has therefore become a major analytical tool in the study of the pattern of flow and the determination of redundancy. More recently selected contributions to a better understanding of the flow patterns are those by Medrano and Gillis [16]. The difficulty encountered in successive 'smoothing' of computer derived flow patterns, has been partly removed by the modifications to the analysis introduced by Medrano and Gillis and substantiated by their experiments with lead. A study of the incidence of redundant shearing in cold extrusion of lead, copper and aluminium rods, as well as in cold and hot wax model materials was made by Blazynski, [17].

An interesting approach to the determination of extrusion pressure, combining an adaptation of the upper-bound technique to sub-grain size and prediction of temperature rise, has been proposed by Sheppard and Raybould [18]. Their experiments, carried out on super-pure aluminium, aluminium-zinc and aluminium-zinc-magnesium an encouraging measure of agreement between the calculated and measured quantities.

The solution of the problems involved in impact extrusion is generally complex. Approximate theoretical and experimental approaches were made by, for instance, Cole and Bakhtar [19] and Parsons, Laycock and Cole [20] in connection with the cold extrusion of solid bar. The reverse impact extrusion of tubular components has been extensively analysed by Bishop and Avitzur [21] using the upper-bound technique, and predicting the incidence of defects such as, cavitation, rounded edges, or "fishskin".

From both the theoretical and experimental information available on the extrusion orifices, it is believed that an energy absorbing system employing the extrusion process as the absorbing portion, could be developed practically. The apparent versatility of such an extrusion device is considerable as the device should be able to absorb or dissipate large of small amounts of energy, have long or short absorption distances, with high or low decelerations. Some other apparent desirable features of the extrusion device are: low cost, compactness and virtually maintenance free. Such an energy absorbing system, may be a "one off" device with no automatic reset capabilit, but, by coupling this device to an energy converter its potential would be greatly increased.

The purpose of this investigation was to establish experimentally the practicability of using the extrusion process to absorb the kinetic energy in an impacting situation. The four main approaches to the theoretical analysis of the extrusion process were examined and they were found to be useful when applied to conventional, slow speed operations. The four main approaches are; i) Equilibrium of forces, ii) Slip-line field, iii) Upper-bound, iv) Visioplasticity. When the speed of extrusion process is increased, dynamic effects have to be considered and this feature leads to the development of a fifth approach.

The forming energy in impact extrusion is supplied through the medium of a ram which, in turn, is actuated by a sudden expansion of gas or by a mass falling under the influence of gravity.

Relatively high strain rates can be attained and these will, in the case of some alloys, lead to a substantial increase in the value of the yield stress, combined with a reduction in the strain to fracture. This is particularly noticeable towards the end of the operation, when a high degree of deceleration is reached. It is also at this stage that high tensile stresses are reached at the base of the extruded bar and result in eigher necking of breaking-off of the extruded portion. Maximum possible deformations depend mainly on the ability of the tools to withstand the shock of impact.

In general, the investigation of an impact extrusion process is best approached from the point of view of the energy balance. This can be done either in the form of an overall equilibrium-type assessment or by a detailed examination of the energy components provided by the upper-bound technique. The 'equilibrium technique' is used to

analyse the reverse extrusion of bar.

This analysis, which cannot differentiate between the homogeneous and inhomogeneous effects, is based on the assumptions that the billet is rigid-plastic, the dead metal zone is relatively small, the tools are rigid, friction is negligible, and that for a given situation the work of deformation per unit volume is constant. The latter assumption does not, of course, take into account the effect of strain rate, unless the value of yield stress is suitably adjusted. If it is further assumed that it is reasonable to exclude rebounds and other elastic phenomena. Consequently the energy delivered by the ram is assumed to be entirely absorbed by the billet.

CHAPTER TWO

DESIGN OF RIG.

2.1 Introduction

The first part of any design work, must be to carefully select the parameters that control the design of the rig and divide them into two groups; that is, one group enforces strict design limits and the other group lax design limits. For example: a parameter that requires strict control is the axis of the extrusion which should coincide with the axis of the impacting mass. This makes all the calculations regarding the extrusion process relatively simple when compared with the case of non-coincident axis. For the other group, a parameter requiring only lax control is the shape of the impacting mass. It could be any shape so long as the impacting face is square to the direction of travel, and its centre of gravity travels along the axis of the extrusion.

From the parameters in the two groups, the necessary limits of the performance of the rig can be established. The last step before any real design work starts, is to set a maximum limit to the cost of building the rig, (£2000 in this case).

Each sub-assembly of the rig was designed with all the other sub-assemblies in mind, to ensure an overall design that was both functional and compatible.

2.2 Guidance System of Impacting Mass.

The basic concept of an impact extrusion test rig is that a moving mass strikes the extrusion device against a rigid base. The methods of accelerating the moving mass to the desired speed fall into two groups: a) acceleration due to gravity and b) acceleration due to a mechanical device. Both groups have many advantages and disadvantages over each other. Since the methods in group b); that is employing a mechanical device to accelerate the moving mass, are generally more difficult to produce, and at higher costs than those methods in group a), a method from group a) was the natural choice.

There are three methods in group a) using gravity to accelerate the moving mass: i) simple pendulum, ii) sloping trolley and iii) falling mass. See Fig.2.1. The simple pendulum has several disadvantages. The impact load will not be axial to the axis of the extrusion device, as the impacting mass swings through an arc of a circle, and so considerable side loads will be generated in the extrusion device. The maximum working stroke is also limited by this same arc of circle. Another important factor is that a swinging mass is difficult to control and this could lead to some safety problems. There is very little difference between the last two methods, that is sloping trolley and falling mass. The falling mass is a more compact unit than the equivalent sloping trolley, but the guidance of the impacting mass is more complex. The limitations of space in the laboratory outweighed the difficulties of a more complex guidance system, so finally the selection of a vertical impacting mass where acceleration was due to gravity was adopted. Thus a simple rig was built which was very economical on laboratory floor space. The major disadvantage is that the impacting mass needs constraint in two dimensions.

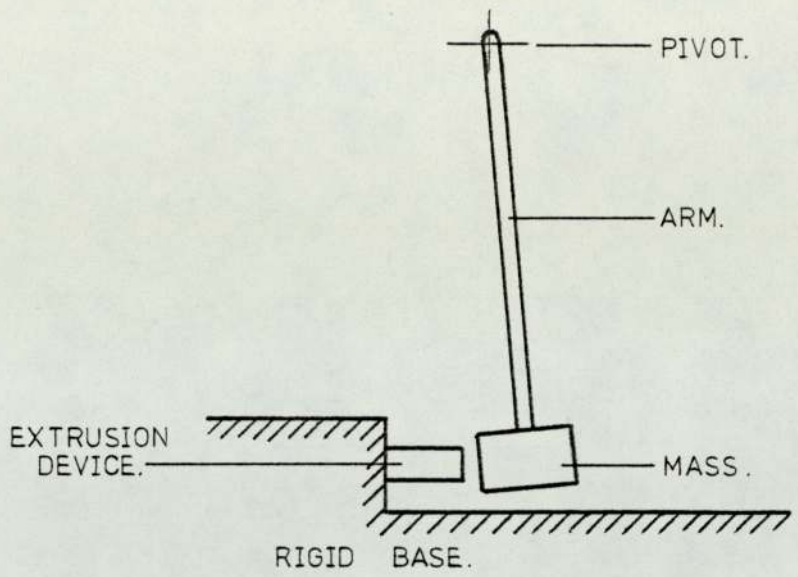

i) SIMPLE PENDULUM.

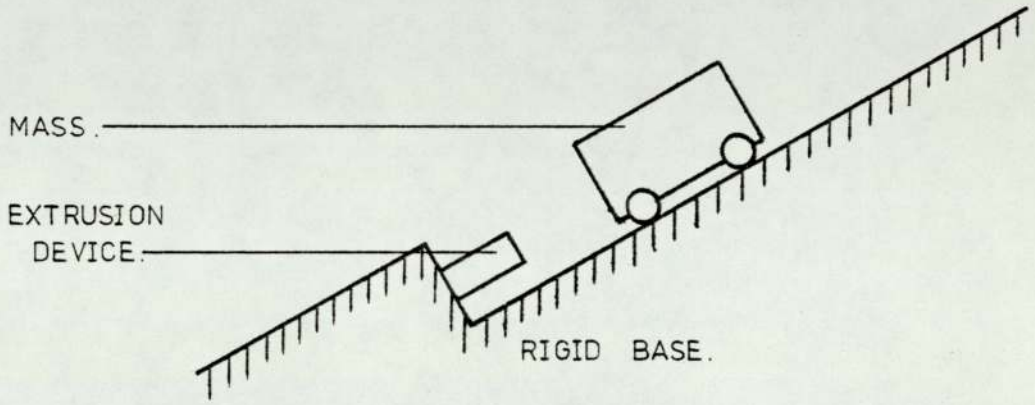

ii) SLOPING TROLLEY.

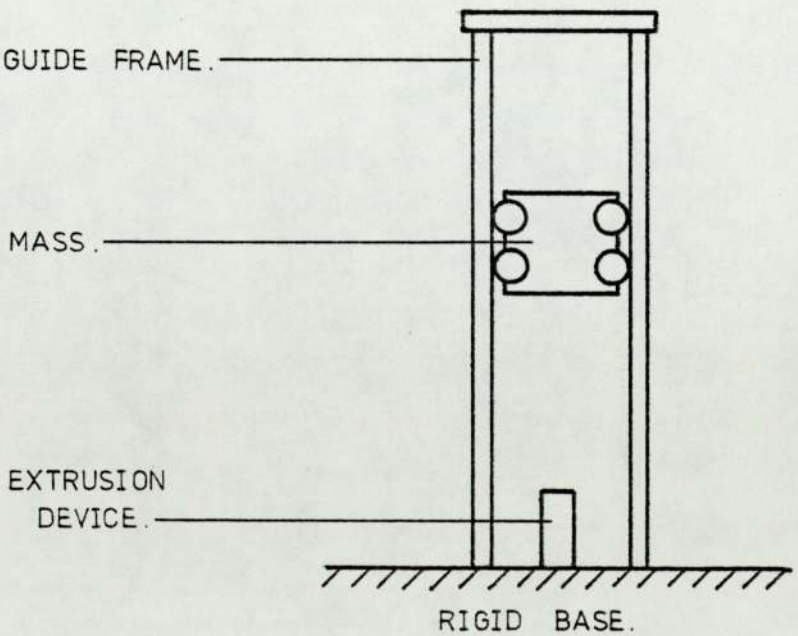

iii) FALLING MASS.

FIG.2-1. METHODS OF ACCELERATING A MASS EMPLOYING GRAVITY.

and guiding in the third.

The impacting mass required about three metres of free fall to gain the maximum velocity proposed in the testing schedule. During this fall the mass must not on impact be able to move sideways, twist, tilt or jump out of its guides. The rig had to be considerably higher than three metres to accommodate the release and lifting mechanisms and the standing height of the extrusion device. Extra height was incorporated for the effect of friction in the guides to be taken into account. Thus the accelerating force is now the force due to gravity minus the force due to friction. With a careful selection of the guidance system this effect is minimized. Two types of bearings, sliding bearings or rolling bearings, offered the necessary guidance to the mass. Although sliding bearings cost less to manufacture than rolling bearings, the coefficient of sliding friction is about fifty times greater than that of rolling friction. The final choice of bearings rested with the actual physical layout of the guidance system. From Fig. 2.2 seven possible configurations are shown that give the necessary constraints and guidance. The first four systems are similar to each other and they all have the same disadvantages, that is all the bearings (minimum of eight for a) and b), and twelve for c) and d), have to be individually adjustable. This would make the manufacture of the trolley or cross-head unnecessarily complicated and therefore expensive: firstly the single central guide tube or bar could only be supported at the top. This would leave about four to five metres of unsupported tube or bar which could lead to excessive vibrations of the guide tube; secondly, the impacting mass has a large hole in the centre, so some form of an adaptor would be necessary to transfer the impacting

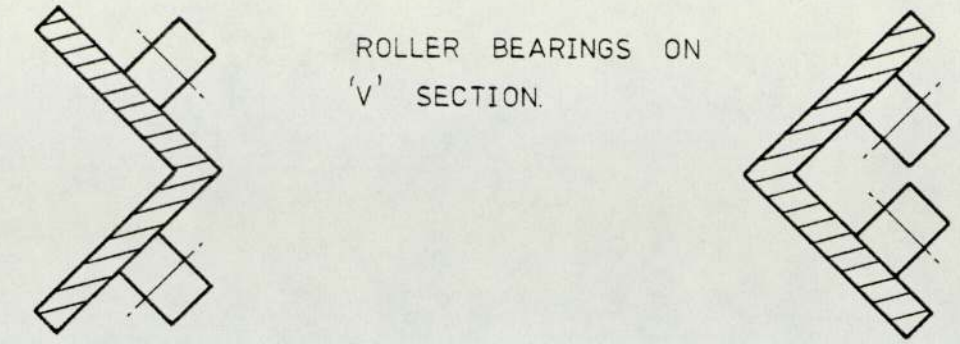

a) EXTERNAL.

b) INTERNAL.

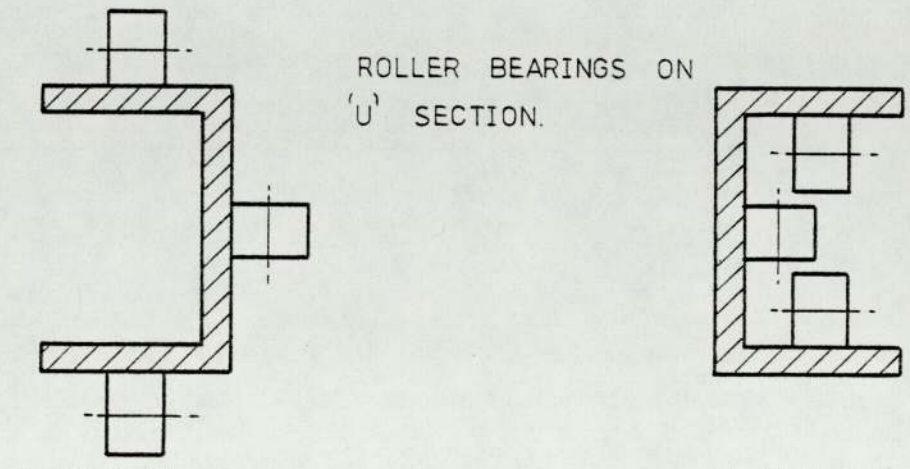

c) EXTERNAL.

d) INTERNAL.

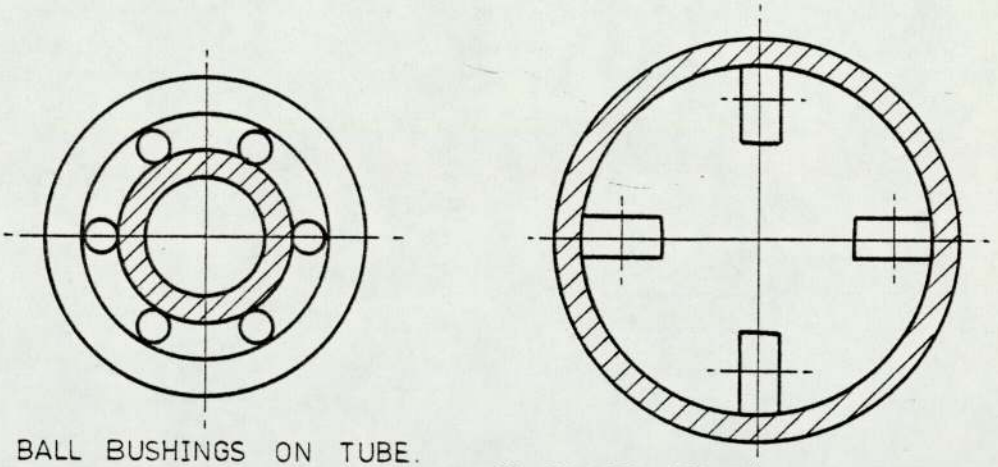

e) BALL BUSHINGS ON TUBE.

f) ROLLER BEARINGS IN TUBE.

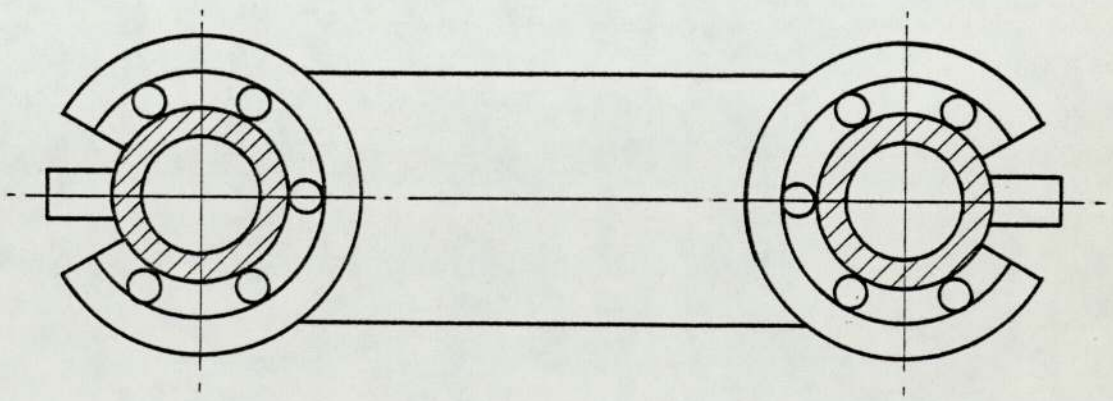

g) OPEN BALL BUSHINGS ON TUBES WITH SIDE MOUNTINGS.

FIG. 2-2. POSSIBLE CONFIGURATIONS OF GUIDANCE SYSTEMS FOR FALLING MASS.

energy to the extrusion device. System f) would cost too much as the price of large diameter tube (350mm bore) is high. As with systems a), b), c) and d) the bearings would have to be individually adjustable, again adding to the cost of the system. The straightness and parallelism of the guideways would affect the efficiency of all the above systems. System g) was chosen as the best compromise between cost and accuracy. The system consisted of two open ball bushings, see Drg. 100, mounted in the cross-head at fixed distance apart. The guide tubes are held top and bottom in tension, this tension helps to pull the tubes straight. The rigidity of the tubes was increased by the addition of four side mountings per tube. These side mountings are adjustable to increase the straightness and parallelism of the tubes. See Fig. 2.3. Both the ball bushings and the tubes were readily available from stockholders, leaving only simple parts to be manufactured.

2.3 Main Frame and Safety Cage.

The main purpose of the main frame was to give support and increase the rigidity of the guidance system. The frame consists of a heavy cast iron block, which acted as the base of the rig, two upright U-shaped sections fastened to the base by two base supports of similar U-shaped sections. The uprights are cross stiffened by four pairs of cross braces equally spaced along the uprights. The top of the frame consists of two U-shaped sections which provide support for the guide tubes and the upper half of the rope pulley system. See Drg. 500. The whole frame was bolted together rather than welded, to allow any modifications, or complete disassembly. The final frame was only slightly less rigid than a welded one.

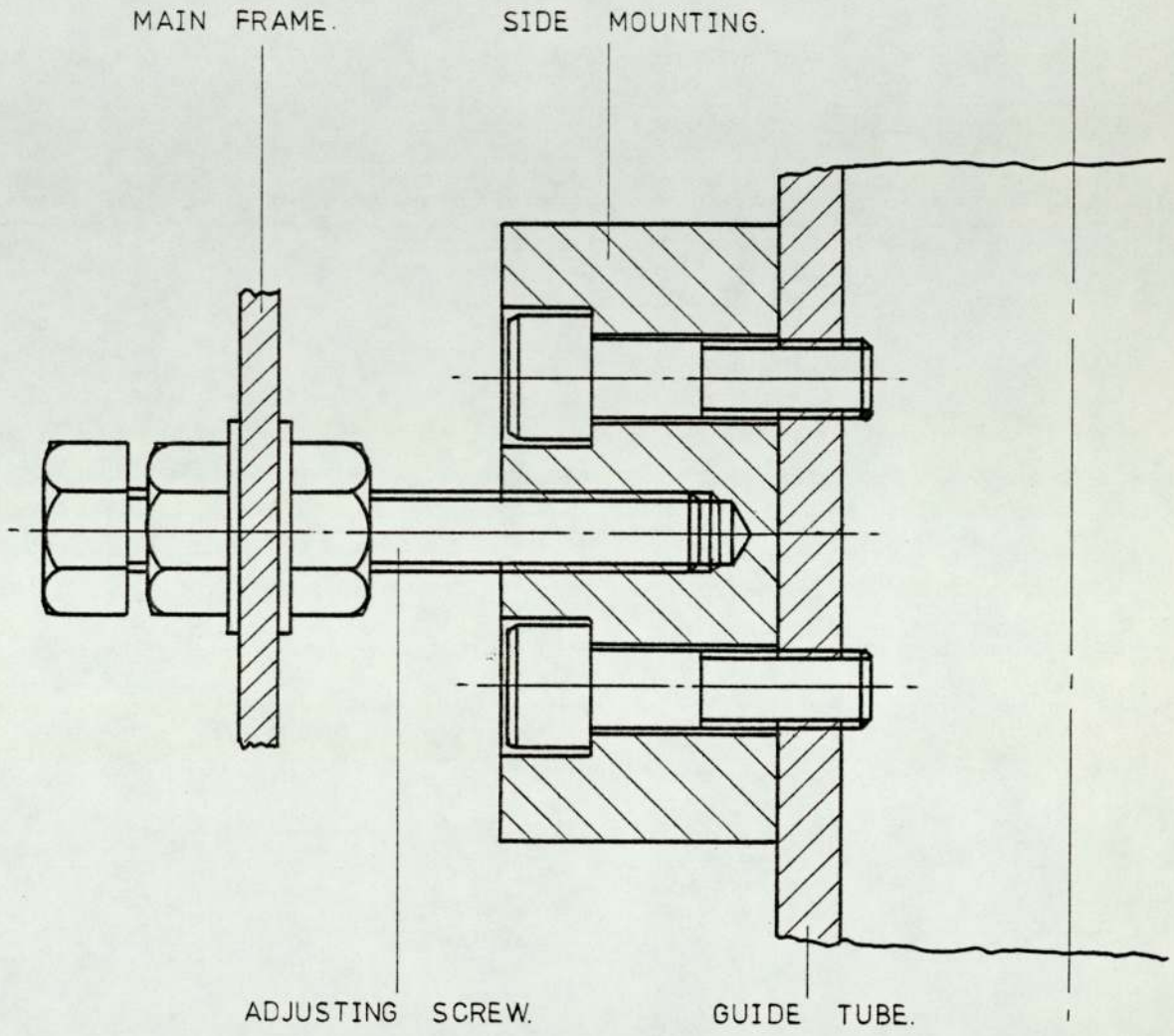

FIG. 2·3. METHOD OF INCREASING RIGIDITY OF GUIDE TUBE.

The lower half of the rig was surrounded by a protective wire mesh cage to prevent any accidental contact between the falling mass and any observers. The door of the cage was connected via a simple system of pulleys and levers to two heavy bars. These bars rested across a pair of side braces of the main frame when the door of the cage was open, thus preventing the falling mass from reaching the lower half of the rig if it was accidentally released. When the door was closed the bars are pulled clear onto a supporting frame, this allows a clear passage for the falling mass. The bars are 'spring loaded', so the system is 'fail safe', that is, if the connecting cable breaks the bars return to the safe position. See Fig. 2.4.

2.4 Falling Mass.

The actual design of the mass was determined by the design of the rest of the rig. Flat discs were chosen rather than the slightly cheaper rectangular plates. The diameter of the discs which was the maximum possible was limited by the distance between the guide tubes. Any smaller diameter would increase the standing height of the mass unnecessarily. The mass was adjustable to allow for a full range of tests. The discs which were made in 10, 5, 2 and 1 kg weights were firmly bolted to the crosshead, to prevent them flying about on impact. Two lifting rings were fastened to the top of the mass to allow it to be coupled to the combined release-lifting mechanism.

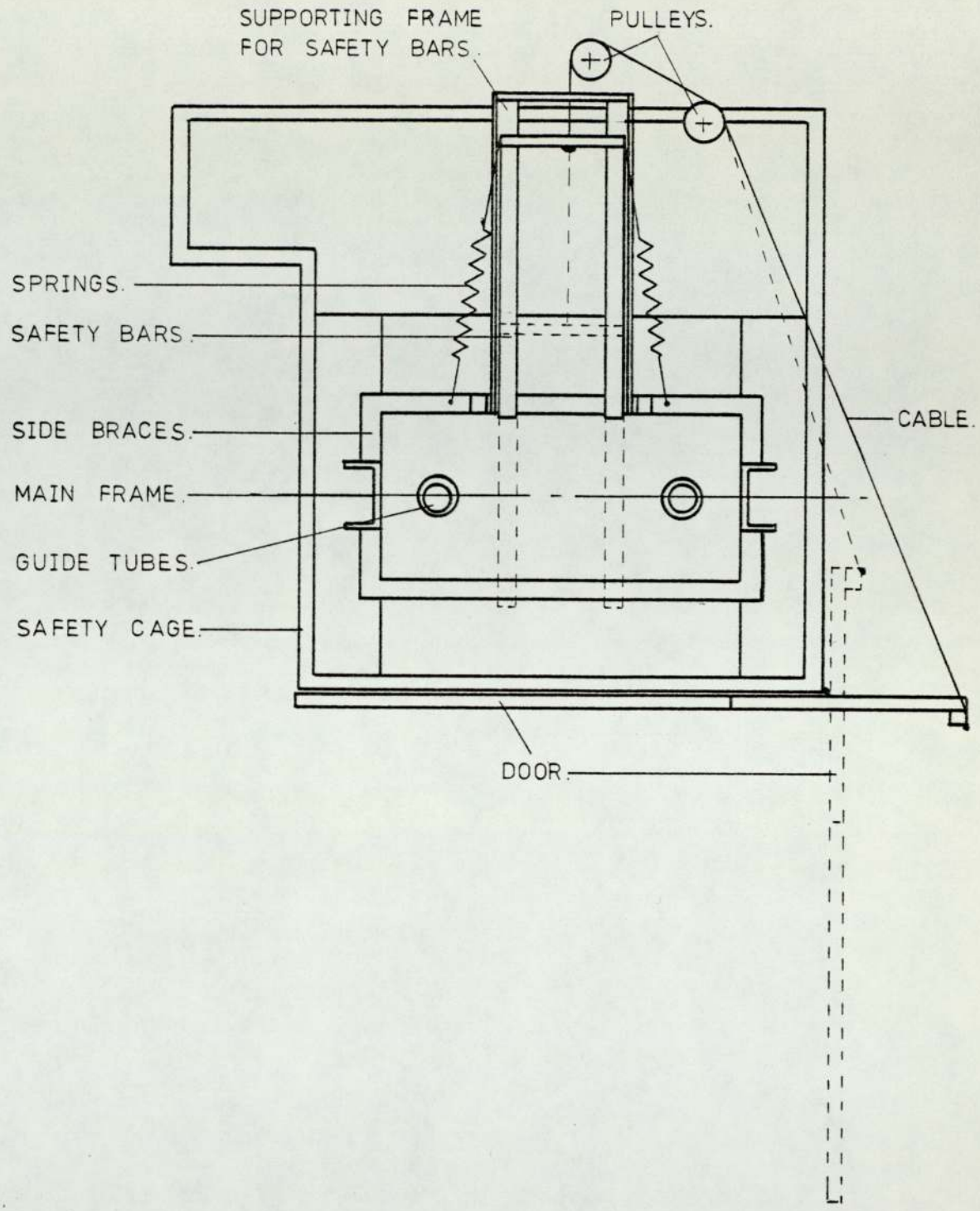

FIG. 2·4. SHOWING OPEN AND CLOSED POSITIONS OF DOOR AND SAFETY BARS. (PLAN VIEW).

2.5 Combined Release - Lifting Mechanism.

The first requirement of the release mechanism was that it should release the mass under load and without shock to greatly reduce the amount of vibration set up in the rig. There are numerous load release mechanisms on the market, but most have some degree of shock at the moment of release. A truly shock free system would be one employing electro-magnets. For safety reasons a system using both a mechanical and a electro-magnetic release mechanism was designed. See Drg. 400. The system operates as follows: under normal lifting and waiting conditions the mechanical system takes all the load with the electro-magnets switched off. A few seconds before the mass is released the magnets are switched on, taking all the load off the mechanical system. The mechanical system is actuated by a small solenoid. Switching off the electro-magnets released the mass, shock free.

The release mechanism consisted of a lifting head with two bronze bearings to guide the mechanism on the same path as the mass. Fitted onto the lifting head was the mechanical release mechanism and the electro-magnets. The mechanical release mechanism consisted of two sets of pins and rings actuated through a system of levers by a single solenoid. The electro-magnets were positioned just above a plate fastened to the mass, so that when activated they would lift the mass up until physical contact was made. This slight movement was just enough to take all the load off the pins in the mechanical system. See Fig. 2.5.

The release machanism was combined with the lifting mechanism

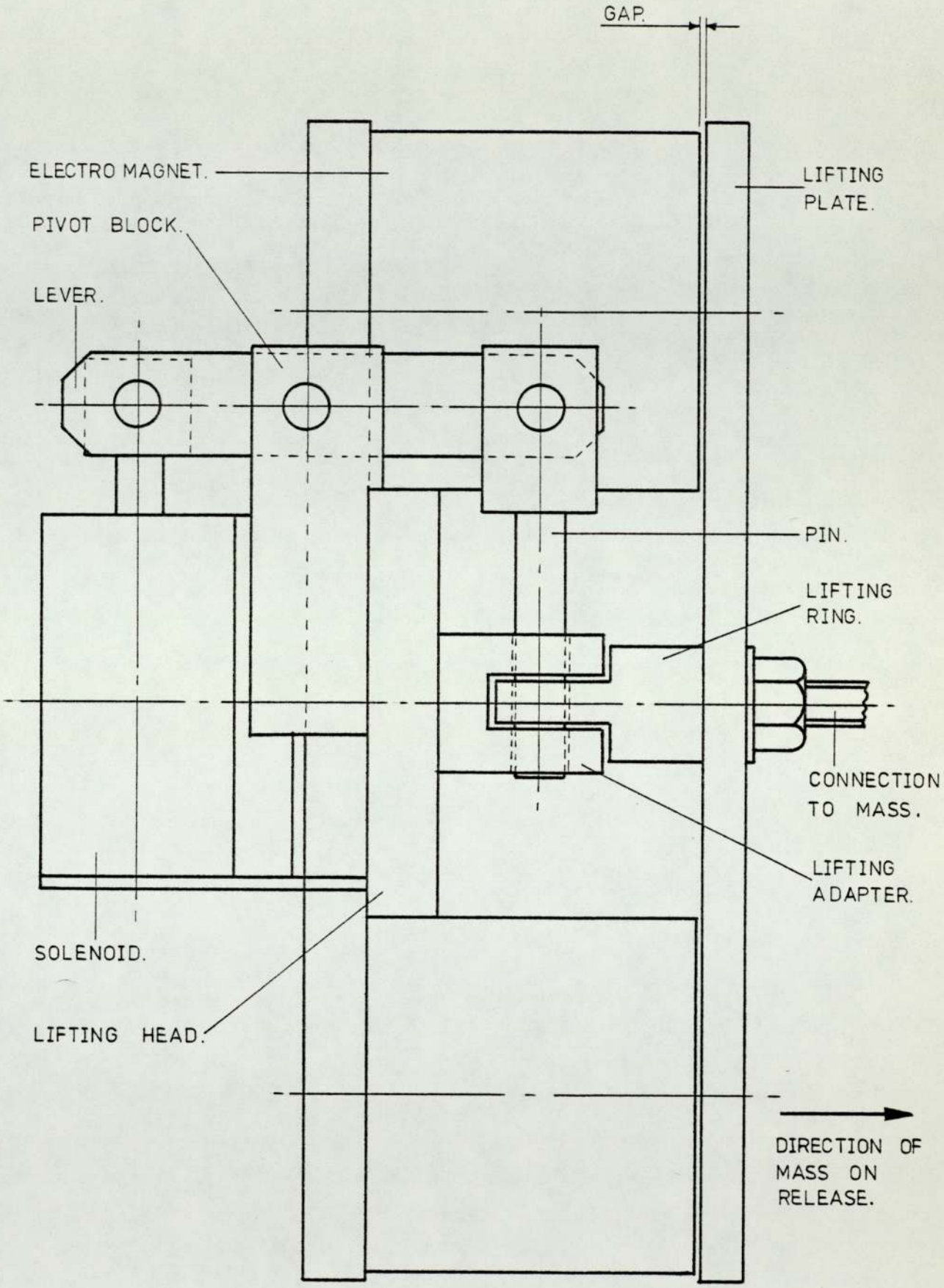

FIG. 2·5. CONFIGURATION OF RELEASE MECHANISM.

as a good connection with the mass was already made. The lifting mechanism consisted of an electric motor coupled through a flexible coupling to a 40:1 reduction gearbox and then through another flexible coupling to the rope drum. The pre-stretched Terylene rope passed through a system of pulleys, which gave a further reduction of 3:1 and was attached to the release mechanism. See Fig. 2.6.

2.6 The Extrusion System

The main design feature of the extrusion system to be satisfied was that there should be the fewest possible equipment changes for different tests. The original test programme called for a large spread of the variables. See Fig. 2.7. Each extrusion set consisted of; die, ram, container and container base plate. The requisite design of the die was a simple orifice plate normal to the axis with a small lead-in radius. Originally it was intended that a sharp-edged die would be used but life of the edge was uncertain. The incorporation, initially, of a small radius would minimise this problem. The thickness of the dies necessary to prevent excessive bending was estimated by calculating the deflection of a circular plate with a concentric hole under the action of a uniformly distributed load. After a parallel section of 10mm. the bore of the die was relieved by a taper of 10^{o} to prevent excessive frictional contact between the extruded portion and the die. See Fig. 2.8.

The design of the ram proved to be quite difficult as consideration had to be given to the following points: the ram would have to provide its own guidance in the container, the ram should not bend in the container due to lateral expansion when under load,

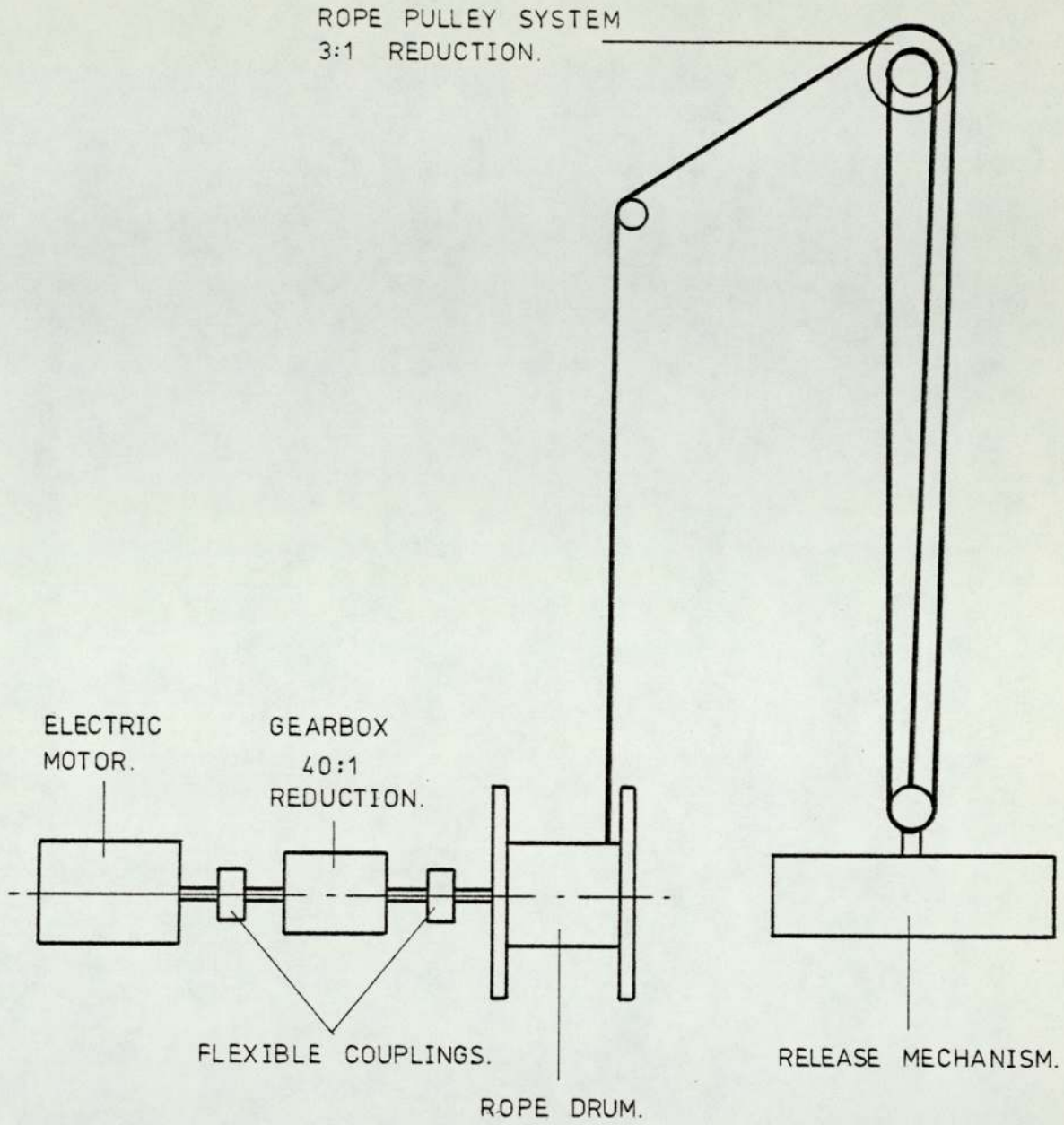

FIG. 2·6. SCHEMATIC LAYOUT OF LIFTING MECHANISM.

PARAMETER	ORIGINAL REQUIREMENTS	REVISED REQUIREMENTS
Material	i) Aluminimum ii) L.D. Polythene iii) Delvin iv) Polypropylene G.S.E. 20	i) Aluminimum Alcoa C800 ii) Polypropylene G.S.E.20 iii) Lead 99.9%
Billet Diameter	i) $\frac{1}{2}$in ii) 1in iii) $1\frac{1}{2}$in iv) 2in v) $2\frac{1}{2}$in vi) 3in	i) 12.5mm ii) 25.0mm iii) 37.5mm iv) 50.0mm v) 75.0mm
Billet Length	i) $\frac{1}{2}$in ii) 1in iii) $1\frac{1}{2}$in iv) 2in v) $2\frac{1}{2}$in vi) 3in	i) 12.5mm ii) 25.0mm iii) 37.5mm iv) 50.0mm v) 75.0mm
Tempera-ture	i) 40°c ii) 20°c iii) 0°c iv) 20°c v) 40°c vi) 60°c	i) 20°c
Impact Speed	i) Static ii) 15ft s^{-1} iii) 30ft s^{-1} iv) 45ft s^{-1}	i) Static ii) 4m s^{-1} iii) 6m s^{-1} iv) 8m s^{-1}
Reduction of Area	i) 50% ii) 60% iii) 70% iv) 80% v) 90% vi) 95%	i) 50% ii) 60% iii) 70% iv) 80% v) 90% vi) 95%
Type of Extrusion	i) Backward rod ii) Backward tube	i) Backward rod

Fig.2.7 Comparision of Original and Revised Parameters.

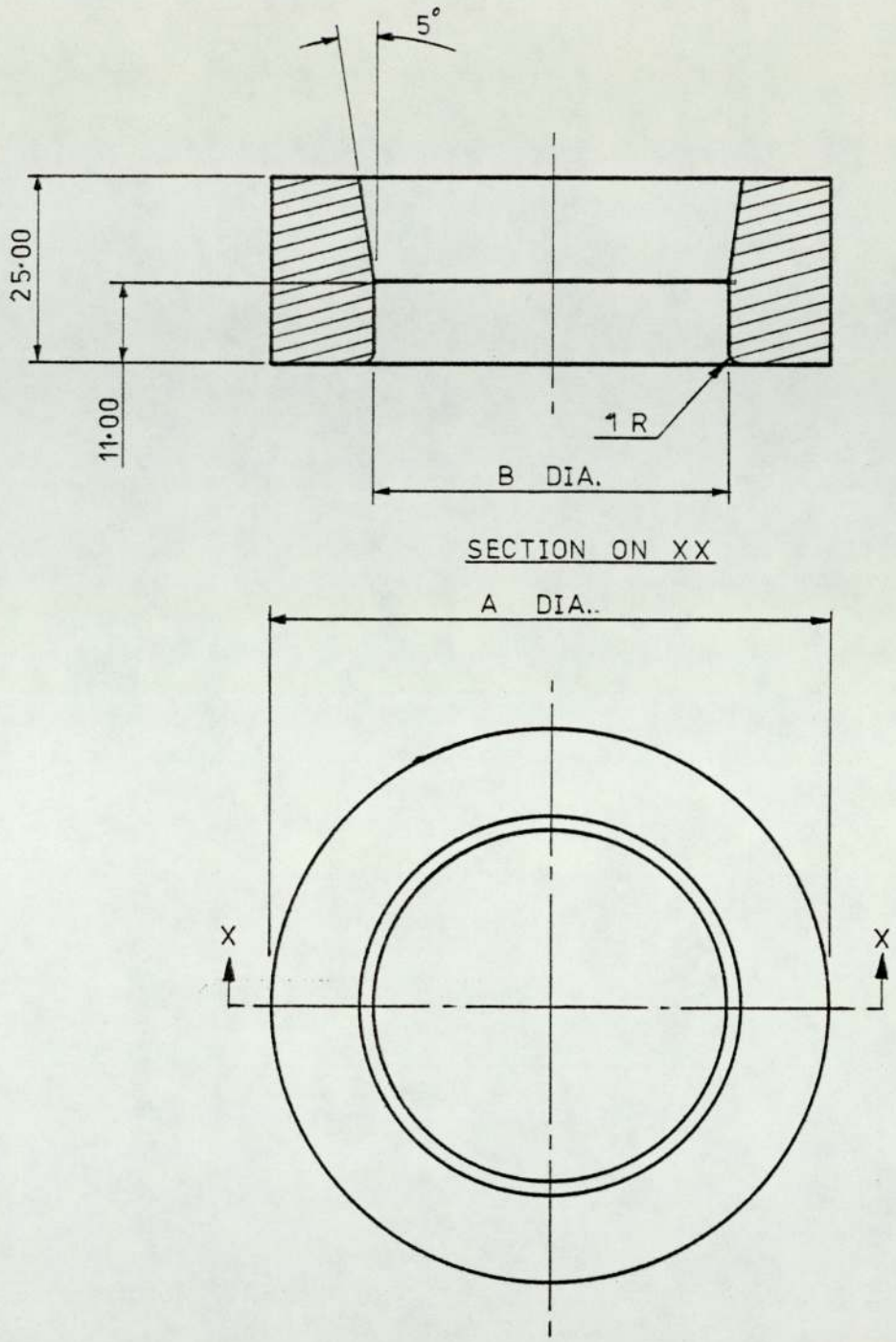

MATERIAL. SVERKER 3. HEAT TREATED TO GIVE HARDNESS 60 HRC ± 2.

FIG. 2·8. DIAGRAM SHOWING THE PROFILE OF THE DIES.

the stress imposed on the ram should be less than its yield stress, the ram should not buckle and should be able to withstand the shock loadings due to impact. The material of the ram necessary to meet the above specification, could only be found in the steels normally associated with dies, hence the cost of the rams would be high. For the ram to provide its own guidance, the minimum length had to be at least equal to its diameter. Since the design called for as much standardization as possible all the rams were the same length, except for the smallest diameter (12.5mm nominal) which would have had slenderness ratio of 13:1 while the maximum permitted was 7:1. This was easily overcome by packing out the container and shortening the ram; this still left enough of the ram in contact with the container to provide the necessary guidance. The rams were also to be connected to a load cell, which was achieved through a simple screwed adaptor. Two adaptors were made to cater for the range of ram sizes, as a single adaptor would entail a large wastage of ram material. See Fig. 2.9.

The container and container base plate required very little design work. Only two factors needed to be considered, the length of the container and the wall thickness to prevent bursting. The length was set by the longest length of billet to be tested and the minimum length for the guidance of the largest ram. The wall thickness was calculated from thick cylinder theory using as the internal pressure, the extrusion pressure. This over-estimated the wall thickness as the pressure felt by the container is always less than the extrusion pressure. The container was designed to have a removable base, for if a billet or possibly the ram jammed in the container, the base would have to be removed and the billet or ram driven out. This

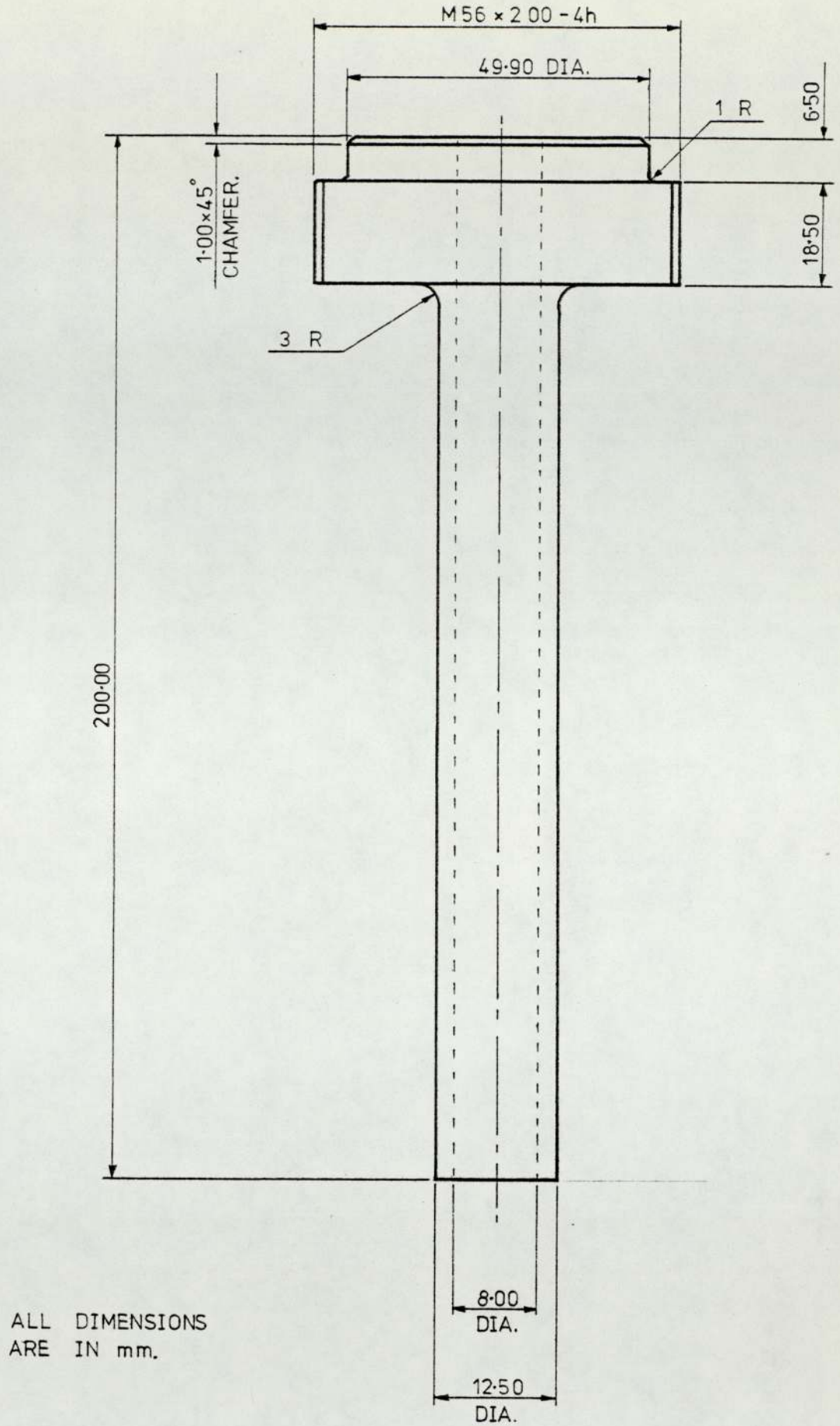

MATERIAL. SVERKER 3. HEAT TREATED TO GIVE HARDNESS 58 HRC ± 2.

FIG. 2·9. DIAGRAM OF A TYPICAL RAM.

would be impossible with a one piece container.

2.7 Load Cell.

The material chosen for the load cell was a titanium alloy, as this material combines high strength with a low Young's Modulus of Elasticity, about half that of steel. This means that for the same load, the strain in the titanium alloy is twice that in the steel, assuming they have the same cross-sectional area. When coupled into the design of a strain gauge type of load cell, the extra straining produced in the strain gauges increases the signal from the load cell. Thus to produce a reasonable amount of deflection on a U.V. recorder trace, less amplification of the signal was required. Since the range of loads to be measured by the load cell was large (500 N to 300 kN), the amount of amplification is critical.

The load cell could have been mounted in two places, i.e., on top of the ram or below the container; but there was some doubt as to which position would give the most accurate measurement of extrusion load. Two identical load cells were made and the results could then be compared. The load cell was of hollow construction to allow the extruded products to pass through. The size of the bore was chosen as a compromise between the smallest size allowable by the extruded product and the size necessary to prevent excessive bending stresses in the adaptors. See Fig. 2.10. The outer diameter was set by the cross-sectional area necessary to support the maximum load of 300kN at a strain of 0.5%. The load cell was threaded at both ends to allow it to be fastened to the associated parts. As all the loads measured were compressive the force transmitted from the impact cover to load cell was transferred by the ends of the load cell and

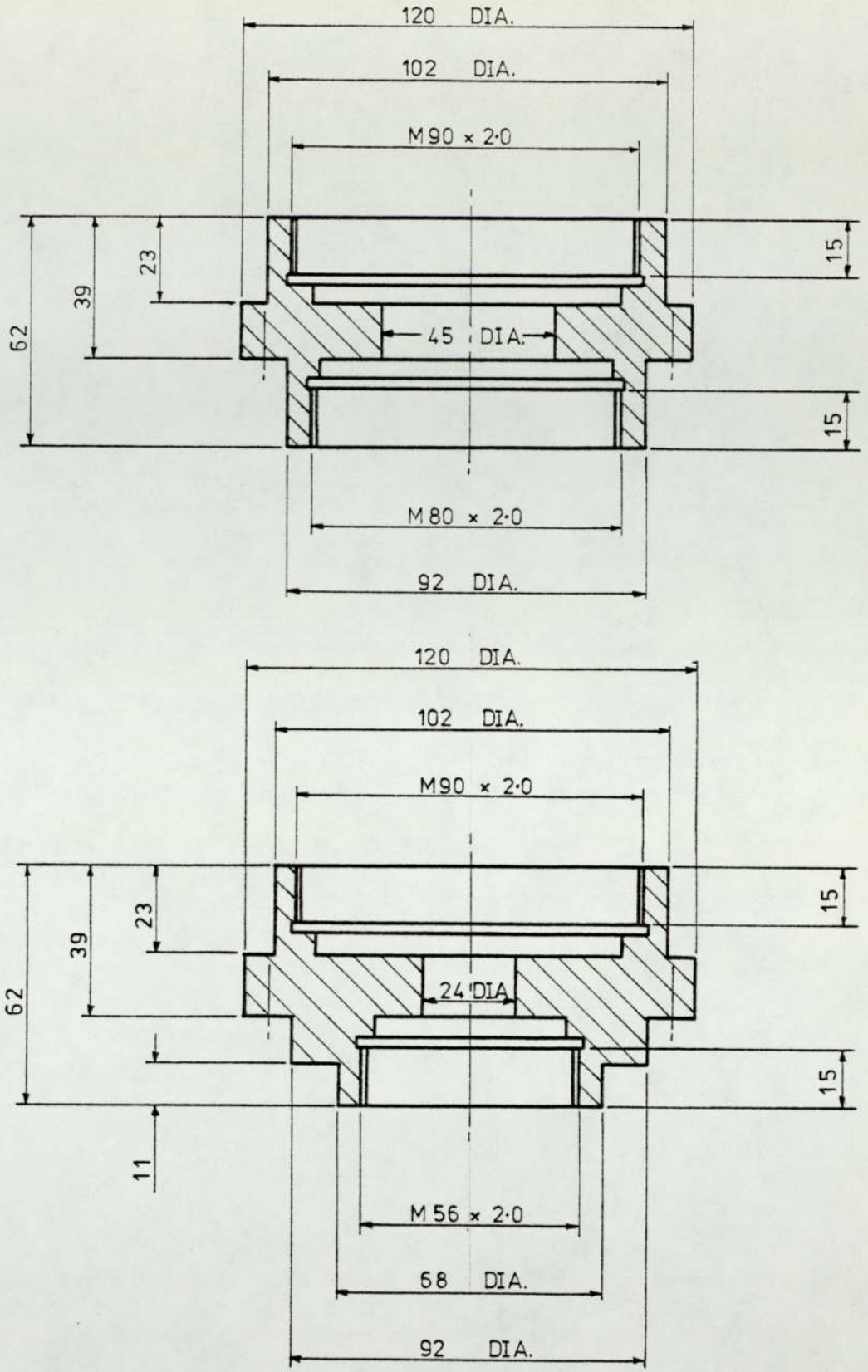

ALL DIMENSIONS ARE IN mm.

FIG. 2·10. SECTION THROUGH BOTH ADAPTORS SHOWING DIFFERENCE IN CONNECTING DIAMETERS FOR THE RAMS.

not by the thread. To ensure a stress concentration in the load cell, the outside diameter had to be less than the minor diameter of the thread. The stress lines should be parallel to where the measurements are taken. Previous experiments had shown that to ensure parallel stress lines the length to diameter ratio should be 1:1.1 to 1.5.

2.8 Outer Sleeve Assembly.

The purpose of the outer sleeve was to hold the extrusion device concentric and parallel to the axis of impact. Since the sleeve was manufactured from an available length of a thick cylinder, this necessitated the additional manufacture of a packing sleeve for the container as the bore of the outer sleeve was larger than expected. The size of the other packing sleeves and the two covers for the bottom load cell had to be increased accordingly. This was still far cheaper to produce than purchasing a length of thick cylinder of the correct size. An outer jacket was made to fit over the outer sleeve leaving a gap between the two; this was to allow a heating/cooling liquid to be pumped around the extrusion device. See Fig. 2.11. Due to the cost and time available the rest of the equipment necessary to carry out tests at different temperatures could not be purchased.

Placed on top of the outer sleeve was the displacement arm guide. This together with the displacement arm was to prevent any rotation of the ram. Since the displacement arm was coupled directly to the displacement transducer any rotation of the ram, and hence the displacement arm, would damage the transducer. The arm was designed

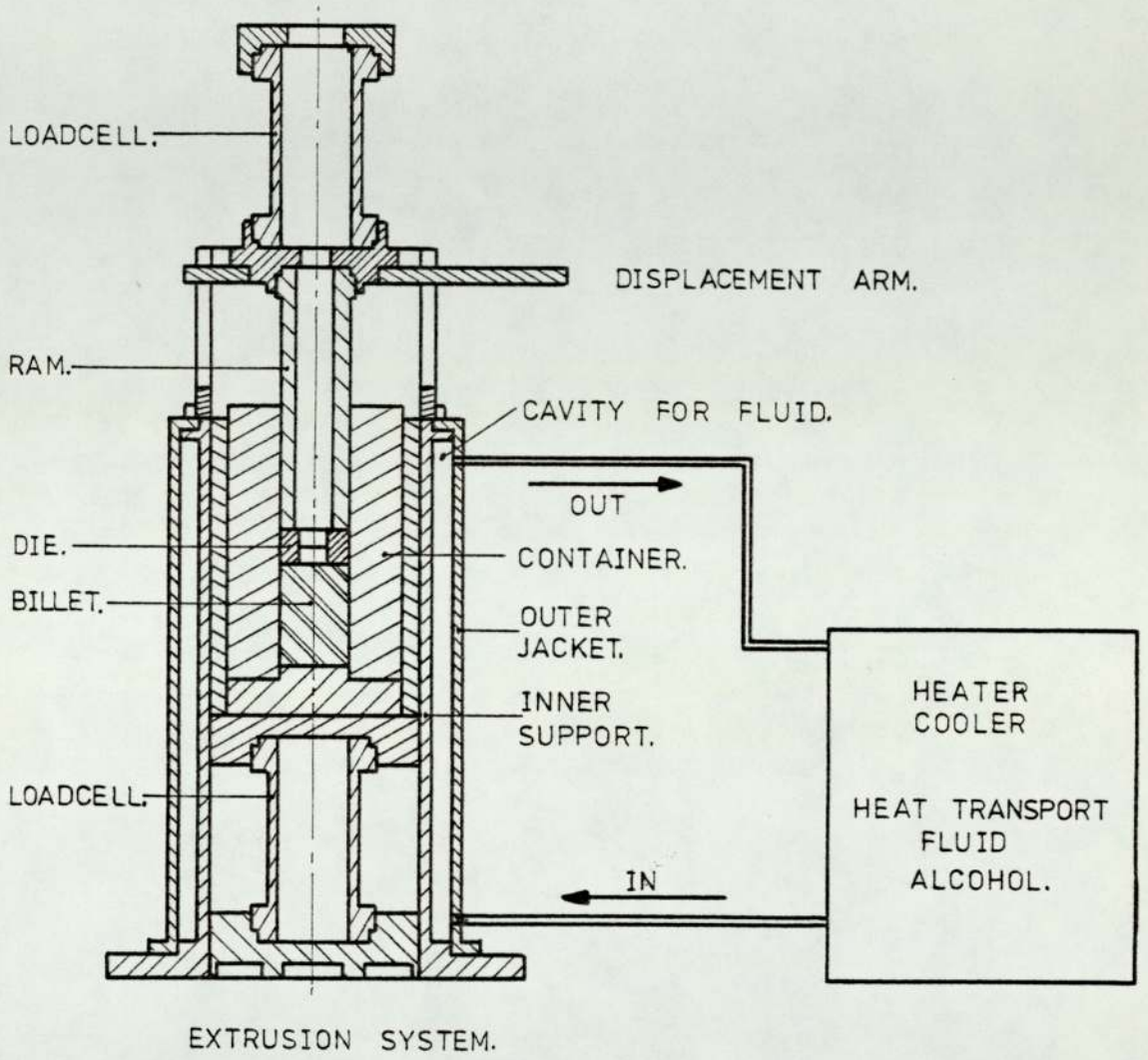

FIG. 2·11. PROPOSED HEATER COOLER ARRANGEMENT COUPLED TO THE EXTRUSION SYSTEM.

to be strong enough to withstand any side loads imposed on it by any rotation of the ram and the bending loads imposed by the inertia of the arm when accelerated in the impact.

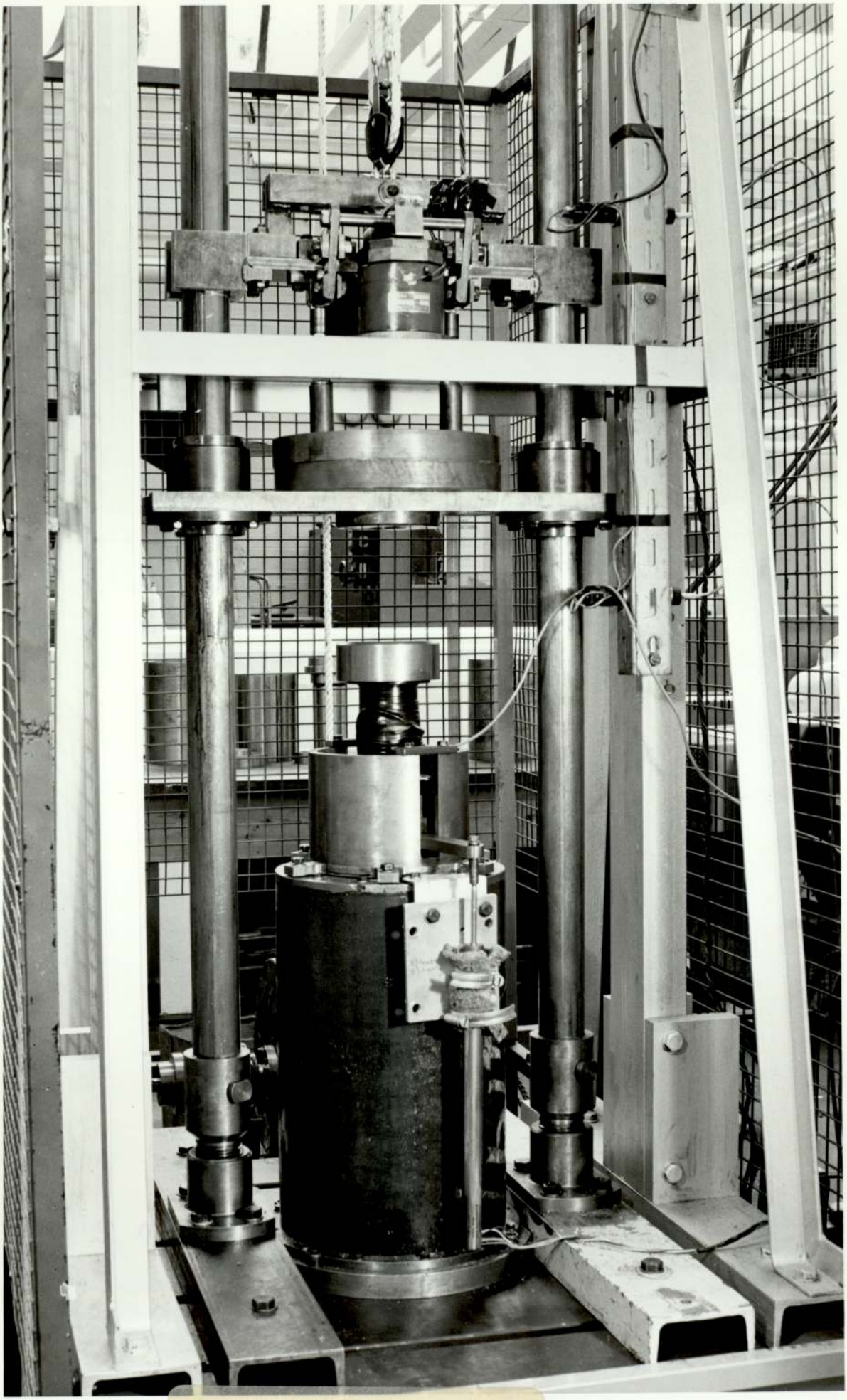

FIG 2.12
THE EXTRUSION RIG

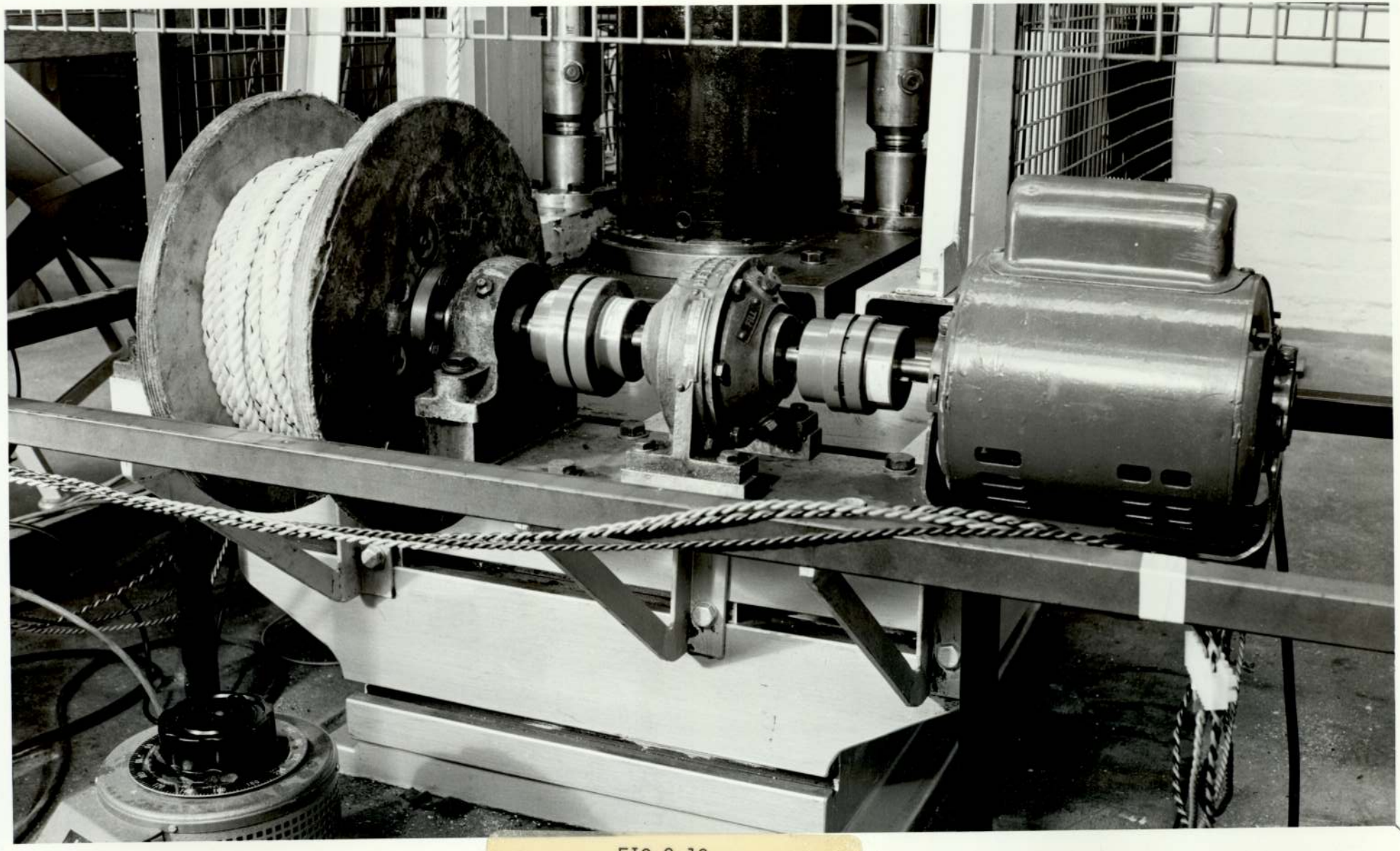

FIG 2.13
HOIST MECHANISM

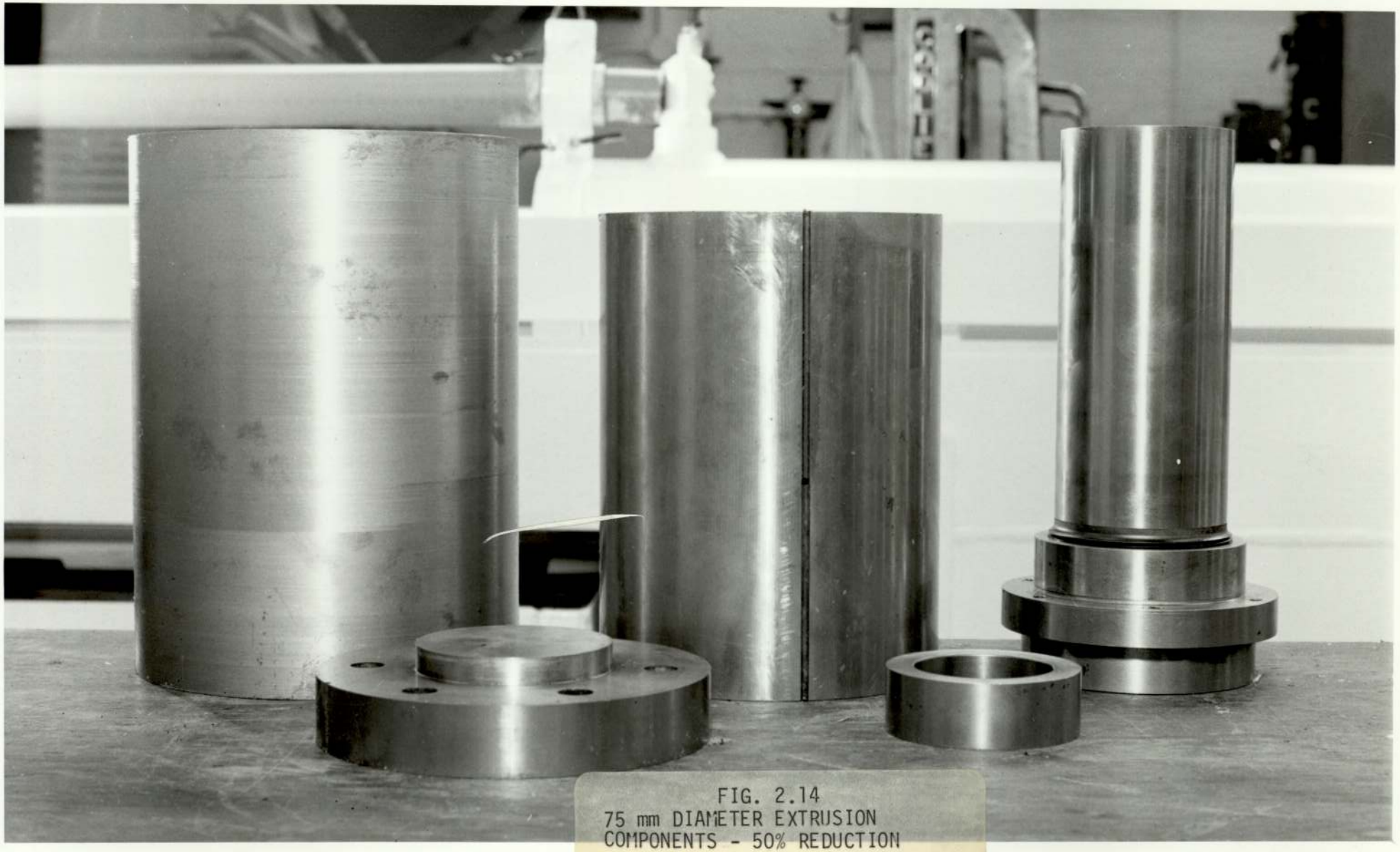

FIG. 2.14
75 mm DIAMETER EXTRUSION
COMPONENTS - 50% REDUCTION
OF AREA

FIG. 2.15.

12.5 mm DIAMETER EXTRUSION
COMPONENTS - 50% - 60% - 70% -
80% REDUCTION OF AREA.

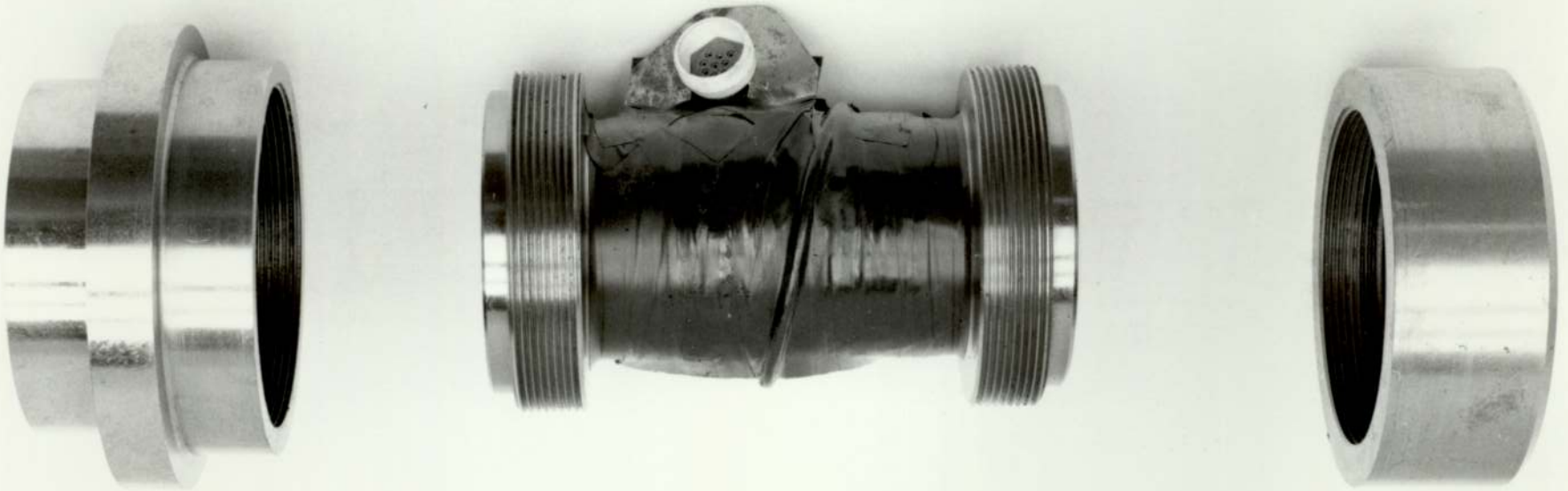

FIG 2.16
TOP LOAD CELL WITH ADAPTOR
AND IMPACT COVER

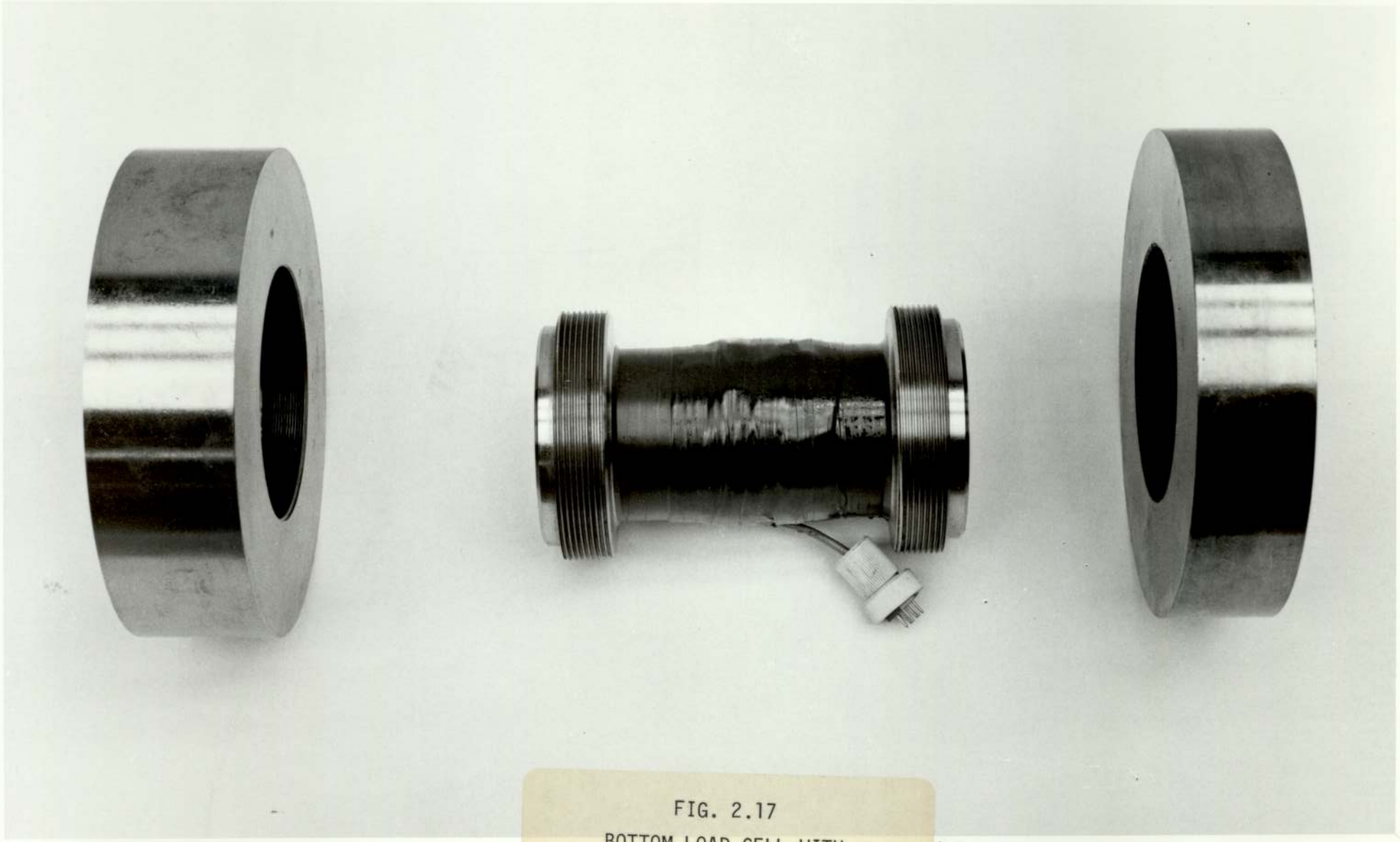

FIG. 2.17

BOTTOM LOAD CELL WITH
TOP AND BASE COVERS

FIG. 2.18
INNER SUPPORT AND
OUTER JACKET

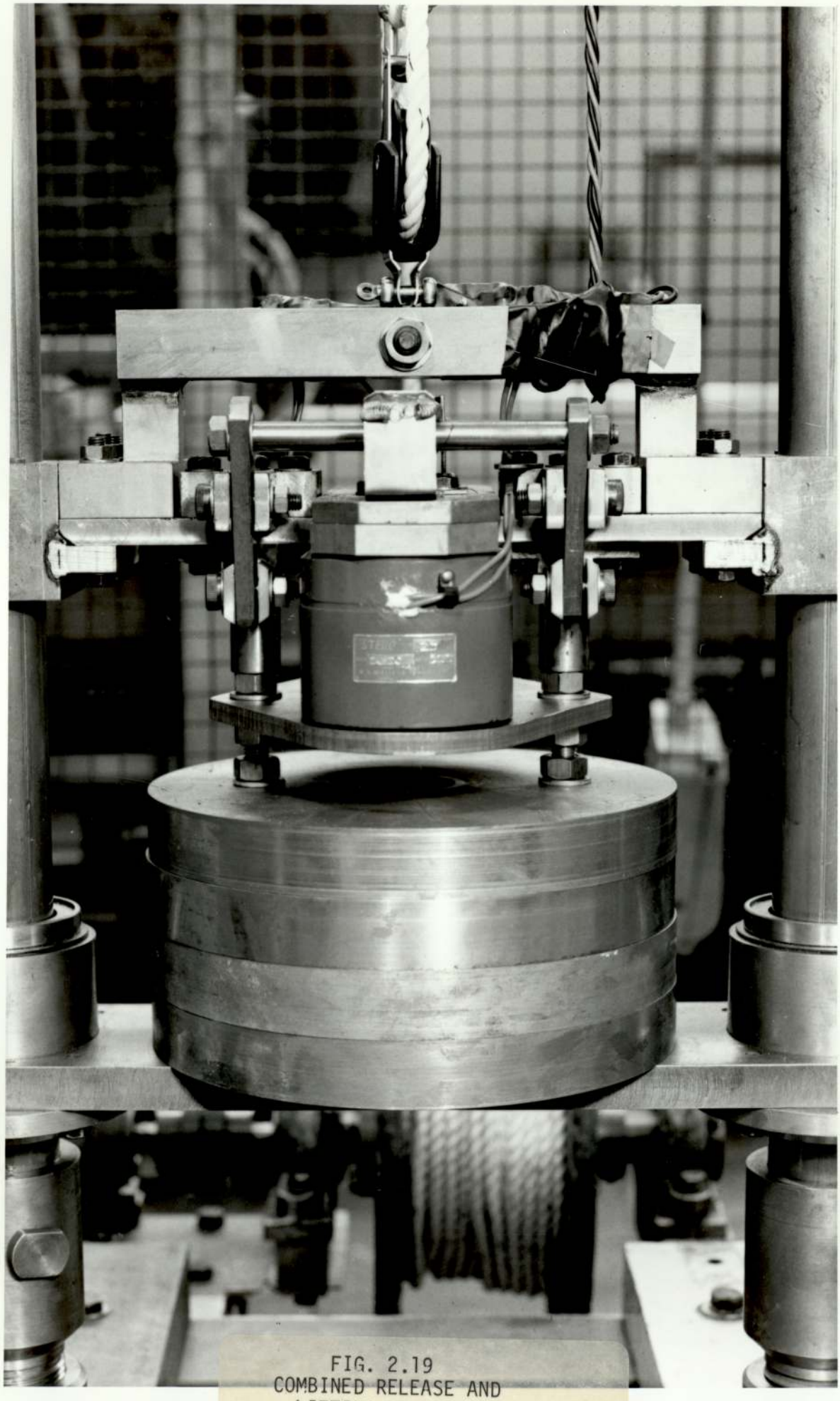

FIG. 2.19
COMBINED RELEASE AND
LIFTING MECHANISM

CHAPTER 3.

INSTRUMENTATION AND CALIBRATION

To ensure that a complete analysis of the energy absorbed in impact extrustion would be made, measurements were taken of the extrusion force, the displacement of the ram and the velocity of the falling mass.

3.1 The Load Cells.

The extrusion force was measured directly by two load cells, positioned above and below the extrusion system. See Fig.3.1.

The central region of the surface of the load cell, on which the strain gauges were bonded, was slightly roughened by fine emery paper and subsequently degreased with 'Inhibisol'. Eight foil strain gauges, each of 120 ohms resistance and dimensions 17.7mm x 5.5mm were bonded on the the centre of the load cell with Loctite Cyanoacrylate adhesive 15495. The arrangement of the gauges on each load cell is shown in Fig. 3.2, where the gauges numbered 1,2,3, and 4 are the active gauges and those numbered 5,6,7, and 8 are the passive or dummy gauges. After bonding, each gauge was checked for continuity and resistance to earth. The gauges were protected from the atmosphere and any accidental knocks by wrapping Self-Amalgamating Rubber tape around the load cell completely covering the gauges. The strain gauges were connected to the strain gauge conditioning amplifier in a Wheatstone bridge arrangement as shown in Fig.3.2. The conditioning amplifier controlled the bridge supply voltage and the zero setting of the bridge as well as the amplification. The conditioning amplifier was powered from a cross-linked stabilised d.c. dual power supply. The

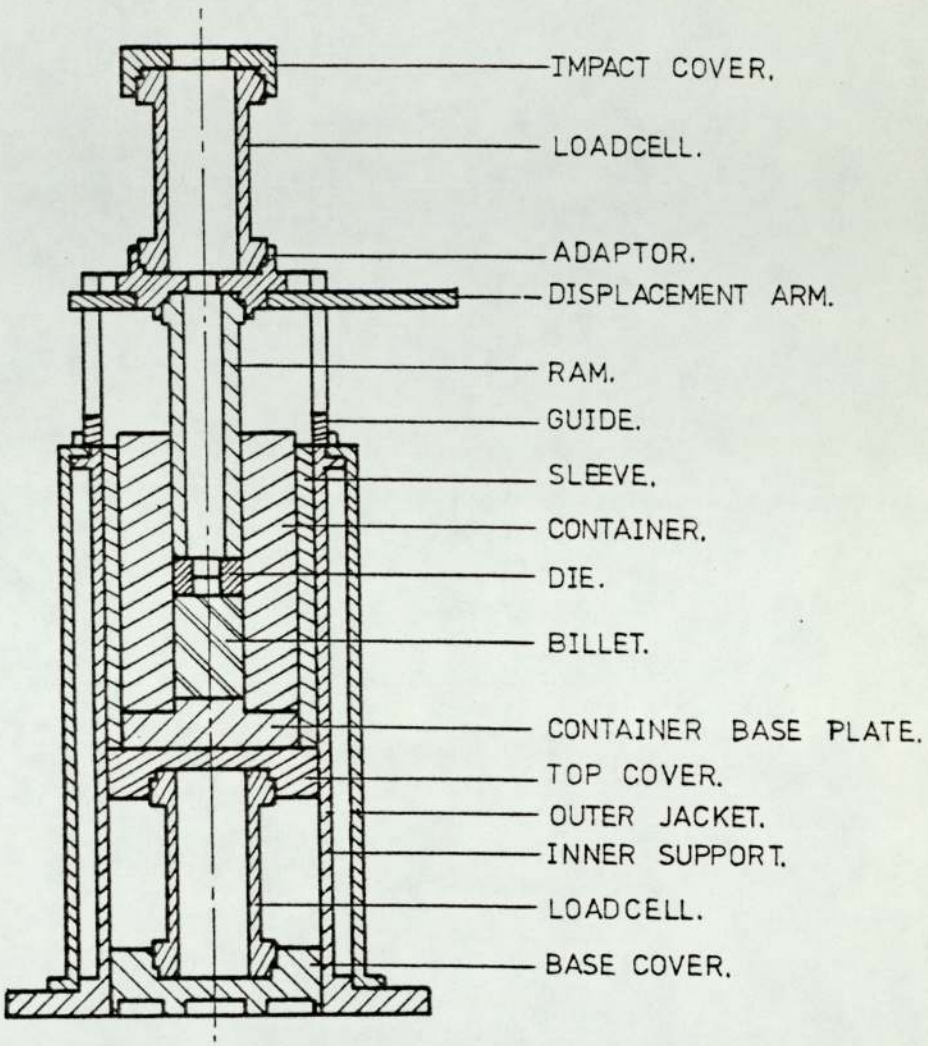

FIG. 3·1. EXTRUSION SYSTEM ASSEMBLY.

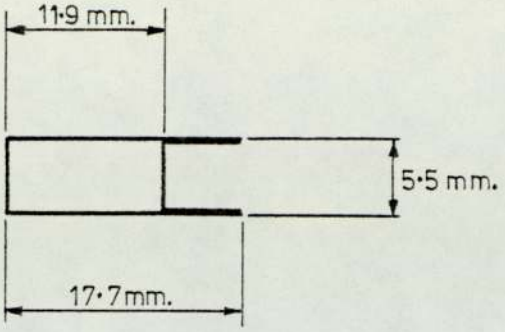

STRAIN GAUGES.
TINSLEY TELCON.
TYPE. 13/120/EC.

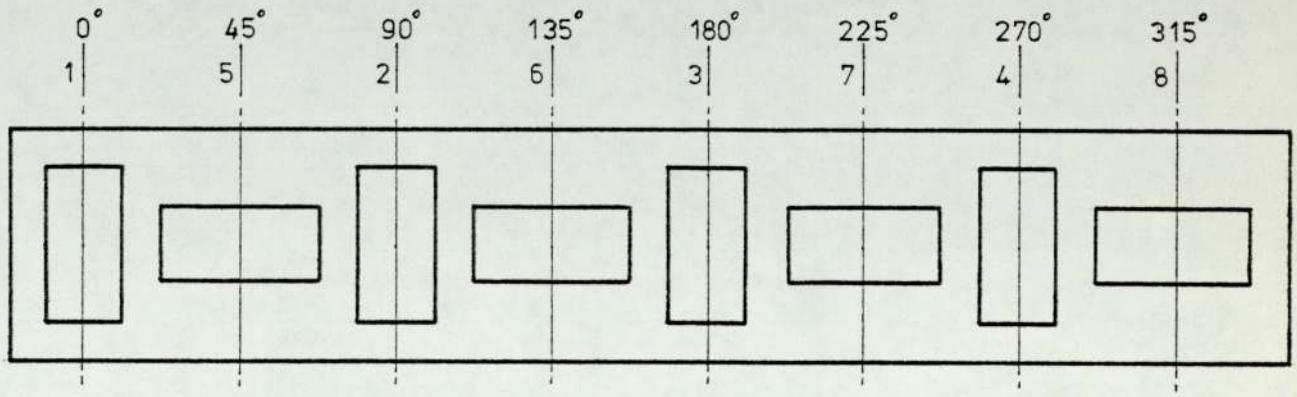

ARRANGEMENT OF STRAIN GAUGES ON THE LOADCELLS.

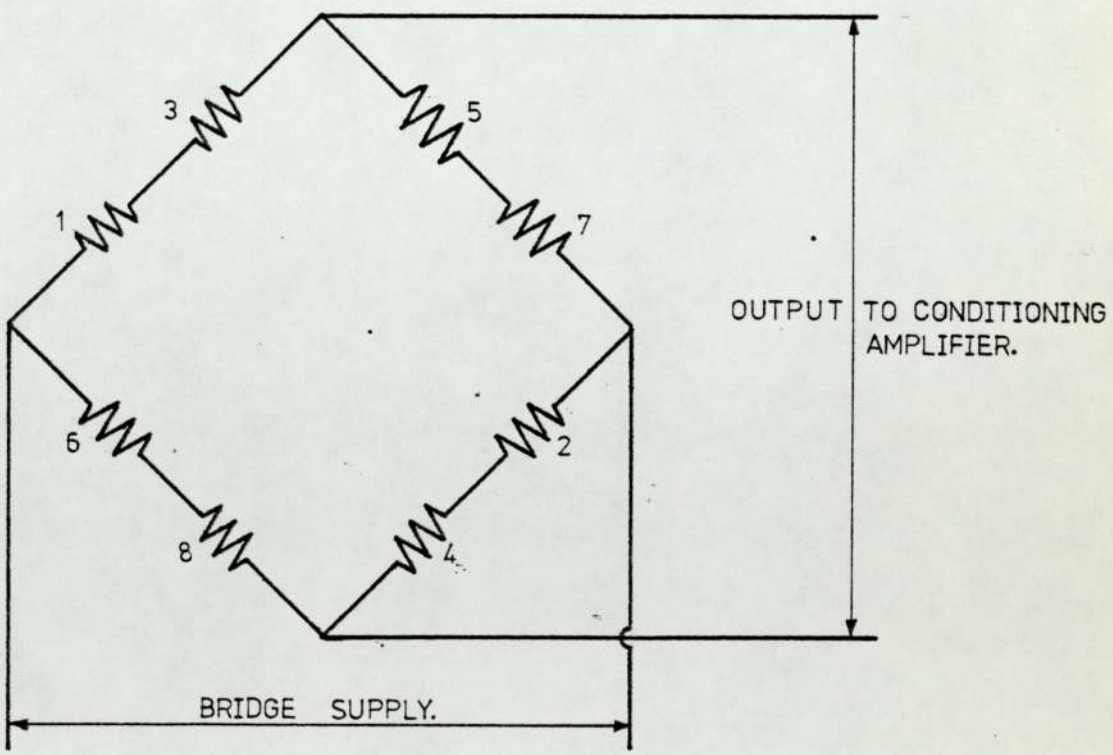

FIG. 3·2. THE WHEATSTONE BRIDGE FOR THE LOADCELLS.

output from the conditioning amplifier was fed directly to the recording oscilloscope. See Fig. 3.3

3.2 The Calibration of the Load Cells.

Before each calibration test, each load cell had the maximum load (30,000 kgf) applied approximately fifteen times by the 50,000 kgf Mohr and Federhaff Universal Testing Machine used for the calibration tests.

The load cell was loaded to its maximum load of 30,000 kgf (approximately 294 kN). The bridge supply voltage was set to 6 volts and the gain of the amplifier adjusted until the maximum output, without saturation, was achieved. The load cell was calibrated by recording the deflection of the oscilloscope trace for a number of consecutive steps of 5000 kgf up to the maximum load. The sensitivity of the oscilloscope was set at 0.2 volts/div for the above test. The test was repeated using decreasing steps of 5000 kgf from the maximum load.

The calibration procedure was repeated a further four times, using different oscilloscope sensitivity settings and load steps; i.e. at 0.1 volt/div, in steps of 2000 kgf to 16,000 kgf (full scale deflection); 0.05 volts/div, in steps of 1000 kgf to 9000 kgf; 0.02 volts/div, in steps of 500 kgf to 3000 kgf; and 0.01 volts/div, in steps of 250 kgf to 1500 kgf.

This calibration procedure was repeated for the other load cell. Both load cells were calibrated several times to ensure the results were repeatable. The calibration results are shown in Appendix E.

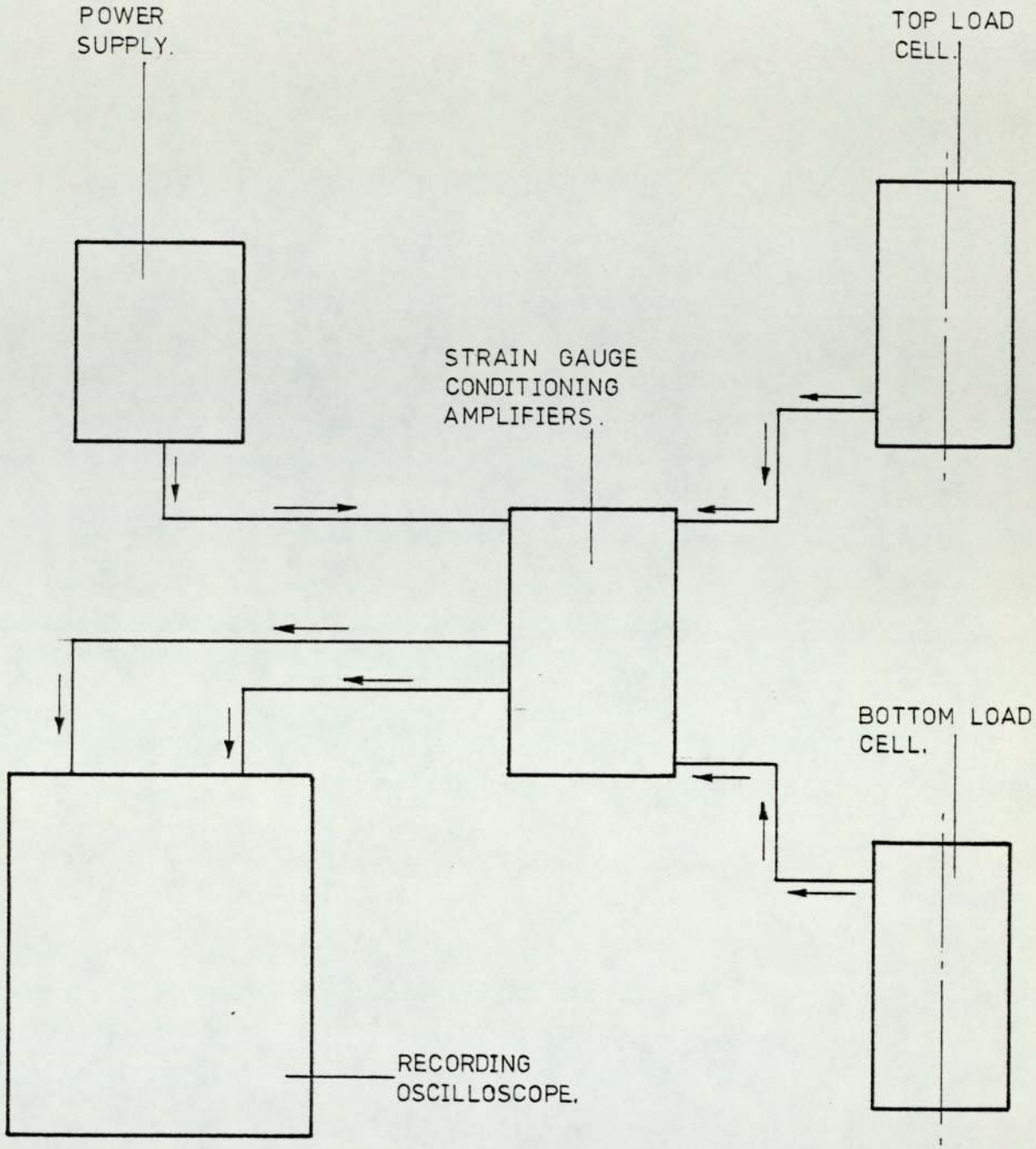

FIG. 3·3. SCHEMATIC LAYOUT OF THE LOAD MEASUREMENT SYSTEM.

3.3 Measurement of Ram Displacement.

The displacement of the ram was to have been measured by an inductive displacement transducer, coupled directly to the recording oscilloscope, See Fig.3.4. This would have produced a recording showing both displacement and extrusion force traces on the same time scale.

The transducer, a DC LUDT Linear Displacement transducer, type D2/2000 manufactured by R.D.P. Electronics Ltd., was used successfully on another impact test but the output signal from the transducer was very "noisy" and hence it did not give a clear usable recording. The fault appeared to be in the demodulator, which could not be repaired as it was sealed inside the transducer. The only other displacement transducer available was a resistive type LP1B/85 Rectilinear Potentiometer manufactured by Penny and Giles. This transducer gave a very clear trace at slow speeds, but at high speeds the noise produced by the pick-up elements of the transducer made it unsuitable for the application.

Since no suitable displacement transducer was available, or could be obtained quickly at a reasonable cost, the displacement of the ram was measured by a dial test indicator; this meant that only an overall displacement measurement could be taken. This displacement was assumed to vary linearly during the period that the extrusion force was present.

3.4 The Falling Mass Velocity Measurement System.

The velocity of the falling mass was measured indirectly by recording the time taken for the mass to pass by three fixed points,

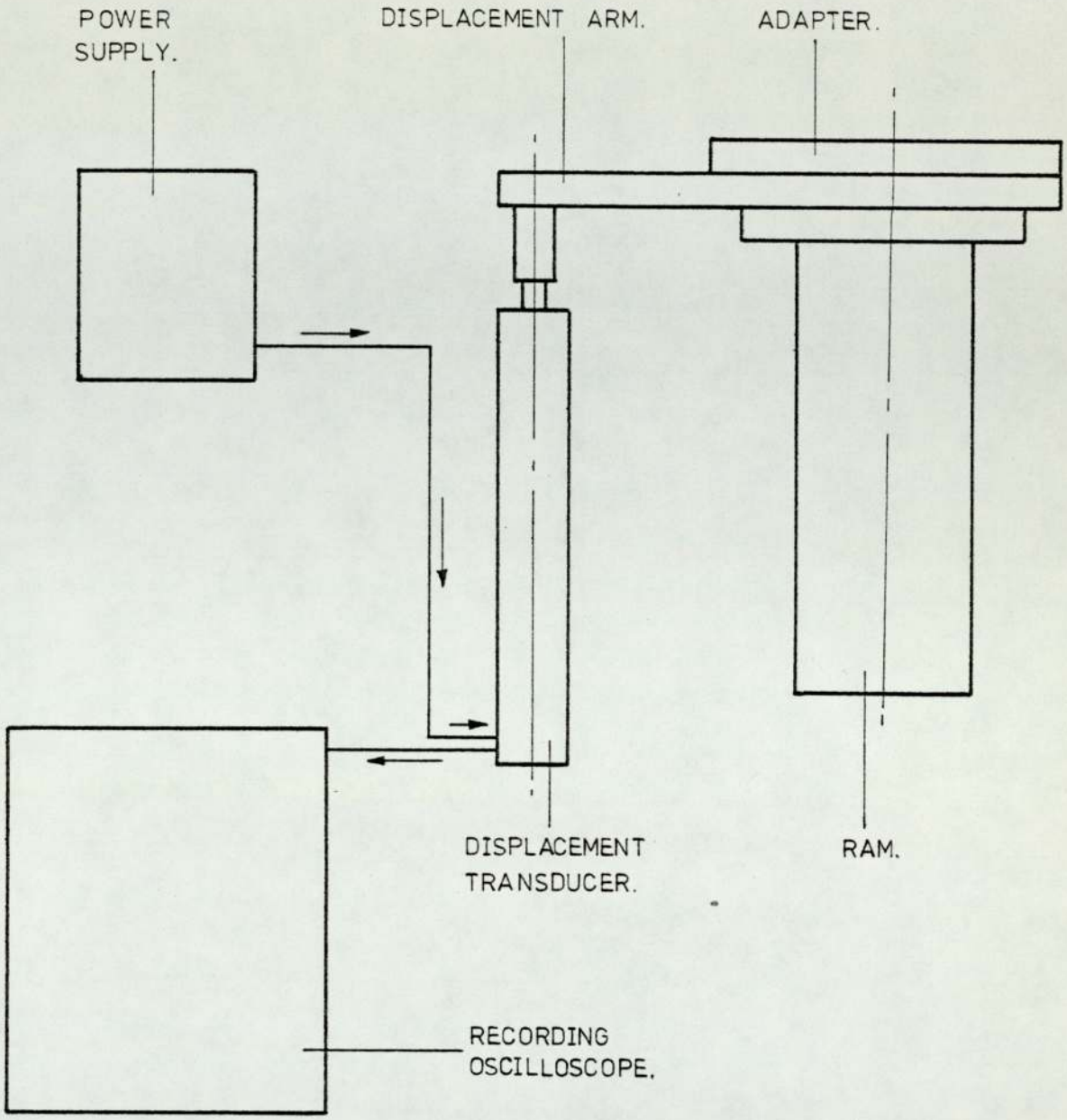

FIG. 3·4. SCHEMATIC LAYOUT OF THE RAM DISPLACEMENT MEASUREMENT SYSTEM.

400mm apart. Three fixed points were used to enable the acceleration of the falling mass to be calculated, since the acceleration of the mass is dependent on the force due to gravity minus the force due to friction in the bearings which is an unknown quantity.

A U-shaped channel was used to mount the light-activated switches and light sources 400 mm apart. The channel was attached to the main frame so that the lowest pair of light source and corresponding switch were in the same horizontal plane as the impact cover on the top load cell. This ensured that the final velocity calculated was the velocity at impact. See Fig. 3.5. The light sources were standard 6 volt bulbs mounted in housings that only allowed light to be emitted in a small round parallel beam. The light-activated switches, mounted in similar housings, could only receive light from the light sources opposite. See Fig. 3.6. A bar was attached to the crosshead to break the light beam and thus operate the light-activated switches.

When the first light beam was broken, a pulse from the switch operated the reed relay system which in turn started both of the electronic timing clocks. As the second light beam was broken, another pulse operated the reed relay system and stopped the first timing clock. A third pulse from the third switch operated the reed relay system and stopped the second timing clock at the instant of impact. A specimen calculation of impact velocity is shown in Appendix E.

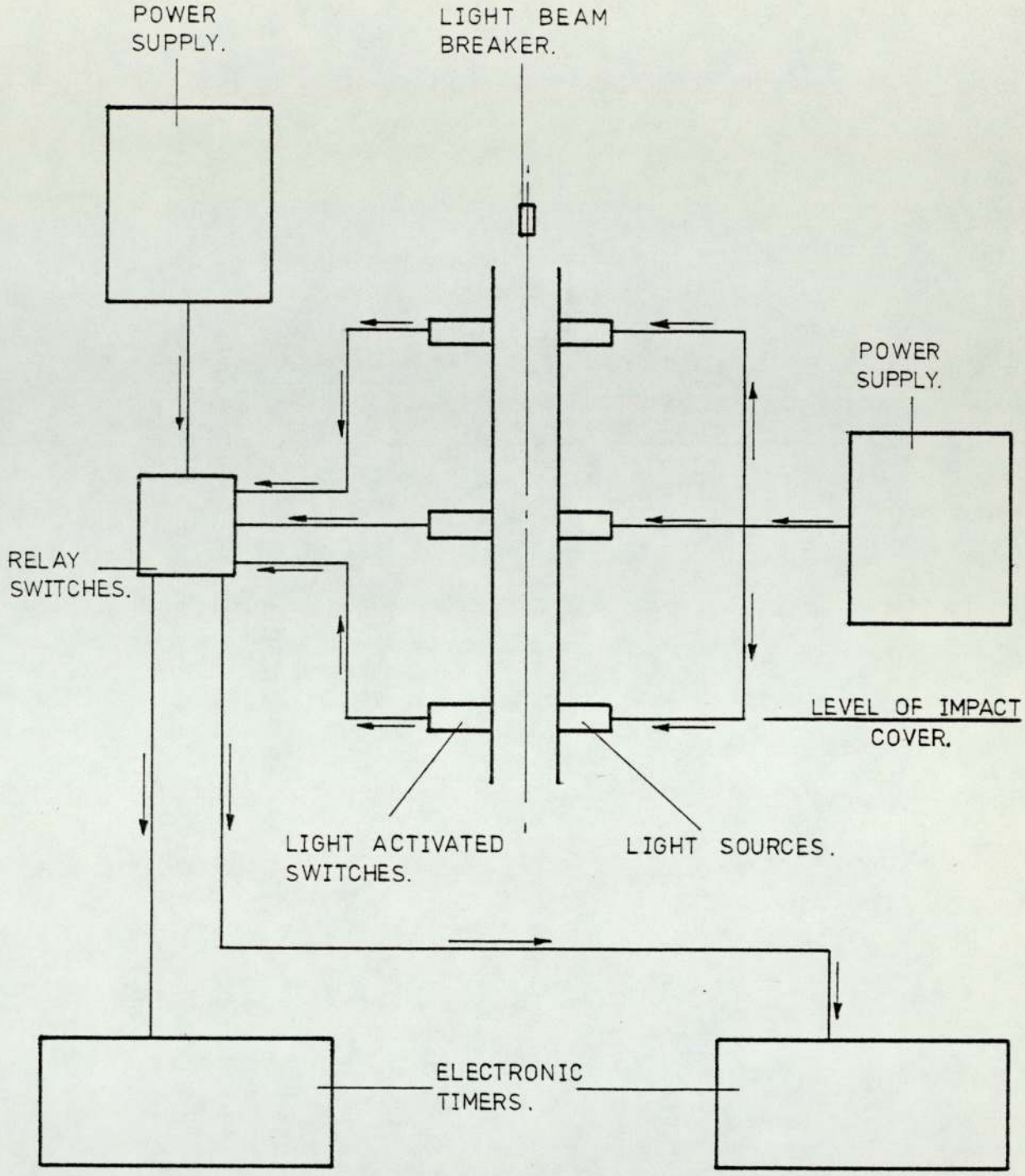

FIG. 3-5. SCHEMATIC LAYOUT OF THE FALLING MASS VELOCITY MEASUREMENT SYSTEM.

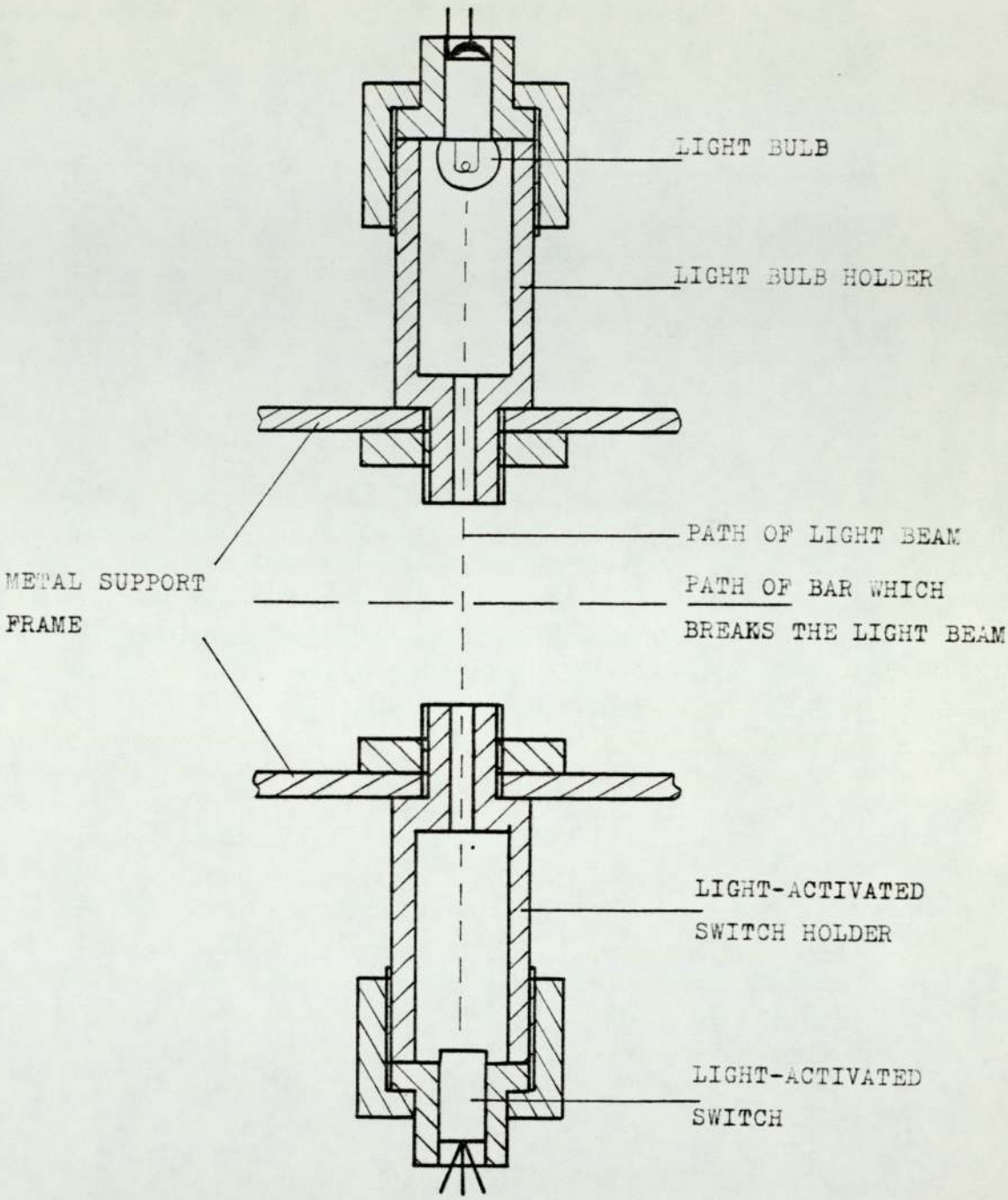

FIG. 3.6. SECTION THROUGH LIGHT ACTIVATED SWITCH AND BULB HOLDERS.

3.5 The Recording Oscilloscope.

Since the period of impact was in the order of a few milliseconds, it was difficult to obtain a reasonably long trace on a standard U.V. recorder chart. For an impact duration of 5 milliseconds, the paper speed would have to be 12 m/s in order to obtain a trace 60mm long. The paper drive motor requires a certain amount of time to run-up to speed and to stop. This would use a lot of paper and therefore, each test would be expensive to run.

A "Medelec" Recording Oscilloscope was purchased which allows traces of up to 90mm long to be recorded on stationary paper, i.e. across the paper. The running costs are comparatively very low. The sweep velocities of the "Medelec", range from 0.5 s/cm to 50 s/cm in 14 calibrated steps, which are equivalent to paper speeds of 0.02 m/s to 200 m/s.

The signals from the two load cells and the displacement transducer were fed directly into the "Medelec". The mode of recording was for a single sweep across the paper on a time basis to suit the extrusion period. The sweep was triggered internally by the signal from the top load cell. The force required, on the top load cell, to trigger the recording was about 600 N. The sensitivity of the "Medelec" was set to give optimum deflection for each recording with reference to the calibration settings.

A complete specification of all the instruments and power supplies is given in Appendix I.

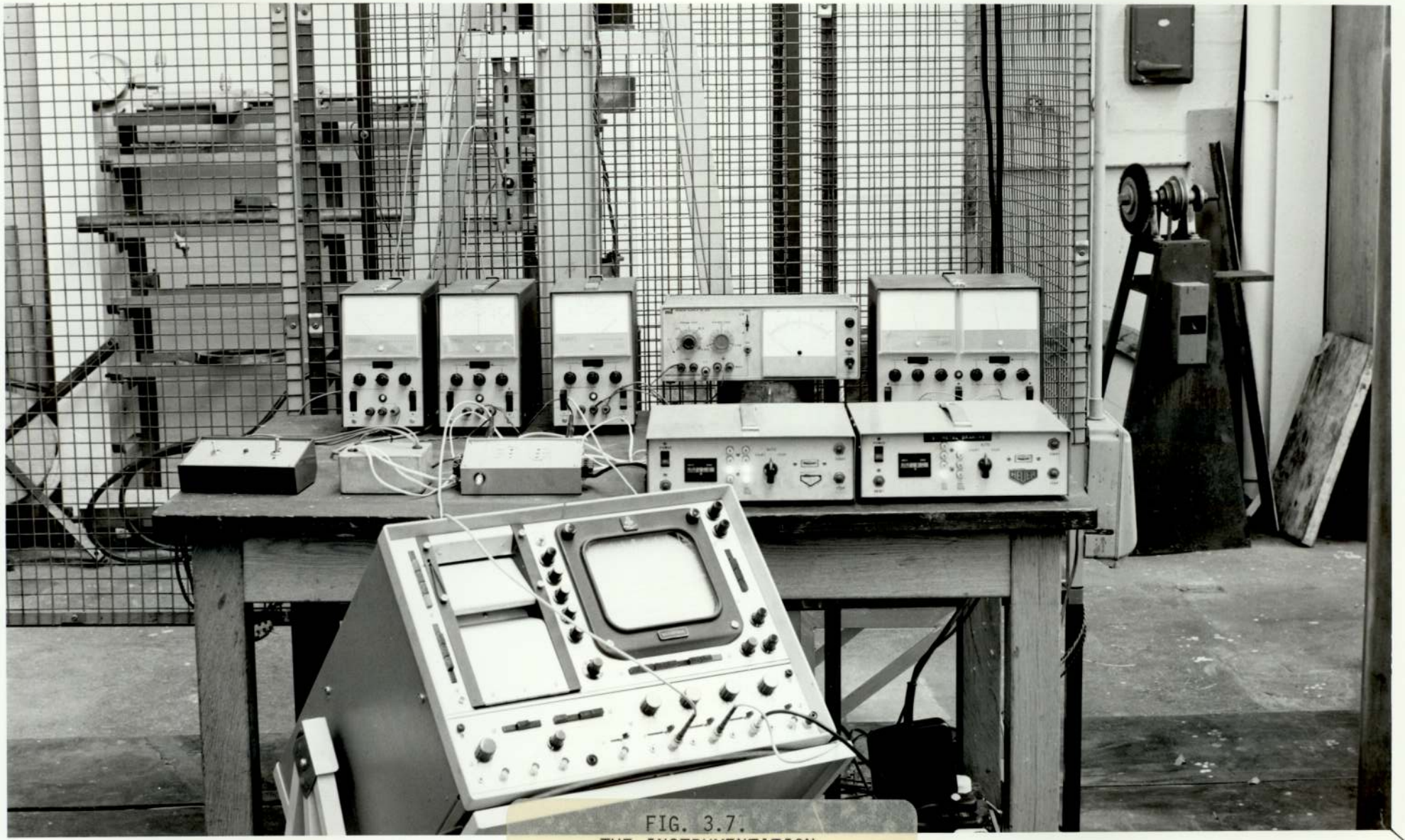

FIG. 3.7.
THE INSTRUMENTATION

CHAPTER 4.

EXPERIMENTAL METHOD

4.1 Determination of Stress - Strain Curves - Simple Compression.

The method used was that of incremental loading with re-lubrication of the dies between each loading. The length and diameter of a aluminium specimen were measured and recorded. Both ends of the specimen were coated with the lubricant and placed centrally on the bottom platen of the Denison Universal Testing Machine. The top platen was brought down until it just touched the specimen. An increment of load was applied and released, recording the value of load. The specimen was removed and the length measured and recorded. Both ends of the specimen were re-lubricated and the specimen placed back between the platens. Another increment of load was applied, released and recorded. The specimen was re-measured and the new length recorded. This was repeated, re-lubricating between each incremental loading, until about 90 - 95% length reduction was achieved. See Fig. 4.1.

This method was repeated for several more aluminium specimens of the same size, but made from different size bars.

Both the lead and polypropylene specimens were compressed in the same way, but without the application of a lubricant to the specimen ends. The specimens of lead and polyproplene were of the same length to diameter ratio, but varied in different size.

The curves of true stress versus percentage compression and true

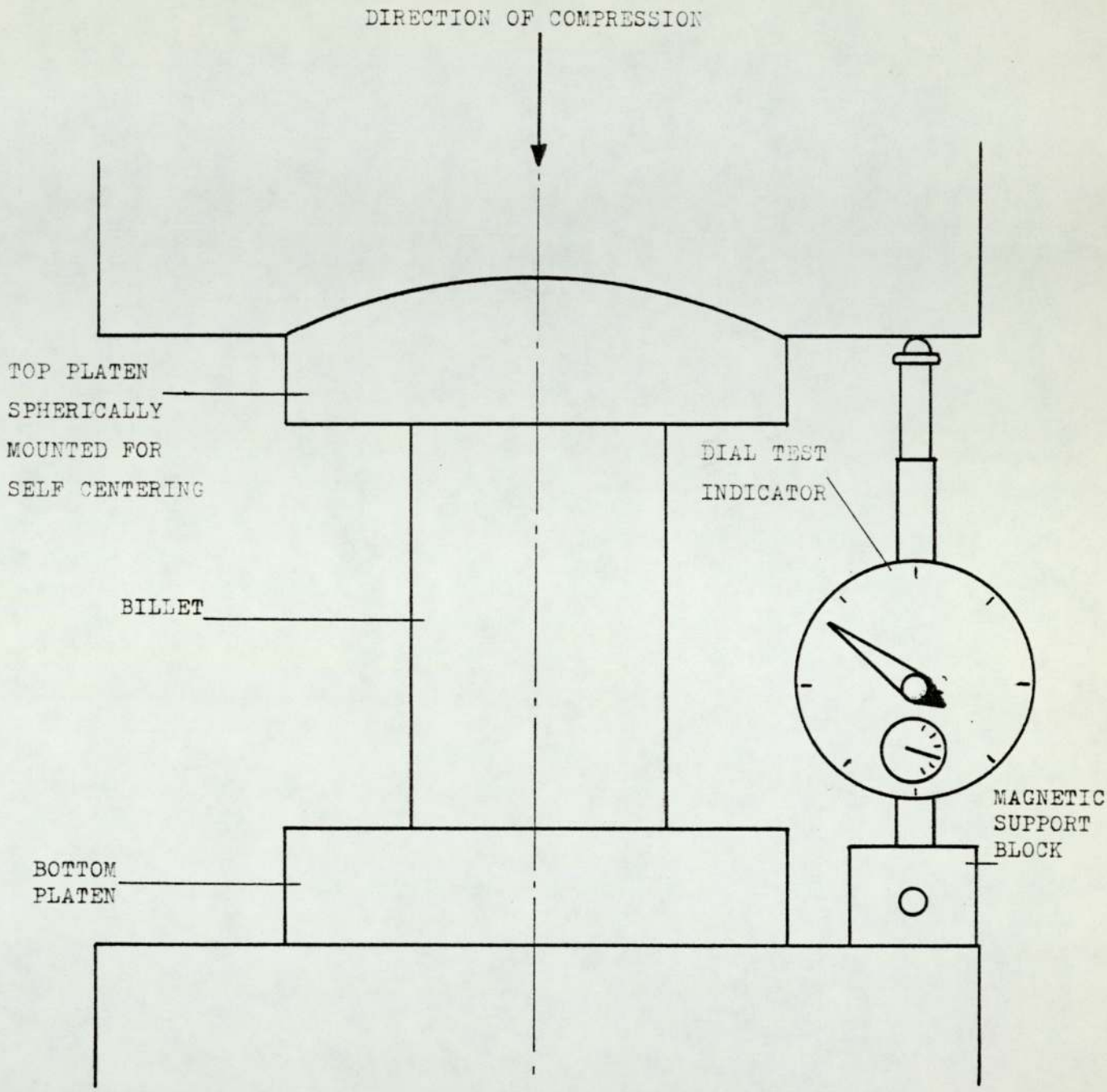

FIG. 4.1. SYSTEM FOR UNIAXIAL COMPRESSION TESTS OF LEAD, ALUMINIUM AND POLYPROPYLENE G.S.E.20.

stress versus logarithmetic strains are shown in Appendix F.

4.2 Slow Speed Extrusion Tests.

The length and diameter of a billet were measured and recorded. The billet was placed in the container followed by the die and the assembly was placed on the bottom platen of the Avery Universal Testing Machine. The ram was placed into the container and the top platen lowered until it was just touching the ram. See Fig. 4.2. The dial test indicator was placed under the displacement arm and set to zero.

The load was applied until slow movement of the ram occurred. (0.1mm per second or less). Values of displacement and the corresponding loads were recorded. The load was applied until the steady state was passed; this was noticed by a large increase in the load.

The load was released and the top platen raised to give access to the ram and container. The container and ram were removed and separated. The container base plate was removed and the extruded part with the discard and die were driven out. The die was removed from the extruded portion by pushing the extruded portion back through the die using the Mohr and Federhaff See Fig. 4.3.after removing the portion of billet remaining.

This method was repeated for all the lead billets extruded in the slow speed tests and the results are shown in Chapter 5.

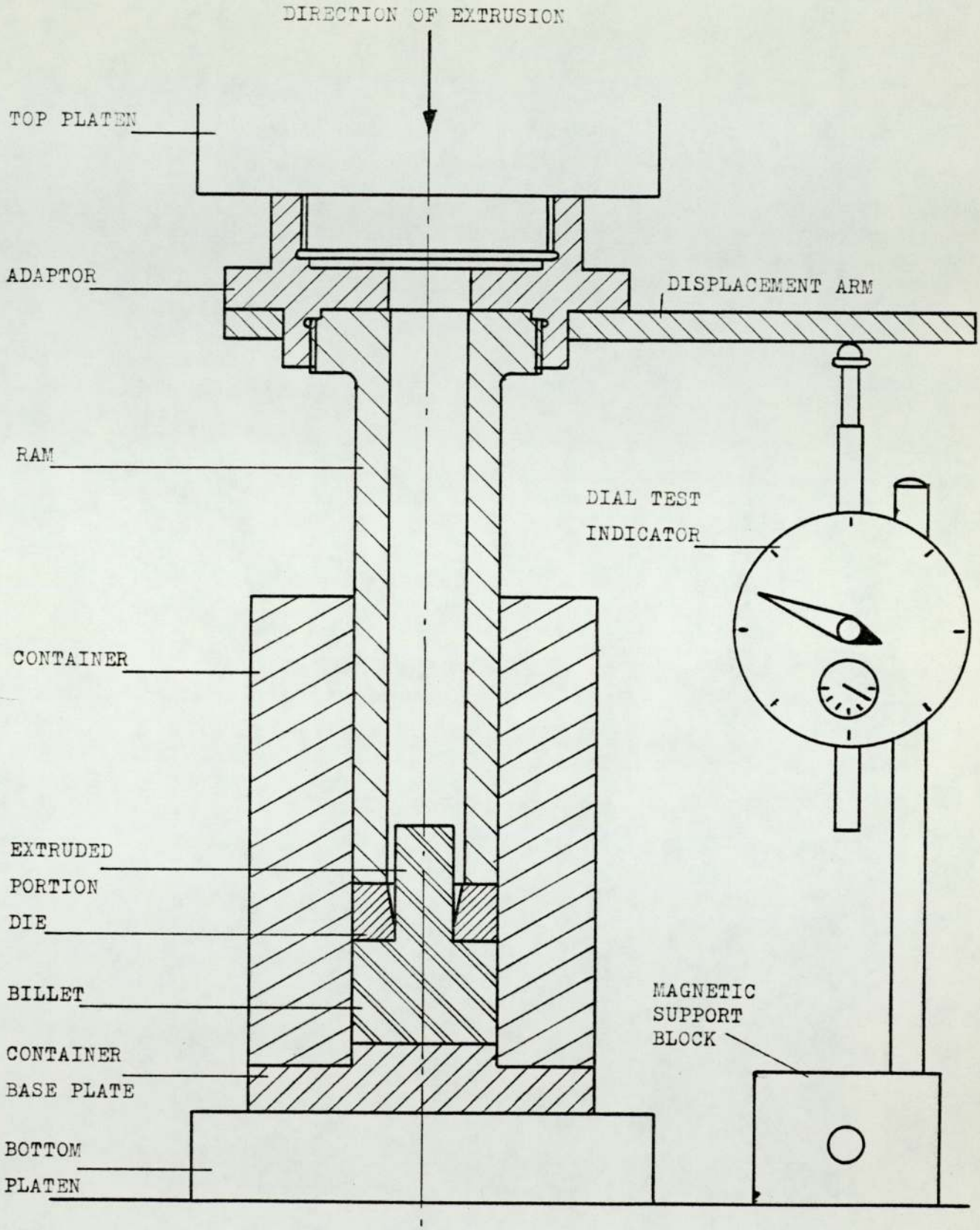

FIG. 4.2. SYSTEM FOR SLOW SPEED EXTRUSION TESTS OF LEAD.

CUT THROUGH BILLET

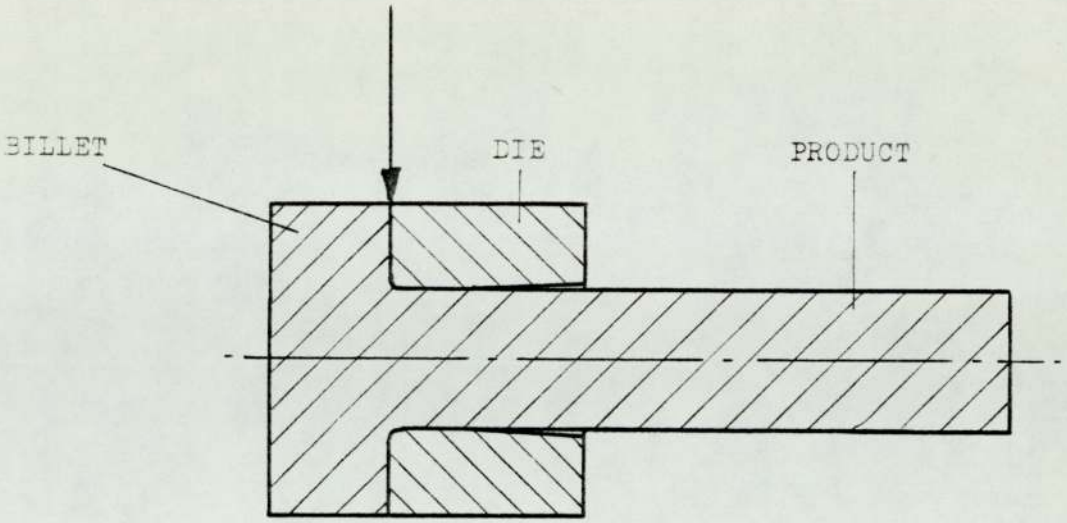

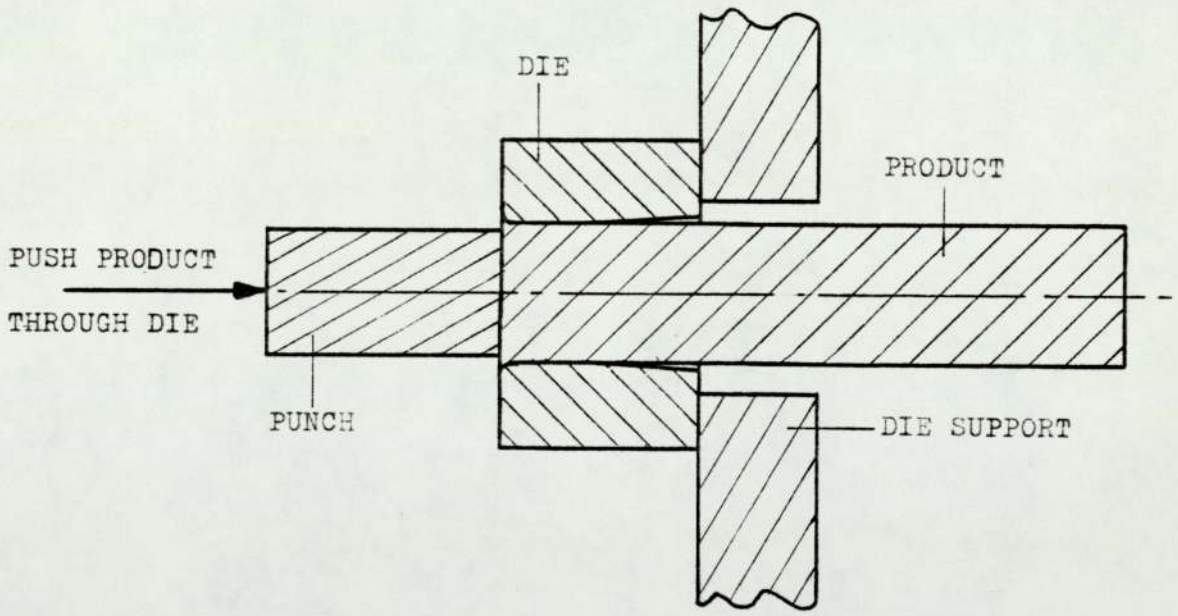

FIG. 4.3. METHOD USED TO REMOVE THE PRODUCT FROM THE DIE.

4.3 Impact Extrusion Tests.

The sleeve was placed inside the outer support on top of the bottom loadcell and cover. The container was placed inside the sleeve and the guide fitted on top of the outer support. The length and diameter of the billet were measured and recorded. The billet and die were placed in the container and the ram assembly placed on the top. The two bars to stop the ram from jumping out were put into place and the dial test indicator was placed under the displacement arm. See Fig. 4.4. The crosshead was lowered on to the impact cover on the top load cell and the mass adjusted to the required amount, determined from the theoretical results. The dial test indicator was set to zero and removed complete with its base plate: this was to protect its delicate mechanism from the shock of the impact. The crosshead was raised to the calculated drop height and the door of the safety cage closed. The timing clocks were set to zero and the Medelec recording oscilloscope set to single sweep with internal triggering from the top load cell. All the instrumentation was allowed to warm up and stabilise for at least one hour before being used.

The crosshead was released by activating the electro-magnets, operating the solenoid and the de-activating the electro-magnets.

After the crosshead came to rest, the door of the safety cage was opened and the dial test indicator replaced. The ram displacement and the times from the clocks were recorded with the U.V. trace from the Medelec recording oscilloscope.

The dial test indicator was removed and the lifting release

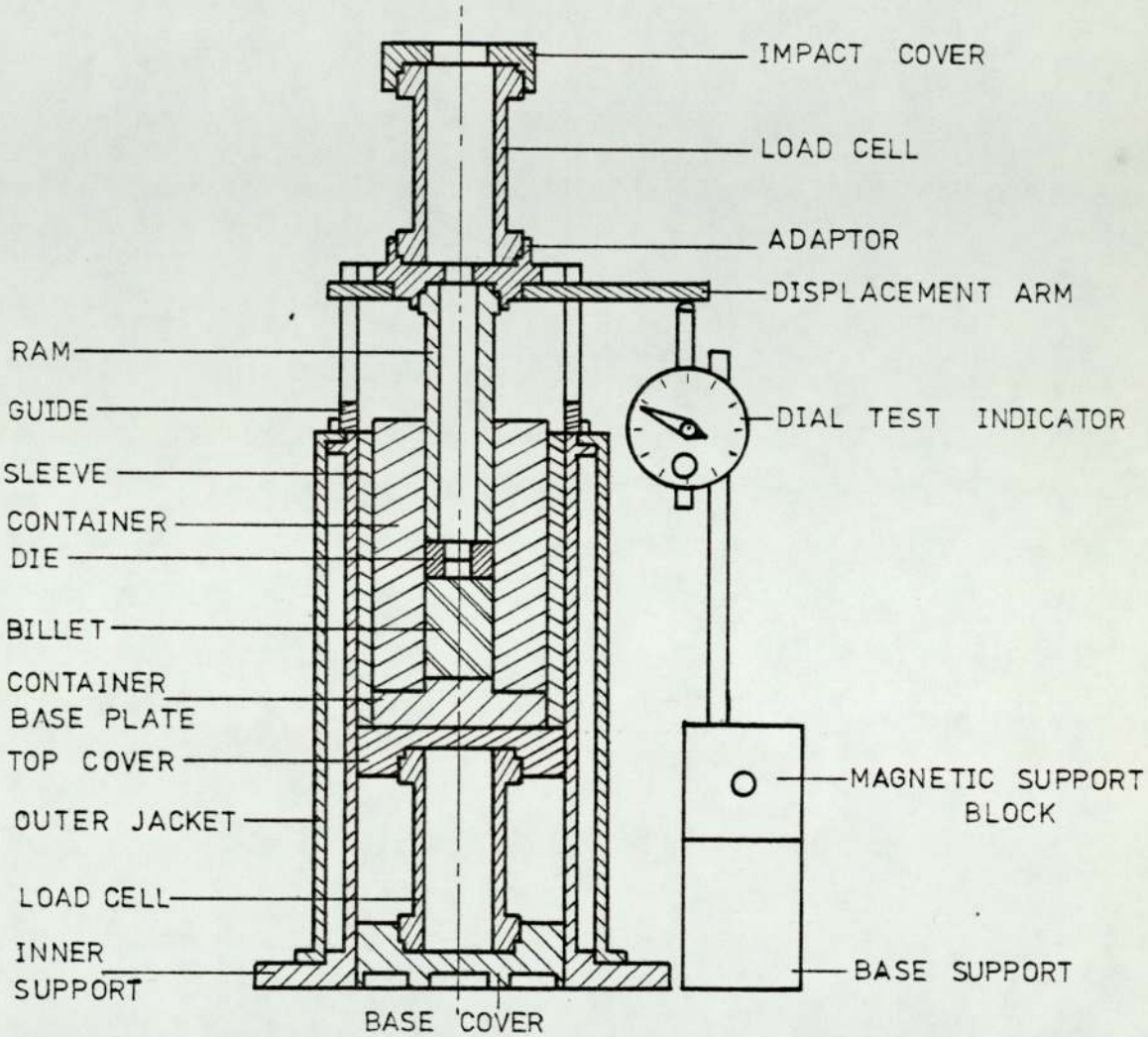

FIG. 4·4. POSITION OF DIAL TEST INDICATOR FOR THE IMPACT EXTRUSION TESTS.

mechanism lowered on to the crosshead. The release mechanism was re-connected to the crosshead and the combined system raised above the safety bars. The two bars on the guide were removed and the ram was withdrawn from the container. The sleeve and container were removed from the outer support. The container base plate was removed and the extruded part with the discard and die were driven out. The die was removed from the extruded portion by pushing the extruded portion back through the die using the Mohr and Federhaff.

This method was used in all the impact extrusion tests, using the drop height and mass as calculated from the theory initially; this value was then adjusted until complete extrusion of the billet was achieved. The results of these tests are shown in Chapter 5.

CHAPTER FIVE

RESULTS

RECORDED RESULTS

Billet Material : LEAD

Test No.	Billet Dia. mm	Size Length mm	Reduction of Area %	Falling Mass kg	Ram Displacement mm	Time of Fall T_1 Sec	Time of Fall T_2 Sec
1	74.96	75.01	50	100	-	0.061	0.120
2	74.96	75.01	50	100	-	0.062	0.121
3	74.96	75.01	50	100	-	-	0.121
4	74.96	75.01	50	100	-	0.061	0.121
5	74.96	75.01	50	100	-	0.062	0.121
6	74.96	75.01	50	100	-	0.061	0.120
7	74.96	75.01	50	100	-	-	-
8	74.98	75.09	50	100	-	0.062	-
9	74.98	75.09	50	100	-	0.061	0.121
10	74.98	75.09	50	100	-	0.061	0.120
11	74.98	75.09	50	100	-	0.061	0.121
12	74.98	75.09	50	100	-	0.061	0.121
13	74.98	75.09	50	100	7.85	0.062	-
14	74.98	75.09	50	100	7.75	-	-
15	74.98	75.09	50	100	7.70	-	0.121
16	74.95	75.10	50	100	8.00	0.063	0.121
17	74.95	75.10	50	100	7.75	0.062	0.121
18	74.95	75.10	50	100	6.39	0.087	0.162
19	74.95	75.10	50	100	6.47	0.086	0.162
20	74.95	75.10	50	110	4.97	0.105	0.190
21	74.95	75.10	50	110	4,83	0.106	0.192

Mass of ram, displacement arm, load cell, impact cover, adaptor and die = 8.85 kg.

RECORDED RESULTS

Billet Material : LEAD

Test No.	Billet Dia mm	Size Length mm	Reduction of Area %	Falling Mass kg	Ram Displacement mm	Time of Fall T_1 Sec	Time of Fall T_2 Sec
22	12.45	12.59	50	15	12.59	-	-
23	12.46	12.53	50	15	12.53	0.067	-
24	12.49	12.57	50	15	12.57	-	-
25	12.48	12.59	50	15	12.59	0.068	0.129
26	12.47	12.56	60	15	12.56	0.068	0.130
27	12.48	12.52	70	15	12.25	0.069	0.130
28	12.45	12.54	80	15	11.61	0.068	0.129
29	12.47	12.59	50	25	12.59	0.099	0.180
30	12.44	12.58	60	25	12.58	0.100	0.182
31	12.46	12.55	70	25	12.41	0.100	0.181
32	12.46	12.58	80	25	12.12	-	0.180
33	12.47	12.57	80	25	12.24	-	-
34	12.44	12.55	80	25	12.18	-	-
35	12.46	12.53	80	25	12.22	0.099	0.180
36	12.45	25.44	50	25	25.44	0.067	0.128
37	12.46	25.38	50	25	25.38	0.097	0.177
38	12.49	25.39	60	25	-	0.067	0.129
39							
40							
41							
42							

Mass of ram, displacement arm, load cell, impact cover, adaptor and die = 6.44 kg

CALCULATED RESULTS

Billet Material: LEAD

Test No	Total Mass — Kg	Impact Speed ms^{-1}	Initial Extrusion Speed ms^{-1}	Available Energy Nm	Total Mass / Billet Mass
16	108.85	7.19	6.61	2378	28.9
17	108.85	7.14	6.56	2342	28.9
18	108.85	5.77	5.31	1535	28.9
19	108.85	5.79	5.32	1540	28.9
20	118.85	5.13	4.75	1341	31.6
21	118.85	5.09	4.71	1318	31.6
25	21.44	6.84	4.79	246.0	1232
26	21.44	6.81	4.76	242.9	1232
27	21.44	6.80	4.75	241.8	1232
28	21.44	6.84	4.79	246.0	1232
29	31.44	5.33	4.24	282.6	1807
30	31.44	5.28	4.20	277.3	1807
31	31.44	5.30	4.21	278.6	1807
35	31.44	5.30	4.21	278.6	1807
36	31.44	6.83	5.43	463.5	904
37	31.44	5.39	4.53	325.4	904

CALCULATED RESULTS

Billet Material: LEAD

Test No.	Available Energy Nm	Energy Absorbed		Average Extrusion Pressure		Energy Absorbed / Available Energy	
		Top Nm	Bottom Nm	Top Nm^{-2}	Bottom Nm^{-2}	Top %	Bottom %
16	2378	1529	1501	43.3	42,5	64.3	63.1
17	2342	1468	1498	42.9	43.8	62.7	64.0
18	1535	1249	1120	44.2	39.7	81.4	73.0
19	1540	1077	1096	37.7	38.3	69.9	71.2
20	1341	928	918	42.3	41.8	69.2	68.5
21	1318	904	890	42.4	41.7	68.6	67.5
25	246.0	-	99.4	-	64.3	-	40.4
26	242.9	-	151.2	-	98.1	-	62.2
27	241.9	-	219.8	-	146.2	-	90.8
28	246.0	-	239.8	-	168.3	-	97.5
29	282.6	-	111.9	-	72.4	-	39.6
30	277.3	-	156.3	-	101.2	-	56.4
31	278.6	-	201.9	-	132.6	-	72.5
35	278.6	-	244.5	-	163.0	-	87.8
36	463.5	-	269.7	-	86.4	-	58.2
37	325.4	-	228.6	-	73.4	-	76.4

THEORETICAL PREDICTIONS

Billet Material: LEAD

Billet Size		Reduction of Area	Impact Velocity	Extrusion Pressure		Impact Mass Required for Complete Extrusion	Energy of Impact
Dia.	Length.			Initial	Final		
mm	mm	%	ms^{-1}	Nmm^{-2}	Nmm^{-2}	kg	Nm
12.48	12.59	50	4.79	65.5	64.5	8.73	100.2
12.47	12.56	60	4.76	76.5	74.9	10.17	115.2
12.48	12.52	70	4.75	94.7	91.9	12.67	142.9
12.45	12.54	80	4.79	142.2	135.6	18.48	212.0
12.47	12.59	50	4.24	65.4	64.6	11.12	100.0
12.44	12.58	60	4.20	76.3	75.1	13.12	115.7
12.46	12.55	70	4.21	94.4	92.2	15.00	141.8
12.46	12.53	80	4.21	141.4	136.4	23.95	212.2
12.45	25.44	50	5.43	65.6	64.4	13.65	201.2
12.46	25.38	50	4.55	65.5	64.5	19.43	201.1
74.95	8.00	50	6.61	66.0	64.0	105.0	2294
74.95	7.75	50	6.56	66.0	64.0	103.3	2223
74.95	6.39	50	5.31	65.6	64.4	130.0	1833
74.95	6.47	50	5.32	65.6	64.4	131.1	1855
74.95	4.97	50	4.75	65.5	64.5	126.3	1425
74.95	4.83	50	4.71	65.5	64.5	124.9	1385
74.95	75.10	50	6.6	66.0	64.0	988.8	21536

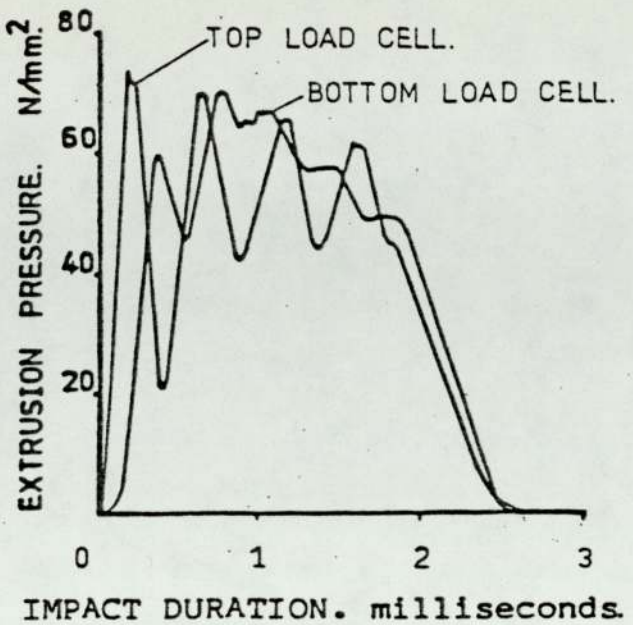

Material.	99.9% LEAD
Reduction of Area	50%
Billet size	74.95mm DIA. 75.10mm LONG
Impacting Mass	100.00kg.
Total Moving Mass	108.85kg
Impact Speed.	7.19 m s^{-1}
Initial Extrusion Speed.	6.61m s^{-1}
Energy Available at Impact.	2378Nm.
Energy Absorbed top Loadcell.	1529Nm
Energy Absorbed bottom Loadcell	1501Nm.
Ram displacement	8.00mm
Impact on Billet	FIRST

TEST No. 16.

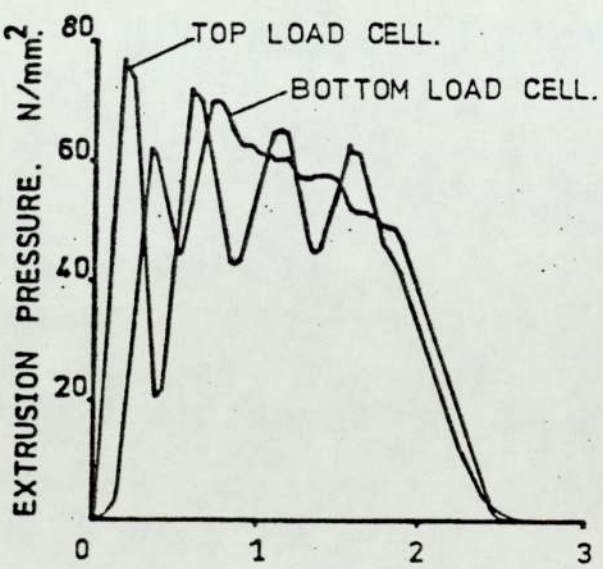

Material	99.9% LEAD
Reduction of Area	50%
Billet size	74.95mm DIA 75.10mm LONG
Impacting Mass	100.00kg
Total Moving Mass	108.85kg
Impact Speed	7.14m s^{-1}
Initial Extrusion Speed	6.56 ms^{-1}
Energy Available at Impact	2342Nm
Energy Absorbed top Loadcell	1468Nm
Energy Absorbed bottom Loadcell	1498Nm
Ram Displacement	7.75mm
Impact on Billet	SECOND

TEST No. 17.

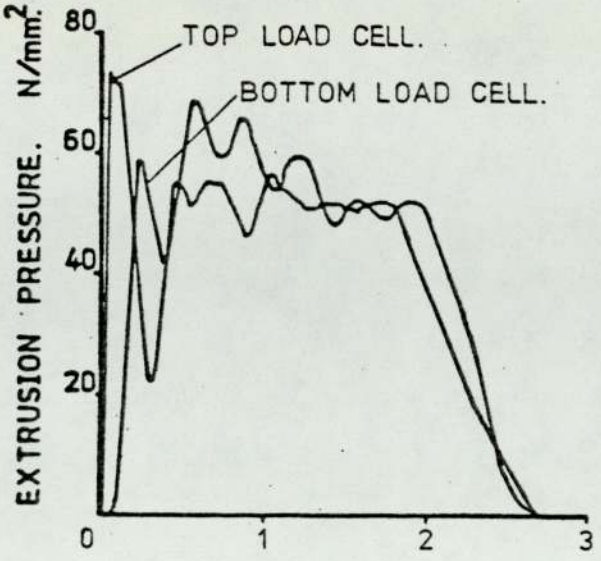

IMPACT DURATION milliseconds.

TEST No. 18.

Material	99.9%LEAD
Reduction of Area	50%
Billet size	74.95 mmDIA 75.10 mm LONG
Impacting Mass	100.00kg
Total Moving Mass	108.85kg
Impact Speed	$5.77ms^{-1}$
Initial Extrusion Speed	$5.31ms^{-1}$
Energy Available at Impact	1535Nm
Energy Absorbed top loadcell	1249Nm
Energy Absorbed bottom loadcell	1120Nm
Ram Displacement	6.39mm
Impact on Billet	THIRD

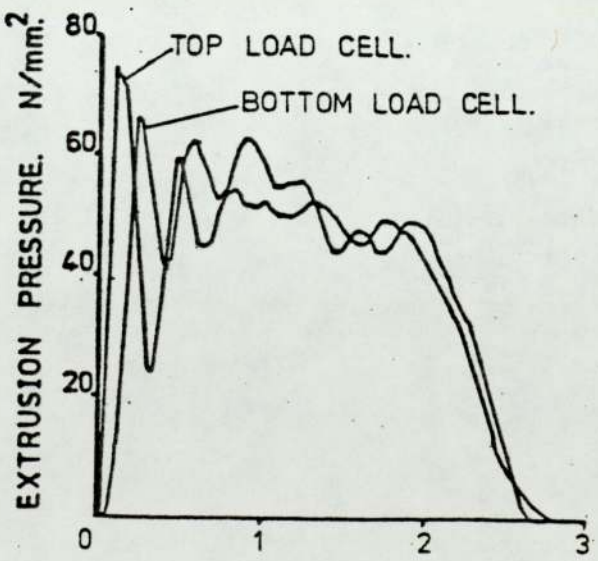

IMPACT DURATION milliseconds.

TEST No. 19.

Material	99.9%LEAD
Reduction of Area	50%
Billet Size	74.95mmDIA 75.10mmLONG
Impacting Mass	100.00kg
Total Moving Mass	108.85kg
Impact Speed	$5.79ms^{-1}$
Initial Extrusion Speed	$5.32ms^{-1}$
Energy Available at Impact	1540Nm
Energy Absorbed top loadcell	1077Nm
Energy Absorbed Bottom loadcell	1096Nm
Ram Displacement	6.47mm
Impact on Billet	FOURTH

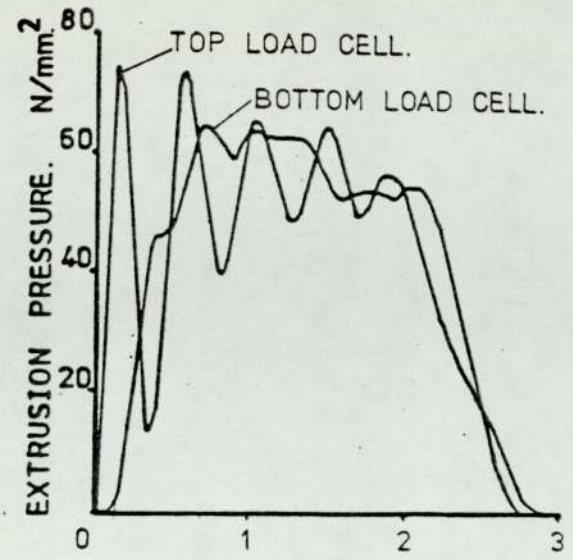

IMPACT DURATION. milliseconds.

Material	99.9%LEAD
Reduction of Area	50%
Billet size	74.95mmDIA 75.10mmLONG
Impacting Mass	110.00kg
Total Moving Mass	118.85kg
Impact Speed	$5.13ms^{-1}$
Initial Extrusion Speed	$4.75ms^{-1}$
Energy Available at Impact	1341Nm
Energy Absorbed top loadcell	928Nm
Energy Absorbed bottom loadcell	918Nm
Ram Displacement	4.97mm
Impact on Billet	FIFTH

Test No. 20.

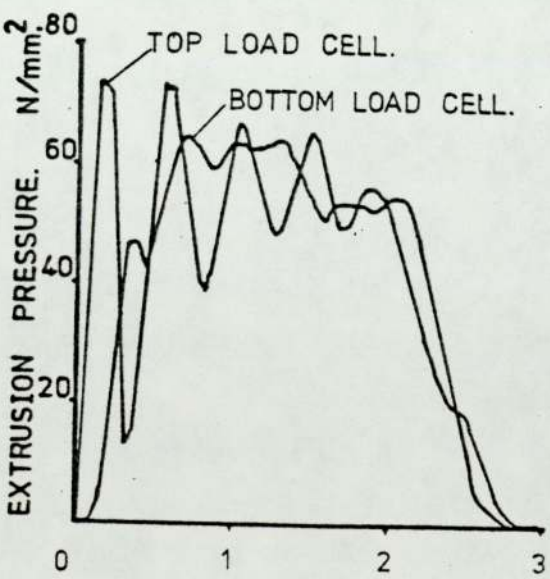

IMPACT DURATION. milliseconds.

Material	99.9%LEAD
Reduction of Area	50%
Billet size	74.95mmDIA 75.10mm LONG
Impacting Mass	110.00kg
Total Moving Mass	118.85kg
Impact Speed	$5.09ms^{-1}$
Initial Extrusion speed	$4.71ms^{-1}$
Energy Available at Impact	1318Nm
Energy Absorbed top loadcell	904Nm
Energy Absorbed bottom loadcell	890Nm
Ram Displacement	4.83mm
Impact on Billet	SIXTH

TEST No. 21.

Material	99.9% LEAD
Reduction of Area	60%
Billet size	12.47mm DIA 12.56mm LONG
Impacting Mass	15.00kg
Total Moving Mass	21.44kg
Impact speed	$6.81 ms^{-1}$
Initial Extrusion speed	$4.76 ms^{-1}$
Energy Available at Impact	242.9Nm
Energy Absorbed bottom loadcell	151.2Nm
Ram Displacement	12.56mm

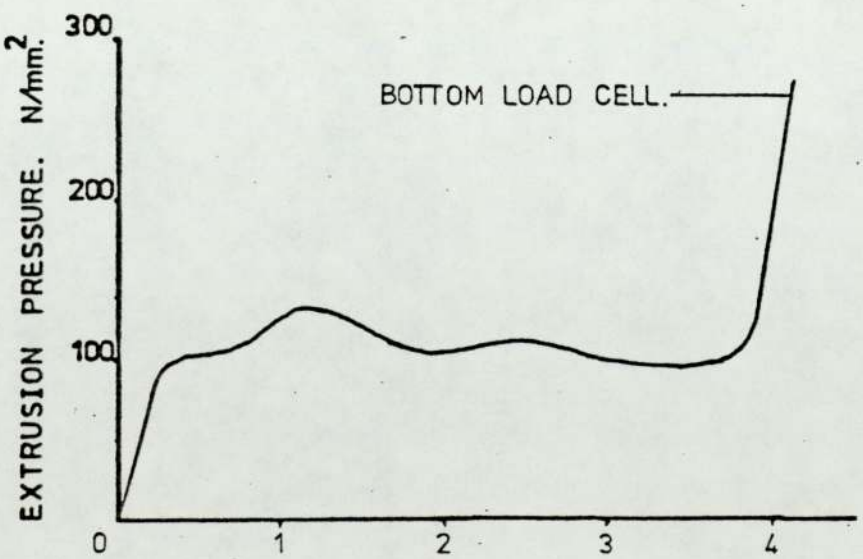

IMPACT DURATION. milliseconds.

TEST No. 26.

Material	99.9% LEAD
Reduction of Area	60%
Billet size	12.44mm DIA 12.58mm LONG
Impacting Mass	25.00kg
Total Moving Mass	31.44kg
Impact speed	$5.28ms^{-1}$
Initial Extrusion speed	$4.20ms^{-1}$
Energy Available at Impact	277.3Nm
Energy Absorbed bottom loadcell	156.3Nm
Ram Displacement	12.58mm

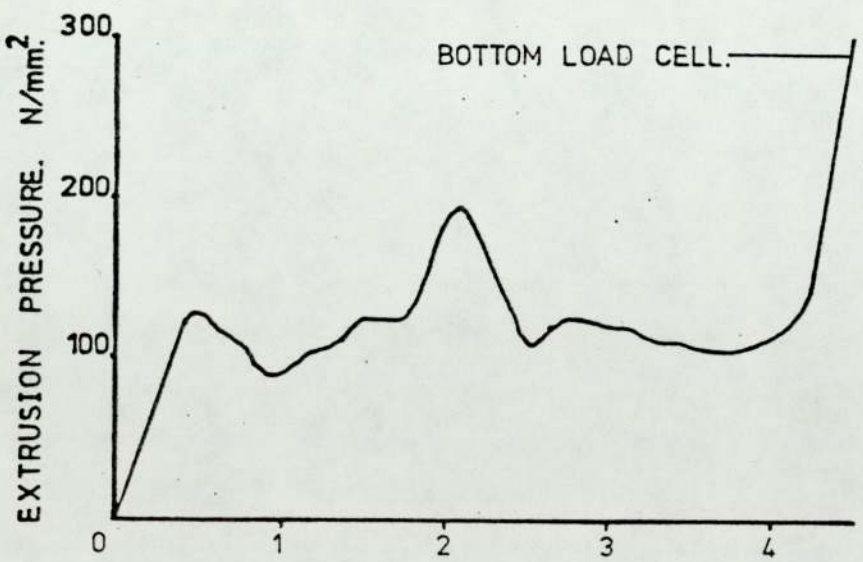

TEST No. 30.

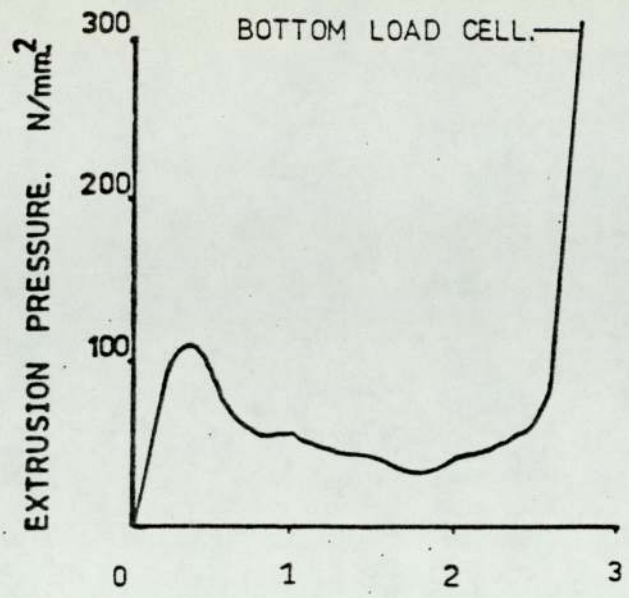

IMPACT DURATION. milliseconds.

TEST No. 25.

Material	99.9%LEAD
Reduction of Area	50%
Billet size	12.48mmDIA 12.59mmLONG
Impacting Mass	15.00kg
Total Moving Mass	21.44kg
Impact Speed	$6.84ms^{-1}$
Initial Extrusion Speed	$4.79ms^{-1}$
Energy Available at Impact	246.0Nm
Energy Absorbed bottom loadcell	99.4Nm
Ram displacement	12.59mm

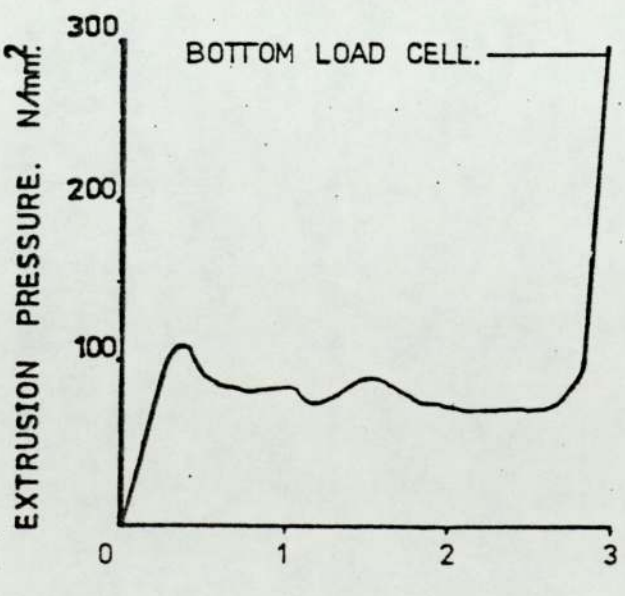

IMPACT DURATION. milliseconds.

TEST No. 29.

Material	99.9%LEAD
Reduction of Area	50%
Billet size	12.47mm DIA 12.59mm LONG
Impacting Mass	25.00kg
Total Mo ing Mass	31.44kg
Impact Speed	$5.33ms^{-1}$
Initial Extrusion Speed	$4.24ms^{-1}$
Energy Available at Impact	282.6Nm
Energy Absorbed bottom loadcell	111.9Nm
Ram displacement	12.59mm

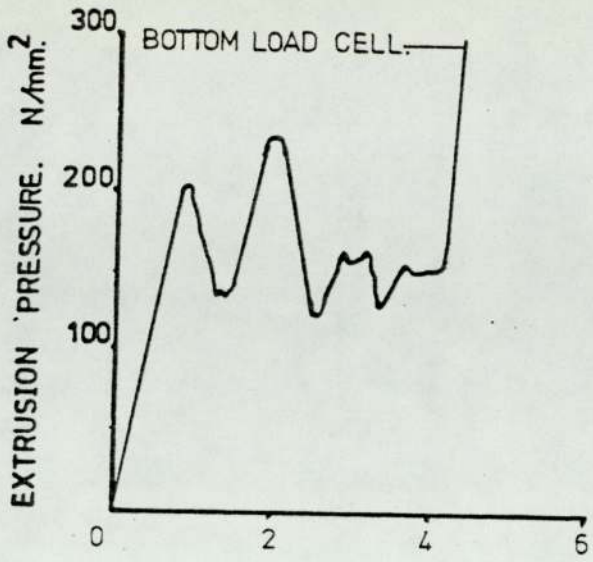

Material	99.9% LEAD
Reduction of Area	70%
Billet size	12.48mm DIA 12.52mm LONG
Impacting Mass	15.00kg
Total Moving Mass	21.44kg
Impact Speed	$6.80ms^{-1}$
Initial Extrusion speed	$4.75ms^{-1}$
Energy Available at impact	241.9Nm
Energy Absorbed bottom loadcell	219.8Nm
Ram Displacement	12,25mm

IMPACT DURATION. milliseconds.

TEST No. 27.

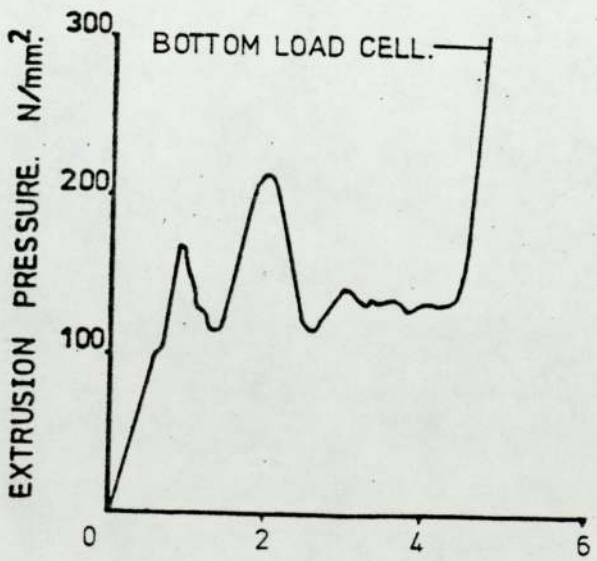

Material	99.9% LEAD
Reduction of Area	70%
Billet size	12.46mm DIA 12.55mm LONG
Impacting Mass	25.00kg
Total Moving Mass	31.44kg
Impact speed	$5.30ms^{-1}$
Initial Extrusion speed	$4.21ms^{-1}$
Energy Available at Impact	278.6Nm
Energy Absorbed bottom loadcell	201.9Nm
Ram Displacement	12.41mm

IMPACT DURATION. milliseconds.

TEST No. 31.

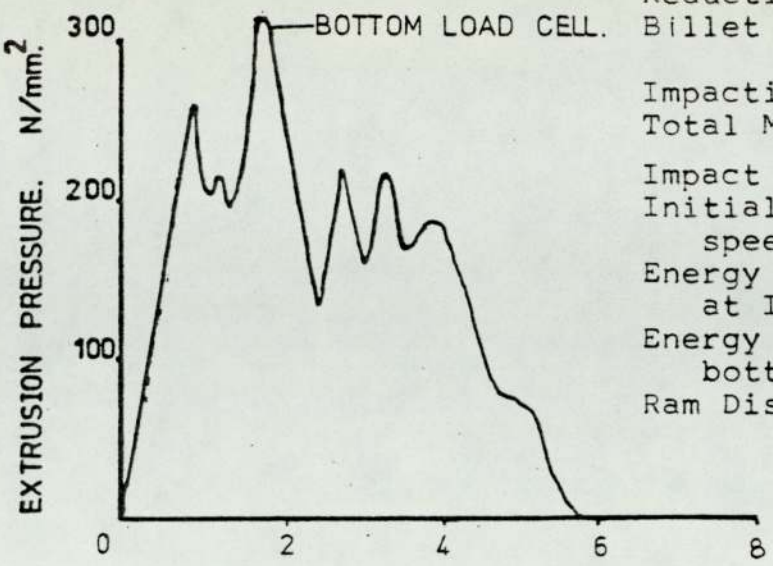

Material	99.9% LEAD
Reduction of Area	80%
Billet size	12.45mm DIA
	12.54mm LONG
Impacting Mass	15.00kg
Total Moving Mass	21.44kg
Impact speed	$6.84ms^{-1}$
Initial Extrusion speed	$4.79ms^{-1}$
Energy Available at Impact	246.0Nm
Energy Absorbed bottom loadcell	239.8Nm
Ram Displacement	11.61mm

IMPACT DURATION. milliseconds.

TEST No. 28.

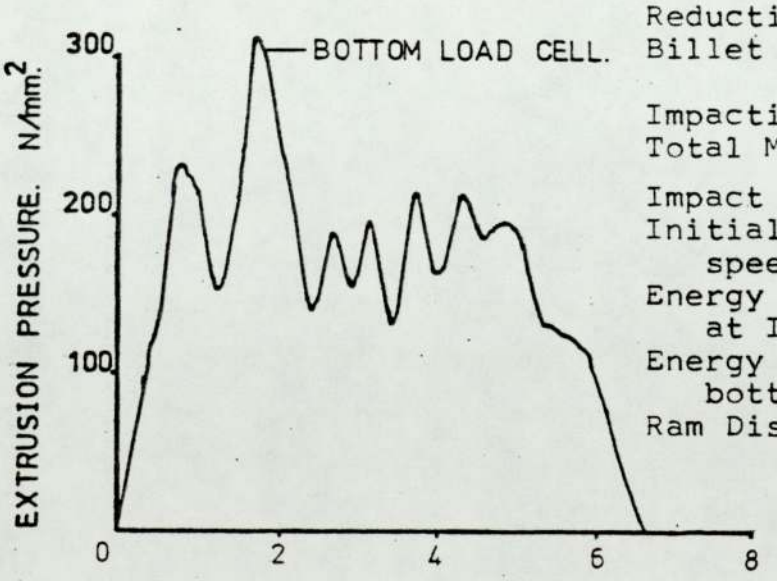

Material	99.0% LEAD
Reduction of Area	80%
Billet size	12.46mm DIA
	12.53mm LONG
Impacting Mass	25.00kg
Total Moving Mass	31.44kg
Impact speed	$5.30ms^{-1}$
Initial Extrusion speed	$4.21ms^{-1}$
Energy Available at Impact	278.6Nm
Energy Absorbed bottom loadcell	244.5Nm
Ram Displacement	12.22mm

IMPACT DURATION. milliseconds.

Test No. 35.

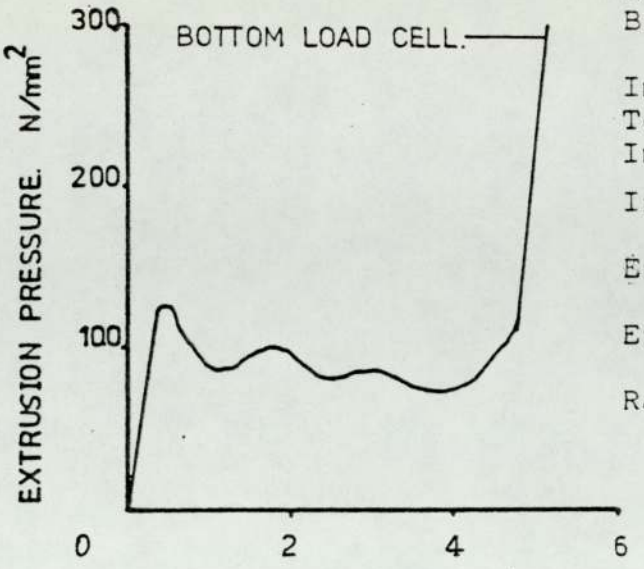

Material	99.9% LEAD
Reduction of Area	50%
Billet size	12.45mm DIA
	25.44mm LONG
Impacting Mass	25.00kg
Total Moving Mass	31.44kg
Impact speed	$6.83ms^{-1}$
Initial Extrusion speed	$5.43ms^{-1}$
Energy Available at Impact	463.5Nm
Energy Absorbed bottom loadcell	269.7Nm
Ram Displacement	25.44mm

IMPACT DURATION. milliseconds.

TEST No. 36.

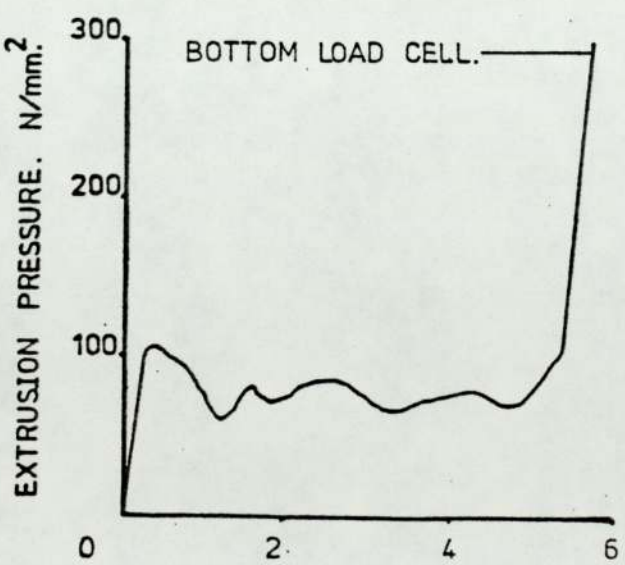

Material	99.9% LEAD
Reduction of Area	50%
Billet size	12.46mm DIA
	25.38mm LONG
Impacting Mass	25.00kg
Total Moving Mass	31.44kg
Impact speed	$5.39ms^{-1}$
Initial Extrusion speed	$4.55ms^{-1}$
Energy Available at Impact	325.4Nm
Energy Absorbed bottom loadcell	228.6Nm
Ram Displacement	25.38mm

IMPACT DURATION. milliseconds.

TEST No. 37.

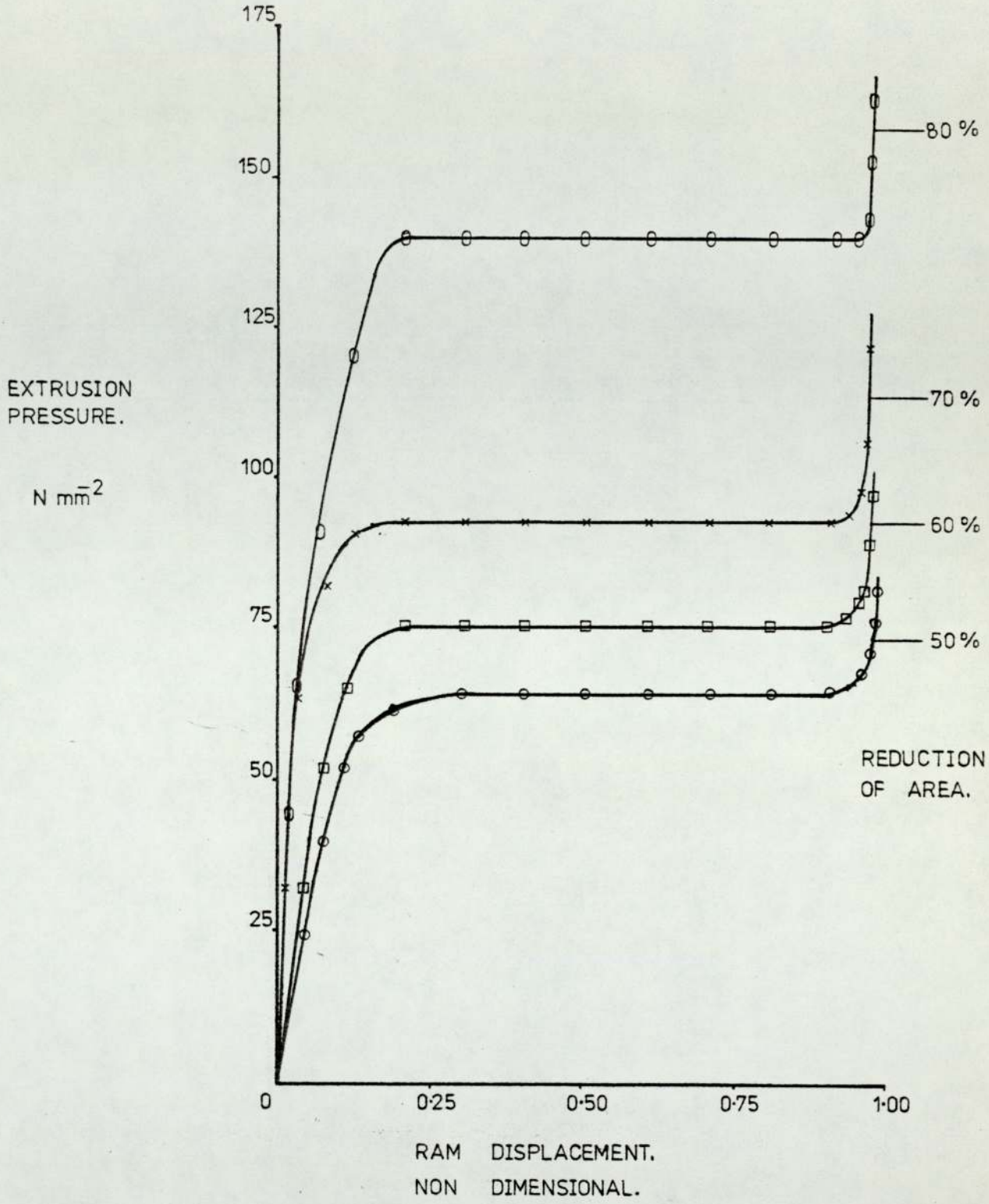

NOMINAL BILLET SIZE 12·5 mm DIAMETER
12·5 mm LENGTH.

GRAPH 5·1 SLOW SPEED EXTRUSION OF LEAD.–EXPERIMENTAL.

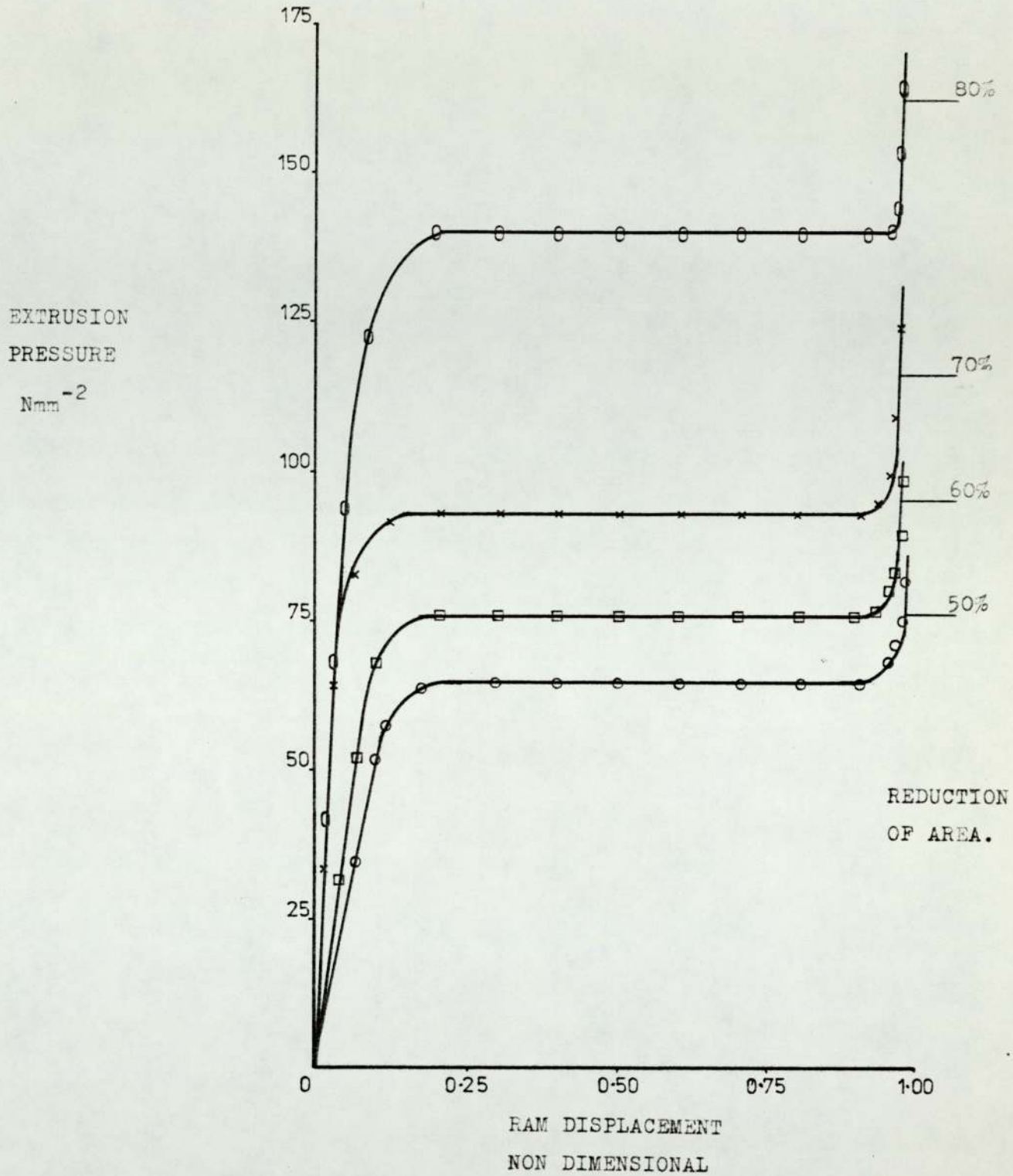

NOMINAL BILLET. SIZE. 12.5mm DIAMETER.
25.0mm LONG.

GRAPH 5.2. SLOW SPEED EXTRUSION OF LEAD.—EXPERIMENTAL.

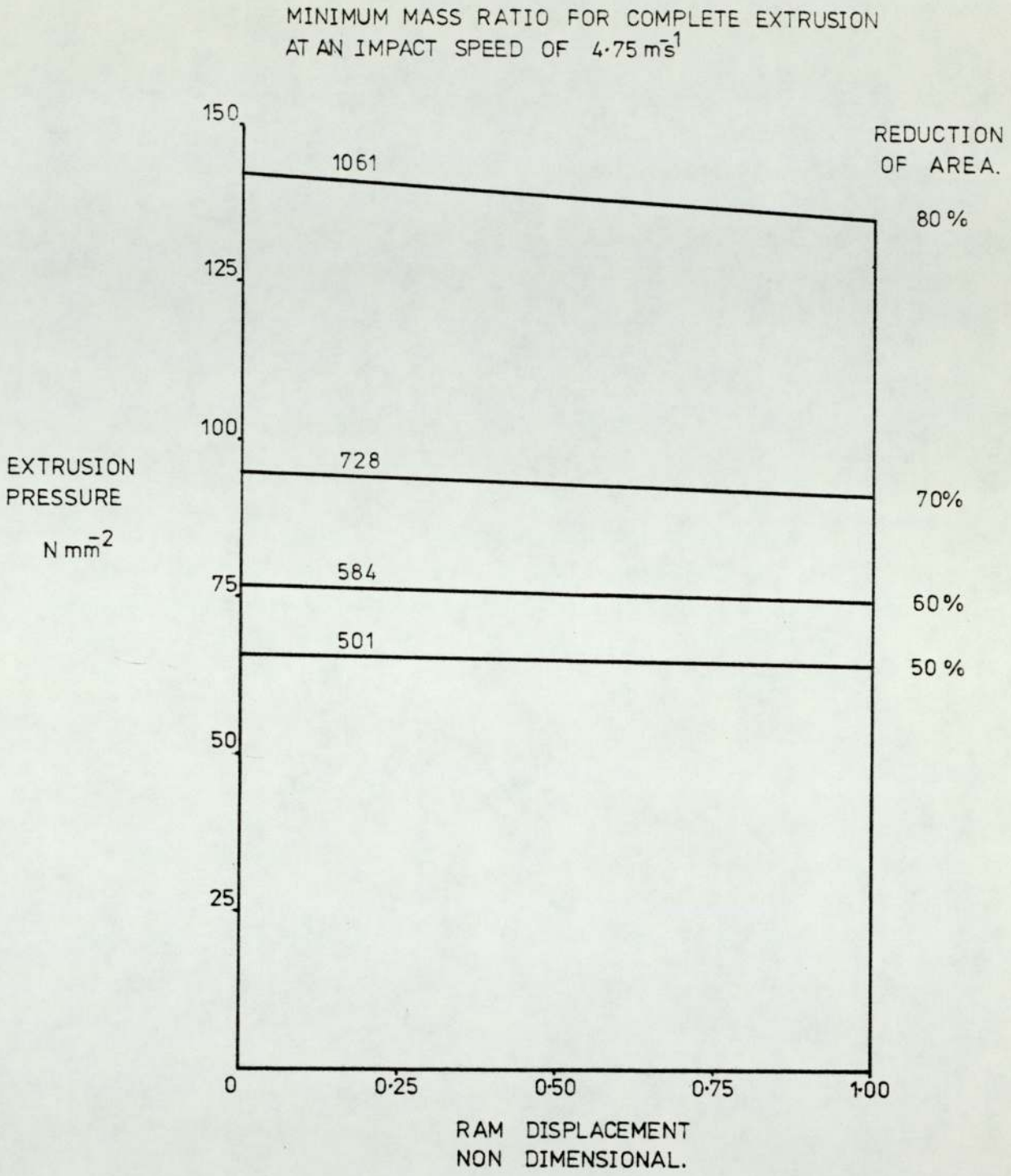

GRAPH. 5·3. EXTRUSION PRESSURE VERSUS RAM DISPLACEMENT FOR MINIMUM MASS RATIO OF IMPACTING MASS TO BILLET MASS.—THEORETICAL.

50 % REDUCTION OF AREA.

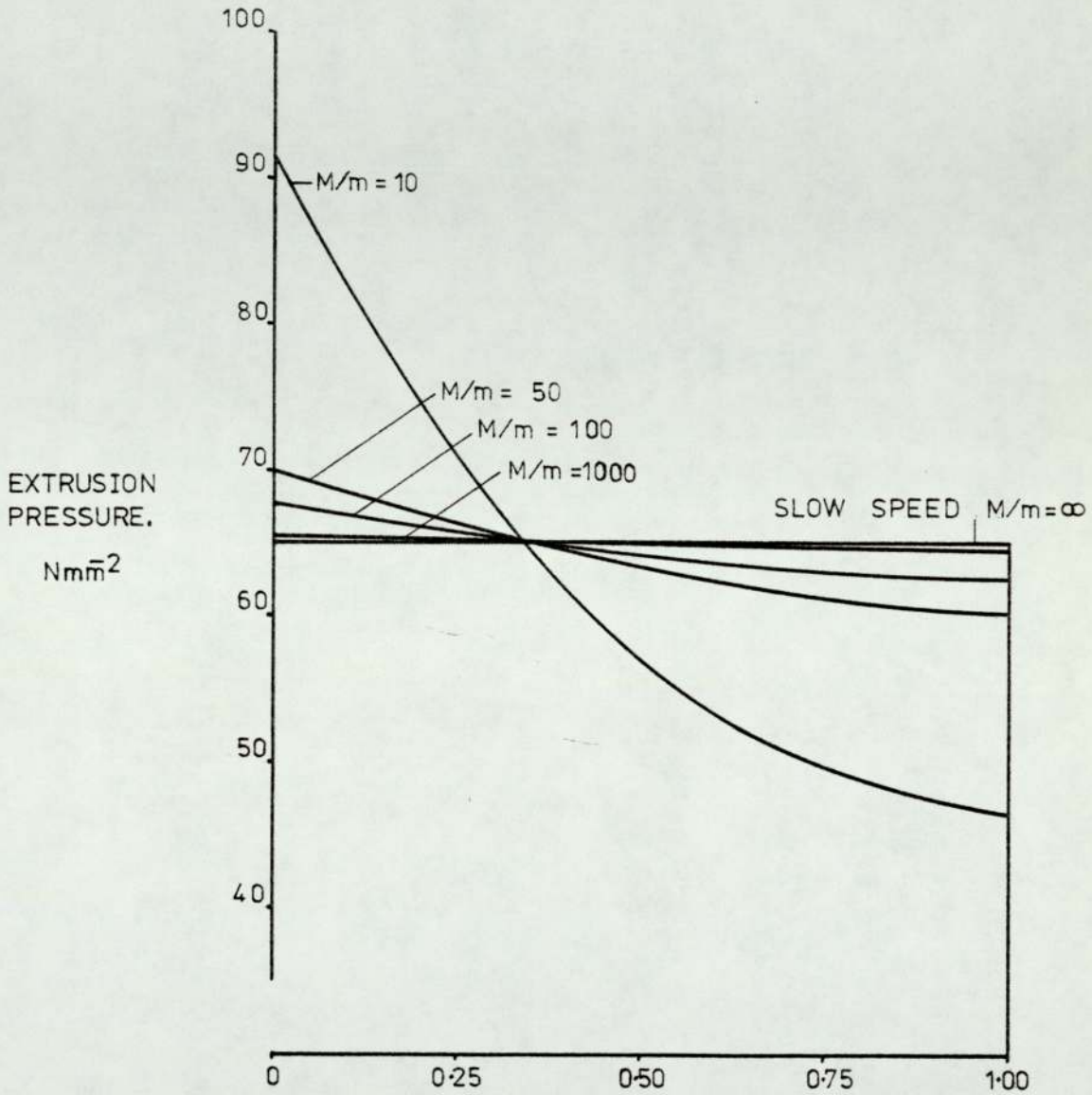

NOMINAL BILLET SIZE. 12·5 mm DIAMETER.
12·5 mm LONG.

BILLET MATERIAL.
LEAD.

GRAPH. 5·4. EXTRUSION PRESSURE VERSUS RAM DISPLACEMENT FOR VARIOUS MASS RATIOS OF IMPACTING MASS TO BILLET MASS, —THEORETICAL.

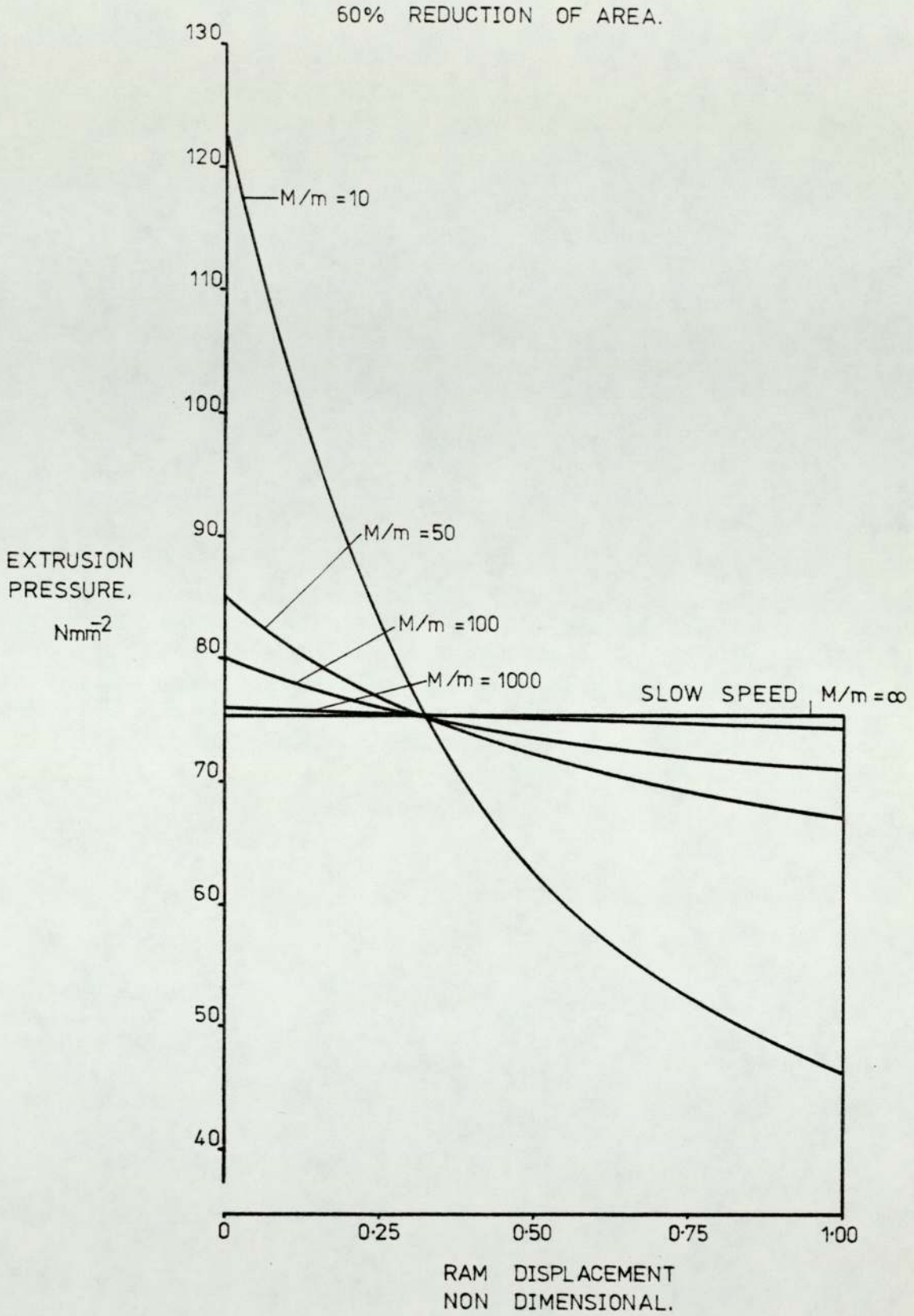

GRAPH. 5·5. EXTRUSION PRESSURE VERSUS RAM DISPLACEMENT FOR VARIOUS MASS RATIOS OF IMPACTING MASS TO BILLET MASS.—THEORETICAL.

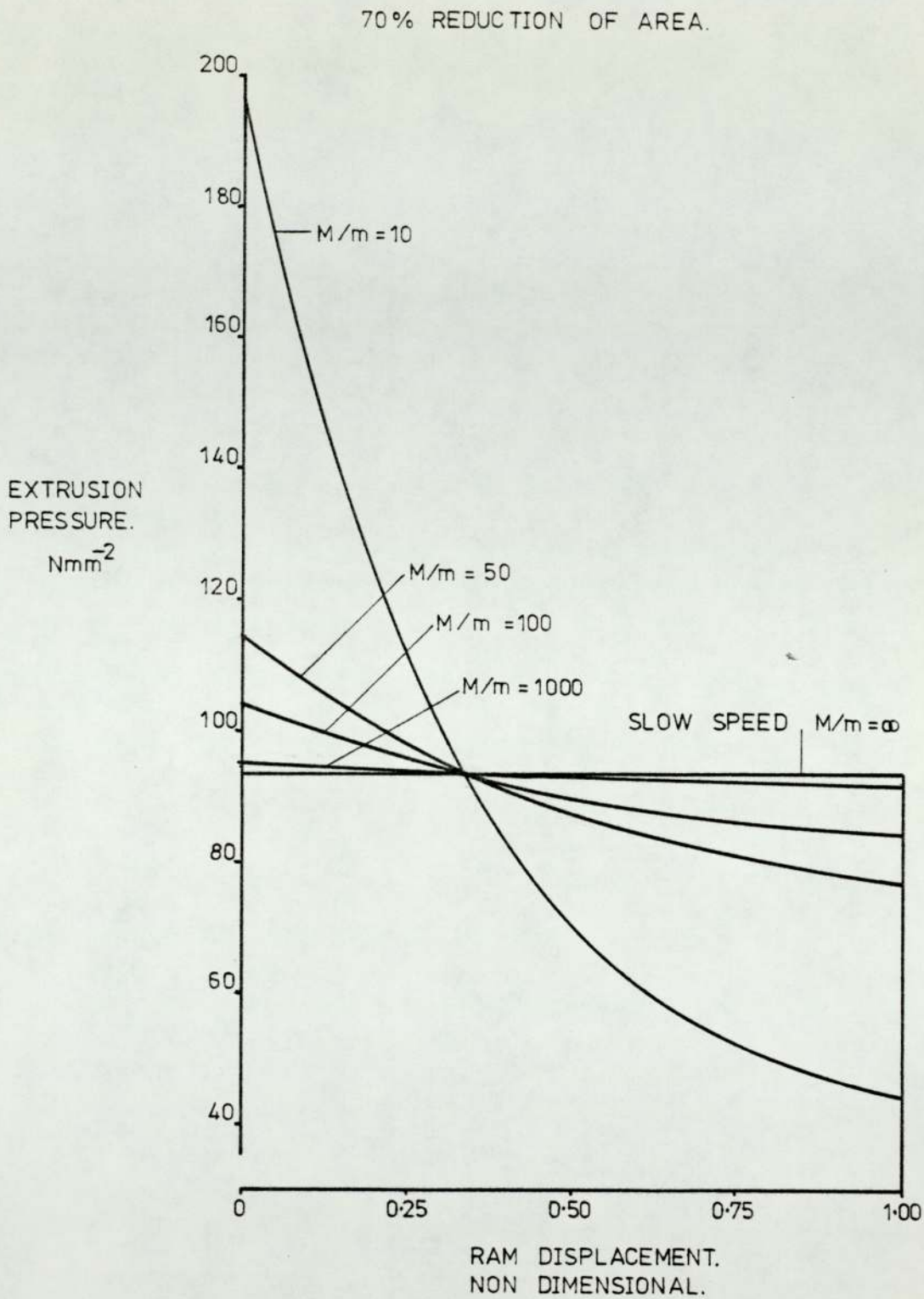

GRAPH. 5·6. EXTRUSION PRESSURE VERSUS RAM DISPLACEMENT FOR VARIOUS MASS RATIOS OF IMPACTING MASS TO BILLET MASS. - THEORETICAL.

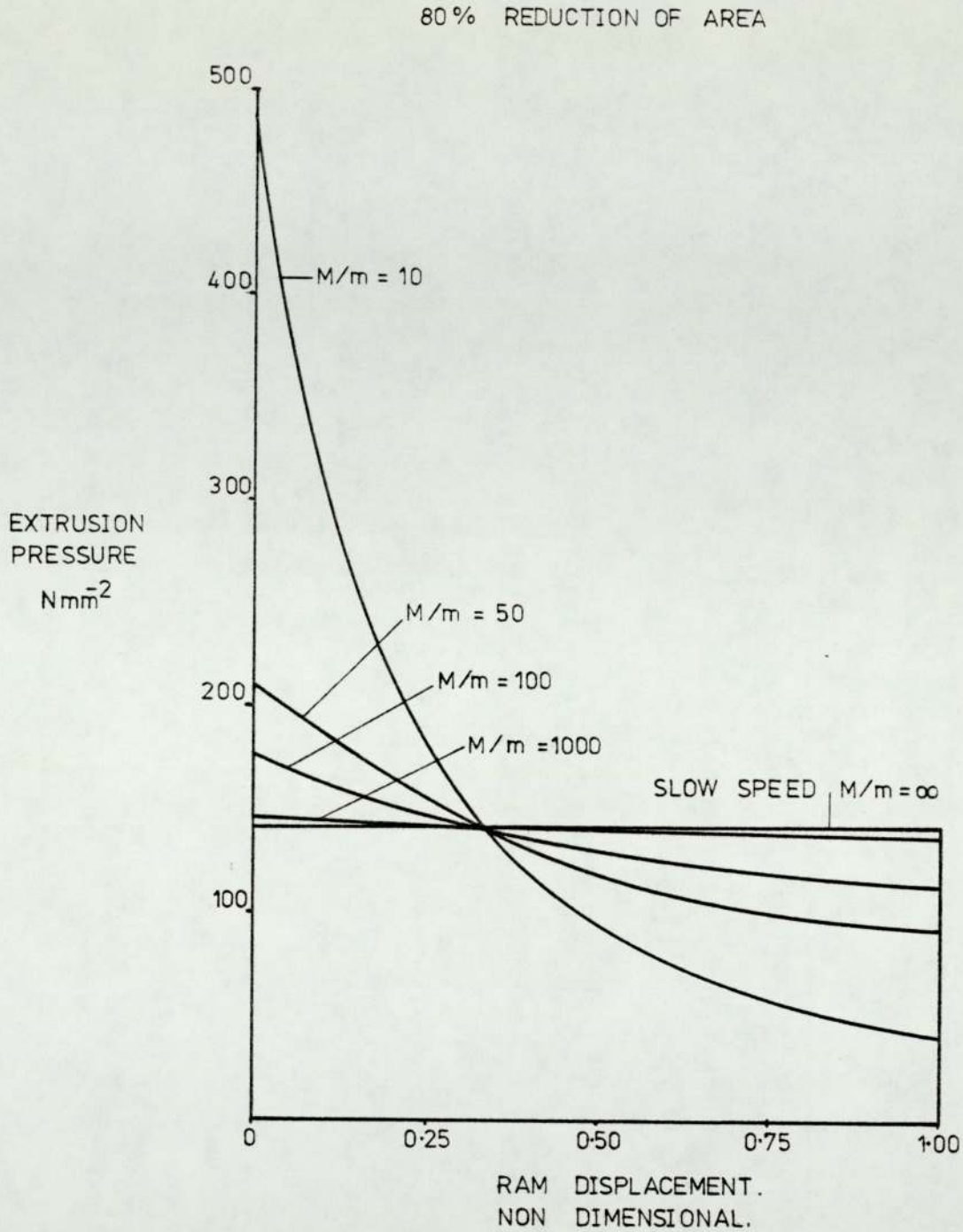

GRAPH. 5·7. EXTRUSION PRESSURE VERSUS RAM DISPLACEMENT FOR VARIOUS MASS RATIOS OF IMPACTING MASS TO BILLET MASS. – THEORETICAL.

50% REDUCTION OF AREA.

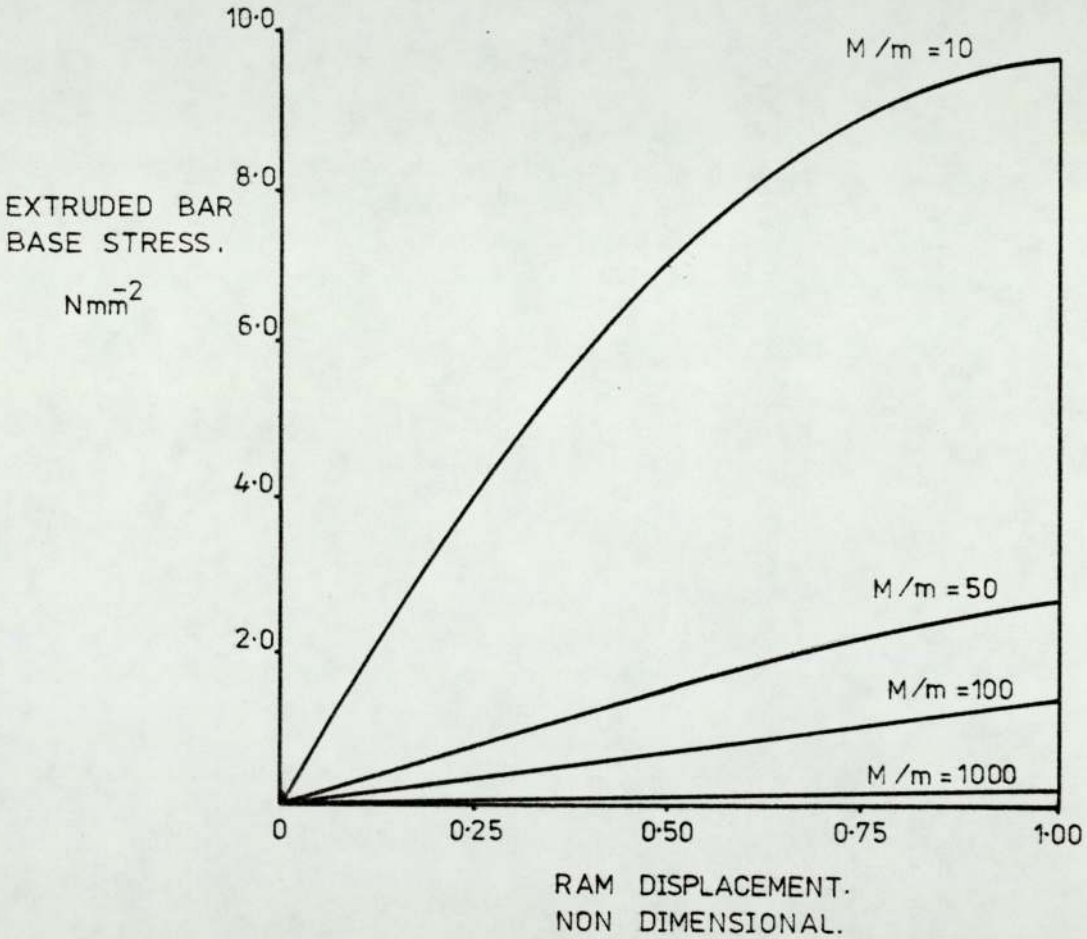

NOMINAL BILLET SIZE, 12·5 mm DIAMETER.
12·5 mm LONG.

BILLET MATERIAL.
LEAD

GRAPH. 5·8. EXTRUDED BAR BASE STRESS VERSUS RAM DISPLACEMENT FOR VARIOUS MASS RATIOS OF IMPACTING MASS TO BILLET MASS, — THEORETICAL.

60% REDUCTION OF AREA.

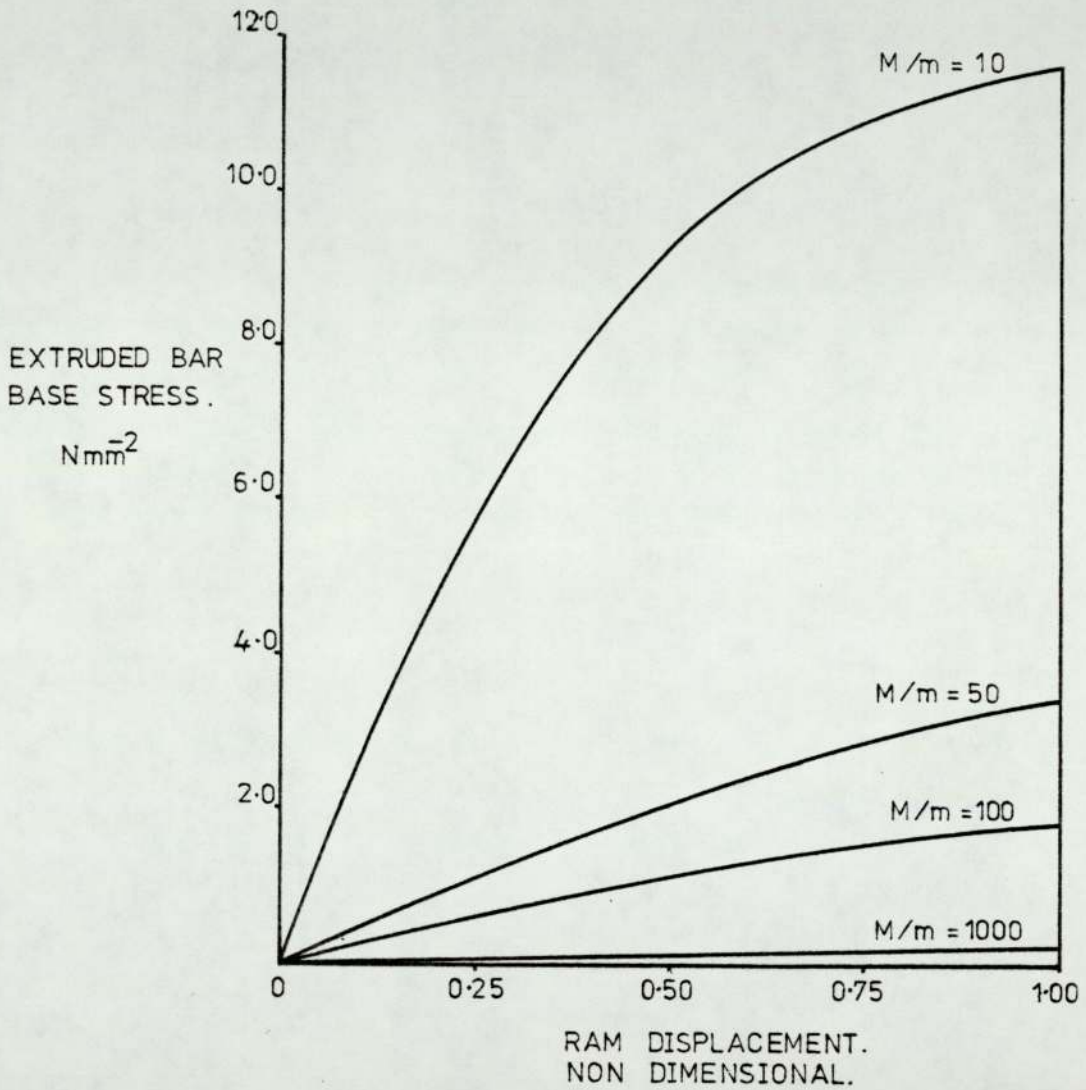

NOMINAL BILLET SIZE. 12·5 mm DIAMETER
12·5 mm LONG.

BILLET MATERIAL.
LEAD.

GRAPH. 5·9. EXTRUDED BAR BASE STRESS VERSUS RAM DISPLACEMENT FOR VARIOUS MASS RATIOS OF IMPACTING MASS TO BILLET MASS.— THEORETICAL.

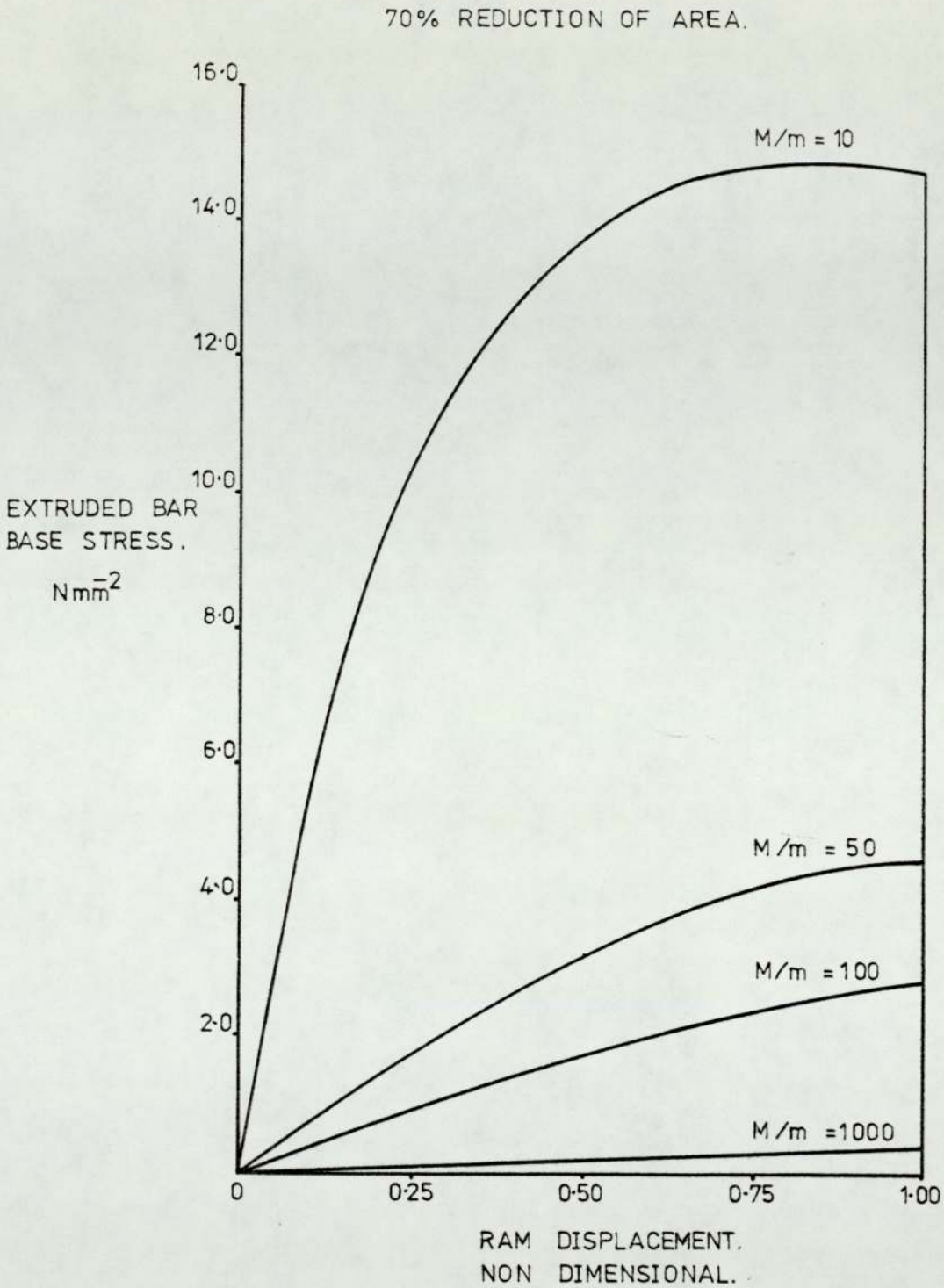

NOMINAL BILLET SIZE, 12·5 mm DIAMETER.
12·5 mm LONG.

BILLET MATERIAL.
LEAD.

GRAPH. 5·10. EXTRUDED BAR BASE STRESS VERSUS RAM DISPLACEMENT FOR VARIOUS MASS RATIOS OF IMPACTING MASS TO BILLET MASS.—THEORETICAL.

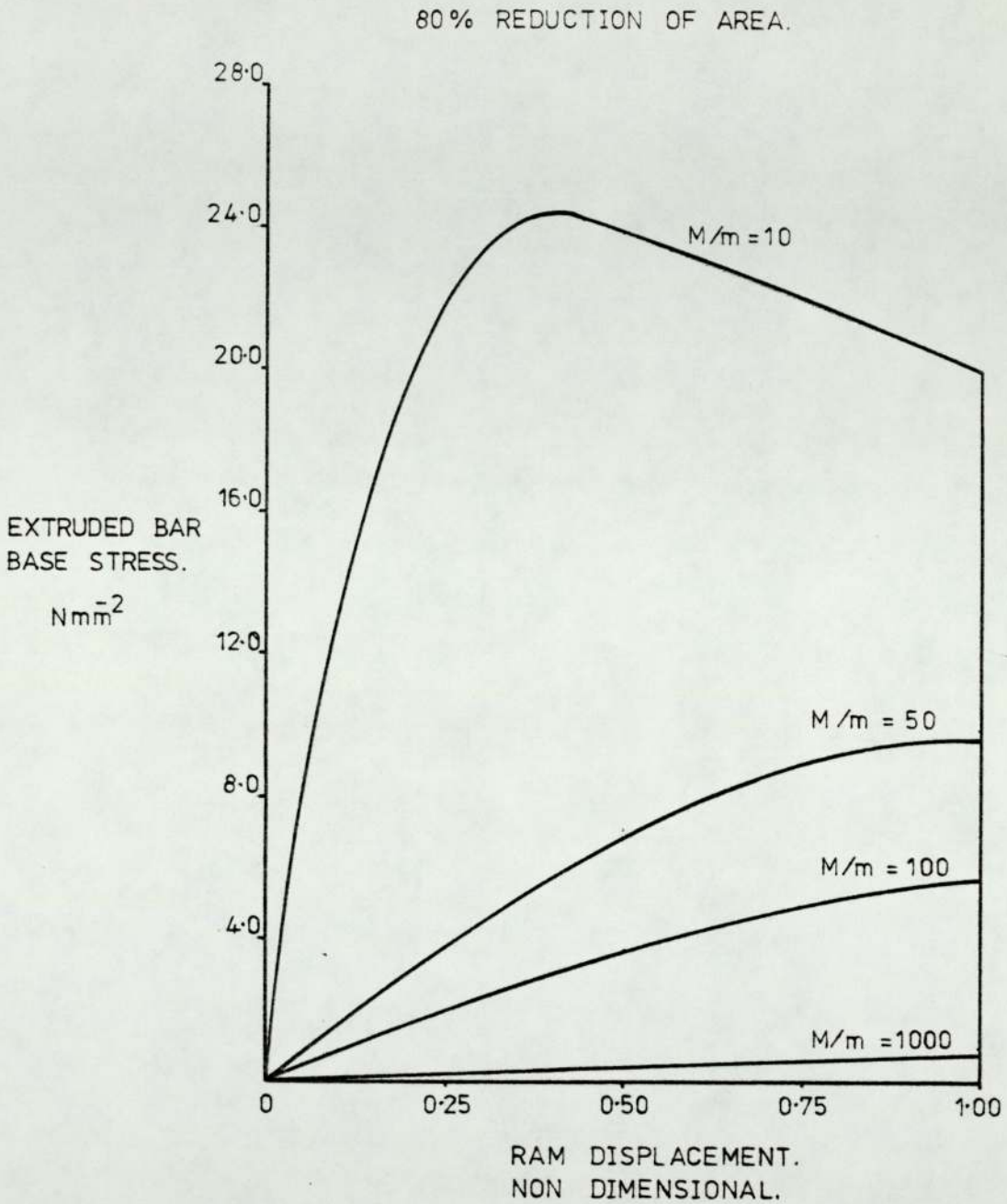

NOMINAL BILLET SIZE. 12·5 mm DIAMETER.
12·5 mm LONG.

BILLET MATERIAL.
LEAD.

GRAPH. 5·11. EXTRUDED BAR BASE STRESS VERSUS RAM DISPLACEMENT FOR VARIOUS MASS RATIOS OF IMPACTING MASS TO BILLET MASS.—THEORETICAL.

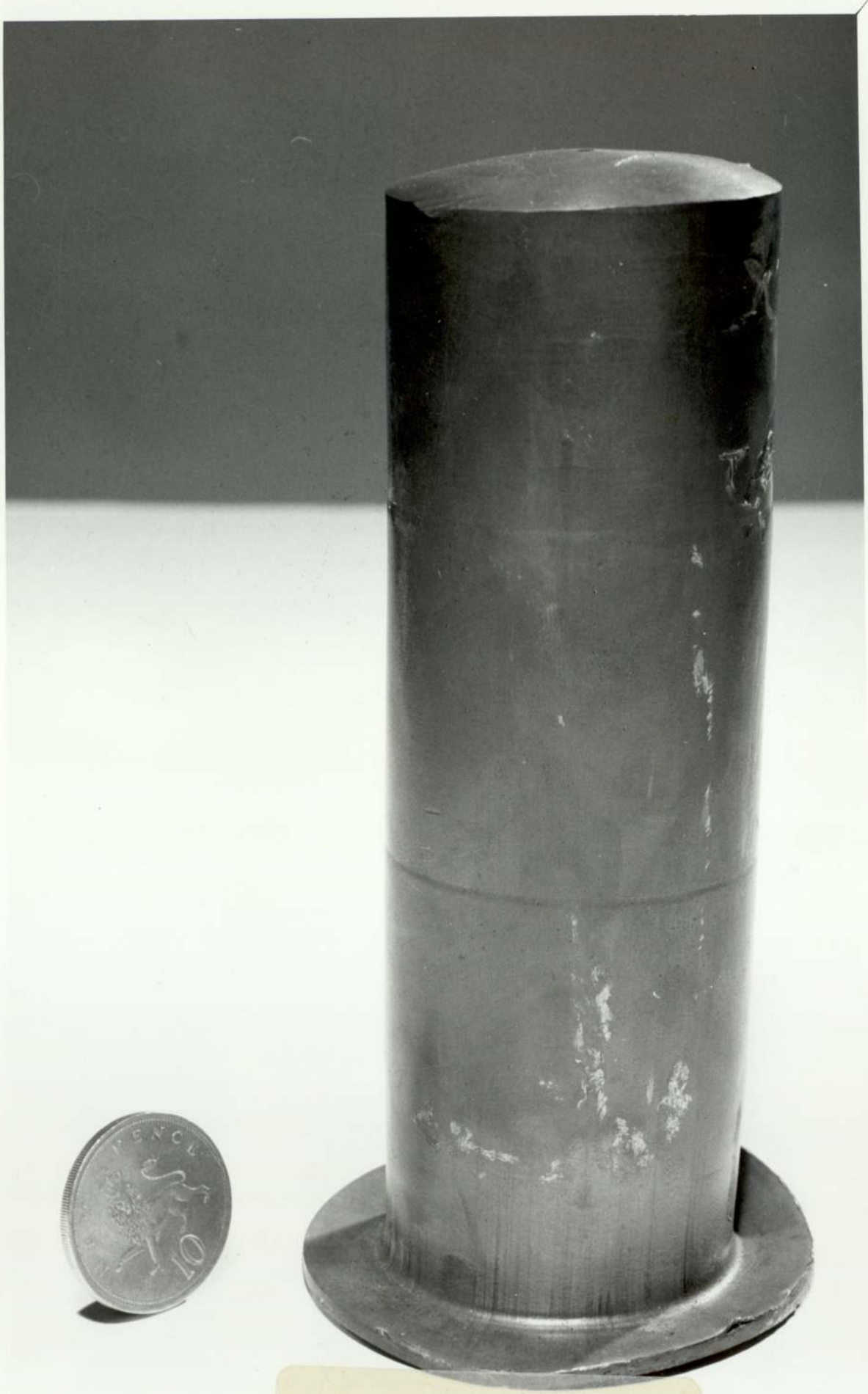

FIG. 5.3.
SLOW SPEED EXTRUSION OF LEAD,
75 mm DIAMETER, 75 mm LONG
BILLET- 50% REDUCTION OF AREA

FIG. 5.4.

IMPACT EXTRUSION OF LEAD - 75 mm DIAMETER, 75 mm LONG BILLET - REDUCTION OF AREA, TEST 1 to 6.

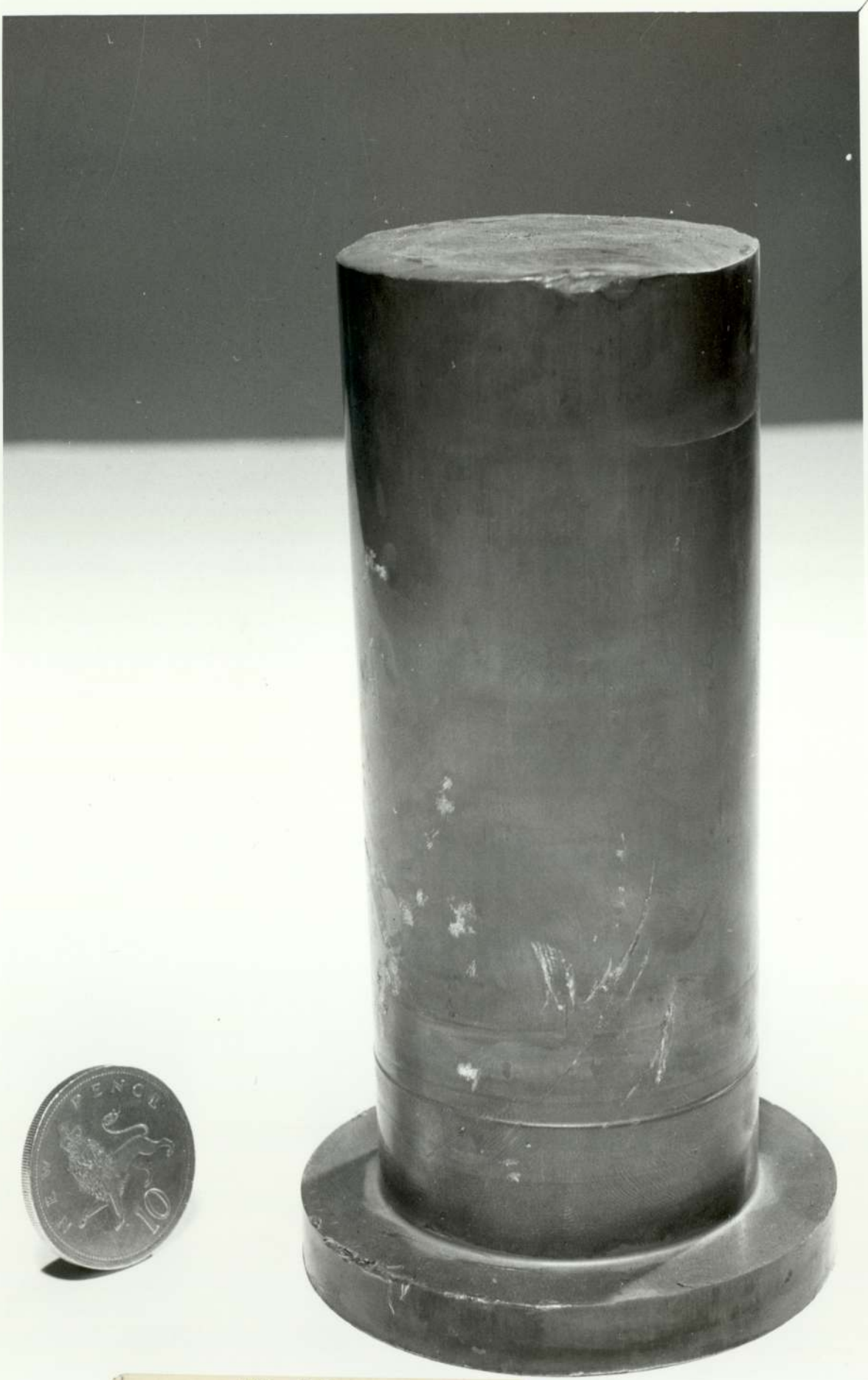

FIG. 5.5.
IMPACT EXTRUSION OF LEAD - 75 mm DIAMETER, 75 mm LONG BILLET - 50% REDUCTION OF AREA, TEST 7 to 15

FIG. 5.6.
IMPACT EXTRUSION OF LEAD - 75 mm DIAMETER, 75 mm LONG BILLET - 50% REDUCTION OF AREA, TEST 16 to 21

FIG. 5.7.

SLOW SPEED EXTRUSION OF LEAD - 12.5 mm DIAMETER, 12.5 mm LONG BILLET - 50% - 60% - 70% - 80% REDUCTION OF AREA.

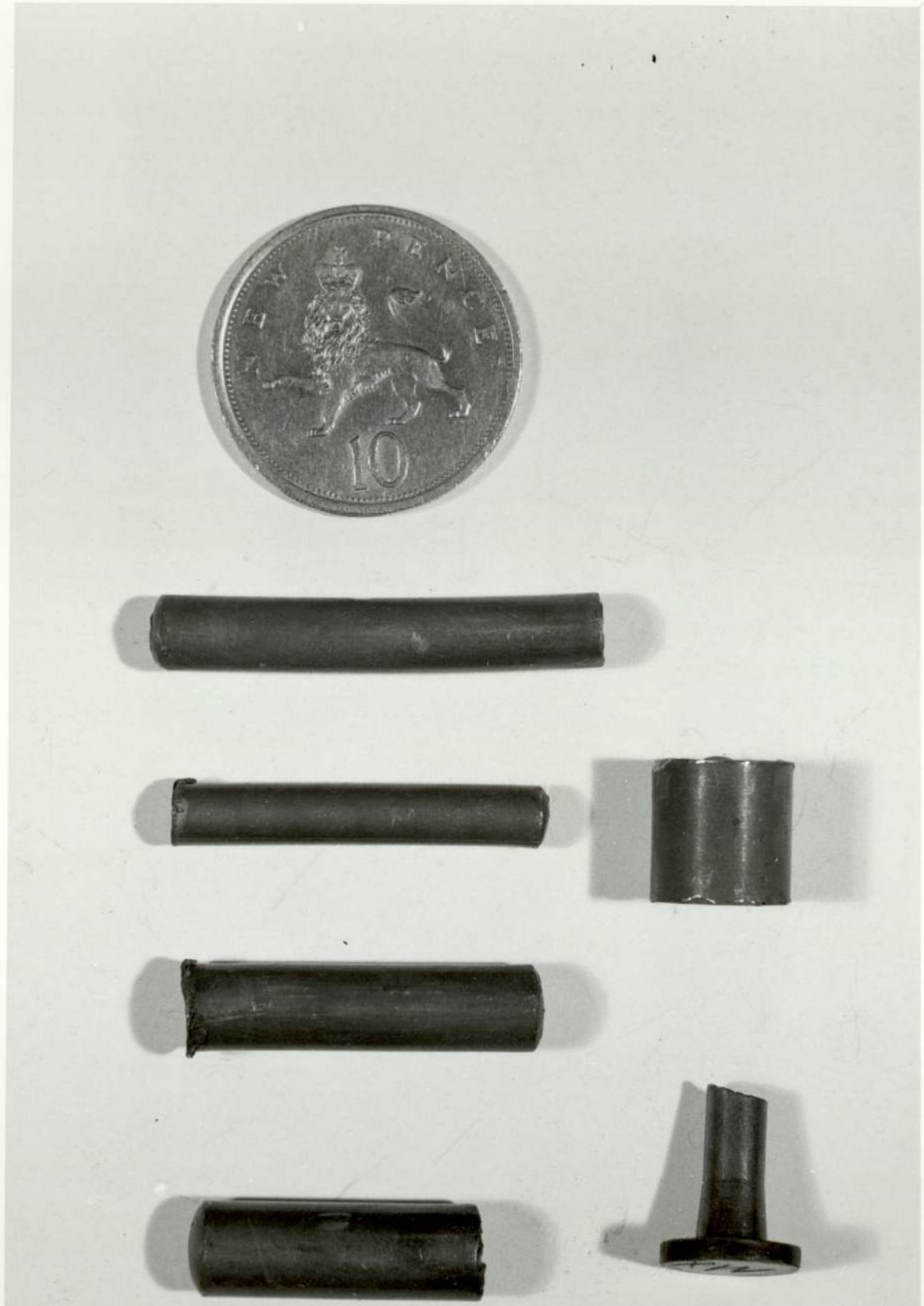

FIG. 5.8.
IMPACT EXTRUSION - 12.5 mm DIAMETER
12.5 mm LONG BILLET, 50% - 60% -
70% - 80% REDUCTION OF AREA, TESTS.

FIG. 5.9.
SLOW SPEED EXTRUSION OF POLY-PROPYLENE G.S.E. 20 - 70 mm DIAMETER, 75 mm LONG BILLET - 50% REDUCTION OF AREA.

CHAPTER SIX

DISCUSSION

6.1 The Rig

The fundamental design of the rig is correct, but the actual physical design of some components was not ideal for this application. There were two basic reasons for the short-comings in the component design; i) the cost of manufacture, ii) the time required for manufacture. The cost of components was controlled by the overall budget allowable for the building of the rig. The Apprentice School of Imperial Metal Industries helped in reducing costs, by manufacturing a considerable number of components and supplying them free of charge. Some time was saved by manufacturing some of the basic components in the University workshop and in the laboratory workshop. All the construction of the main frame, the guide tubes, the safety cage, and the lifting mechanism was carried out in the laboratory. Some delay in the manufacture of the dies, rams and containers occurred at Aston Services as they did not have the necessary capacity to heat treat and machine to the required tolerances. This necessitated the factoring out by Aston Services of some of this work to the appropriate specialists.

Following the extensive use of the rig, weaknesses have become apparent and these, with suggested improvements are now discussed. As the guide tubes were manufactured from mild steel, they were easily 'brinelled' by the ball bushings. This 'brinelling' was caused by a small amount of misalignment in the guide tubes. Very small hair like pieces of swarf were also produced by the action of the ball

bushings on the guide tubes. These hair like pieces of swarf quickly penetrated the ball tracks making theit motion sticky. This problem can be overcome in two ways; i) change the mild steel guide tubes for ones which have been hardened. This would be very expensive, as to obtain two straight and parallel tubes of this length would involve very careful heat treatment to avoid major distortion and a large amount of grinding to remove the small distortions, ii) change the ball bushings to roller bushings. These are similar to the ball bushings, in as much as they are recirculating shaped roller bearings, but they differ in only having one track per bearing. See Fig. 6.1. A crosshead using four roller bushings, two at each end set at 120^{o}, would have the same inherent directional stability as a crosshead using ball bushings. The roller bushings spread the load over a large surface of the guide tubes, thus the effect of brinelling would be reduced.

The electric motor, in the lifting mechanism, was a simple capacitor start motor, which normally is not reversible. A simple switching arrangement was constructed which would enable the motor to run in both directions. This was rated at 300W which should have been ample to operate the lifting mechanism. However, at full load the motor could not deliver enough power to operate the lifting mechanism. The main reason for this deficiency was the transmission loss in the reduction gearbox, but frictional losses in the pulleys and the stickiness of the ball bushings must also have contributed to the loss of power in the lifting mechanism. This meant that on a full load test the motor was helped by pulling on the rope before the rope drum.

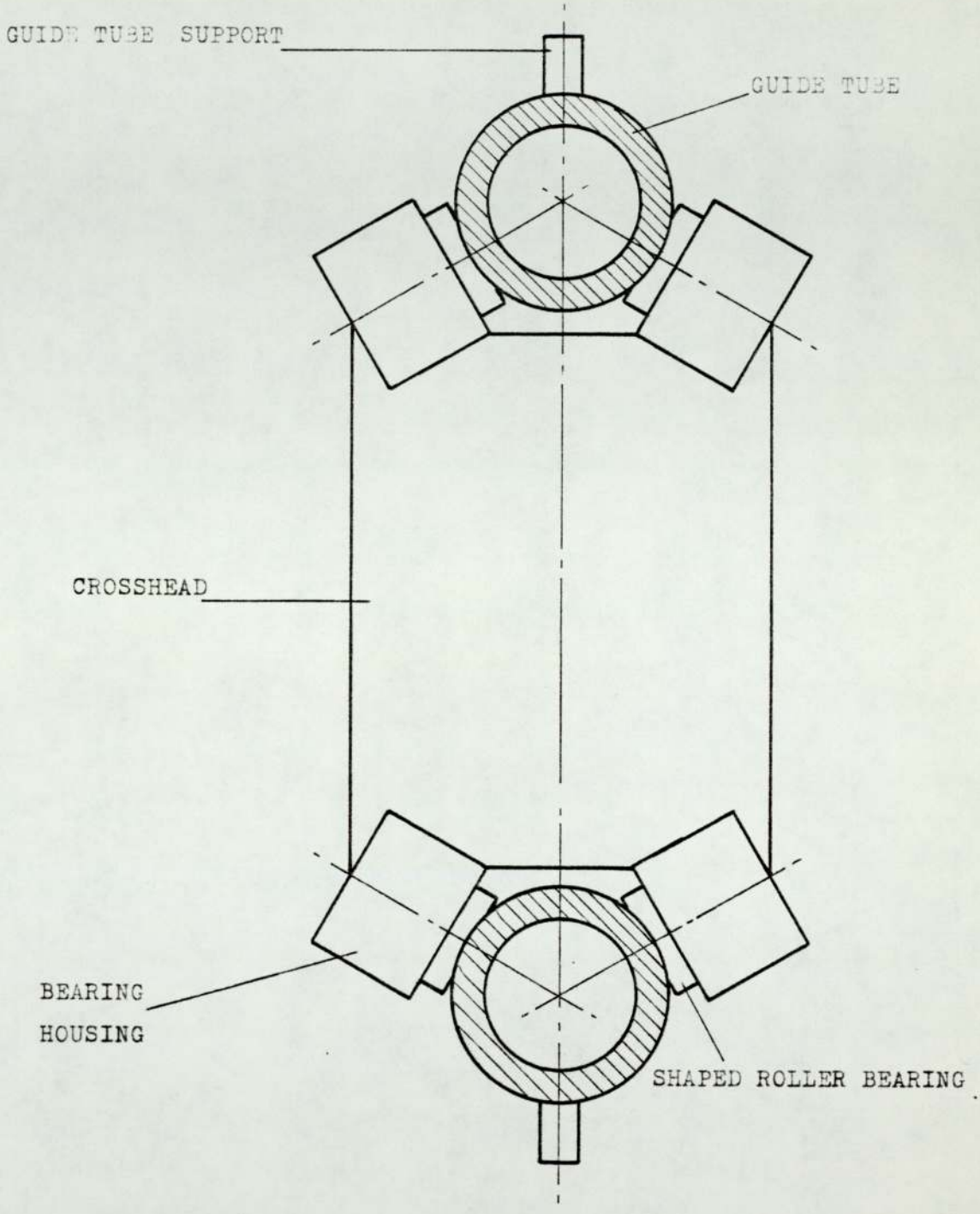

FIG. 6.1. POSSIBLE CONFIGURATION OF A GUIDANCE SYSTEM USING SHAPED ROLLER BEARINGS.

After the first extrusion test a major design fault in the die became apparent. Although the shape of the die was that which was required, it should have been made in two halves. If the die had been made in two halves it would, on removal from the container, have simply spearated from the product. The problem was how to separate the whole die from the product. The method finally adopted was to cut through the remaining portion of the billet and drive the product out of the die. This meant that all the products sustained some damage on extraction from the die. An unfortunate accident proved the suitability of using split dies. A container was dropped on to the 12.5 mm diameter, 60% reduction of area die which split into two halves; this die then worked perfectly as a split die. On removing this die from the container the two halves were easily removed by hand.

Most of the testing was carried out on the 12.5mm diameter series, which brought another problem to light. The wall thickness of the ram used was very small and hence very high stresses were produced in the ram. After only a small number of tests the ram failed and could not be used again. Due to the short amount of time remaining, a new ram could not be made in time. The only other ram available was for the 75 mm diameter series. A 50% reduction of area die was also available for this series, so a few tests on the 75 mm diameter series were carried out. The problem of the 12.5 mm diameter ram breaking were foreseen but could not be prevented. Indirect or reverse extrusion of bar from a small diameter billet is always a problem, as the cross sectional area of the ram is small. This produces very high stress in the ram which leads to failure.

The rest of the rig worked very well and produced no major problems.

6.2 The Instrumentation.

The instrumentation proved to be very difficult to operate in the prevailing conditions. All three areas, load measurement, displacement measurement and velocity measurement gave trouble.

The problem with the load measurement system was the load cells. The bottom load cell had no problems, but the insulation resistance of the top load cell failed frequently, after a few tests on maximum load. The load cell was completely rebuilt with new gauges, but every time the load cell broke down to earth after a few tests. An explanation is that the high transient elastic stress waves present in the top load cell caused the strain gauge backing to fail thus earthing the gauge. The order of magnitude of these elastic stress waves is 50 Nmm^{-2} in the top load cell and 20 Nmm^{-2} in the bottom load cell. The lower magnitude of elastic stress waves in the bottom load cell follows from the attenuation of the waves as they pass through the system during the extrusion process. The top load cell was completely rebuilt again and exchanged with the bottom load cell. After several tests the load cell on top of the extrusion (ex bottom load cell) broke down to earth. This load cell was rebuilt and used again, but after several more tests the load cell broke down to earth again. This suggests that the strain gauges used could not withstand the high values of elastic stress on impact in the top load cell; both load cells worked satisfactorily in the bottom position, where the magnitude of the elastic stress waves were less than half of those in the top load cell. The remainder of the tests were carried out with the

top load cell disconnected.

The problems with the displacement measurement system proved to be insolu ble in the time available. The problem lay with the displacement transducer used. The R.D.P. Electronics transducer type DC LVDT was used successfully on a previous project, but the traces obtained from this transducer were obliterated with noise. The transducer was calibrated at slow speeds, but as soon as the transducer shaft was moved at high speeds the output signal was lost in noise. The cause of this excess noise appeared to arise from the internal demodulator, but this could not be checked as the unit is completely sealed. A low pass filter was included, but the results obtained were useless as the resulting response time was too slow. For example, as the recording was made by a single sweep across the paper, the sweep had almost finished before the displacement trace started to move. The Penny and Giles transducer type LPIB/85 was substituted without success. This type of transducer consisted of a resistive coil and a wiper. At slow speeds the transducer worked very well, but at high speeds the contact noise produced by the wiper obliterated the signal. The displacement of the ram could not be recorded with the load trace as no suitable transducer was available. The displacement of the ram was measured using a dial test indicator before and after a test. The displacement was assumed to vary lineraly from zero to the final value over the length of the load trace.

The problem with the velocity measurement system was only a minor one. Some of the shock of impact of the extrusion system was transferred into the main frame. This shock produced a series of faults in the electronic timing gear. The most common fault was

that the filaments in the light bulbs disintegrated. Some twenty to twenty five light bulbs were used during the tests. Two other faults that occurred less frequently were the unscrewing of either the light bulbs or the light activated switches and the breaking of the connecting wires. Each time a fault occurred, no time for the falling mass was recorded and the results from that test were ignored. To prevent this type of fault recurring the system could be mounted on resilient mounts. To avoid delay this was not carried out as no suitable resilient mounts were readily available and the cost of purchasing commercial mounts was too high.

The Medelec recording oscilloscope produced clear traces with very little trace loss due to internal triggering. The portion of the trace that was lost was assumed to be a straight line. This was projected back to the base line to give a starting point for the trace.

The strain gauge conditioning amplifier gave no problems throughout the tests, it only required re-zeroing each day. This was not really necessary so long as the trace was set to the base line before each test which was easily carried out using the Y shift on the Medelec.

During the testing period all the instruments were left on all the time, thus the instruments were always ready and no warm-up period was necessary to stabilise any of the instruments.

6.3 Experimental Slow Speed Extrusion Tests of Lead.

Two sets of slow speed extrusion tests were carried out using the same die, ram and container set that was used for the impact extrusion tests on the 12.5 mm diameter series. Each set used a common billet size and four different reductions of area, 50%, 60%, 70% and 80%. The results were plotted on graphs of extrusion pressure versus non-dimensional ram positions for each billet size. The shape of the traces was as expected for indirect bar extrusion; that is, three distinct portions. In the first portion the extrusion pressure quickly rose from zero to the steady state extrusion pressure, for very little ram displacement. This corresponds to the elastic compression in length of the billet and the diametral expansion to completely fill the container. The second portion was the steady state extrusion phase, that is, the extrusion pressure remained constant. This phase continued until the length of billet left in the container was 8 - 10% of the diameter. This was the start of the third portion, i.e., the coining phase during which the extrusion pressure increased very rapidly for little more ram displacement.

When the billets and products were removed from the container a defect in the form of a funnel was seen in the remaining portion of the billet. The cause of this defect can be easily explained when flow of the lead in the container and through the die is considered, i.e., during the steady state, the flow of the billet through the centre of the die is more rapid than that along the sides. In a small region bounded by the die, the container wall and the funnel shaped surface, no flow takes place. See Fig. 6.2. Along this

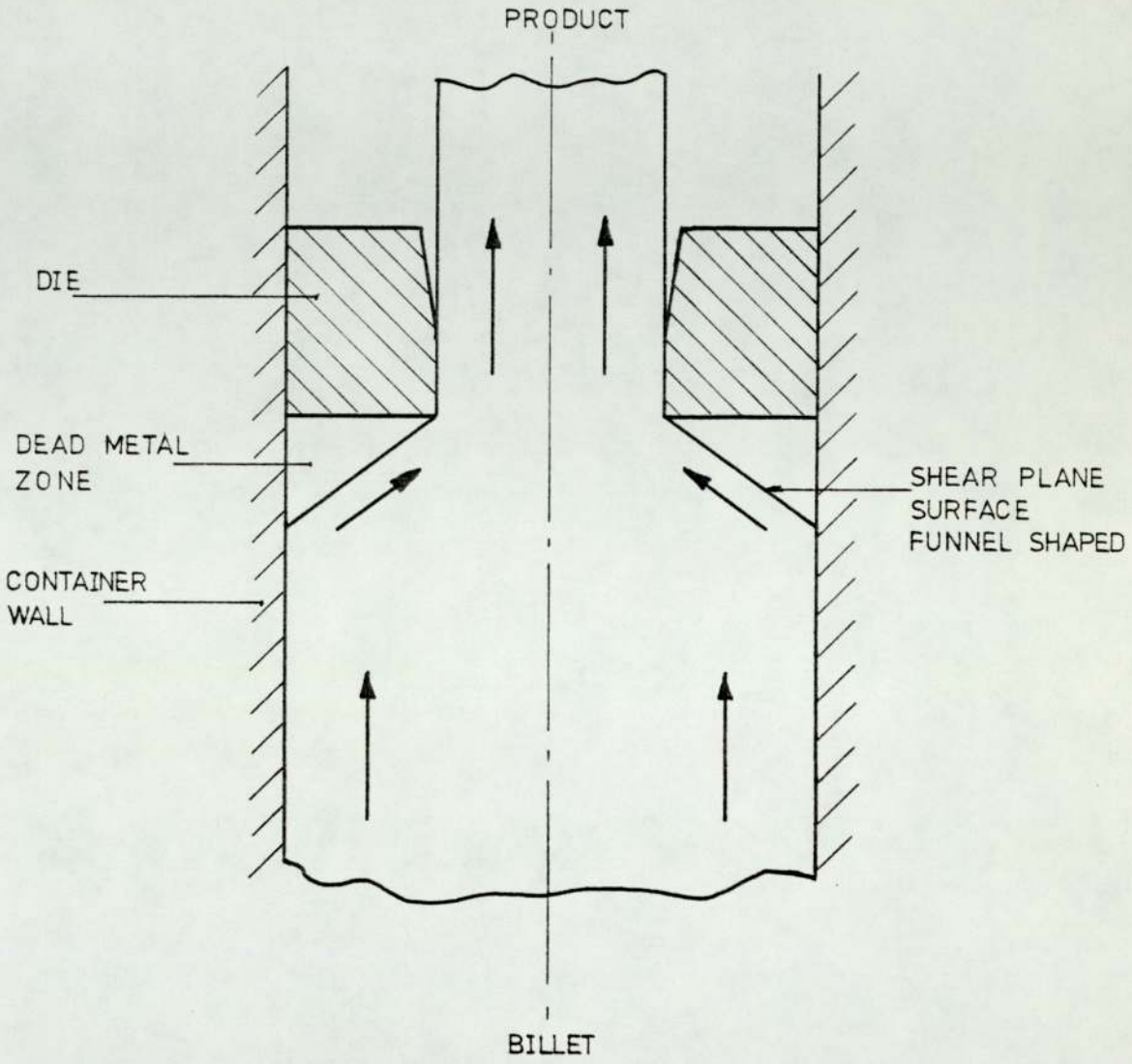

FIG. 6·2. EXTRUSION THROUGH SQUARE DIES SHOWING THE FUNNEL SHAPED SHEAR PLANE SURFACE AND THE DEAD METAL ZONE

funnel shaped surface the distortion of the lead is large. As the outer parts of the billet reach this surface, they are first of all compressed and then pass diagonally with heavy shearing into the die to form the outer part of the extruded bar. The general effect, therefore, is that whereas the centrally-lying elements undergo a minimum of deformation by pure elongation which corresponds to the actual change in cross sections between the billet and the bar, the outer elements have experienced much additional deformation and are stretched out along the sides of the rod. As the deformation zone approaches the rear end of the billet, the rapid inflow directly behind the die aperture creates a tendency for a hollow cavity to be formed in the middle of the base. This happens when the billet has been reduced to a disc of thickness about one - quarter of it's diameter. The funnel increases if the extrusion is pressed to the limit.

6.4 Impact Extrusion Tests of Lead.

The impact extrusion tests on the 75 mm dia billets produced some U.V.traces clearly showing the elastic stress waves present during the impact. The difference in magnitude between the elastic stress waves in the top load cell and the bottom load cell are easily seen. The period between two consecutive peaks on the traces corresponds to the time taken for an elastic stress wave to travel from the measuring point, down through the extrusion system, be reflected back by the base block, pass up through the extrusion system, be reflected by the impacting mass and back to the measuring point. The slight time delay in the starting of the bottom load cell after the top load cell also corresponds to the passage of the elastic stress wave between the two load cells.

The energy absorbed by the extrusion was calculated by measuring the area under the pressure versus ram displacement graph and applying the appropriate scale factors. The energy absorbed by the extrusion was calculated for both top and bottom load cell traces, which were almost identical. An average extrusion pressure was calculated by dividing the absorbed energy by the ram displacement and the cross sectional area of the container bore.

The extrusion defect of a cavity in the rear of the billet,(i.e. back-end piping) was also apparent in the impact extrusion tests. The effects of the cavity on the results obtained from the 75 mm diameter billets were ignored as several tests were carried out on one billet before any sign of the pipe appeared. The cavity will have some effect on the traces obtained from the 12.5 mm diameter billets, as most of these were extruded completely with one impact.

The energy available at impact for the 12.5 mm diameter billets was always in excess of that needed for complete extrusion. This corresponds in most cases to the sudden increase in extrusion pressure at the end of the trace as the ram bottomed on the container base. The difference between the energy available at impact from the energy absorbed by the estrusion is the energy lost due to re-bounds, friction between the ram and container and the energy of propagation of the elastic stress waves.

6.5 Theoretical Predictions.

The theory in Appendix A was used to predict the value of the extrusion pressure for the impact tests. The value of K, the process efficiency factor was calculated from the results of the slow speed

extrusion tests. The variation of extrusion pressures with ram displacement is virtually a horizontal line, numerically equal to the slow speed extrusion pressure. This was expected as the mass of the billet was very small when compared with the total moving or driving mass. The ratios were 904, 1232 and 1807 for the 12.5 mm diameter tests. The ratios for the 75 mm diameter tests were small by comparison being, 28.9 and 31.6, but only a small portion of the billet was extruded. The ratios of total moving mass to the actual mass extruded were 550, 690 and 1050, which were of the same order as for the 12.5 mm diameter tests.

The total moving mass required for complete extrusion was calculated using the velocity calculated from the actual extrusion tests. This mass with the actual velocity gave the theroretical energy available at impact, which equalled the energy necessary for complete extrusion.

Some theoretical graphs were plotted showing the variation of extrusion pressure with ram displacement at various mass ratios for constant reductions of area. These showed that as the mass ratio was reduced the initial extrusion pressure increased above the slow speed extrusion pressure, but fell during the extrusion to a load well below the slow speed level.

Theoretical graphs 5·8 - 5·11 showing the variation of product base stress with ram displacement at various mass ratios for constant reduction of area, showed increasing values of base stress for decreasing mass ratios until necking and failure occurred.

The process of high speed impact extrusion was subject to certain simplifying assumptions, to ease the analysis. The main sources of error are i) the neglect of friction, ii) the neglect of the elastic stress waves present, and iii) any strain rate effects.

6.6 Comparison of Theoretical and Experimental Results.

The energy available for extrusion in the 12.5 mm diameter tests usually exceeded the energy necessary for complete extrusion, thus, for this size of billet, the percentage of energy absorbed to energy available is not a meaningful factor. The energy absorbed always, except for one case, exceeded the predicted energy necessary for complete extrusion. The actual extrusion pressure exceeded the theoretical extrusion pressures by a maximum of 50%, average 18%. The actual extrusion pressures were higher than those predicted as the theory does not take into account, i) any friction between the ram and the container, ii) any strain rate effects, iii) the effect of elastic stress waves, and iv) any redundant work. Plastic stress waves may have had some effect on the extrusion pressures.

A detailed comparison of theoretical predictions and experimental results cannot be made as the number of tests performed was too small to allow conclusions of value to be drawn. The theory appears to underestimate the forces, but be of the right order of magnitude.

6.7 Extrusion of Polypropylene G.S.E.20.

The extrusion of polypropylene G.S.E.20 proved to be virtually impossible on the impact test rig. Several attempts were made on 75 mm diameter billets at 50% reduction of area. The impacting mass of 110 kg was dropped from the full height of the rig, which gave it an impact speed of 7.2 ms^{-1}. The resultant speed of the impacting mass and ram was 6.69 ms^{-1} with the available energy for extrusion of 2659.6 Nm. The impacting mass on striking the extrusion, bounced back up the rig to about one third of it's original height, followed by several diminishing rebounds. When the billet was removed from the container, the die had penetrated the billet by 0.25 mm. The polypropylene billet had acted like a very stiff spring, where most of the energy of impact was stored in the billet by elastic compression and released after the impact to propel the mass back up the rig. No actual values of the forces involved were recorded as both the load cells were overloaded, although no actual damage occurred to the load cells. An estimate of the forces involved can be made by estimating the elastic compression of the polypropylene billet. The billet was initially a tight fit in the bore of the container, that is, there was little radial expansion, so assuming no change in volume, the elastic compression would most likely be about 1 or 2 mm. The forces generated in the billet would be 1.33×10^6 to 2.66×10^6N. An attempt was made to extrude a similar polypropylene billet on the slow speed hydraulic press using the same system on container, ram and die. At the maximum load developed by the hydraulic press of 100 tons (0.99×10^6N) extrusion of the billet started. The extrusion of the billet was very slow, taking some 10 minutes for a ram displacement of 2 mm. On removing the polypropylene billet from the container and die, the surface of the

extruded product showed signs of being highly sheared, with thin pieces loosely attached to the surface. On the unextruded portion of the billet, a circumferential line about 15 mm from the die face was seen. This would be the outer edge of the funnel surface of the dead metal zone as shown in Fig. 6.2.

The behaviour of polypropylene in the extrusion tests was a little surprising but not altogether unexpected, for its behaviour in the uniaxial compression was different from that of metals. From observations of the uniaxial compression test and from the plotted results, the following picture of its behaviour is formed. When the polypropylene is compressed it quickly assumes a barrel shape. It has a very well defined elastic stress - strain relationship up to about 5% compression when yielding starts. The yield stress increases to a maximum at 20% compression and then decreases uniformly. At about 40% compression, small internal ruptures were seen in the polypropylene billet. These ruptures grew in size throughout the test with new ruptures continuing to form. From about 65% compression the yield stress increased uniformly for the rest of the test. It appears that these internal ruptures caused the reduction in yield stress. This still does not explain why the polypropylene is so difficult to extrude. Taking into account its unusual stress - strain behaviour, extrusion on the slow speed hydraulic press was expected with the product to be full of internal ruptures with visible surface tears.

Since no information was available on the cold extrusion of polypropylene, theoretical predictions of the extrusion pressure was estimated from $w = KY\ln r$, where K is a measure of the process

efficiency and is dependent on the die geometry, friction, redundant work and strain rate. The extrusion pressure is numerically equal to the energy absorbed per unit volume of the billet, w. The value of K found from the extrusion of lead was used in the prediction of the extrusion pressure for polypropylene, K = 3.54 for 50% reduction of area. The extimated extrusion pressure of polypropylene was 98.2 N mm^{-2} using a yield stress of 40 Nmm^{-2}. The actual extrusion pressure obtained from the slow speed test was 226 Nmm^{-2}. Clearly polypropylene does not behave as lead or other metals.

CHAPTER 7

CONCLUSIONS

1) The theory in its present form, appears to underestimate the magnitude of the extrusion pressure and the amount of energy necessary for complete extrusion.

2) The guidance of the falling mass was not suitable for the high loads generated at impact. The bearing area was too small.

3) The capacity of the rig, i.e. the energy available at impact, was not large enough to carry out extrusion tests on lead with a billet diameter of 75 mm. In further work smaller diameter billets should be used.

4) The loadcell design - which depend on resistive strain gauges bonded on to the loadcell - was not capable of withstanding high transient elastic stress waves.

5) The falling mass measurement system was not accurate enough to give reasonable estimates of the acceleration of the falling mass.

6) For comparison of energy available to energy absorbed to be meaningful, the energy available must be less than the energy necessary for complete extrusion.

7) The extrusion pressures measured in the loadcells above and below the billet are almost the same. The difference between the readings was the pressure of high transient elastic stress waves before the extrusion.

8) The cold extrusion of Polypropylene G.S.E.20 was not possible on this test rig.

CHAPTER 8

SUGGESTIONS FOR FURTHER WORK.

1) Modifications to the Rig.

a) Change the falling mass guidance system to one which will spread the loads of impact over a larger area. Recirculating roller bearings would give a larger area of contact and reduce the amount of "brinelling".

b) A larger capacity electric motor is required for the hoist mechanism, especially if the capacity of the rig is increased.

c) Increase the velocity of the falling mass, which will give more energy available at impact for the same mass. Possible to utilize compressed springs or a compressed air gun on top of the rig to give the mass some initial acceleration. (Alternatively use smaller billets).

2) Modification of the Extrusion System.

a) The extrusion dies should be of the split type, i.e., in two halves along the extrusion axis.

b) The extrusion method, especially for the smaller billet diameters at low extrusion ratios, should be direct. This would enable a solid ram to be used, thus reducing the stress in the ram and preventing failure.

3) Theory.

The use of the Upper Bound Theorem using an incremental finite element computer program, together with a complete revision of the assumptions made, would be the next step in finding a compatible theory.

REFERENCES

1. WISTREICH, J.G., Investigation of the mechanics of wire drawing. Proc. Inst. mech. Engers 169, 643, (1955).
2. WISTREICH, J.G., Back-pull wire drawing. J.Iron Steel Inst. 417, (1947).
3. WISTREICH, J.G., The fundamentals of wire drawing. Met. Rev.2 (10), (1958).
4. SHIELD, R.T., Plastic flow in a converging conical channel, J.Mech. Phys. Solids 3, 246, (1954-55).
5. AVITZUR, B., Analysis of wire drawing and extrusion. Proc. A.S.M.E. paper 62 - Prod. 4, (1963).
6. AVITZUR, B., Analysis of wire drawing and extrusion through conical dies of large cone angle. Proc. A.S.M.E. paper 63-WA-1, (1964).
7. AVITZUR. B., Analysis of central,bursting defects in extrusion and wire drawing. Proc. A.S.M.E. paper 67 - Prod. 5, (1967).
8. JOHNSON, R.W., and ROWE, G.W., Redundant work in drawing cylindrical stock. J.Inst. Met. 96, 97, (1968).
9. CADDELL, R.M., and ATKINS, A.G., The influence of redundant work when drawing rods through conical dies. Proc. A.S.M.E. paper 67 - WA/Prod. 11, (1967).
10. ATKINS, A.G., and CADDELL, R.M., The incorporation of work-hardening and redundant work in rod-drawing analyses. Int. J.mech. Sci. 10, 15, (1968).
11. JOHNSON, W., and KUDO, H., The mechanics of metal extrusion. Manchester University Press (1962).
12. ROWE, G.W., An introduction to the principles of metal working, EDWARD ARNOLD, London (1965).

13. HOFFMAN, O., and SACHS, G., Introduction to the theory of plasticity for engineers. McGRAW-HILL, New York (1953).

14. JOHNSON, W., The pressure for the cold extrustion of lubricated rod through square dies of moderate reduction at slow speeds. J.Inst. Met. 85, 403, (1957).

15. JOHNSON, W., Experiments in plane-strain extrusion. J.Mech. Phys. Solids 4, 269,(1956).

16. MEDRANO, R.E., and GILLIS, P.P., Visioplasticity techniques in axisymmetric extrusion. J.Strain Anal. 7, 170, (1972).

17. BLAZYNSKI, T.Z., Optimization of die design in the extrusion of rod using model materials. Int.J.Mech.Sci. 13, 113, (1971).

18. SHEPPARD, T., and RAYBOULD. D., On load and temperature rise during the extrusion of superpure Al, Al-Zn and Al-Zn-Mg alloys. J.Inst. Met. 101, 33, (1973).

19. COLE, B.N., and BAKHTAR, F., Dynamic effects in very high speed impact extrusion. Int. J. M.T.D.R. 3, 77, (1963).

20. PARSONS, B., LAYCOCK, D.B., and COLE, B.N., Some preliminary investigations of the high-speed impact extrusion of brittle materials. Proc. Inst.Mech. Engrs. 180 (31), (1965-6).

21. BISHOP, E.D., AVITZUR, B., and HAHN, W.C., Impact extrusion: upper-bound analysis of the early stage. Trans. A.S.M.E., B. Eng. Ind. 1079, (1972).

22. FORD, H., Advance Mechanics of Materials. Longman Group Ltd., (1972).

23. JOHNSON, W., and MELLOR, P.B., Engineering Plasticity Van Nostrand Reinhold Company Ltd., (1972).

24. PEARSON, C.E., and PARKINS, R.N., The Extrusion of Metals. Chapman and Hall Ltd., (1961).

25. AVITZUR, B., Metal Forming: Processes and Analysis. McGraw-Hill Book Company. (1968).

26. BLAZYNSKI, T.Z., Metal Forming: Tool Profiles and Flow. The Macmillan Press Ltd.,(1976).

27. JOHNSON, W., Impact Strength of Materials. Edward Arnold Ltd. (1972).

28. CALLADINE, C.R., Engineering Plasticity, Pergamon Press (1969).

29. SPARSHOTT, J.A., Investigations into the Energy Absorption by the Deformation of Metals. The University of Aston in Birmingham, (1974).

30. PUGH, H.U.D., and WATKINS, M.T., Experimental Investigation of the Extrusion of Metals. J.Inst.Metals. Vol. 100 (1972).

31. WALLACE, J.F., Adiabetic Deformation in impact extrusion. J.Inst.Metals Vol. 90. (1962).

32. HENDRY, J.C., Cold Extrusion of six low alloy case hardening steels. NEC. Report No. 642. (1977).

33. THOMPSON, P.J., and SANSOME, D.M., Apparent Strain Method for Analysis of Steady-state Metal Working Operations. Metals Technology. 497. (1976).

34. SHUTT, A., and TURNER, T.W., Extrusion by a True Impact Process. Int. J. Mech. Sci. Vol. 5. 267. (1963).

35. WIRSCHING, P.H., and SLATER, R.C., The Beer Can as a Shock Absorber. Trans. A.S.M.E. Paper 73 - Mat - Y. (1973).

36. GIECK, J.E., WEITAENHOF, D.A., and MERZ, E.J., A High Energy Level pneumatic Energy Absorbing Bumper. S.A.E.Paper 730029. (1973).

37. SLESSOR, J.M., RUSCH, K.C., and PETT, R.A., "After careful consideration of the many characteristics required, natural

rubber was determined to have the best balance of properties ---" Rubber Development Vol. 26. No.1. (1973).

38. BRABIN, E.J., Energy Absorbing Devices used in Crash Testing. MIRA Report.

39. ELLIS, D.T., BRAMLEY, A.N., and ATKINSON, J.R., The Solid Phase Forming (or Forging) of Polypropylene. Leeds University.

40. DEAN, T.A., The Effect of Process Conditions of the Properties of Forged Polypropylene Shapes. University of Birmingham.

ACKNOWLEDGEMENTS.

The author would like to express his sincere gratitude to Professor D.H.Sansome for his keen interest and invaluable guidance throughout the duration of this investigation. Also, his thanks are offered to Mr.M.Elson, of Imperial Metal Industries for his very helpful comments, the Imperial Metal Industries Company for their financial help and the Imperial Metal Industries Apprentice School for their assisance in manufacturing the rig. Further, thanks are due to Mr.G.M.Jones, Mr.A.F.Scott, Mr.S.Twamley and Aston Services for their assistance with the manufacture and instrumentation of the impact test rig. Finally, the author would like to thank all of his friends and colleagues who gave encouragement and help to make this investigation possible.

APPENDIX A

THEORY

IMPACT EXTRUSION

In the impact extrusion of bar, relatively high strain rates can be attained and this will, in the case of some alloys, lead to a substantial increase in the value of the yield stress, combined with a reduction in the strain to fracture. This is particularly noticeable towards the end of the operation, when a high degree of deceleration is reached. It is also at this stage that high tensile stresses are reached at the base of the extruded bar and result in either necking or breaking off of the extruded bar. Maximum possible deformations depend mainly on the tool materials to withstand the shock conditions which prevail.

This analysis, which cannot differentiate between the homogeneous and inhomogeneous work, uses the equilibrium technique of Cole and Bakhtar (Ref.15).

Assumptions

The system consists of three elements: the billet, the surrounding cylindrical container, and the ram-die whose kinetic energy is the chief instrument of the metal forming process. A reasonable generalized diagram of the system is shown in Fig. A.1.

To simplify the analysis the following assumptions are made:

i) No external forces act on the system which consists of ram, billet, and container.

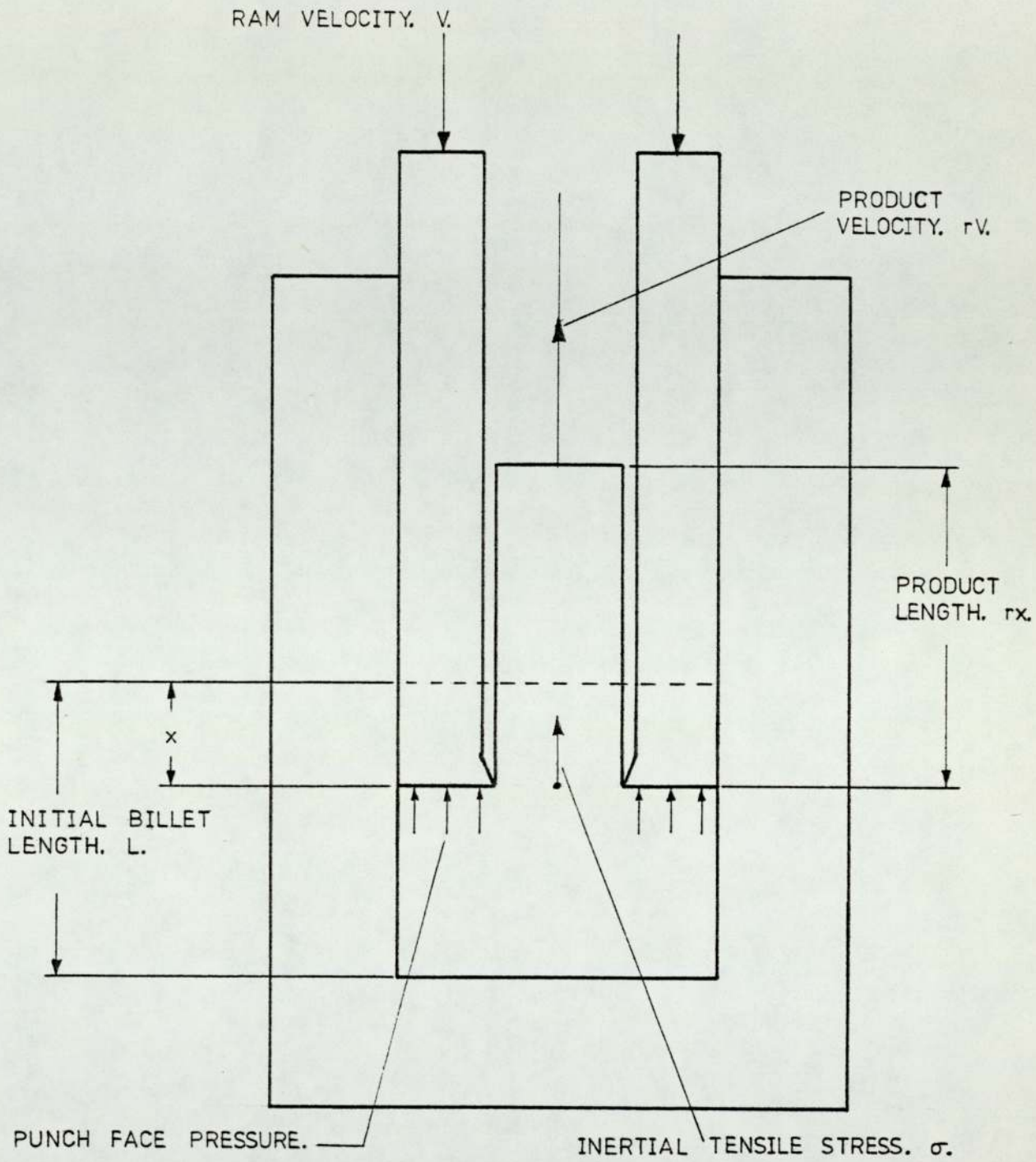

FIG. A.1. SYSTEM FOR REVERSE IMPACT EXTRUSION.

ii) The billet material is assumed to be plastic-rigid and incompressible and unaffected by a rise in temperature.

iii) The billet is initially an exact fit in the container bore.

iv) The ram and container are rigid.

v) The dead metal zone is relatively small.

vi) Friction at the container and ram walls is negligible.

vii) Transverse components of velocity are negligible.

viii) For a given geometry and billet material, the work of deformation per unit volume of billet is an absolute constant w.

The latter assumption does not, of course, take into account the effect of strain rate, unless the value of yield stress Y is suitably adjusted. It is further assumed that, to the exclusion of rebounds and other elastic phenomena, the energy delivered by the ram is entirely absorbed by the billet.

Assumption viii is reasonable in all the circumstances, and numerical values for w could be taken from the data available for conventional low speeds of extrusion. Such choice might be strictly accurate only at the very end of the process when the system comes to rest, for the variation of w with speed of working when the latter is very high, is surrounded by much doubt. Hypothetical strain-rate variations of w in such forms as $w = a + bV$ or $w = a + bV + cV^2$ are amenable to analysis, although from lack of information on the values of the constants a, b and c, this route is not pursued in this analysis. At an exploratory stage, a constant value of w has much to commend it, and it is worth noting that a consistent approximation to

this, for the case of simple bar extrusion, can be taken in the form $w = KY\ln r$ where K is a measure of process efficiency which depends principally on die geometry and friction. The minimum work of deformation per unit volume of billet is the amount of work necessary to cause extrusion through a perfectly smooth cone-shaped die, having an infinitely small cone angle, i.e., when the redundant work is zero; for this minimum value of w, K is unity.

THEORETICAL ANALYSIS

From the Law of Conservation on Linear Momentum, i.e.

$$MV_x = \text{constant}$$

Thus the momentum of the crosshead just before impact is equal to the momentum of the ram and crosshead at the instance of impact. Then the velocity of the combined mass can be expressed as,

$$V_i = \frac{M_c V_c}{M_c + M_r}$$

or

$$V_i = \frac{M_c V_c}{M}$$

At any time t after the impacts considerations of the energy breakdown gives.

Total energy $= 1/2\ MV_i^2$

Energy remaining in ram $= 1/2\ MV^2$

Energy in extruded bar $= 1/2 \rho a r^3 x V^2$

Energy absorbed in extrusion $= wAx$

The balance of energy is thus represented by,

$$1/2MV_i^2 = wAx + 1/2MV^2 + 1/2\rho ar^3xV^2 \qquad (1)$$

The ram velocity at any position after the impact is given by,

$$V = \sqrt{\frac{MV_i^2 - 2wAx}{M + \rho ar^3x}} \qquad (2)$$

The resultant force opposing the motion of the ram is expressible as:

$$F = \frac{-M}{A} V \frac{dV}{dx} \qquad (3)$$

combining (2) and (3) and substituting A = ar

$$F = \frac{M^2}{2}\left[\frac{\rho r^2 V_i \cdot + 2w}{(M + \rho ar^3x)^2}\right] \qquad (4)$$

Assuming that the billet in the container has yielded completely, the compressive container wall pressure can be determined from the criterion of yielding,

$$P = F-Y \qquad (5)$$

The rate of deceleration of the extruded bar is very high and can easily lead to necking and, in the limit, to single or multiple breaks. The incidence of these faults is associated with the magnitude of the tensile stress σ appearing at the instantaneous base of the bar, and supporting the instantaneous acceleration of magnitude (Vr)dV/dx which acts on the mass parx. Hence, in conjunction with equation. (2)

$$\sigma = \frac{Mr^2\rho a}{2}\left[\frac{\rho r^2 V_i 2 + 2w}{(M + \rho ar^3x)\ 2}\right]x \qquad (6)$$

If this at any time exceeds the yield stress Y, then necking at least is bound to occur; should the value exceed the appropriate fracture tensile strength, then fracture will occur.

A physical maximum for the value of σ may arise in either of two ways. Firstly it is possible for the variation of σ with ram displacement x to show a turning point. For this case, putting $d\sigma/dx=o$ in (6) it emerges that:

$$\sigma_{max} = \frac{1}{8r}\left[\rho r^2 V_i^2 + 2w \right] \qquad (7)$$

occurring at ram position $x = \frac{M}{\rho a r^3}$ (8)

Clearly it is necessary that this value of x should be less than the total value of x given by $x = MV_i^2/2Aw$, and it thus follows that a necessary condition for (7) to be meaningful is that:

$$\frac{1}{\rho r^2} \leqslant \frac{V_i^2}{2w} \qquad (9)$$

If this last condition is not satisfied, then no turning point is exhibited, and the physical maximum of σ in this case simply arises for the greatest value of x, i.e., the value at the end of the process.

$$\sigma_{max} = \rho r V_i^2 \frac{w}{2w + \rho r^2 V_i^2} \qquad (10)$$

If either equation (7) or (10) - each within it's range of validity - appears to give a stress exceeding Y, then at least necking of the extruded bar will occur.

NOMENCLATURE

A - cross sectional area of billet.

a - cross sectional area of extruded bar.

F - ram face pressure.

g - acceleration of mass.

K - process efficiency factor.

L - initial billet length.

M - $M_c + M_r$ - mass of ram and crosshead.

M_c - mass of crosshead.

M_r - mass or ram.

m - ρAL - mass of billet.

P - container wall pressure.

r - A/a extrusion ratio.

S_1 - distance between points 1 and 3.

T - time reckoned after instant of impact.

t_1 - time for mass to pass between points 1 and 2.

t_2 - time for mass to pass between points 1 and 3.

U_1 - velocity of mass at point - 1.

U_2 - velocity of mass at point - 2.

U_3 - velocity of mass at point - 3.

V - ram and crosshead velocity at any time after impact.

V_c - velocity of crosshead.

V_i - ram and crosshead velocity at impact.

w - irreversible work of deformation perunit volume of billet.

x - ram displacement after impact.

Y - yield stress of billet in uniaxial tension or compression

ρ - billet density.

σ - tensile stress at base of extruded bar.

APPENDIX B

THEORETICAL CALCULATIONS

To predict the extrusion pressure, the impacting mass and the energy required for complete extrusion, use the corresponding data from each test as necessary.

Test Number 16. Top Load Cell

Impacting Mass

Kinetic energy of mass = $\frac{1}{2} MV_i^2$

Energy absorbed extrusion = wAx

$$M = \frac{2wAx}{V_i^2}$$

now $W = KY\ln r$

$W = 65 N mm^{-2}$

$M = 105$ kg

Extrusion Pressure

From the theory the extrusion pressure,

$$F = \frac{M}{2}\left[\frac{\rho r^2 V_i^2 + 2w}{(M + \rho a r 3x)2}\right]$$

where $a = 2208.93\ mm^2$ = cross sectional area of product

$\rho = 11.37 \times 10^3\ kg\ m^{-3}$ = density of billet

$F = 66.0\ N\ mm^{-2}$ when $x = 0$ (start of the extrusion)

$F = 64.0\ N\ mm^{-2}$ when $x = 8.00$ mm (at the end of the extrusion)

Energy Available at Impact

The energy available at impact = $\frac{1}{2} MV_i^2$

$$\underline{2294 \text{ Nm}}$$

Stress at Base of Product

$$\sigma = \frac{Mr^2\varrho a}{2}\left[\frac{\varrho r^2 V_i^2 + 2w}{(M + \varrho a r^3 x)^2}\right] x$$

Max stress at the end of the extrusion, i.e.,

$$\sigma_{max} = \varrho r V_i^2\left[\frac{w}{2w + \varrho r^2 V_i^2}\right]$$

$$\underline{\sigma_{max} = 0.50 \text{ N mm}^{-2}}$$

Estimation of the Process Efficiency Factor K

Now for slow speed extrusion, the extrusion pressure is numerically equal to the work of deformation per unit volume of billet, i.e.,

$$F = KY \ln r$$

. Therefore the process efficiency factor K

$$K = \frac{F}{Y \ln r}$$

From the slow speed extrusion of lead at 50% reduction of area F = 65.0 N mm^{-2}.

therefore $\underline{K = 3.54}$

for 60% $\underline{K = 3.07}$

70% $\underline{K = 2.81}$

80% $\underline{K = 3.16}$

APPENDIX C

EXPERIMENTAL CALCULATIONS

Velocity measurement

Basic equations

$$S_1 = U_1 t_1 + \tfrac{1}{2} g t_1^2 \qquad (1)$$

$$S_2 = U_1 t_2 + \tfrac{1}{2} g t_2^2 \qquad (2)$$

$$S_2 - S_1 = U_2(t_2 - t_1) + \tfrac{1}{2} g\,(t_2 - t_1)^2 \qquad (3)$$

$$U_3 = U_1 + g t_2 \qquad (4)$$

$$U_3 = U_2 + g(t_2 - t_1) \qquad (5)$$

From (1) and (2) we obtain the following:

$$\frac{S_1}{t_1} - \frac{g t_1}{2} = \frac{S_2}{t_2} - \frac{g t_2}{2}$$

$$g = \frac{2}{t_2 - t_1} \quad \frac{S_2 - S_1}{t_2 - t_1}$$

From test number 16.

$S_1 = 0.4$ m and $S_2 = 0.8$ m

$t_1 = 0.63$ sec and $t_2 = 0.121$ sec

$g = 9.05\ ms^{-1}$

From test number 17.

$S_1 = 0.4$ m and $S_2 = 0.8$ m

$t_1 = 0.62$ sec and $t_2 = 0.121$ sec

$g = 5.42\ ms^{-1}$

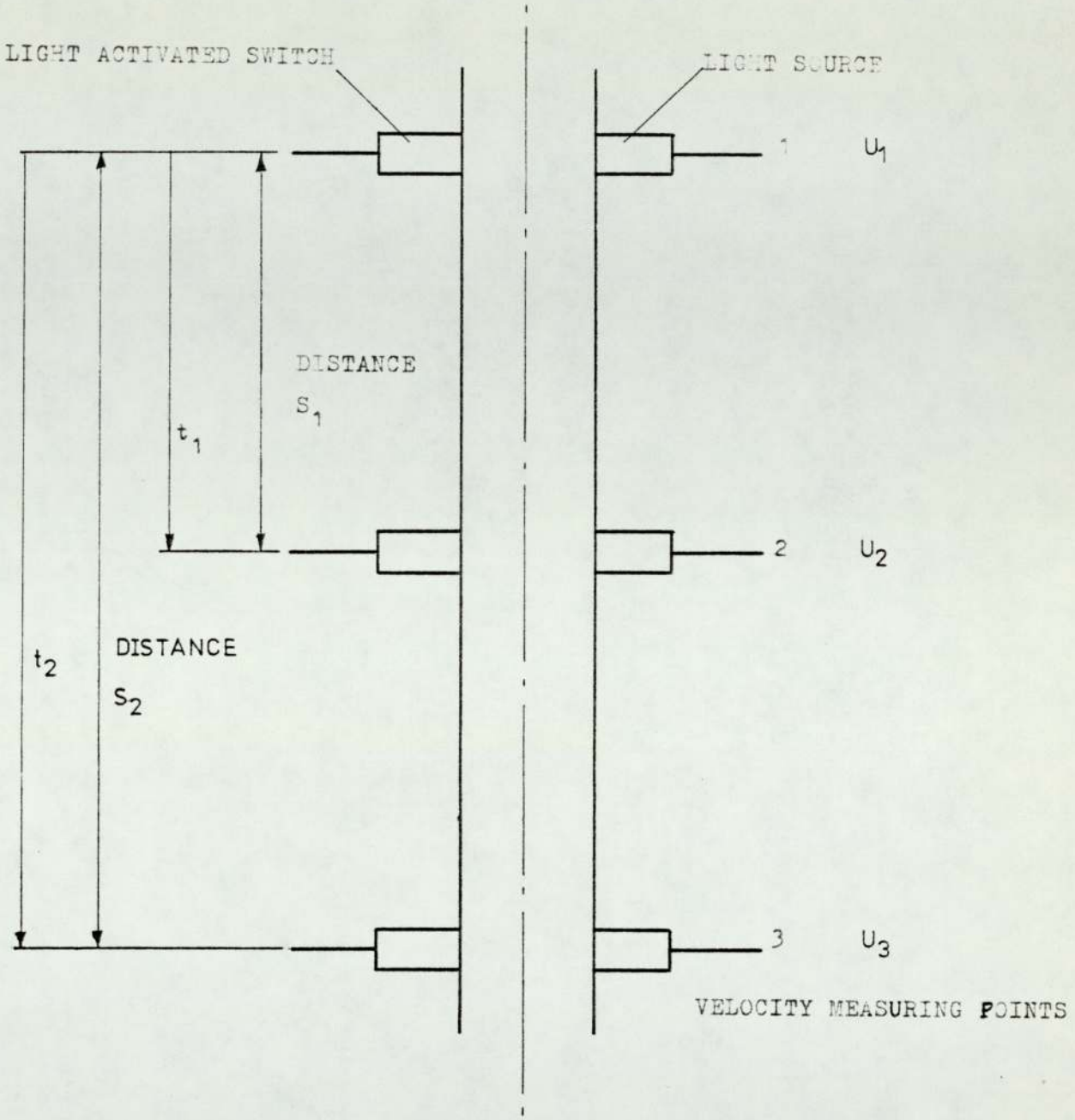

t_1 - TIME FOR MASS TO PASS FROM POSITION 1 TO 2

t_2 - TIME FOR MASS TO PASS FROM POSITION 1 TO 3

FIG. C.1. DIAGRAM SHOWING VELOCITY MEASURING POINTS OF FALLING MASS.

The error in calculating the accceleration of the falling mass is very sensitive to the measured items. The electronic clocks were not sensitive enough to enable accurate estimates of the acceleration during the descent. Acceleration due to gravity was used to calculate the impact velocity, this would (marginally) overestimate the velocity.

Test Number 16.

From equation (2) $U_1 = \frac{S_2}{t_2} - \frac{gt_2}{2} = 6.02\ ms^{-1}$

From equation (4) $U_3 = U_1 + gt_2 = 7.20\ ms^{-1}$

From equation (3) $U_2 = \frac{S_2 - S_1}{t_2 - t_1} - \frac{g(t_2-t_1)}{2} = 6.61\ ms^{-1}$

From equation (5) $U_3 = U_2 + g(t_2-t_1) = 7.18\ ms^{-1}$

The average velocity on impact = $7.19\ ms^{-1}$

Test Number 17.

From equation (2) $U_1 = \frac{S_2}{t_2} - \frac{gt_2}{2} = 6.02\ ms^{-1}$

From equation (4) $U_3 = U_1 + gt_2 = 7.21\ ms^{-1}$

From equation (3) $U_2 = \frac{S_2 - S_1}{t_2 - t_1} - \frac{g(t_2 - t_1)}{2} = 6.49\ ms^{-1}$

From equation (5) $U_3 = U_2 + g\ (t_2 - t_1) = 7.07\ ms^{-1}$

The average velocity of impact = $7.14\ ms^{-1}$

Initial Extrusion Velocity

Test Number 16.

$$V_1 = \frac{Mc \times Vc}{M}$$

$$V_1 = 6.61\ ms^{-1}$$

Energy available at impact.

Kinetic energy available at impact = $\frac{1}{2}MVi^2$

Test number 16. = 2378 Nm

Average velocity of ram.

Test number 16.

Ram displacement = 8.00 mm

Duration of impact = 2.6×10^{-3} sec

average velocity of ram = $3.08 ms^{-1}$

(since the velocity of the ram does not vary linearly during the impact).

Energy absorbed during Impact Extrusion

The energy absorbed during the impact extrusion is the area under a force versus displacement curve, multiplied by the appropriate scale factors.

Since force is the product of pressure and area; displacement is the product of time and velocity, the extrusion force can be calculated from the pressure versus duration curve, from the cross-sectional area of the billet and the ram velocity.

Test number 16

Average ram velocity = $3.08\ ms^{1}$

Cross sectional area of billet = $4417.86\ mm^2$

Extrusion pressure scale factor = $1.3333\ Nmm^{-2}$ per mm

Duration Scale factor = 0.00005 sec per mm

Area under top loadcell's curve = $1687\ mm^2$

Area under bottom loadcell's curve = $1656\ mm^2$

Energy absorbed calculated from top loadcell's curve = 1529 Nm

Energy absorbed calculated from bottom loadcell's curve = 1501 Nm

Average Extrusion Pressure

Test number 16.

To find the average extrusion pressure divide the energy absorbed by the ram's displacement and the cross sectional area of the billet.

From the top load cell, energy absorbed = 1529 Nm.

ram displacement = 8.00 mm

cross sectional area of billet = 44.7.86 mm^2

Average extrusion pressure = 43.3 Nmm^{-2}

From the bottom load cell, energy absorbed = 1501 Nm

ram displacement = 8.00 mm

cross sectional area of billet - 4417.86 mm^2

Average extrusion pressure = 42.5 Nmm^{-2}

Percentage of Energy absorbed to Energy available.

$$\frac{\text{Energy absorbed}}{\text{Energy available}} \times 100$$

Test number 16.

From the top load cell 64.3%

From the bottom load cell 63.1%

APPENDIX D

PROPAGATION OF ELASTIC STRESS WAVES

Speed of Elastic Stress Waves

The longtitude speed of a stress wave is given by;

$$C_L = \frac{E}{\rho}$$

For E.N.26 $E = 204 \times 10^9 Nm^{-2}$

$\rho = 7.83 \times 10^3 kg\ m^{-3}$

For SVERKER.3. $E = 194 \times 10^9 Nm^{-2}$

$\rho = 7.7 \times 10^3\ kg\ m^{-3}$

For TITANIUM $E = 117 \times 10^9 Nm^{-2}$

$\rho = 4.457 \times 10^3 kg\ m^{-3}$

For LEAD $E = 17.23 \times 10^9\ Nm^{-2}$

$\rho = 11.37 \times 10^3\ kg\ m^{-3}$

Therefore, C_L equals:

E.N. 26	$= 5.104 \times 10^3\ ms^{-1}$
SVERKER.3	$= 5.02 \times 10^3\ ms^{-1}$
TITANIUM	$= 5.127 \times 10^3\ ms^{-1}$
LEAD	$= 1.231 \times 10^3\ ms^{-1}$

Equivalent lengths

To calculate the time taken for an elastic stress wave to travel through the extrusion system, replace the Sverker 3, Titanium and the Lead portions by equivalent lengths of E.N.26.

An equivalent length of E.N.26 is one where the time taken for the passage of an elastic stress wave is the same as in the original material.

Therefore to replace the Sverker 3, Titanium and the Lead portions, multiply by the ratio of the propagation speeds.

To replace the Sverker 3 by E.N.26, multiply by 1.0167.

To replace Titanium by E.N.26, multiply by 0.9955.

To replace Lead by E.N.26, multiply by 4.146

From Test number 16

The time taken for the bottom load cell to register the impact after the top load cell was about 0.15 milliseconds; in this time an elastic stress wave passes through 765.6 mm, of E.N.26.

From Fig. D.1., the lengths of the various components are found and by multiplying by their corresponding speed factors, the equivalent lengths of E.N.26 were found and tabulated to give the length of passage of the elastic stress wave between the measuring points on the two load cells.

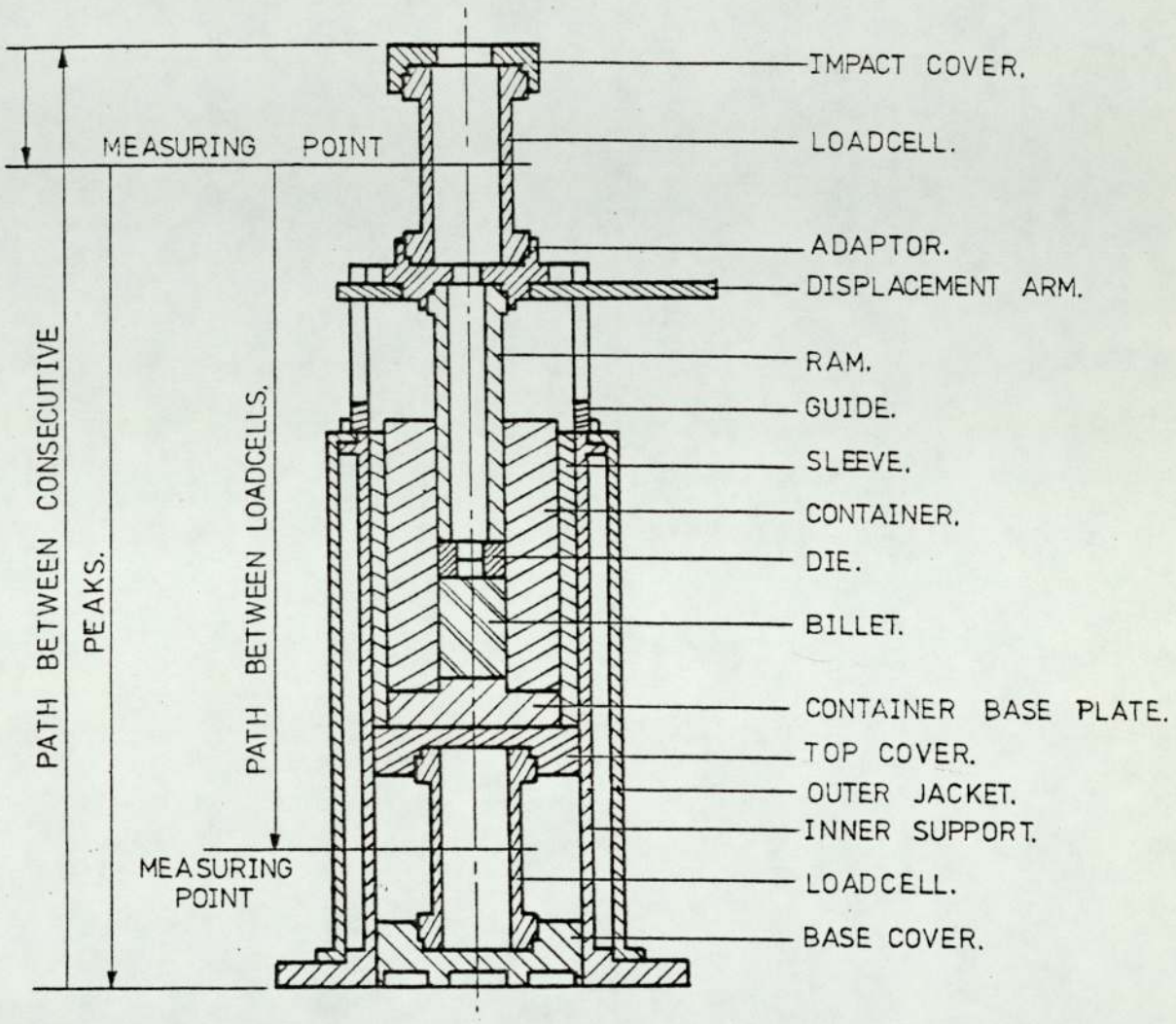

FIG.D.1. EXTRUSION SYSTEM ASSEMBLY SHOWING PATHS AND MEASURING POINTS OF THE ELASTIC STRESS WAVES.

Difference between the Load Cells.

MATERIAL	LENGTH mm	SPEED FACTOR	EQUIVALANT LENGTH mm
Titanium	75.00	0.9955	74.66
E.N.26	16.00	1	16.00
Sverker 3	200.00	1.0167	203.34
Sverker 3	25.00	1.0167	25.42
Lead	75.00	4.146	310.95
E.N.26	36.00	1	36.00
E.N.26	17.00	1	17.00
Titanium	75.00	0.9955	74.66

Total length 758.03 mm

The time taken between the first two consecutive peaks on the top load cell's trace was about 0.4 milliseconds. Thus the length of E.N.26., an elastic stress wave can travel through in this time is 2041.6 mm.

From Fig. D.1. as before.

DIFFERENCE BETWEEN TWO CONSECUTIVE PEAKS ON THE TOP LOAD CELL

MATERIAL	LENGTH mm	SPEED FACTOR	EQUIVALENT LENGTH mm
Titanium	75.00	0.9955	74.66
E.N.26	16.00	1	16.00
Sverken 3	200.00	1.0167	203.34
Sverken 3	25.00	1.0167	25.42
Lead	75.00	4.146	310.95
E.N.26	36.00	1	36.00
E.N.26	17.00	1	17.00
Titanium	150.00	0.9955	149.32
E.N.26	25.00	1	25.00
E.N.26	25.00	1	25.00
Titanium	150.00	0.9955	149.32
E.N.26	17.00	1	17.00
E.N.26	36.00	1	36.00
Lead	75.00	4.146	310.95
Sverker 3	25.00	1.0167	25.42
Sverker 3	200.00	1.0167	203.34
E.N.26	16.00	1	16.00
Titanium	150.00	0.9955	149.32
E.N.26	18.00	1	18.00
E.N.26	18.00	1	18.00
Titanium	75.00	0.9955	74.66

Total length 1900.7 mm

APPENDIX E

CALIBRATION CURVES

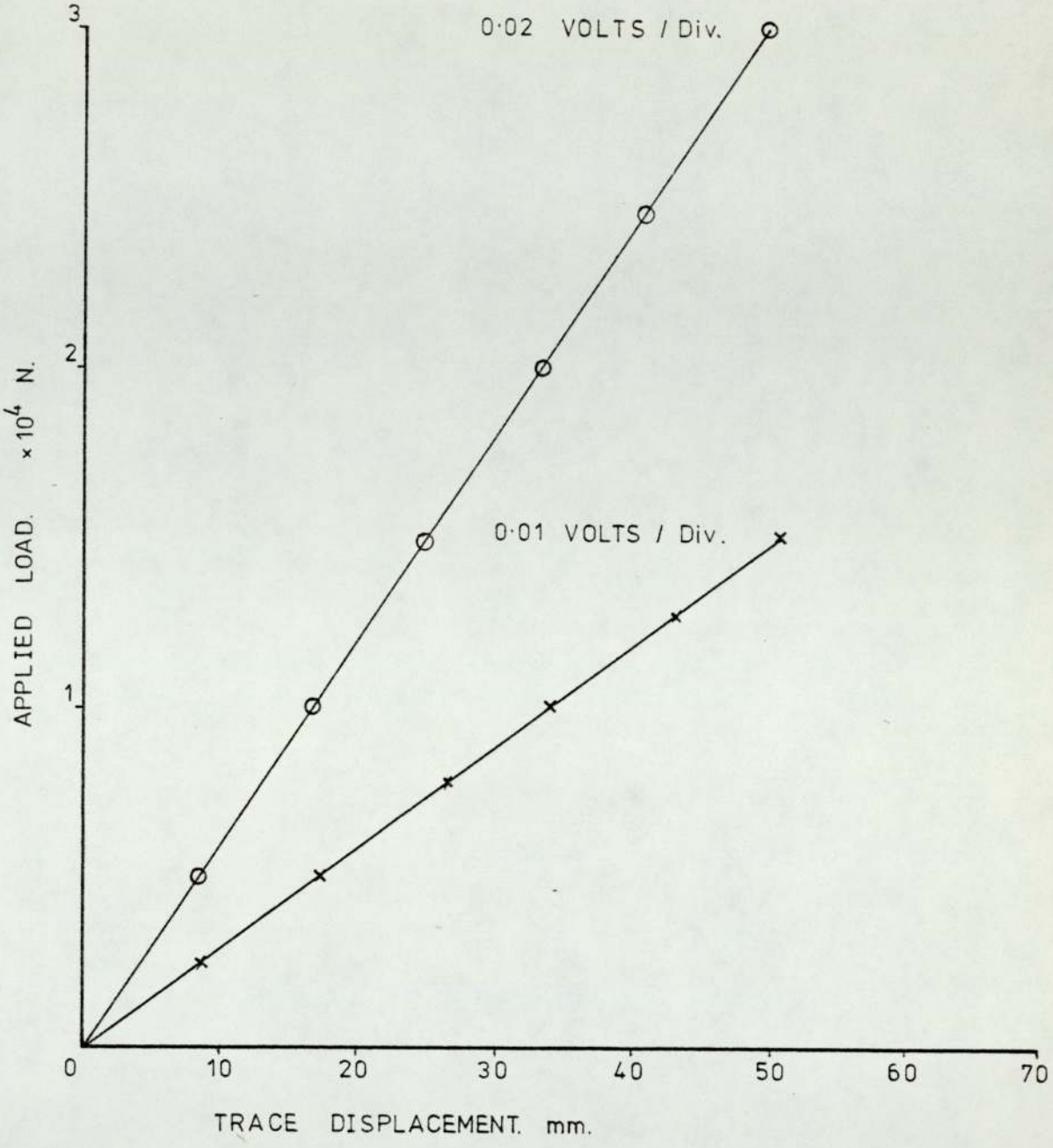

GRAPH. E.1. CALIBRATION OF THE BOTTOM LOAD CELL.

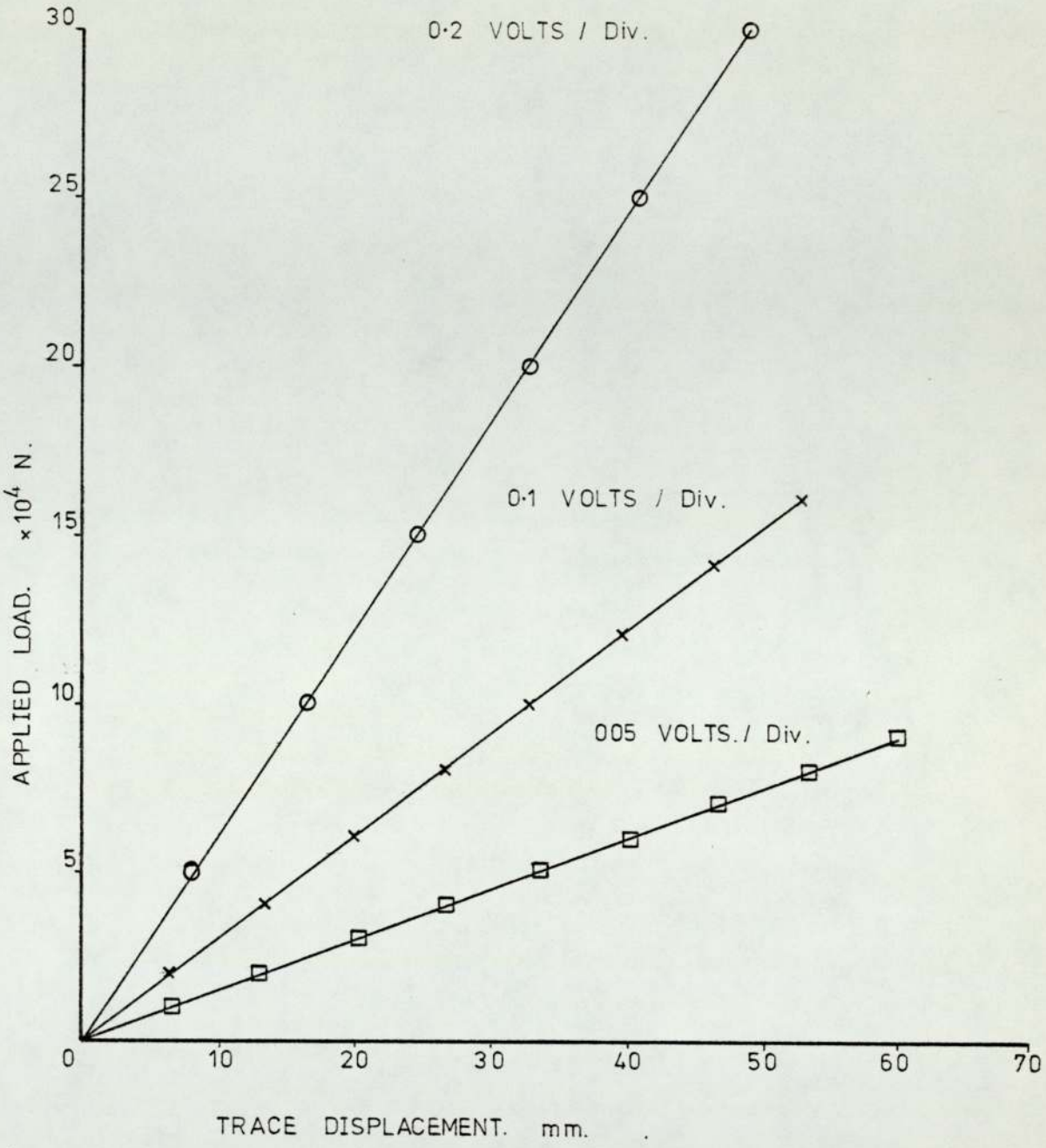

GRAPH. E.2. CALIBRATION OF THE BOTTOM LOAD CELL.

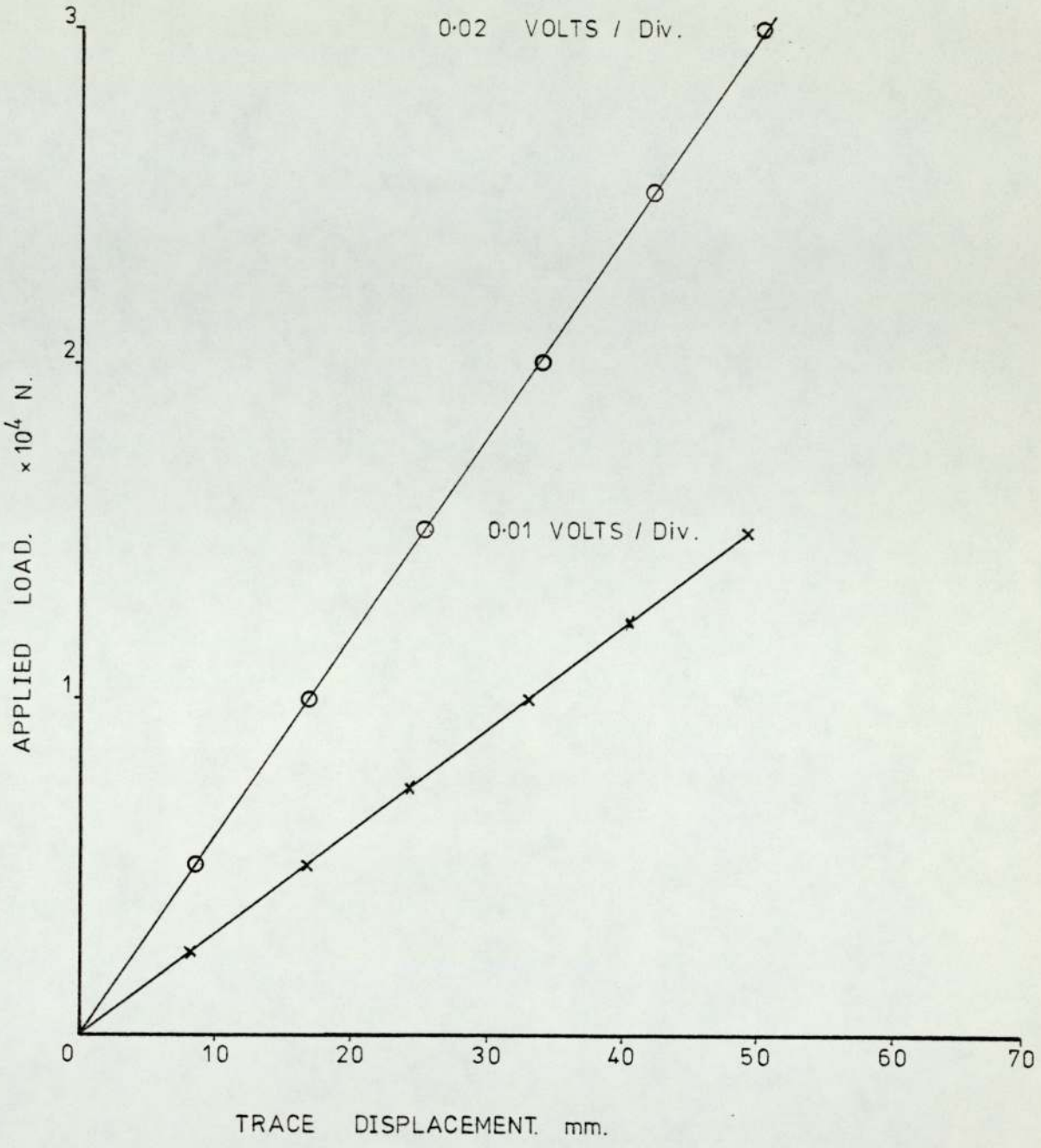

GRAPH. E.3. CALIBRATION OF THE TOP LOAD CELL.

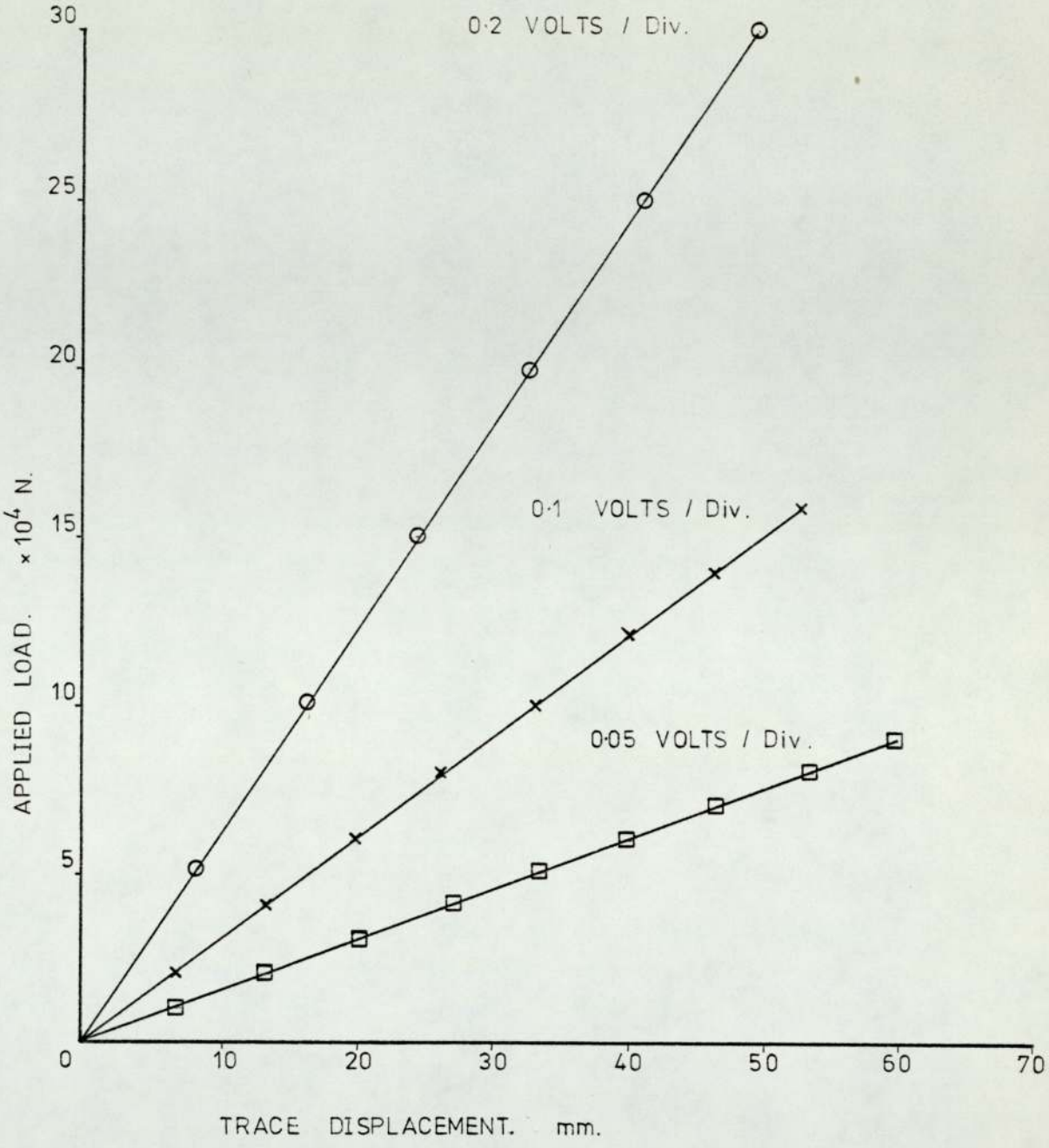

GRAPH. E.4. CALIBRATION OF THE TOP LOAD CELL.

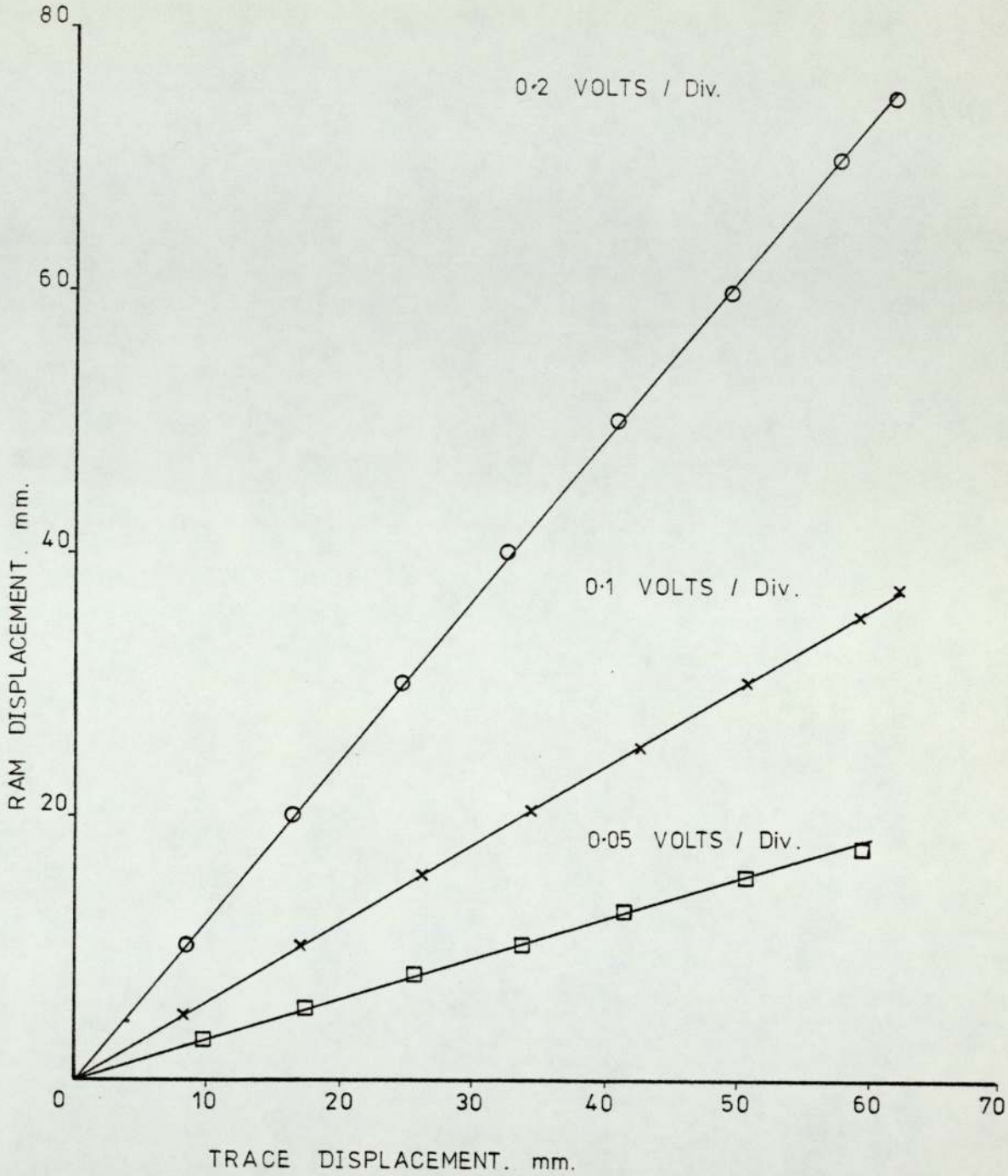

GRAPH. E.5. CALIBRATION OF THE DISPLACEMENT TRANSDUCER.

INDUCTIVE TYPE.

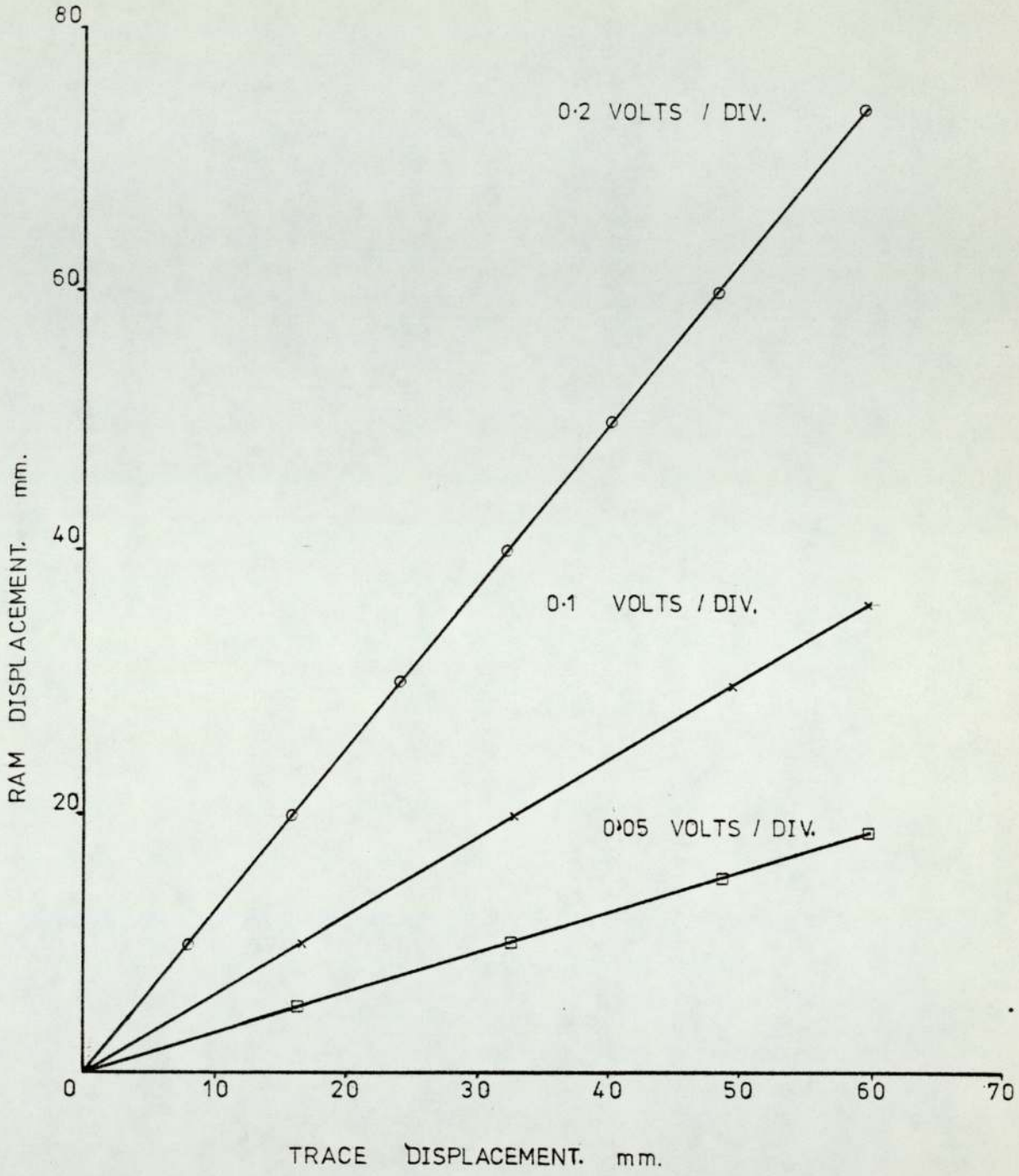

GRAPH. E.6. CALIBRATION OF THE DISPLACEMENT TRANSDUCER.

RESISTIVE TYPE.

APPENDIX F

STRESS - STRAIN CURVES

99.9% pure LEAD

Alcoa C800 ALUMINIUM

G.S.E. 20 POLYPROPYLENE

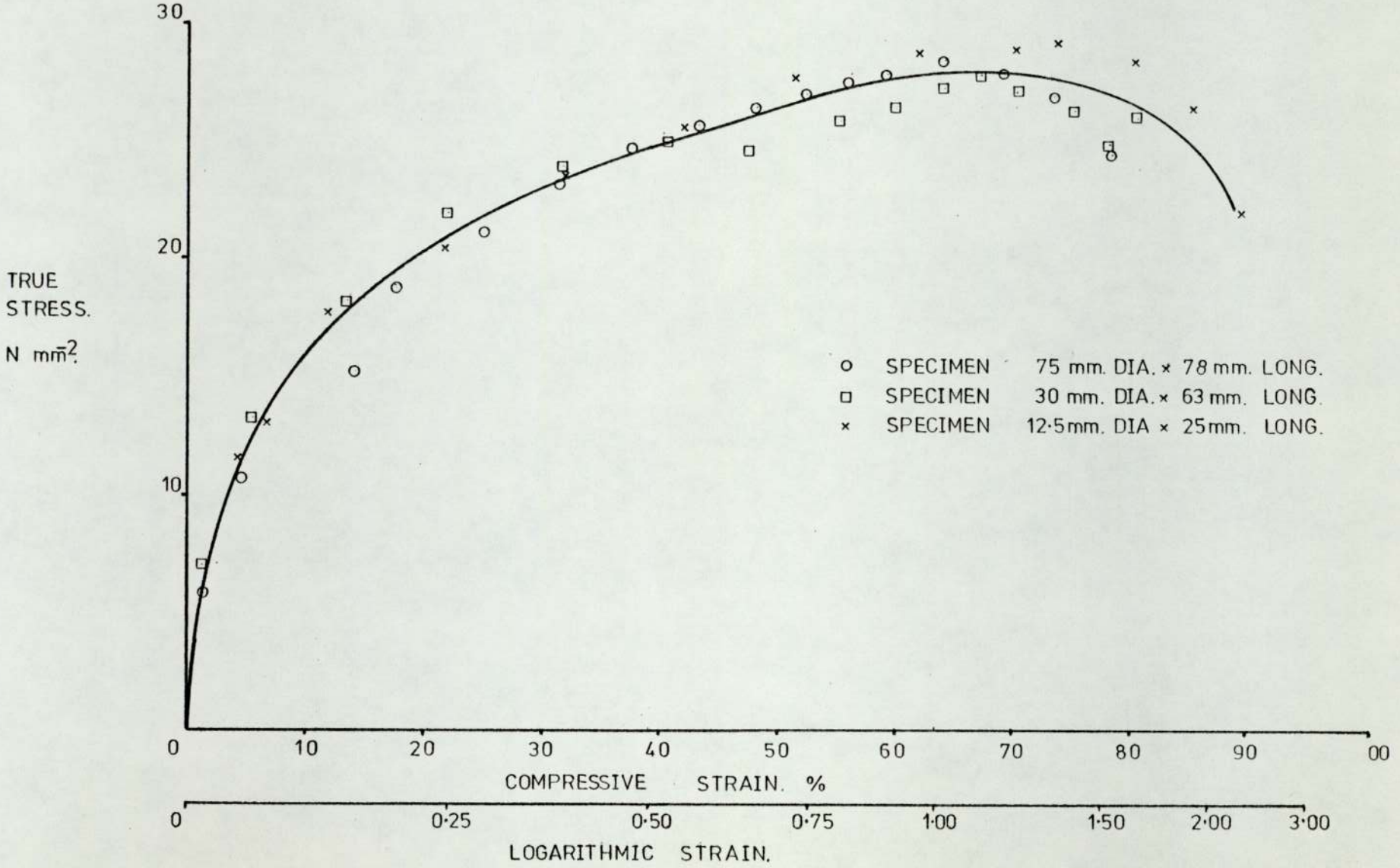

GRAPH F.1. UNIAXIAL COMPRESSION OF LEAD.

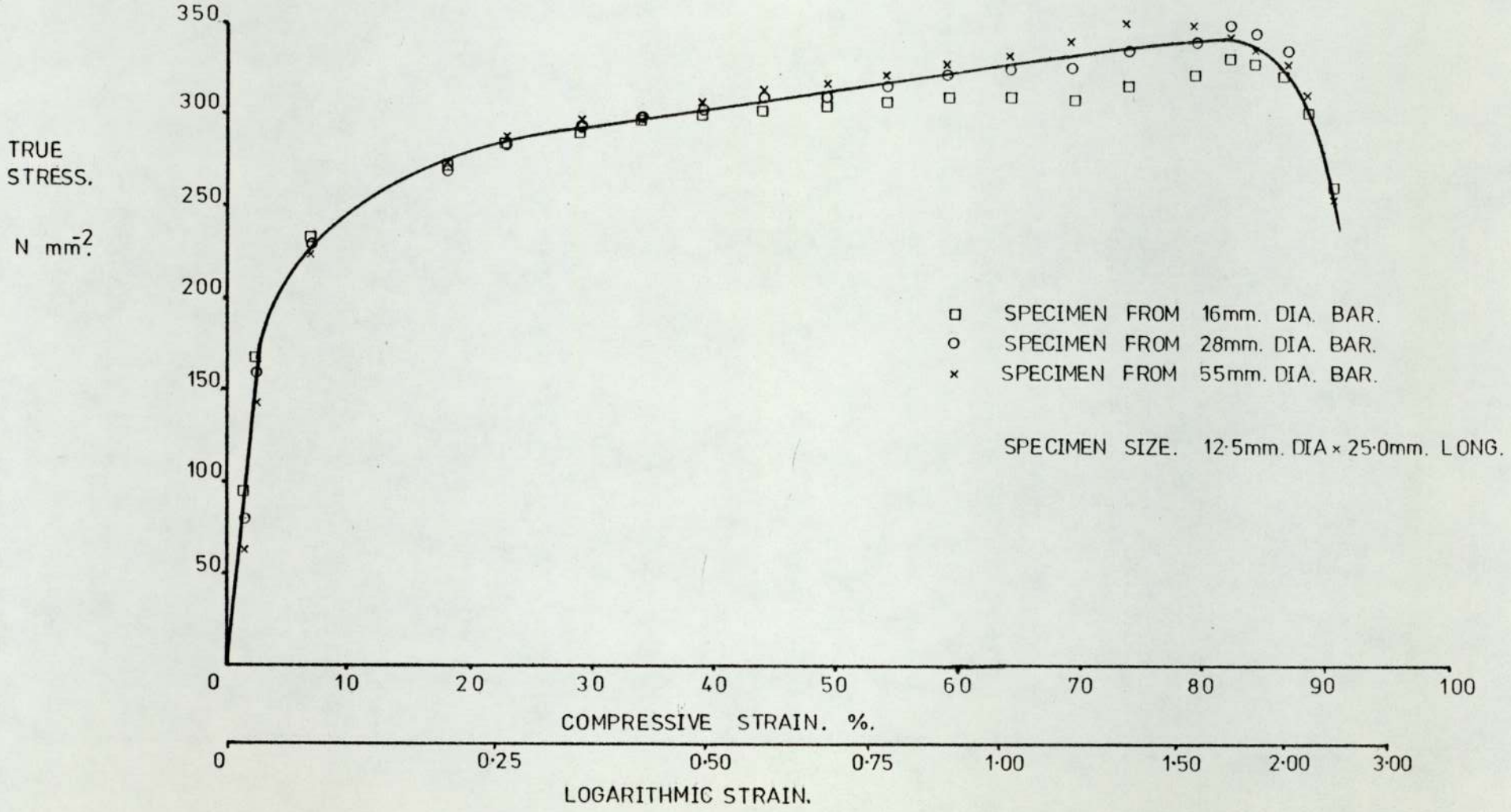

GRAPH F.2. UNIAXIAL COMPRESSION OF ALUMINIUM.

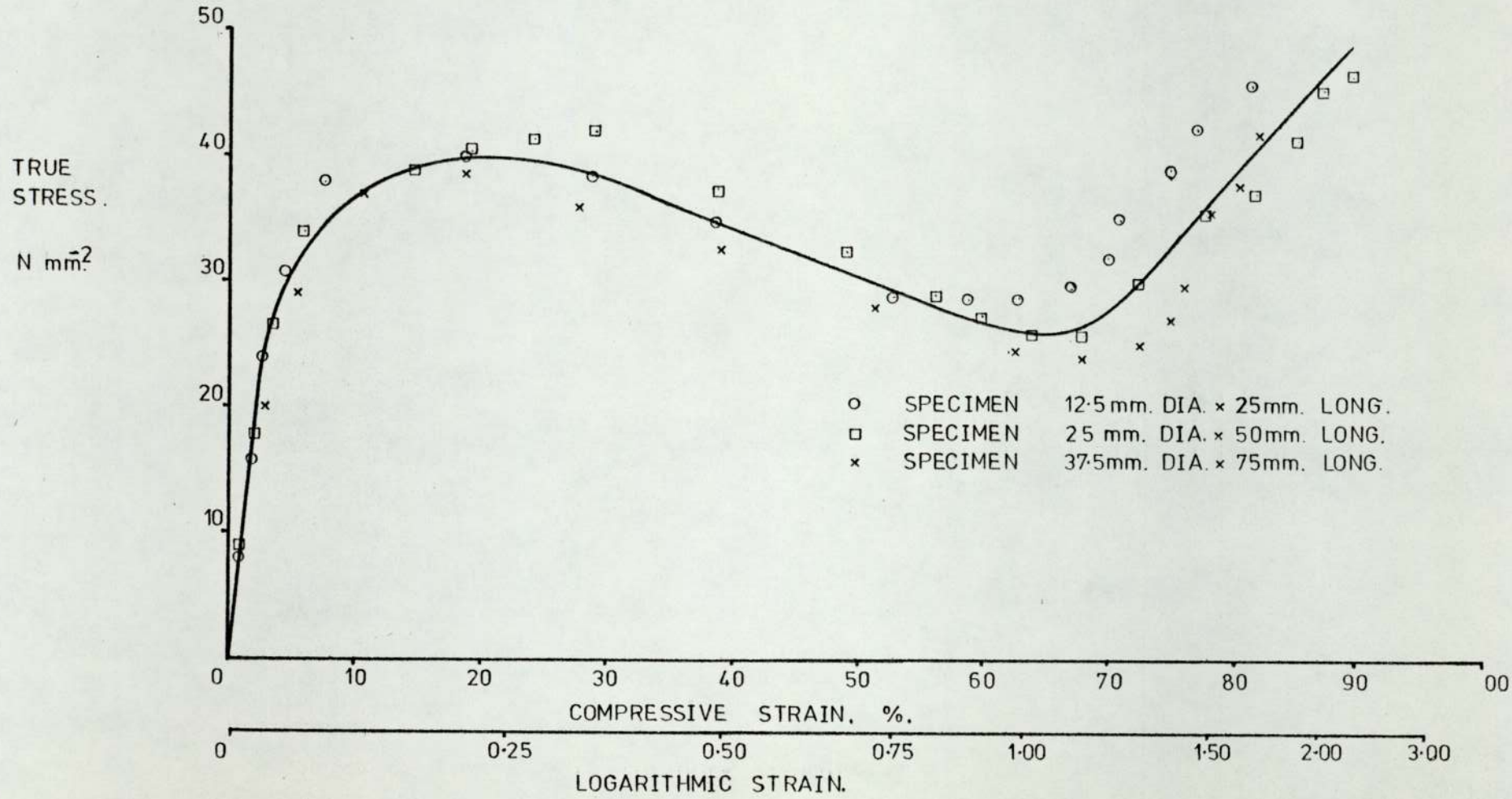

GRAPH F.3. UNIAXIAL COMPRESSION OF POLYPROPYLENE G.S.E. 20.

APPENDIX G

TABULATED RESULTS-

SLOW SPEED EXTRUSION OF LEAD

SLOW SPEED EXTRUSION TEST.

Material: LEAD

Billet Size: 12.46 mm dia.
12.53 mm length.

Reduction of Area: 50%

Speed: Less than 1 mm/minute

Applied Load Tonf	Ram Displacement in.	Extrusion Pressure $N mm^{-2}$	Non-Dimensional Ram Displacement -
0	0	0	0
0.30	0.020	24.5	0.041
0.49	0.037	40.1	0.075
0.64	0.055	52.3	0.111
0.70	0.063	57.2	0.128
0.75	0.094	61.3	0.191
0.79	0.150	64.6	0.304
0.79	0.200	64.6	0.405
0.79	0.250	64.6	0.507
0.79	0.300	64.6	0.608
0.79	0.350	64.6	0.709
0.79	0.400	64.6	0.811
0.79	0.450	64.6	0.912
0.83	0.476	67.8	0.965
0.87	0.481	71.1	0.975
0.93	0.484	76.0	0.981
1.00	0.487	81.7	0.987

SLOW SPEED EXTRUSION TEST.

Material: LEAD

Billet Size: 12.45 mm dia
25.07 mm length

Reduction of Area: 50%

Speed: less than 1mm/minute

Applied Load Tonf	Ram Displacement in	Extrusion Pressure $N mm^{-2}$	Non-Dimensional Ram Displacement -
0	0	0	0
0.28	0.020	16.4	0.020
0.47	0.040	38.5	0.041
0.63	0.060	51.6	0.061
0.74	0.100	60.6	0.101
0.80	0.150	65.5	0.152
0.80	0.200	65.5	0.203
0.80	0.300	65.5	0.304
0.80	0.400	65.5	0.405
0.80	0.500	65.5	0.507
0.80	0.600	65.5	0.608
0.80	0.700	65.5	0.709
0.80	0.800	65.5	0.811
0.81	0.900	66.3	0.912
0.82	0.950	67.1	0.963
0.86	0.969	70.4	0.982
0.93	0.974	76.1	0.987
1.00	0.978	80.1	0.991

SLOW SPEED EXTRUSION TEST.

Material: LEAD

Reduction of Area: 60%

Billet Size: 12.49 mm dia
12.57 mm length

Speed: less than 1 mm/minute

Applied Load Tonf	Ram Displacement in.	Extrusion Pressure $N mm^{-2}$	Non-Dimensional Ram Displacement -
0	0	0	0
0.40	0.020	32.5	0.040
0.64	0.038	52.1	0.077
0.80	0.057	65.1	0.115
0.93	0.100	75.6	0.202
0.93	0.150	75.6	0.303
0.93	0.200	75.6	0.404
0.93	0.250	75.6	0.505
0.93	0.300	75.6	0.606
0.93	0.350	75.6	0.707
0.93	0.400	75.6	0.808
0.93	0.450	75.6	0.909
0.95	0.465	77.3	0.940
0.98	0.473	79.7	0.956
1.00	0.479	81.4	0.968
1.10	0.482	89.5	0.974
1.20	0.485	97.6	0.980

SLOW SPEED EXTRUSION TEST.

Material: LEAD

Reduction of Area: 60%

Billet Size: 12.48 mm dia.
25.08 mm length

Speed: less than 1 mm/minute

Applied Load Tonf	Ram Displacement in	Extrusion Pressure N/mm^{-2}	Non-Dimensional Ram Displacement -
0	0	0	0
0.37	0.020	30.1	0.020
0.61	0.039	49.7	0.039
0.78	0.062	63.6	0.063
0.91	0.100	74.1	0.101
0.93	0.150	75.8	0.152
0.93	0.200	75.8	0.203
0.93	0.300	75.8	0.304
0.93	0.400	75.8	0.405
0.93	0.500	75.8	0.506
0.93	0.600	75.8	0.608
0.93	0.700	76.6	0.709
0.94	0.800	76.6	0.810
0.94	0.900	76.6	0.911
0.94	0.950	76.6	0.962
0.97	0.963	79.0	0.975
1.00	0.969	81.5	0.981
1.10	0.973	89.6	0.985
1.20	0.976	97.8	0.988

SLOW SPEED EXTRUSION TEST.

Material: LEAD

Reduction of Area: 70%

Billet Size: 12.47 mm dia.
12.57 mm length

Speed: less than 1 mm/minute

Applied Load Tonf	Ram Displacement in	Extrusion Pressure $N mm^{-2}$	Non-Dimensional Ram Displacement -
0	0	0	0
0.40	0.005	32.6	0.010
0.78	0.020	63.7	0.040
1.01	0.040	82.4	0.081
1.12	0.060	91.4	0.121
1.14	0.100	93.0	0.202
1.14	0.150	93.0	0.303
1.14	0.200	93.0	0.404
1.14	0.250	93.0	0.505
1.14	0.300	93.0	0.606
1.14	0.350	93.0	0.707
1.14	0.400	93.0	0.808
1.14	0.450	93.0	0.909
1.15	0.469	93.9	0.948
1.20	0.476	97.8	0.962
1.30	0.480	106.1	0.970
1.50	0.482	122.4	0.974

SLOW SPEED EXTRUSION TEST.

Material: LEAD

Reduction of Area: 70%

Billet Size: 12.49 mm dia.
25.0 mm length

Speed: less than 1 mm/minute

Applied Load Tonf	Ram Displacement in	Extrusion Pressure $N mm^{-2}$	Non-Dimensional Ram Displacement -
0	0	0	0
0.35	0.010	28.5	0.010
0.76	0.024	61.8	0.024
1.03	0.045	83.8	0.046
1.13	0.070	91.9	0.071
1.14	0.100	92.7	0.102
1.15	0.150	93.6	0.152
1.15	0.200	93.6	0.203
1.15	0.300	93.6	0.305
1.14	0.400	92.7	0.406
1.14	0.500	93.7	0.508
1.15	0.600	93.6	0.609
1.15	0.700	93.6	0.711
1.15	0.800	93.6	0.812
1.16	0.900	94.4	0.914
1.16	0.950	94.4	0.965
1.18	0.965	96.0	0.980
1.25	0.968	101.7	0.983
1.35	0.971	109.8	0.986
1.50	0.973	122.0	0.988

SLOW SPEED EXTRUSION TEST.

Material: LEAD

Reduction of Area: 80%

Billet Size: 12.48 mm dia.
12.60 mm length.

Speed: less than 1 mm/minute

Applied Load Tonf	Ram Displacement in.	Extrusion Pressure $N mm^{-2}$	Non-Dinensional Ram Displacement -
0	0	0	0
0.55	0.010	44.8	0.020
0.80	0.020	65.2	0.040
1.12	0.034	91.3	0.069
1.48	0.062	120.6	0.126
1.72	0.100	140.2	0.204
1.72	0.150	140.2	0.305
1.72	0.200	140.2	0.407
1.72	0.250	140.2	0.509
1.72	0.300	140.2	0.611
1.72	0.350	140.2	0.712
1.72	0.400	140.2	0.814
1.72	0.450	140.2	0.916
1.72	0.470	140.2	0.957
1.76	0.476	143.4	0.969
1.88	0.480	153.2	0.977
2.00	0.483	162.0	0.983

SLOW SPEED EXTRUSION TEST.

Material: LEAD

Reduction of Area: 80%

Billet Size: 12.45 mm dia
25.09 mm length

Speed: less than 1 mm/minute

Applied Load Tonf	Ram Displacement in.	Extrusion Pressure $N mm^{-2}$	Non-Dimensional Ram Displacement -
0	0	0	0
0.45	0.012	36.8	0.012
0.78	0.024	63.9	0.024
1.09	0.043	89.2	0.044
1.45	0.071	118.7	0.072
1.65	0.100	135.1	0.101
1.67	0.150	136.7	0.152
1.67	0.200	136.7	0.202
1.67	0.300	136.7	0.304
1.67	0.400	136.7	0.405
1.68	0.500	137.6	0.506
1.68	0.600	137.6	0.607
1.68	0.700	137.6	0.709
1.69	0.800	138.4	0.810
1.69	0.900	138.4	0.911
1.69	0.950	138.4	0.962
1.74	0.961	142.5	0.973
1.80	0.969	147.4	0.981
1.90	0.971	155.6	0.983
2.00	0.973	163.8	0.985

APPENDIX H

MATERIAL SPECIFICATIONS.

Test Material

i) LEAD. 99.9% pure, cast over size billets, turned to size.

ii) ALUMINIUM. Alco C800

Tensile strength	310N mm^{-2} min.
0,2% Proof stress	255N mm^{-2} min.

Chemical Composition

Silicon	0.4%
Iron	0.7%
Copper	5.0-6.0%
Zinc	0.3%
Lead	0.2-0.6%
Bismuth	0.2-0.6%
Aluminium	the remainder.

State received - as extruded bar - over size.

Turned to size and annealed.

iii) POLYPROPYLENE G.S.E. 20 (no technical information available).

Test Rig Materials.

Dies and Rams - Uddholm Steels	SVERKER.3.
Young's Modulus of Elasticity	194 kN mm^{-2}
Density	7.70 x 10^{3} kg m^{-3}
Specific Heat	0,110 cal per gm ^{o}C
Thermal Conductivity	49 x 10^{-3} cal per cm.s.^{o}C
Coefficient of Thermal Expansion	11 x 0^{-6} per ^{o}C

Chemical Composition

Carbon	1.90 - 2.30 %
Silicon	0.60 % max.
Chromium	12.00 - 13.00 %
Vanadium	0.50 % max.
Manganese	0.70 %

Delivery soft annealed 245 HB.

Hardness	H.R.C.	Tensile Nmm^{-2}	0.2% proof stress Nmm^{-2}
	62	3250	2250
	60	3100	2150
	55	2750	1900
	50	2400	1650
	45	2000	1350

Protection against decarbonization ; neutral salt bath.

Containers, Adaptors Impact Covers, etc.

E.N.26.

Young's Modulus of Elasticity	204 kN mm^{-2}
Density	7.83 x 10^{3} kg m^{-3}
Specific Heat	0.118 cal per gm ^{o}C
Thermal Conductivity	83 x 10^{-3} cal per cm.s.^{o}C
Coefficient of Thermal Expansion	11.4 x 10^{-6} per ^{o}C

Chemical Composition

Carbon	0.36 - 0.44 %
Silicon	0.10 - 0.35 %
Manganese	0.50 - 0.70 %
Nickel	2.30 - 2.80 %
Chromium	0.50 x 0.80 %
Molybdenum	0.40 - 0.70 %
Sulphur	0.50 % max.
Phosphorus	0.50 % max.

Delivery soft annealed HB 277.

Hardness	H.R.C.	Tensile Nmm^{-2}	0.2% proof stress Nmm^{-2}
	54	1750	1400
	48	1550	1240
	37	1240	990
	31	1080	850
	28	1000	770
	23	930	710

Loadcells

Titanium Alloy - Actual specification unknown.

Known data (obtained from supplier).

Young's Modulus of Elasticity 103 kN mm^{-2}

Yield Stress as delivered minimum 800 N mm^{-2}

Density 4.457×10^{3} kg m^{-3}

APPENDIX I

Equipment Specification

Strain Gauges — 16 off

Make	TINSLEY TELECON
Type	Foil 13/120/EC
Size	17.7mm x 5.5mm
Resistance	120 ohms.
Supply Voltage	6 volts d.c.

Strain Gauge Amplifiers — 2 off

Make	CREATIVE INSTRUMENTS LTD.
Type	Miniature strain gauge conditioning unit series SGA 700
Supply Voltage	$\pm$ 12 volts d.c. stabilised.

Displacement Transducer (Inductive) — 1 off

Make	R.D.P.ELECTRONICS LTD.
Type	DC LVDT Series D2/2000
Serial No.	108
Supply Voltage	6 volts d.c. stabilised.

Displacement Transducer (Resistive) — 1 off

Make	PENNY AND GILES LTD.
Type	LP IB/85
Supply Voltage	4.5 volts stabilised.

Timing Clocks	2 off
Make	HEUER ELECTRONICS CORP.
Type	DITIAL 1006-3
Serial No.	031 and 032
Accuracy	1 millisecond
Supply Voltage	Mains.

Light Activated Switches	3 off
Make	RADIO SPARES
Type	LAS 15
Supply Voltage	-12 volts

Recording Oscilloscope	1 off
Make	MEDELEC
Type	FOR - 4 M-SCOPE
Serial No.	22459
Channels	4
Supply Votlage	Mains

Stabilised Power Supplies	3 off
Make	FARNELL INSTRUMENTS
Type	L30B
Serial No.	005470, 003804, 003521
Output Voltages	0-30 volts d.c.
Output Current	1 ampere maximum
Supply Voltage	Mains.

Dual Stabilised Power Supply — 1 off

Make	FARNELL INSTRUMENTS
Type	L30BT
Serial No.	003503
Output Voltage	0-30 volts d.c. each channel
Output Current	1 ampere maximum each channel
Supply Voltage	Mains.

Electron Magnets — 2 off

Make	R.A.WILLIAMS (B'HAM) LTD.
Type	STERO LM7
Supply Voltage	24 volts d.c.

Power Supply — 1 off

Make	MARCONI INSTRUMENTS LTD
Type	TF 2151
Serial No.	50841
Output Voltage	0-30 volts d.c.
Output Current	4 amperes maximum
Supply Voltage	Mains.

Solenoid — 1 off

Make	R.A.WILLIAMS (B'HAM) LTD.
Type	STERO SOL 4
Supply Voltage	24 volts d.c.

Electric Motor		1 off
Make	TACON INC.	
Type	Capacitor start	
Serial No.	2-7521	
Supply Voltage	110 volts a.c.	

Power Supply		1 off
Make	CLAUDE LYONS LTD.	
Type	REDULAC RK13-M	
Output Voltage	0-240 volts a.c.	
Output Current	15 amperes maximum	
Supply Voltage	Mains.	

Reduction Gearbox		1 off
Make	SANDERSON BROTHERS AND NEWBOULD LTD.	
Type	Heliocentre speed reducer type E	
Serial No.	7520	
Gear Ratio	40:1	

Flexible Couplings		1 off
Make	FENNER	
Type	65F H.R.C. and 85F H.R.C.	

APPENDIX J

DESIGN CALCULATIONS

Drop Height

$$V^2 = U^2 + 2gS$$

where V = final velocity
U = initial velocity
S = distance of fall
g = acceleration due to gravity

U = 0 at moment of release

$$S = \frac{V^2}{2g}$$

Maximum velocity = 8 ms^{-1} and g = 9.81 ms^{-2}

maximum height required. S = 3.262 m

Overall Height of Test Rig

Base height	0.760 m
Extrusion device height	0.710 m
Drop height	3.262 m
Mass height	0.250 m
Release mechanism height	0.170 m
Rope pulley system height.	0.258 m
Total height	5.410 m

Load Cell

Maximum force - 300 kN.

E.Young's modulus of elasticity for Titanium Alloy 103 kN/mm^2.

Maximum allowable strain in load cell 0.5%.

$E = \frac{\text{stress}}{\text{strain}}$ stress = E x strain = 515 $N\ mm^{-2}$

Area necessary to support 300 kN at a maximum stress of 515 Nmm^{-2} is 582.5 mm^2.

Bore of load cell d = 55.00 mm.

from $\frac{\pi}{4} (D^2 - d^2) = 582.5\ mm^2$

$D = 61.40$ mm

manufacture at 62.00 mm dia.

Die

Maximum bending stresses will be found in the larger dies with the highest extrusion ratios.

Approximated to a plate under uniform pressure and supported at outer edges.

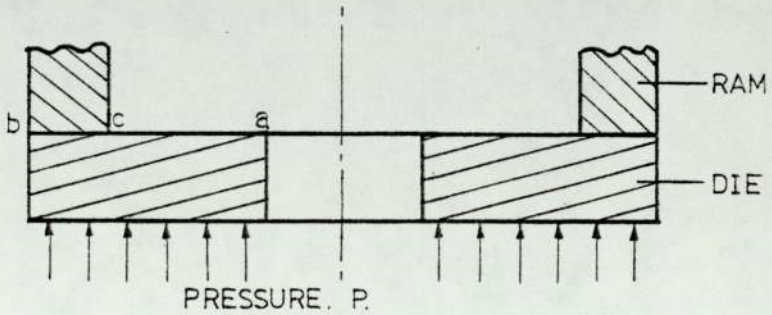

Boundary conditions at $r = a$, $Mr = 0$, $r = b$, $Mr - 0$,
$r = c$, $w = 0$, $r = b$, $w = 0$

$$\frac{1}{r}\frac{d}{dr}\left[r\frac{d}{dr}\left[\frac{1}{r}\frac{d}{dr}\left[r\frac{dw}{dr}\right]\right]\right] = \frac{P}{D}$$

$$r\frac{d}{dr}\left[\frac{1}{r}\frac{d}{dr}\left[r\frac{dw}{dr}\right]\right] = \frac{1}{D}\int_a^r pr\,dr$$

$$r\frac{d}{dr}\left[\frac{1}{r}\frac{d}{dr}\left[r\frac{dw}{dr}\right]\right] = \frac{P}{2D}\left[r^2 - a^2\right]$$

$$\frac{1}{r}\frac{d}{dr}\left[r\frac{dw}{dr}\right] = \frac{Pr^2}{4D} - \frac{Pa^2\ln r}{2D} + C_1$$

$$r\frac{dw}{dr} = \frac{Pr^4}{16D} - \frac{Pa^2r^2\ln r}{4D} + \frac{Pa^2r^2}{8D} + \frac{C_1r^2}{2} + C_2$$

$$w = \frac{Pr^4}{64D} - \frac{Pa^2r^2\ln r}{8D} + \left[\frac{Pa^2 + C_1}{8D\quad 4}\right]r^2 + C_2\ln r + C_3$$

$r = C, \quad w = 0$

$$0 = \frac{Pc^4}{64D} - \frac{Pa^2c^2 \ln r}{8D} - \frac{Pa^2c^2}{8D} + \frac{C_1c^2}{4} + C_2 \ln c + C_3 \qquad (1)$$

also $Mr = -D\left[\frac{d^2w}{dr^2} + \nu\frac{1}{r}\frac{dw}{dr}\right] \qquad M\psi = D\left[\frac{1}{r}\frac{dw}{dr} + \nu\frac{d^2w}{dr}\right]$

$$\frac{dw}{dr} = \frac{Pr^3}{16D} - \frac{Pa^2 r \ln r}{4D} + \frac{Pa^2 r}{8D} + \frac{C_1 r}{2} + \frac{C_2}{r}$$

$$\frac{d^2w}{dr} = \frac{3Pr^3}{16D} - \frac{Pa^2 \ln r}{4D} - \frac{Pa^2}{8D} + \frac{C_1}{2} - \frac{2C_2}{r^2}$$

$$Mr = -D\left[(3+\nu)\frac{Pr^2}{16D} - (1+\nu)\frac{Pa^2 \ln r}{4D} - (1-\nu)\frac{Pa^2}{8D} + (1+\nu)\frac{C_1}{2} - (2-\nu)\frac{C_2}{r^2}\right]$$

$\nu = 0.3$ for Titanium alloy

at $r = b$

$$Mr = 0 = -D\left[\frac{3.3Pb^2}{16D} - \frac{1.3\,Pa^2 \ln b}{4D} - \frac{0.7Pa^2}{8D} + \frac{1.3C_1}{2} - \frac{1.7C_2}{b^2}\right] \qquad (2)$$

at $r = a$

$$Mr = 0 = -D\left[\frac{3.3\,Pa^2}{16D} - \frac{1.3Pa^2 \ln a}{4D} - \frac{0.7\,Pa^2}{8D} + \frac{1.3C_1}{2} - \frac{1.7C_2}{2}\right] \qquad (3)$$

(2) - (3)

$$\frac{3.3P}{16D}(b^2-a^2) - \frac{1.3Pa^2 \ln b/a}{4D} - 1.7C\left|1/b^2 - 1/a^2\right|$$

$$C = \frac{1}{1.7}\left[\frac{1}{1/b^2 - 1/a^2}\right]\left[\frac{3.3P}{16D}\left[b^2 - a^2\right] - \frac{1.3Pa^2}{4D} \ln b/a\right]$$

$b = 37.5$ mm $a = 8.5$ mm $c = 27.5$ mm

$$D = \frac{Eh^3}{12(1-\nu^2)} = 17.77 \times 10^3 h^3 \ N\ mm^{-2}$$

$$C_2 = -10.765 \times \frac{10^3 P}{D} = -0.6057 \frac{P}{h^3} \frac{mm^6}{N}$$

from (2)

$$C_1 = \frac{2}{1.3}\left[\frac{1.3\ Pa^2 \ln b}{4D} - \frac{3.3Pb^2}{16D} + \frac{0.72Pa^2}{8D} + \frac{1.7C_2}{b^2}\right]$$

$$C = 5.499 \times 10^{-3} \frac{P}{h^3} \frac{mm^4}{N}$$

From (1)

$$C_3 = \frac{Pa^2c^2 \ln c}{8D} - \frac{Pc^4}{64D} + \frac{Pa^2c^2}{8D} - \frac{C_1c^2}{4} - C_2 \ln c$$

$$C_3 = 2.123 \frac{P}{h^3} \frac{mm^6}{N}$$

$P = 300\ kN / 4.417 \times 10^{3}\ mm^{2} = 67.91\ N\ mm^{-2}$

let $h = 25$ mm

hence W at inner edge $a = 8.5$ mm

$\underline{w = 3.867 \times 10^{-3}\ mm}$ very small

Container

Thick cylinder theory.

$$\sigma_1 = \left[(D^2 + d^2) / (D^2 - d^2) \right] P$$

Smallest dia. $d = 12.5$ mm area $= 122.7\ mm^2$

Extrusion pressure for pure Aluminium at 94% reduction of area(from Johnson and Mellor page 337) $= 600\ N\ mm^{-2}$.

Assume liquid.

$$\sigma_2 = -600\ N\ mm^{-2}$$

let $D = 87.5$ mm

$\sigma_1 = 625\ N\ mm^{-2}$

Tresca Yield criterion.

$$\frac{\hat{\sigma} - \check{\sigma}}{2} = k$$

$k = 612.5\ N\ mm^{2}$

0.2% Proof stress of E.N. 26. $(2k) = 1400\ N\ mm^{-2}$

(at H.R.C. 54)

Power required to lift the falling mass.

Maximum falling mass	120 kg
Mass of release mechanism	30 kg
Total moving mass	150 kg

Reduction gearbox ratio	40:1
Rope pulley ratio	3:1
Total reduction	120:1

Force on rope drum 50 kg $\simeq$ 500 N

Assume maximum diameter of 300 mm

Torque on rope drum 150 Nm

Motor Speed	980 r.p.m.
Drum Speed	24.5 r.p.m.

Power = 193 W

Allow efficiency of rope pulley system	90%
Allow efficiency of gearbox	80%
System efficiency	72%

Power required = 270W = 0.35 h.p.

APPENDIX K

PARTS LIST AND MANUFACTURING

DRAWINGS

EXTRUSION DIE ASSEMBLY.

DRG. No. 000 PART LIST.

PART No.	No. OFF.	DESCRIPTION.	MATERIAL.
001-006	30	DIE.	SVERKER .3.
007-012	5	CONTAINER.	EN.26.
013-018	5	CONTAINER BASE PLATE.	EN.26.
019-024	18	RAM.	SVERKER.3.
025-026	2	ADAPTOR.	EN.26.
027	1	BASE COVER.	EN.26.
028	1	TOP COVER.	EN.26.
029	2	LOAD CELL.	TITANIUM ALLOY.
030	1	IMPACT COVER.	EN.26.
031-036	6	SLEEVE.	MILD STEEL.
037	1	INNER SUPPORT.	MILD STEEL.
038	1	OUTER JACKET.	MILD STEEL.
039	1	GUIDE.	MILD STEEL.
040	1	DISPLACEMENT ARM.	MILD STEEL.
041	4	SOCKET SCREW.	M12x50 - 6g.
042	4	T-NUT.	MILD STEEL.
043	4	WASHER.	24 O/D-13 I/D -2.5
044	24	SET SCREW.	M6 x 20-6g.
045	30	WASHER.	12.5 O/D-6.4 I/D-1.6
046	6	SET SCREW.	M8 x 20 - 6g.
047	6	WASHER.	17 O/D-8.4 I/D - 1.6
048	6	SOCKET SCREW.	M6 x 22 - 6g.
049	6	SOCKET SCREW.	M12x30 - 4 h.

DO NOT SCALE.

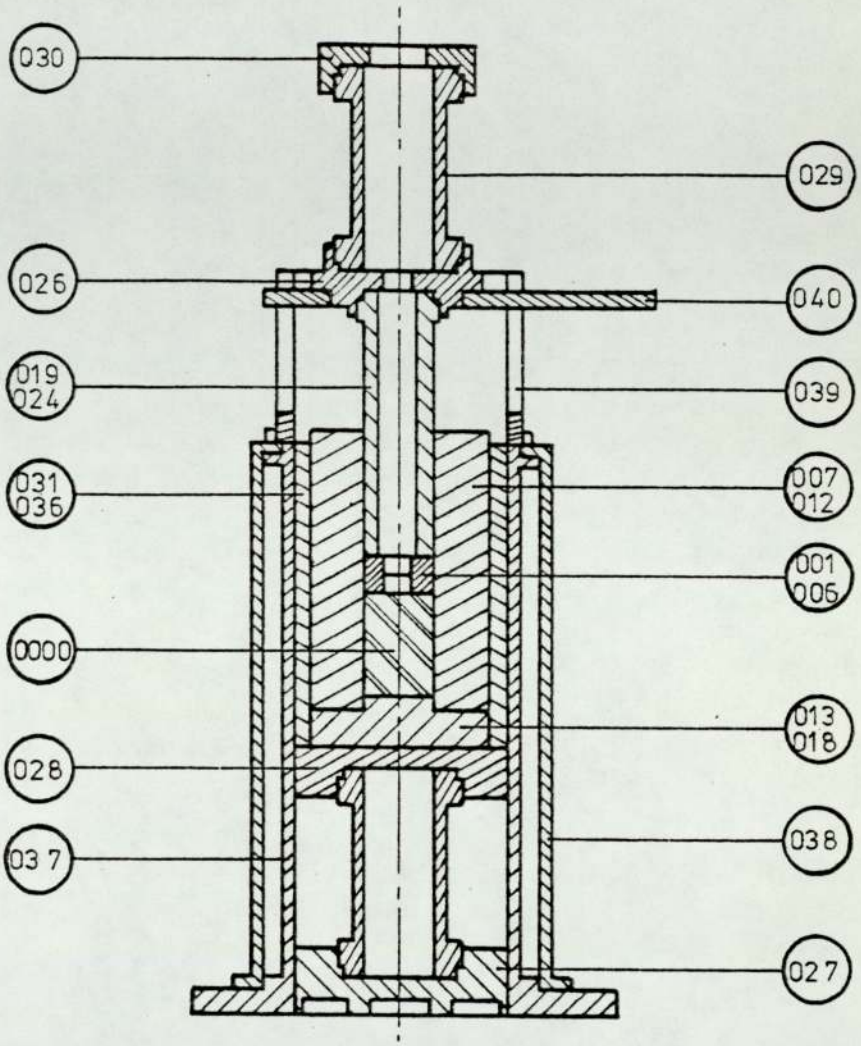

MATERIAL. MILD STEEL.

TOLERANCE EXCEPT WHERE OTHERWISE STATED ± 0·20.

ALL DIMENSIONS ARE IN mm. UNLESS OTHERWISE STATED.

EXTRUSION DIE ASSEMBLY.	DRG. No. 000.
THE UNIVERSITY OF ASTON IN BIRMINGHAM.	SCALE. 1:2
DEPARTMENT OF PRODUCTION ENGINEERING.	P.J. LEAVESLEY.

DO NOT SCALE.

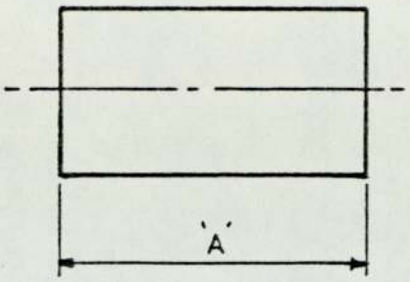

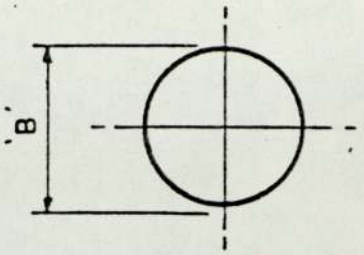

ALUMINIUM TEST BILLETS.

SLUG DIAMETER. 'B'	SLUG LENGTH. 'A'				
	12·50	25·00	37·50	50·00	75·00
12·50	25	25	25	25	25
25·00	25	21	20	15	11
37·50	22	12	11	6	6
50·00	20	11	6	6	6
75·00	-	-	-	-	-

POLYPROPYLENE TEST BILLETS

SLUG DIAMETER. 'B'	SLUG LENGTH. 'A'				
	12·50	25·00	37·50	50·00	75·00
12·50	25	25	25	25	25
25·00	25	25	25	25	25
37·50	25	25	25	21	20
50·00	25	21	20	15	11
75·00	23	12	11	6	6

ALL DIMENSIONS ARE IN mm UNLESS OTHERWISE STATED.

TOLERANCE SLUG LENGTH ± 0·10.

SLUG DIAMETER $^{+\ 0\cdot00}_{-\ 0\cdot10}$

TEST BILLETS.	DRG. No. 0000.
THE UNIVERSITY OF ASTON IN BIRMINGHAM.	SCALE: FULL SIZE.
DEPARTMENT OF PRODUCTION ENGINEERING.	P.J. LEAVESLEY.

DO NOT SCALE.

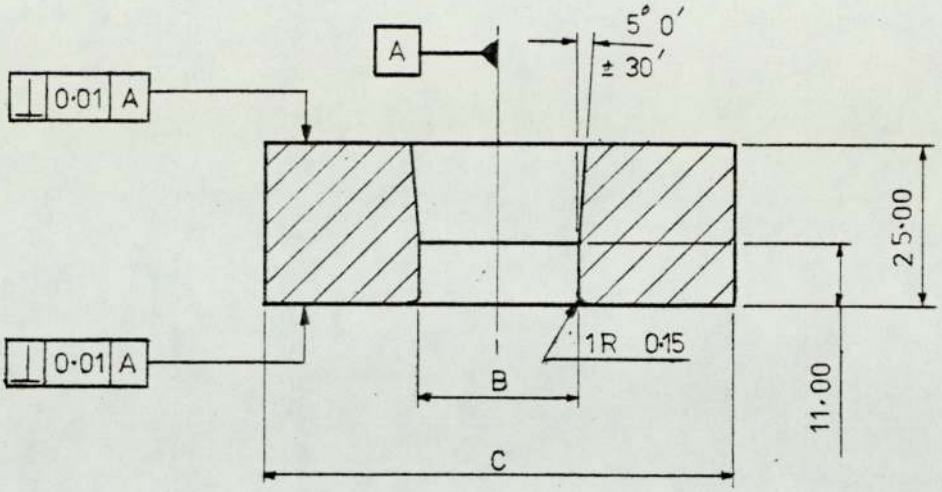

Diameter C	Diameter B
75.000	53.033
75.000	47.434
75.000	41.079
75.000	33.541
75.000	23.717
75.000	16.771
62.500	44.194
62.500	39.528
62.500	34.223
62.500	27.951
62.500	19.764
62.500	13.975
50.000	53.355
50.000	31.623
50.000	27.836
50.000	22.361
50.000	15.811
50.000	11.180

Diameter C	Diameter B
37.500	26.517
37.500	23.717
37.500	20.540
37.500	16.771
37.500	11.859
37.500	8.358
25.000	17.678
25.000	15.811
25.000	13.693
25.000	11.180
25.000	7.906
25.000	5.590
12.500	8.839
12.500	7.906
12.500	6.847
12.500	5.590
12.500	3.953
12.550	2.795

MATERIAL

UDDHOLM STEEL. UHB SVERKER 3.

HEAT TREATMENT

PROTECTION AGAINST DECARBORIZATION. NEUTRAL SALT BATH OR PROTECTIVE ATMOSPHERE

PRE-HEAT TEMPERATURE. 600-700°C

AUSTENITINZING 920°C 60min SOAK 65 HRC
960°C 30min SOAK 66 HRC
1000°C 15min SOAK 66 HRC

QUENCHING MEDIA OIL OR AIR

TEMPERING TWICE. SLOW HEATING. NO COLOURS.
300°C TO GIVE HARDNESS 60 HRC ± 2

TOLERANCE EXCEPT WHERE OTHERWISE STATED ± 0·20.

ALL DIMENSIONS ARE IN mm. UNLESS OTHERWISE STATED.

DIE	DRG. No. 001-006
THE UNIVERSITY OF ASTON IN BIRMINGHAM.	SCALE : FULL SIZE.
DEPARTMENT OF PRODUCTION ENGINEERING.	P.J. LEAVESLEY.

DO NOT SCALE.

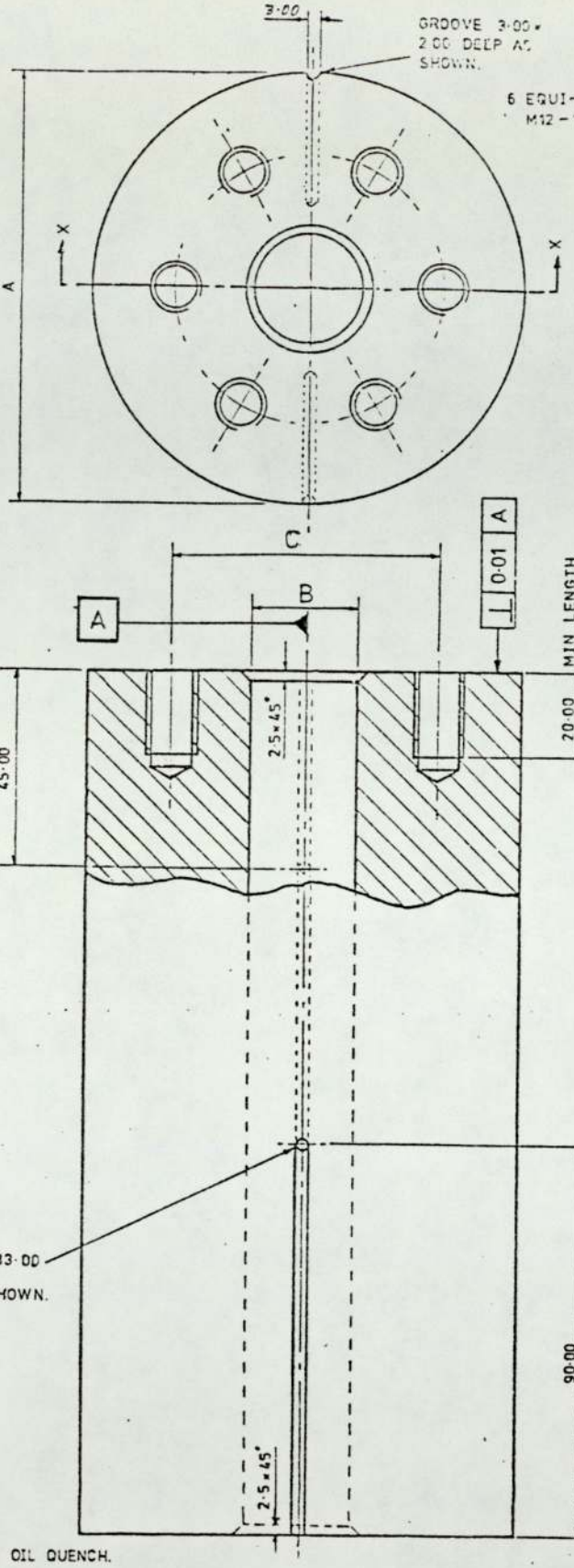

DIAMETER A	DIAMETER B	P.C.D. C
150·000	75·040	112·500
137·500	62·540	100·000
125·000	50·040	87·500
112·500	37·540	75·000
100·000	25·040	62·500
87·500	12·540	50·000

MATERIAL.
EN. 26.
HARDENING. 820-850°C OIL QUENCH.
TEMPERING. 250°C AIR COOL.
TO GIVE HARDNESS 54 HRC ± 2.

TOLERANCE ON DIAMETERS A ±0·015 B ±0·005

TOLERANCE EXCEPT WHERE OTHERWISE STATED ± 0·20.

ALL DIMENSIONS ARE IN mm. UNLESS OTHERWISE STATED.

CONTAINER

DRG. No. 007-012

THE UNIVERSITY OF ASTON IN BIRMINGHAM.

SCALE 1:2

DEPARTMENT OF PRODUCTION ENGINEERING.

P.J. LEAVESLEY.

DO NOT SCALE.

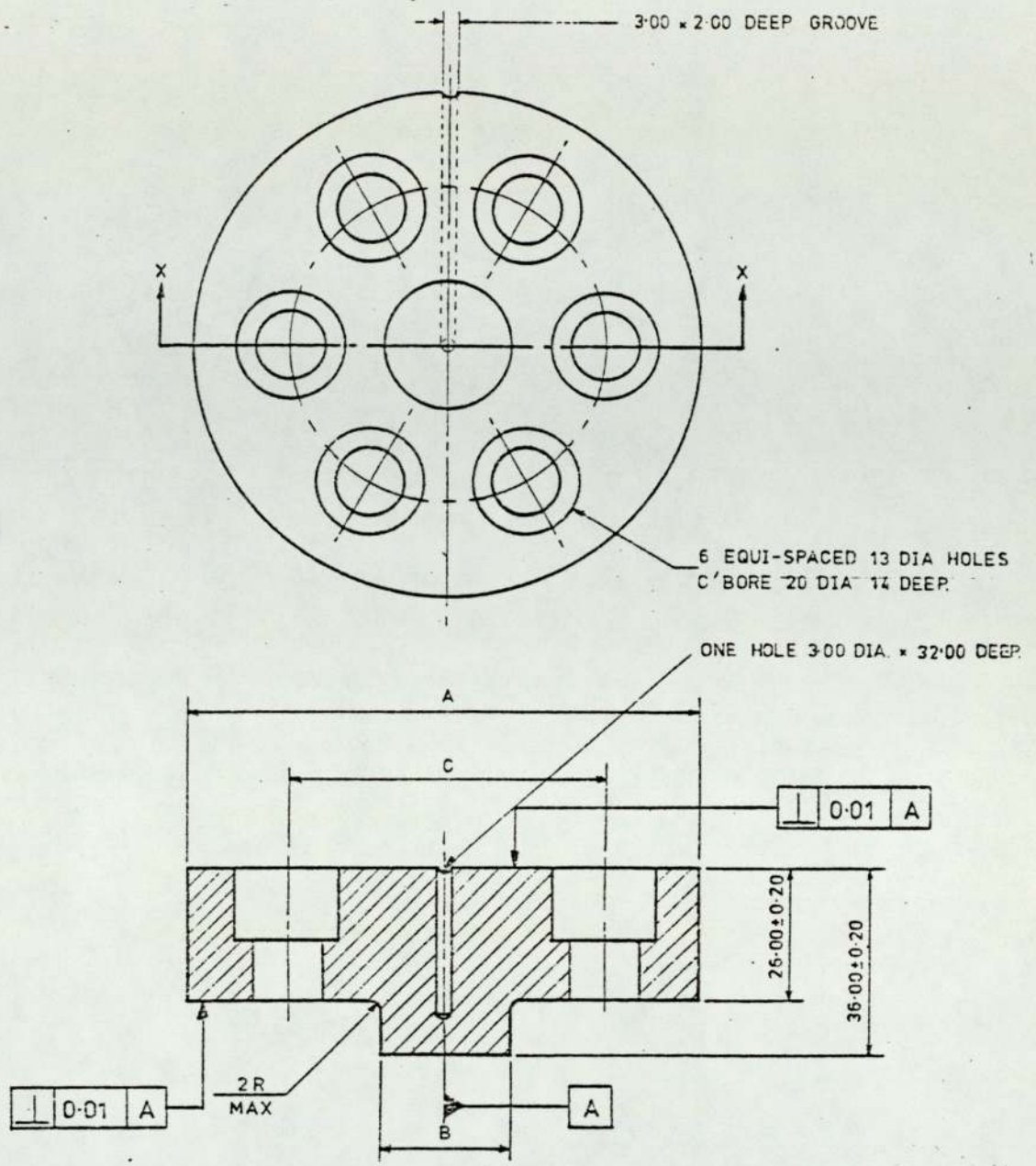

SECTION ON XX

DIAMETER A	DIAMETER B	P.C.D. C	NO OFF.	PART NUMBER.
150·000	75·000	112·500	1.	013.
137·500	62·500	100·000	1.	014.
125·000	50·000	87·500	1.	015.
112·500	37·500	75·000	1.	016.
100·000	25·000	62·500	1.	017.
87·500	12·500	50·000	1.	018.

MATERIAL.

EN. 26.

HARDENING. 820 - 850°C OIL QUENCH.

TEMPERING. 250°C AIR COOL.

TO GIVE HARDNESS 54 HRC ± 2.

TOLERANCE ON DIAMETERS B ±0·005
A ±0·015

TOLERANCE EXCEPT WHERE OTHERWISE STATED ± 0·20.

ALL DIMENSIONS ARE IN mm. UNLESS OTHERWISE STATED.

CONTAINER BASE PLATES.	DRG. No. 013-018
THE UNIVERSITY OF ASTON IN BIRMINGHAM.	SCALE: FULL SIZE.
DEPARTMENT OF PRODUCTION ENGINEERING.	P.J. LEAVESLEY.

DO NOT SCALE.

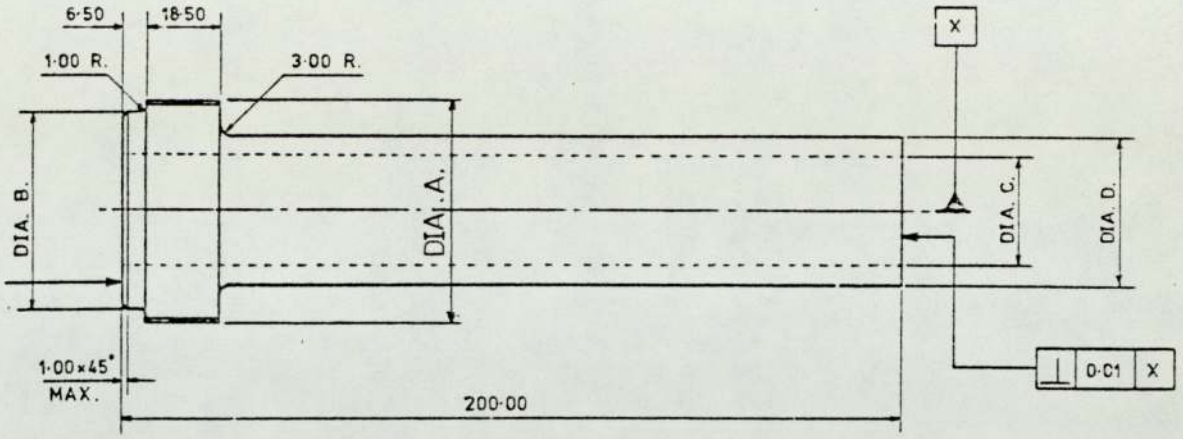

DIAMETER. A.	DIAMETER. B. ±0·05	DIAMETER. C. ±0·05	DIAMETER. D. $^{+0.000}_{-0.020}$	NO. OFF.	PART. NO.
M80×2·0-4h.	75·90	55·00	75·000	1.	019.
M80×2·0-4h.	75·90	45·50	62·500	1.	020.
M80×2·0-4h.	75·90	36·50	50·000	1.	021.
M56×2·0-4h.	49·90	27·50	37·500	1.	022A.
M56×2·0-4h.	49·90	25·00	37·500	1.	022B.
M56×2·0-4h.	49·90	22·00	37·500	1.	022C.
M56×2·0-4h.	49·90	19·00	25·000	1.	023A.
M56×2·0-4h.	49·90	17·00	25·000	1.	023B.
M56×2·0-4h.	49·90	14·80	25·000	1.	023C.
M56×2·0-4h.	49·90	12·50	25·000	1.	023D.
M56×2·0-4h.	49·90	9·00	25·000	1.	023E.
M56×2·0-4h.	49·90	6·80	25·000	1.	023F.
M56×2·0-4h.	49·90	10·00	12·500	1.	024A.
M56×2·0-4h.	49·90	9·00	12·500	1.	024B.
M56×2·0-4h.	49·90	8·00	12·500	1.	024C.
M56×2·0-4h.	49·90	6·80	12·500	1.	024D.
M56×2·0-4h.	49·90	5·00	12·500	1.	024E.
M56×2·0-4h.	49·90	4·00	12·500	1.	024F.

MATERIAL.

UDDHOLM STEEL. UHB SVERKER 3.

HEAT TREATMENT.

PROTECTION AGAINST DECARBURIZATION. NEUTRAL SALT BATH.
OR PROTECTIVE ATMOSPHERE.

PRE-HEAT TEMPERATURE. 600-700°C.

AUSTENITINZING 920°C 60 min. SOAK. 65 HRC.
960°C 30 min. SOAK. 66 HRC.
1000°C 15 min. SOAK. 66 HRC.

QUENCHING MEDIA. OIL OR AIR.

TEMPERING. TWICE. SLOW HEATING. NO COLOURS.
500°C TO GIVE HARDNESS 58 HRC ± 2.

TOLERANCE EXCEPT WHERE OTHERWISE STATED ± 0·20.

ALL DIMENSIONS ARE IN mm. UNLESS OTHERWISE STATED.

RAM.	DRG. No. 019–024.
THE UNIVERSITY OF ASTON IN BIRMINGHAM.	SCALE. 1:2
DEPARTMENT OF PRODUCTION ENGINEERING.	P.J. LEAVESLEY.

DO NOT SCALE.

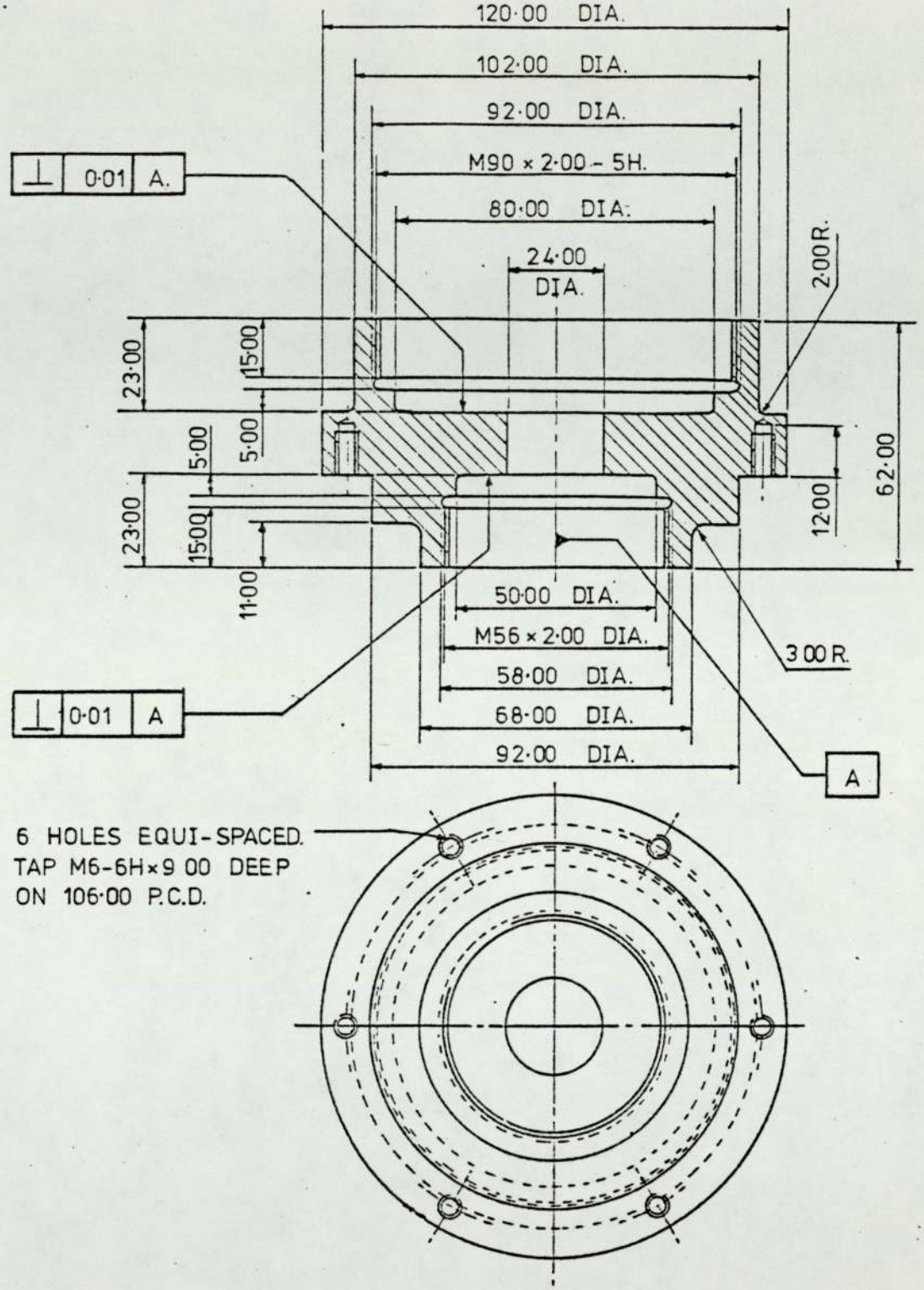

MATERIAL.

EN 26.
HARDENING 820-850°C OIL QUENCH.
TEMPERING 600°C AIR COOL.
TO GIVE HARDNESS 38 HRC ±2

TOLERANCE EXCEPT WHERE OTHERWISE STATED ± 0·20.

1 OFF.

ALL DIMENSIONS ARE IN mm. UNLESS OTHERWISE STATED.

ADAPTOR.	DRG. No. 025
THE UNIVERSITY OF ASTON IN BIRMINGHAM.	SCALE. 1:2
DEPARTMENT OF PRODUCTION ENGINEERING.	P.J. LEAVESLEY.

DO NOT SCALE.

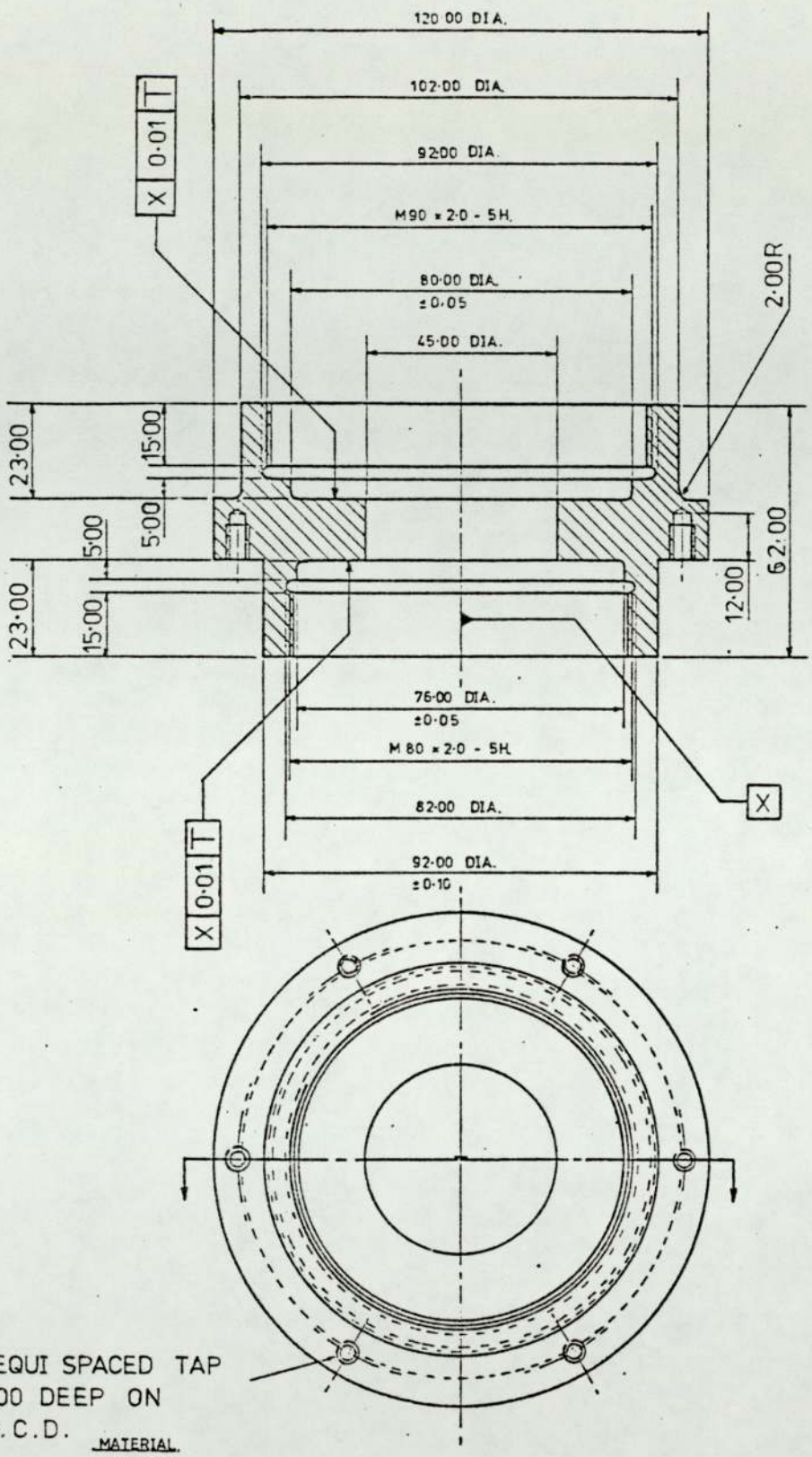

6 HOLES EQUI SPACED TAP
M6-6H × 9·00 DEEP ON
106·00 P.C.D.

MATERIAL.

EN. 26.
HARDENING 820-850°C OIL QUENCH.
TEMPERING 600°C AIR COOL.
TO GIVE HARDNESS 38 HRC ± 2.

MATERIAL.

TOLERANCE EXCEPT WHERE OTHERWISE STATED ± 0·20.

ALL DIMENSIONS ARE IN mm. UNLESS OTHERWISE STATED.

ADAPTOR.	DRG. No. 026.
THE UNIVERSITY OF ASTON IN BIRMINGHAM.	SCALE. 1:2
DEPARTMENT OF PRODUCTION ENGINEERING.	P.J. LEAVESLEY.

DO NOT SCALE.

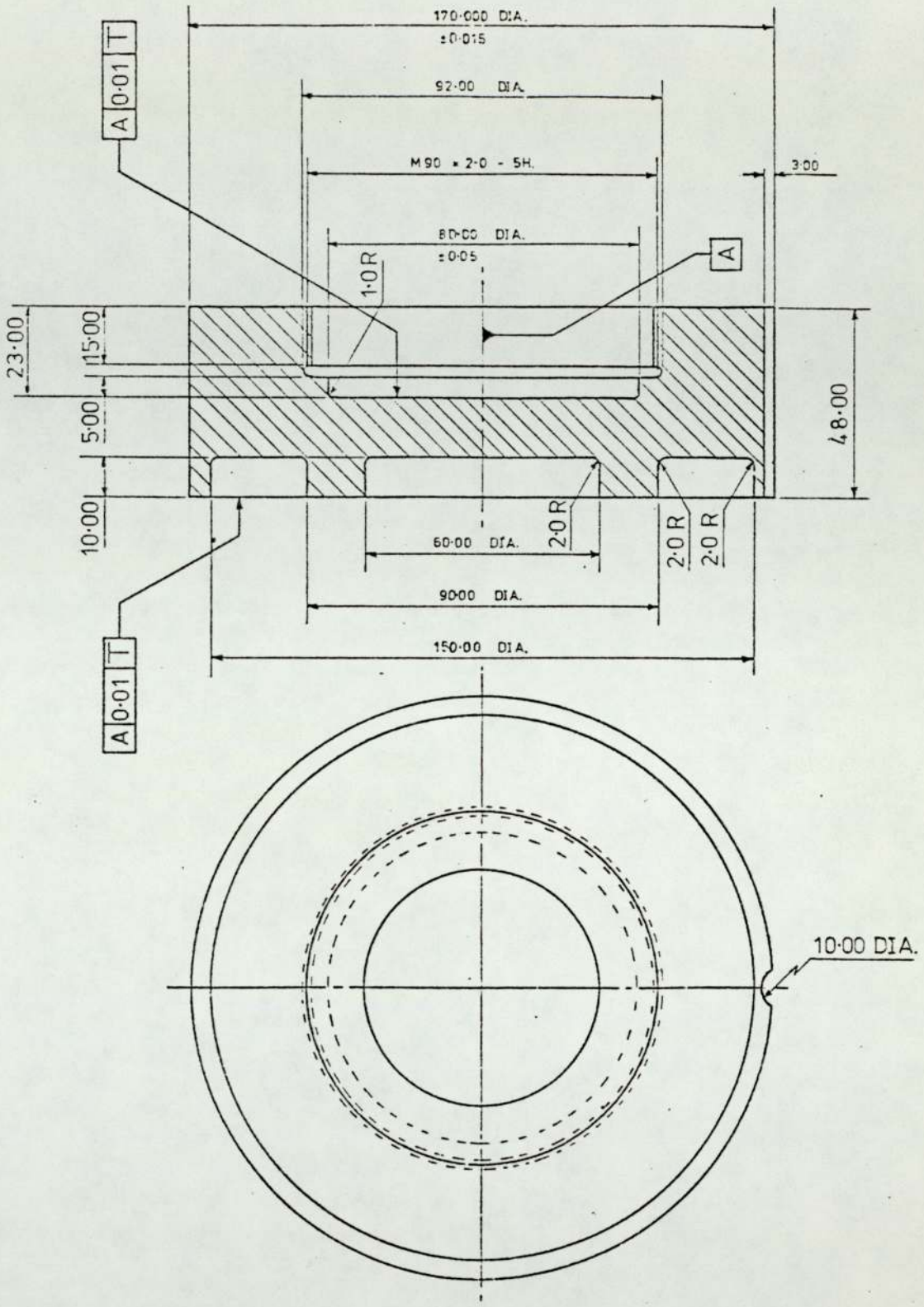

MATERIAL.

EN. 26.

HARDENING 820–850°C OIL QUENCH.

TEMPERING 600°C AIR COOL.

TO GIVE HARDNESS 38 HRC ±2.

TOLERANCE EXCEPT WHERE OTHERWISE STATED ± 0·20.

ALL DIMENSIONS ARE IN mm. UNLESS OTHERWISE STATED.

BASE COVER	DRG. No. 027
THE UNIVERSITY OF ASTON IN BIRMINGHAM.	SCALE 1:2
DEPARTMENT OF PRODUCTION ENGINEERING.	P.J. LEAVESLEY.

DO NOT SCALE.

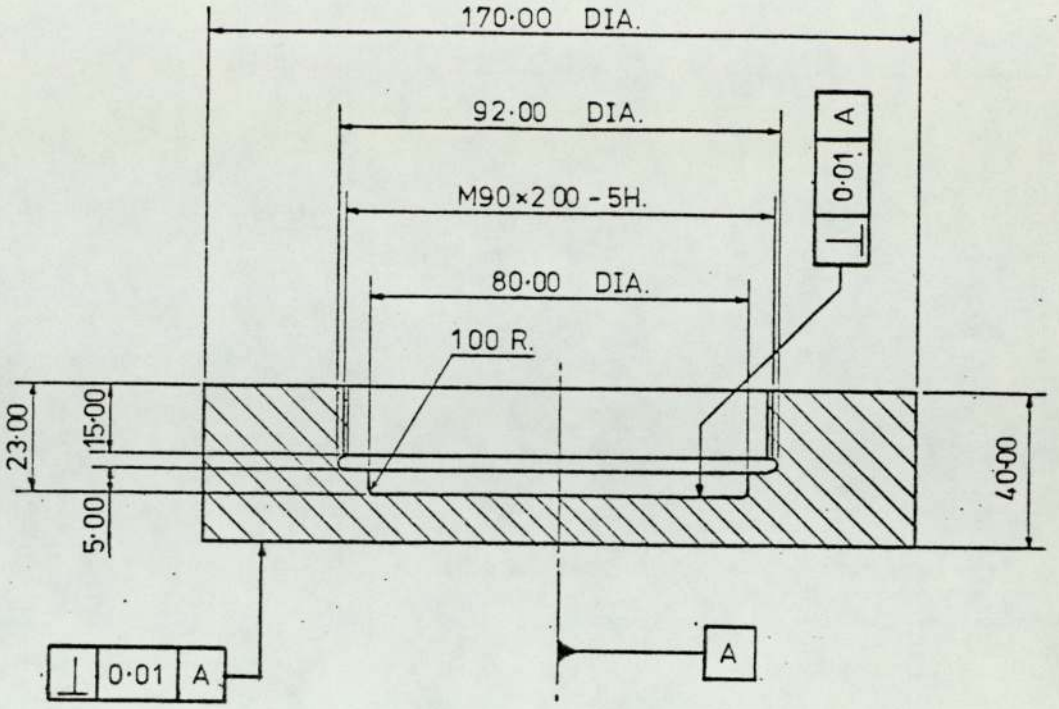

SECTION AA.

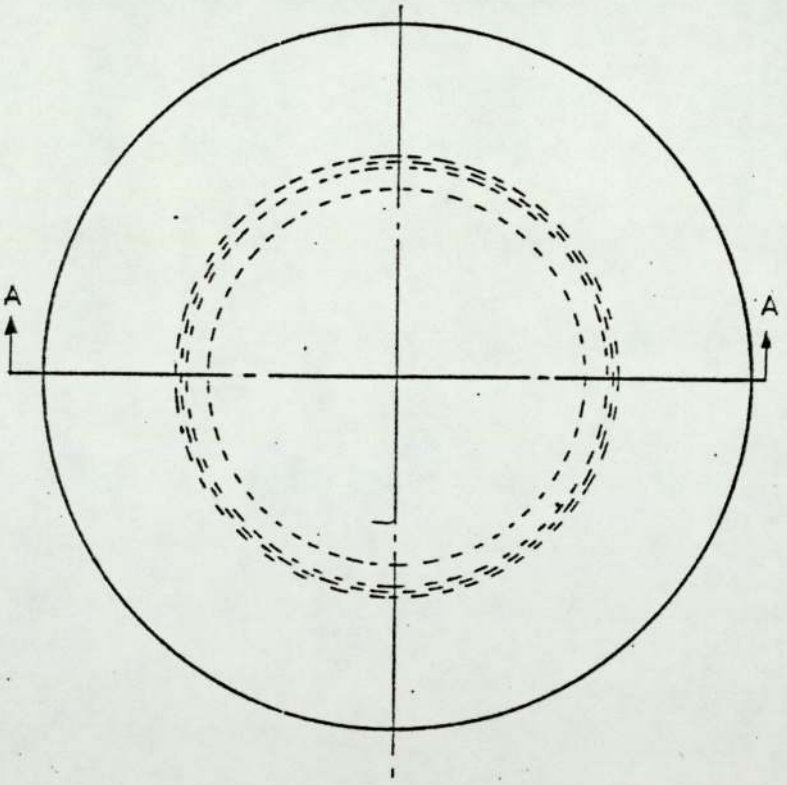

MATERIAL.

EN 26.
HARDENING 820 850°C OIL QUENCH.
TEMPERING 600°C AIR COOL.
TO GIVE HARDNESS 38 HRC ± 2.

1 OFF.

TOLERANCE EXCEPT WHERE OTHERWISE STATED ± 0·20.

ALL DIMENSIONS ARE IN mm. UNLESS OTHERWISE STATED.

TOP COVER.	DRG. No. 028
THE UNIVERSITY OF ASTON IN BIRMINGHAM.	SCALE 1:2
DEPARTMENT OF PRODUCTION ENGINEERING.	P.J. LEAVESLEY.

DO NOT SCALE.

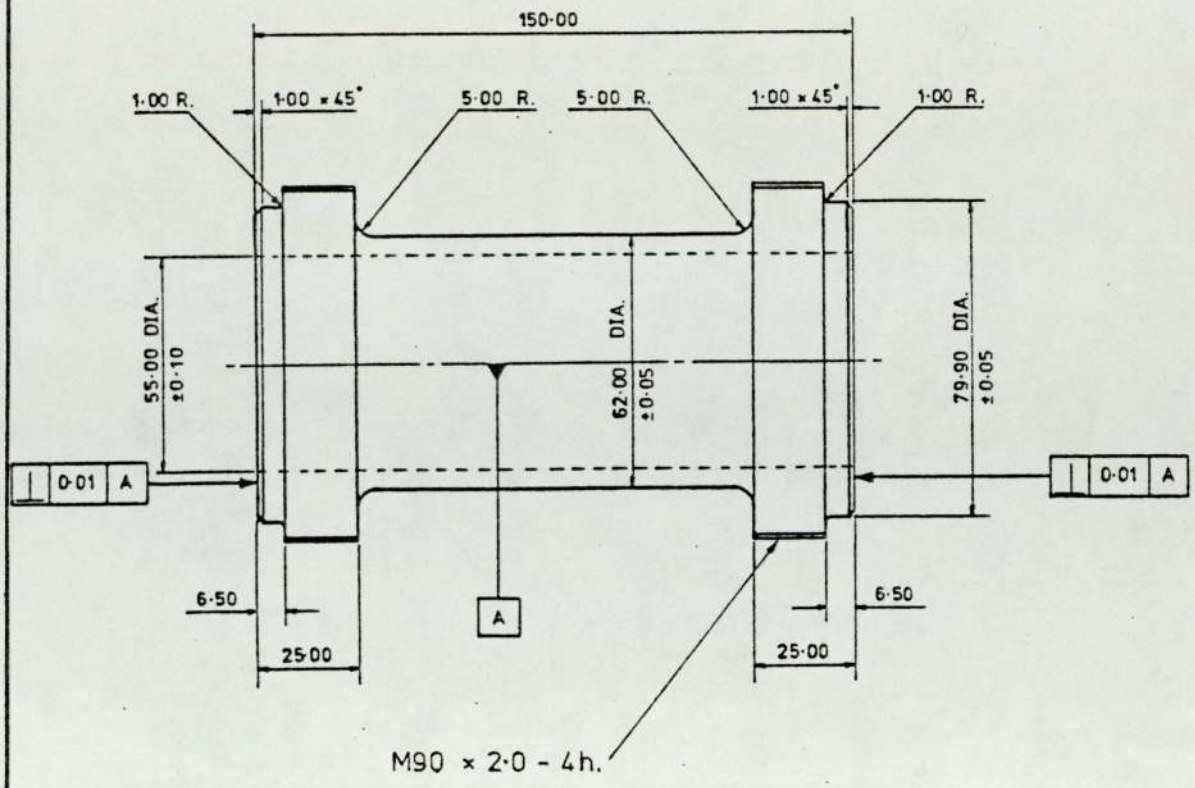

MATERIAL. TITANIUM ALLOY.

TOLERANCE EXCEPT WHERE OTHERWISE STATED ± 0·20.

ALL DIMENSIONS ARE IN mm. UNLESS OTHERWISE STATED.

LOAD CELL.	DRG. No. 029.
THE UNIVERSITY OF ASTON IN BIRMINGHAM.	SCALE. 1:2
DEPARTMENT OF PRODUCTION ENGINEERING.	P.J. LEAVESLEY.

DO NOT SCALE.

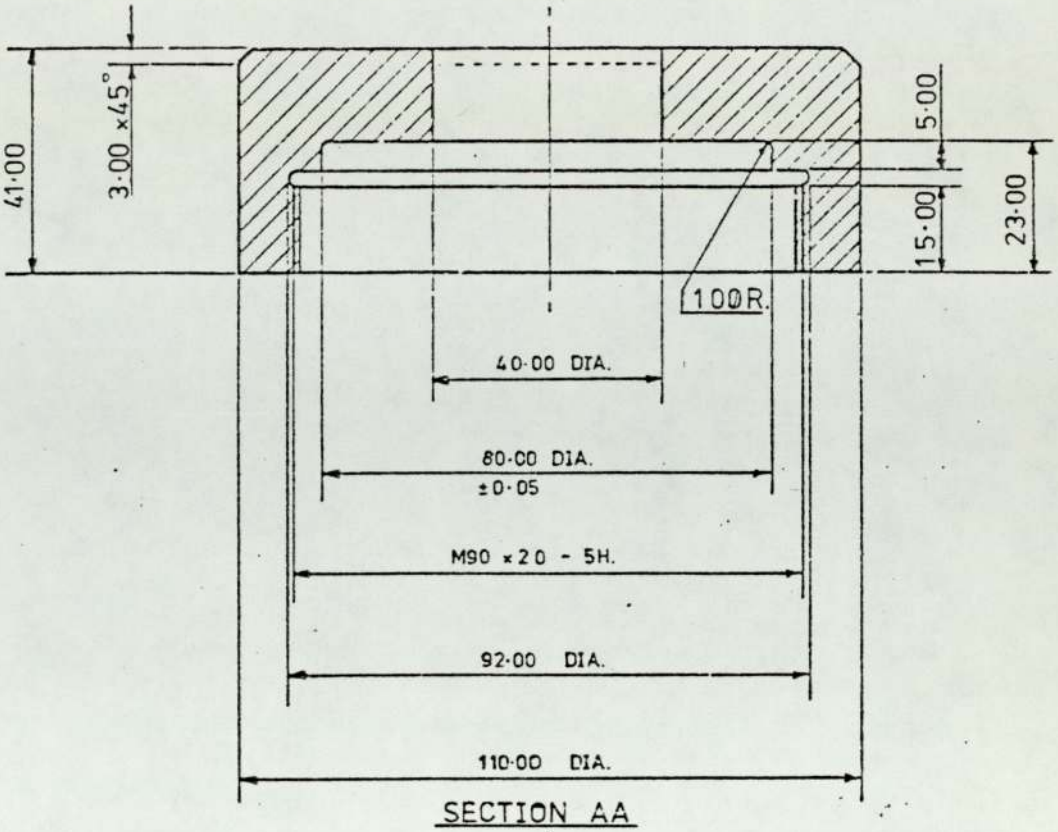

SECTION AA

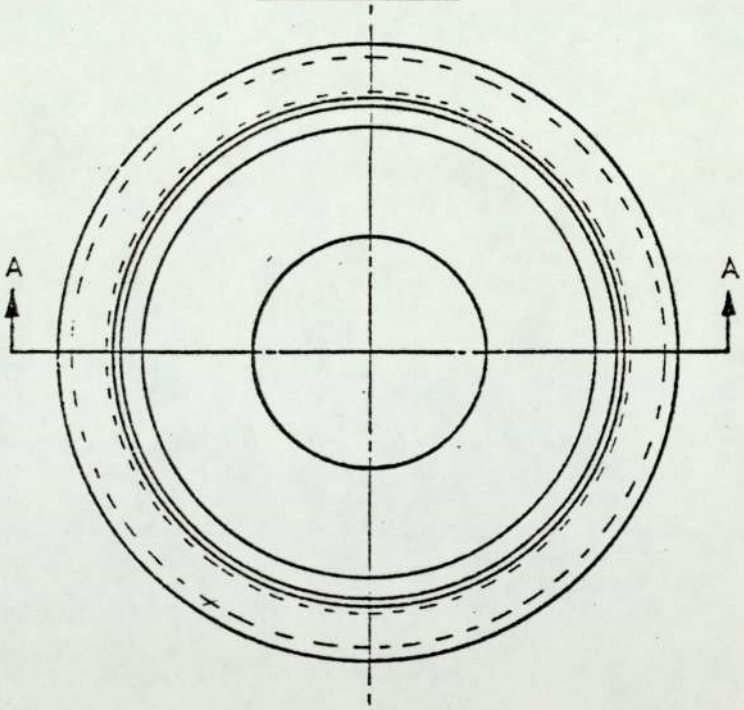

MATERIAL.

EN 26.

HARDENING 820–850°C OIL QUENCH.

TEMPERING 650°C AIR COOL.

TO GIVE HARDNESS 33 HRC ± 2.

1 OFF.

TOLERANCE EXCEPT WHERE OTHERWISE STATED ± 0·20.

ALL DIMENSIONS ARE IN mm. UNLESS OTHERWISE STATED.

IMPACT COVER.	DRG. No. 030
THE UNIVERSITY OF ASTON IN BIRMINGHAM.	SCALE: FULL SIZE.
DEPARTMENT OF PRODUCTION ENGINEERING.	P.J. LEAVESLEY.

DO NOT SCALE.

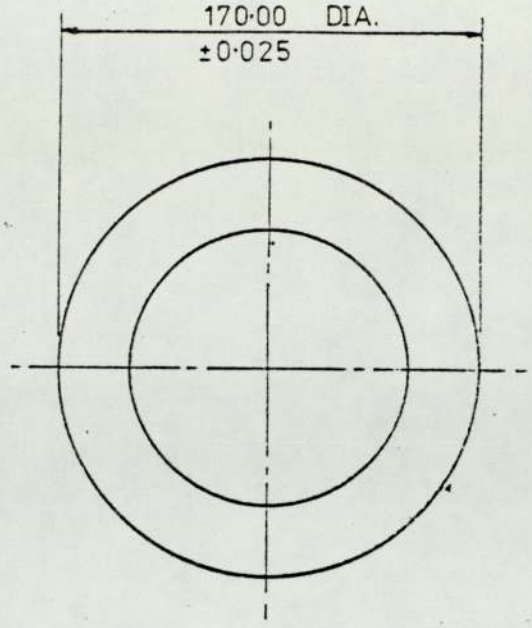

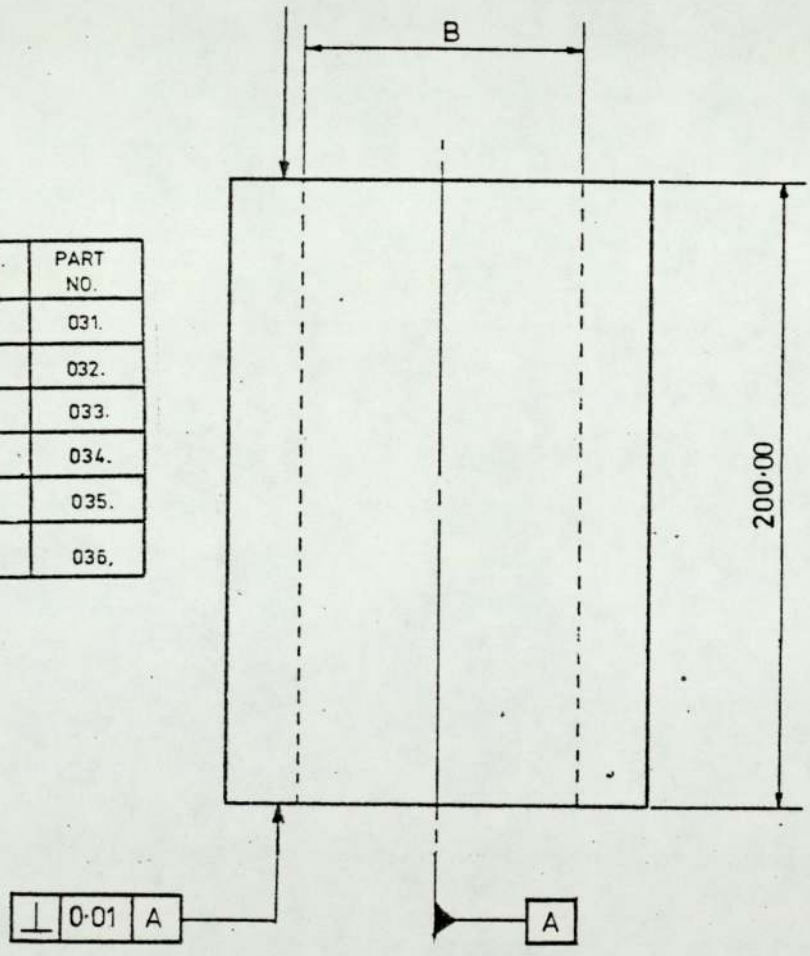

DIAMETER. B	NO. OFF.	PART NO.
150·045	1.	031.
137·545	1.	032.
125·045	1.	033.
112·545	1.	034.
100·045	1.	035.
87·545	1.	036.

MATERIAL. MILD STEEL.

TOLERANCE EXCEPT WHERE OTHERWISE STATED ± 0·20.

ALL DIMENSIONS ARE IN mm. UNLESS OTHERWISE STATED.

SLEEVE.	DRG. No. 031 - 036
THE UNIVERSITY OF ASTON IN BIRMINGHAM.	SCALE 1:3
DEPARTMENT OF PRODUCTION ENGINEERING.	P.J. LEAVESLEY.

DO NOT SCALE.

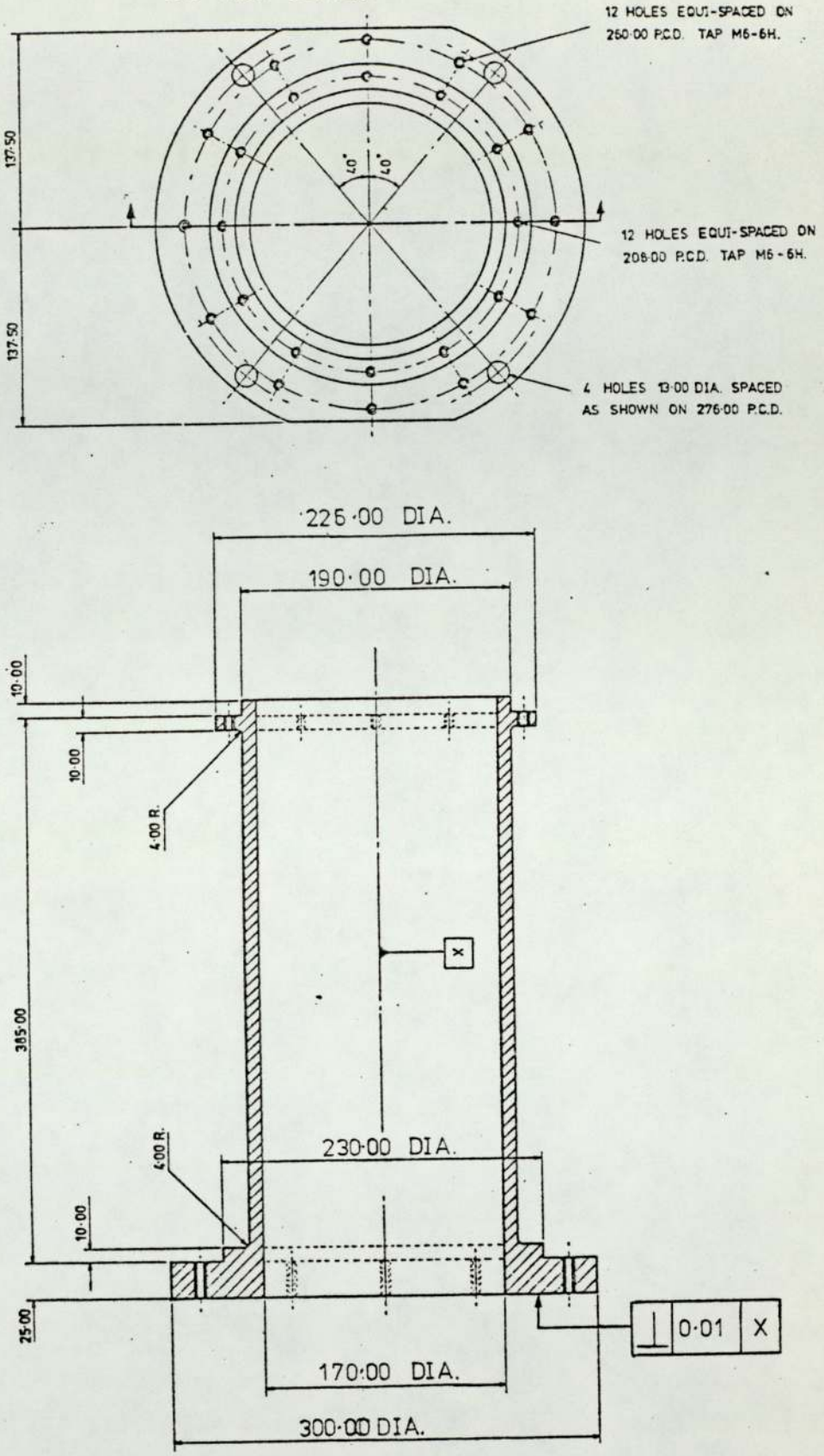

MATERIAL. MILD STEEL.

TOLERANCE EXCEPT WHERE OTHERWISE STATED ± 0·20.

ALL DIMENSIONS ARE IN mm. UNLESS OTHERWISE STATED.

INNER SUPPORT.	DRG. No. 037.
THE UNIVERSITY OF ASTON IN BIRMINGHAM.	SCALE. 1:2
DEPARTMENT OF PRODUCTION ENGINEERING.	P.J. LEAVESLEY.

DO NOT SCALE.

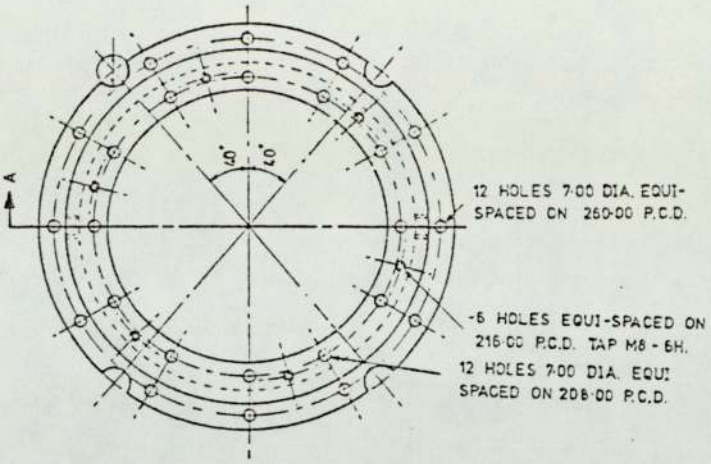

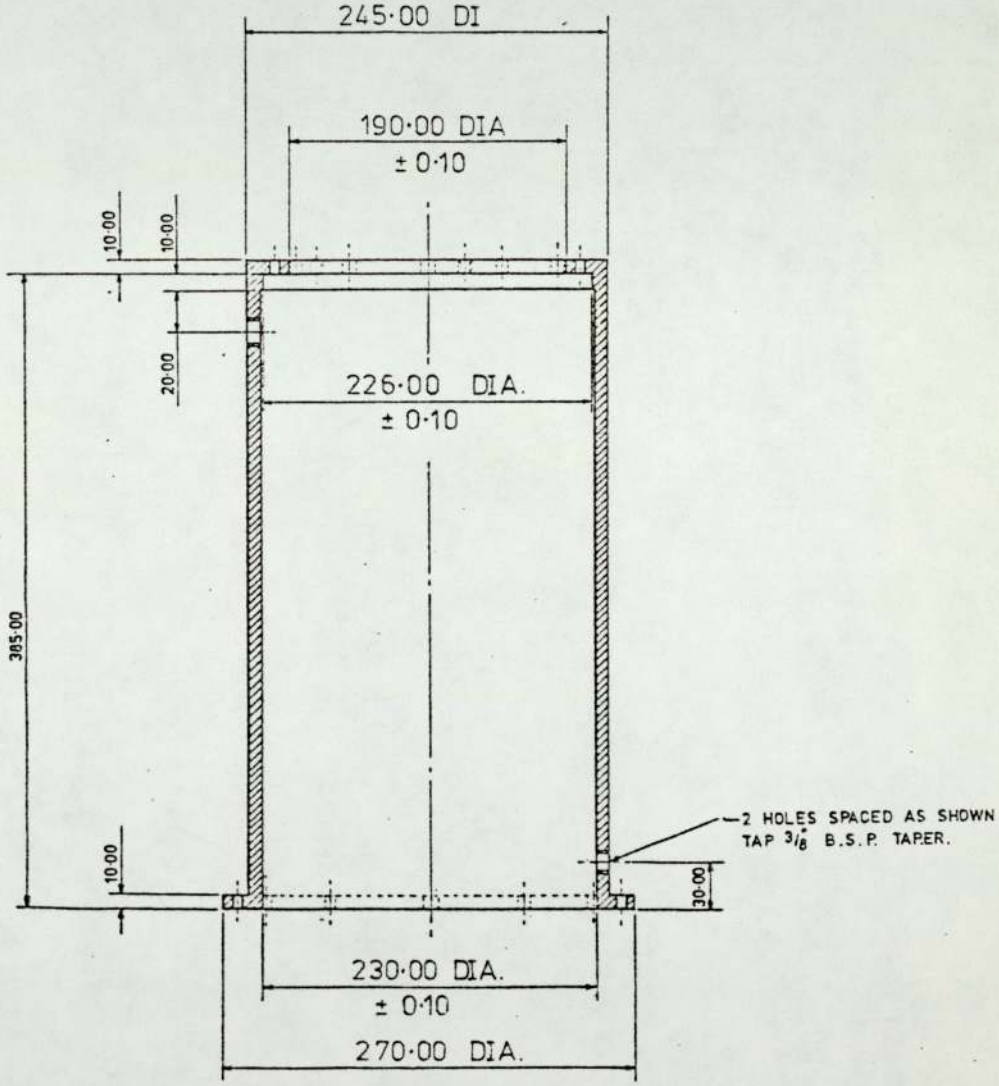

MATERIAL. MILD STEEL.

TOLERANCE EXCEPT WHERE OTHERWISE STATED ± 0·20.

ALL DIMENSIONS ARE IN mm. UNLESS OTHERWISE STATED.

OUTER JACKET	DRG. No. 038
THE UNIVERSITY OF ASTON IN BIRMINGHAM.	SCALE 1:5
DEPARTMENT OF PRODUCTION ENGINEERING.	P.J. LEAVESLEY.

DO NOT SCALE.

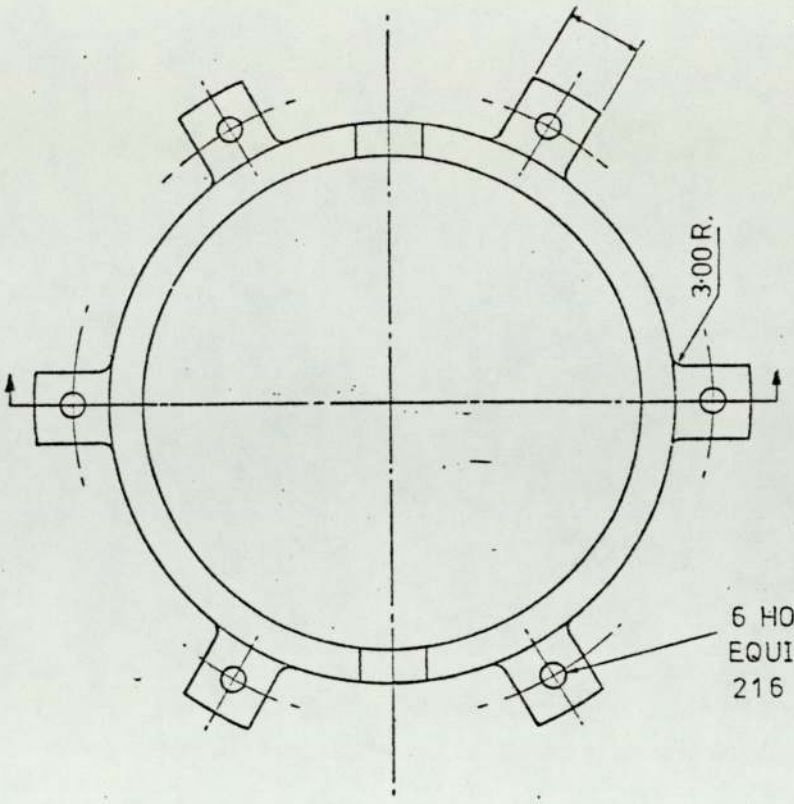

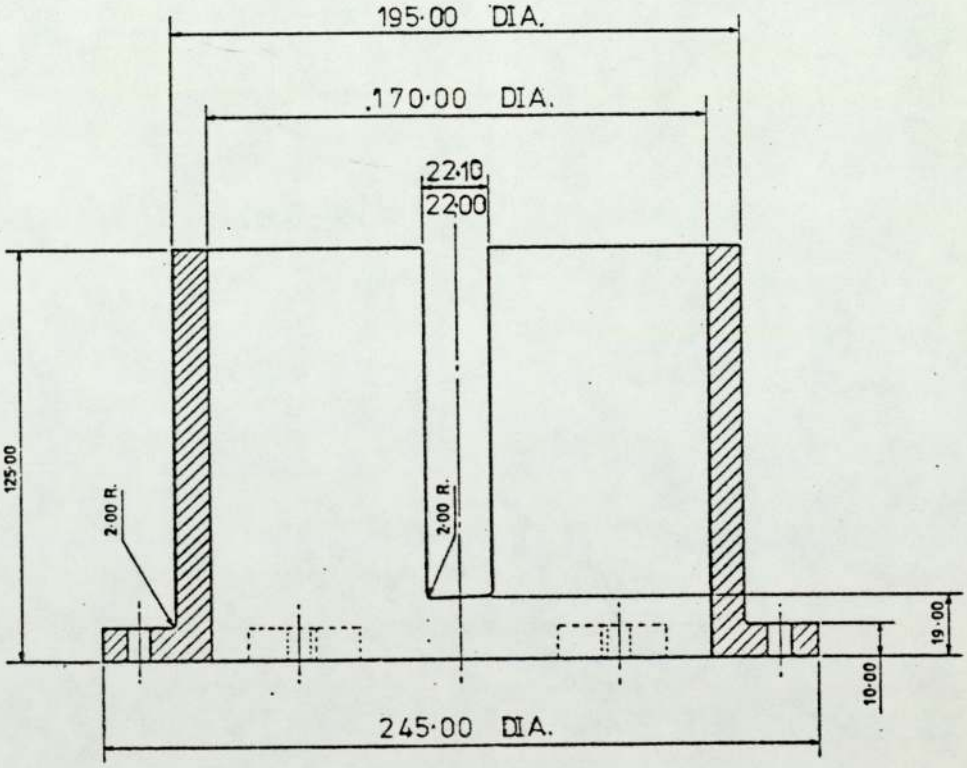

MATERIAL. MILD STEEL.

TOLERANCE EXCEPT WHERE OTHERWISE STATED ± 0·20.

ALL DIMENSIONS ARE IN mm. UNLESS OTHERWISE STATED.

GUIDE.	DRG. No. 039.
THE UNIVERSITY OF ASTON IN BIRMINGHAM.	SCALE. 1:2
DEPARTMENT OF PRODUCTION ENGINEERING.	P.J. LEAVESLEY.

DO NOT SCALE.

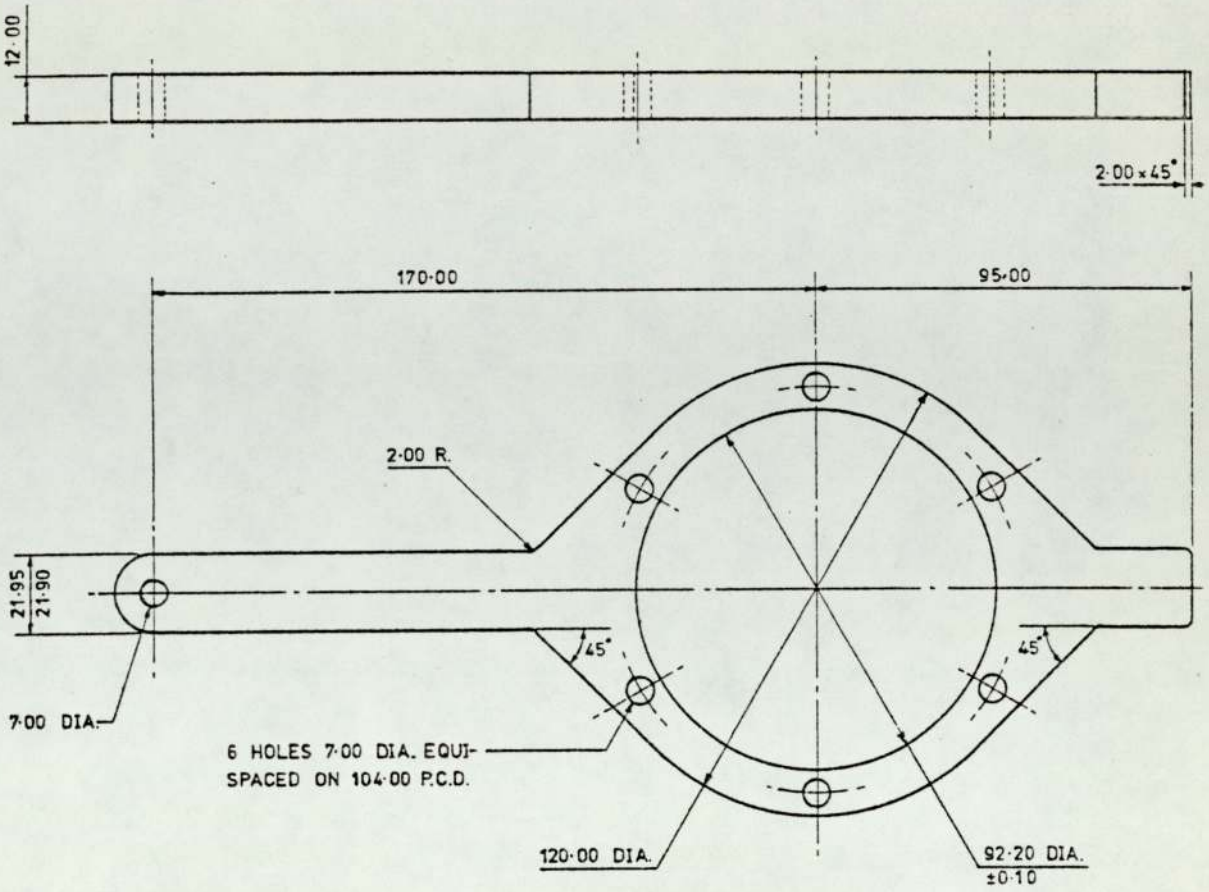

MATERIAL. MILD STEEL.

TOLERANCE EXCEPT WHERE OTHERWISE STATED ± 0·20.

ALL DIMENSIONS ARE IN mm. UNLESS OTHERWISE STATED.

DISPLACEMENT ARM.	DRG. No. 040.
THE UNIVERSITY OF ASTON IN BIRMINGHAM.	SCALE. 1:2
DEPARTMENT OF PRODUCTION ENGINEERING.	P.J. LEAVESLEY.

CROSS HEAD ASSEMBLY.

DRG. No. 100 PART LIST.

PART No.	No. OFF.	DESCRIPTION.	MATERIAL.
101	1	CROSS-HEAD.	MILD STEEL.
102	2	BEARING HOUSING.	MILD STEEL.
103	2	IMPACT PAD.	EN.26.
104	2	STUD.	MILD STEEL.
105	-	WEIGHTS (VARIOUS).	MILD STEEL.
106	2	LIFTING RING.	MILD STEEL.
107	2	BALL BUSHING.	OPN 324864.
108	4	CIRCLIP.	EN.42.
109	8	SET SCREW.	M6x25-6g.
110	8	WASHER.	12.5 O/D-6.4 I/D-1.6
111	6	NUT.	M12-6H.
112	6	WASHER.	24 O/D-13 I/D-2.5
113	1	LIFTING PLATE.	MILD STEEL.
114	4	SOCKET SCREW.	M6x20-6g.

DO NOT SCALE.

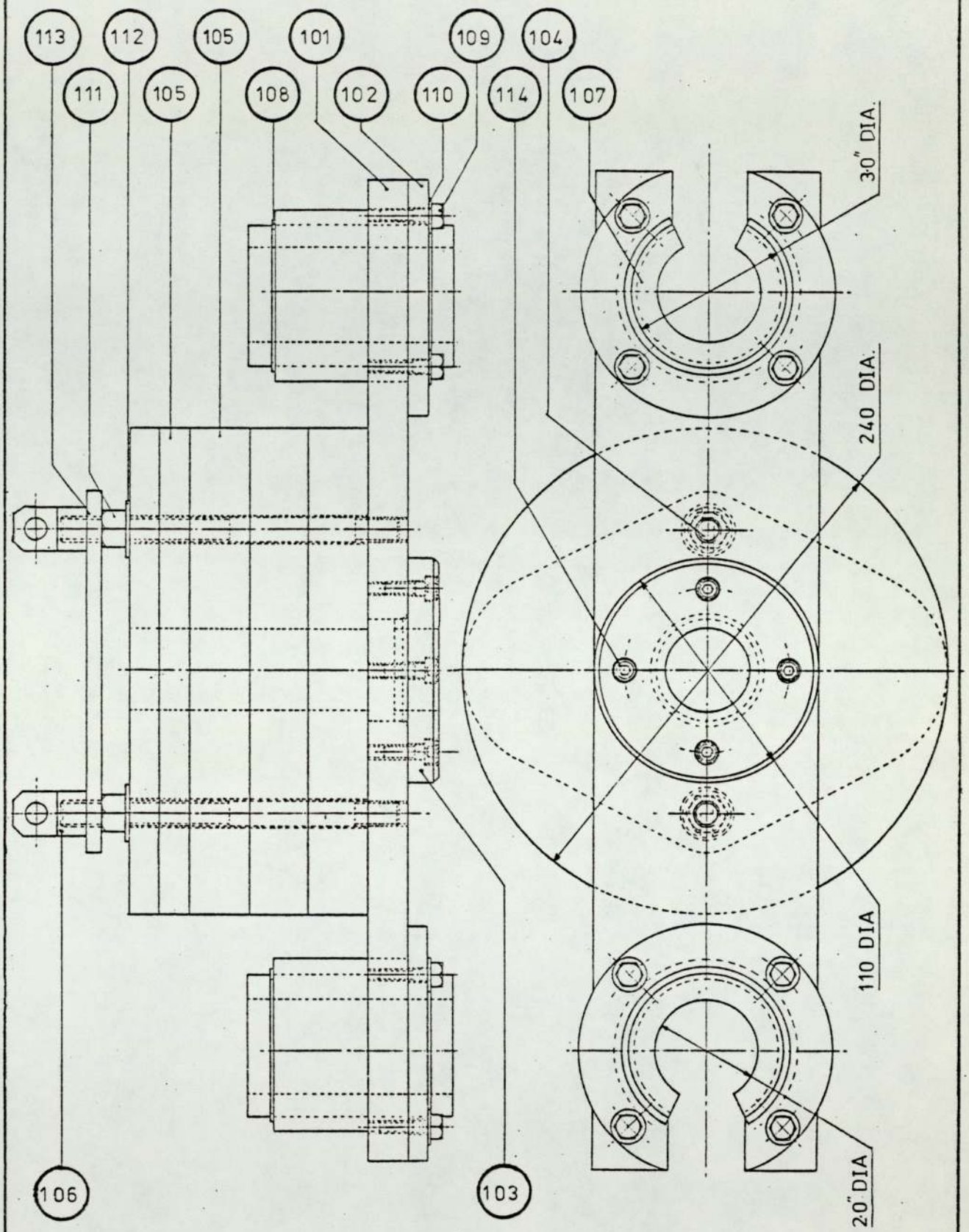

TOLERANCE EXCEPT WHERE OTHERWISE STATED ± 0·20.

ALL DIMENSIONS ARE IN mm. UNLESS OTHERWISE STATED.

CROSSHEAD ASSEMBLY.	DRG. No. 100
THE UNIVERSITY OF ASTON IN BIRMINGHAM.	SCALE: FULL SIZE.
DEPARTMENT OF PRODUCTION ENGINEERING.	P.J. LEAVESLEY.

DO NOT SCALE.

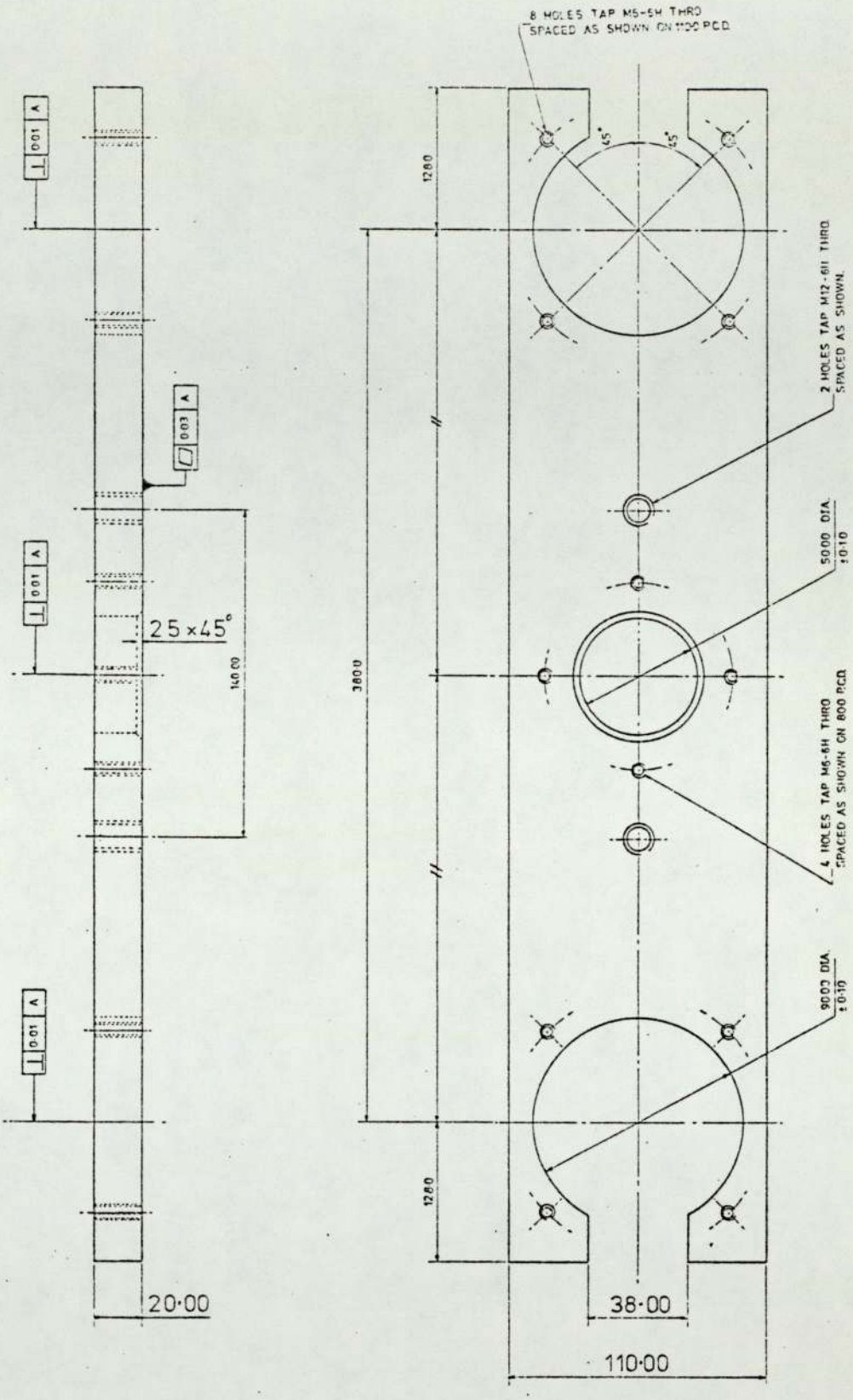

MATERIAL. MILD STEEL.

TOLERANCE EXCEPT WHERE OTHERWISE STATED ± 0·20.

ALL DIMENSIONS ARE IN mm. UNLESS OTHERWISE STATED.

CROSSHEAD	DRG. No. 101
THE UNIVERSITY OF ASTON IN BIRMINGHAM.	SCALE 1:2
DEPARTMENT OF PRODUCTION ENGINEERING.	P.J.LEAVESLEY.

DO NOT SCALE.

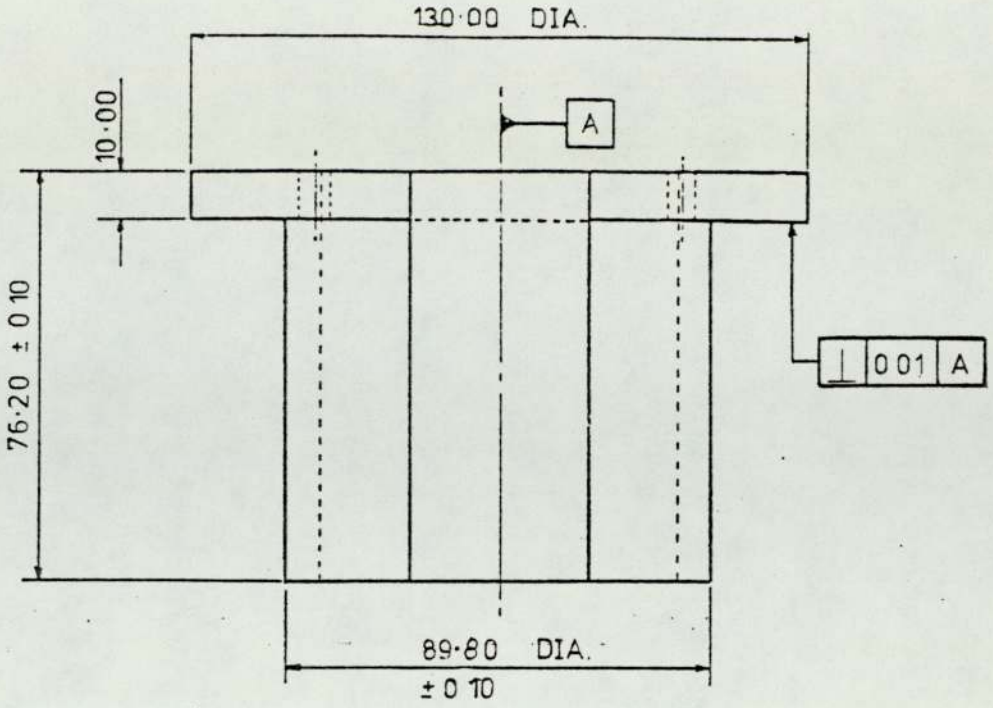

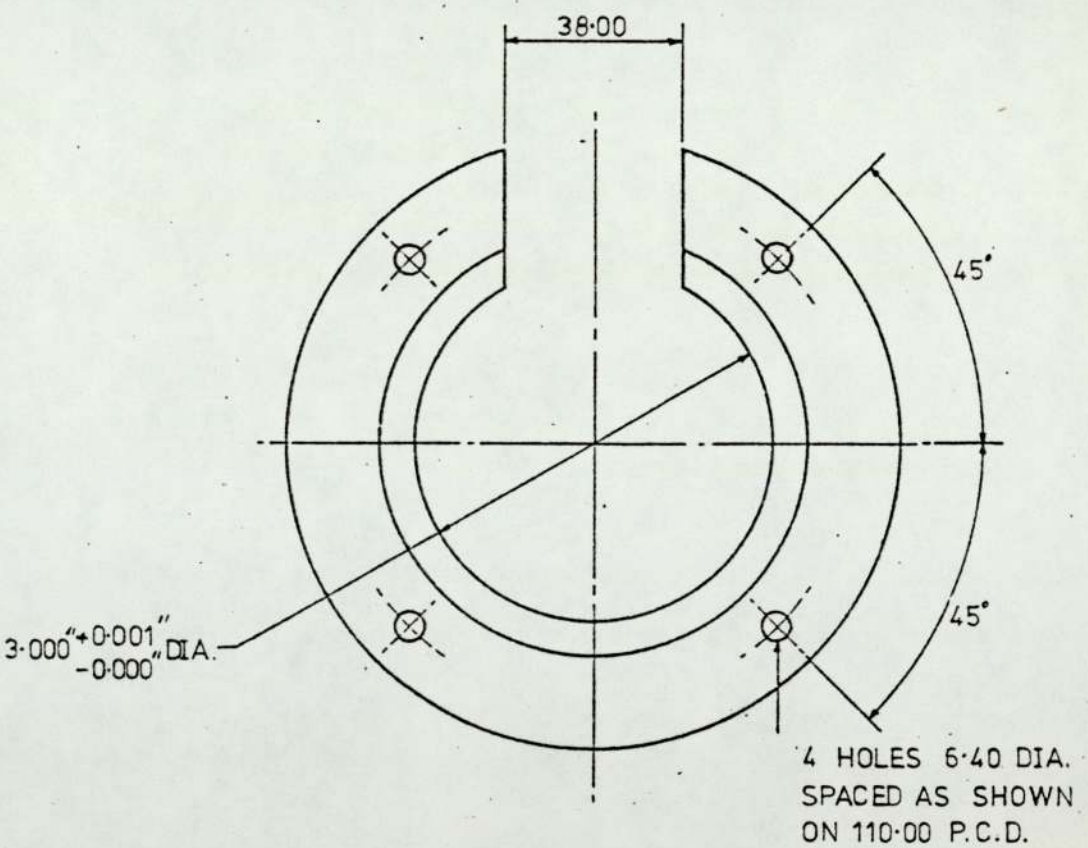

MATERIAL. MILD STEEL.

2 OFF.

TOLERANCE EXCEPT WHERE OTHERWISE STATED ± 0·20.

ALL DIMENSIONS ARE IN mm. UNLESS OTHERWISE STATED.

BEARING HOUSING.	DRG. No. 102
THE UNIVERSITY OF ASTON IN BIRMINGHAM.	SCALE: FULL SIZE.
DEPARTMENT OF PRODUCTION ENGINEERING.	P.J. LEAVESLEY.

DO NOT SCALE.

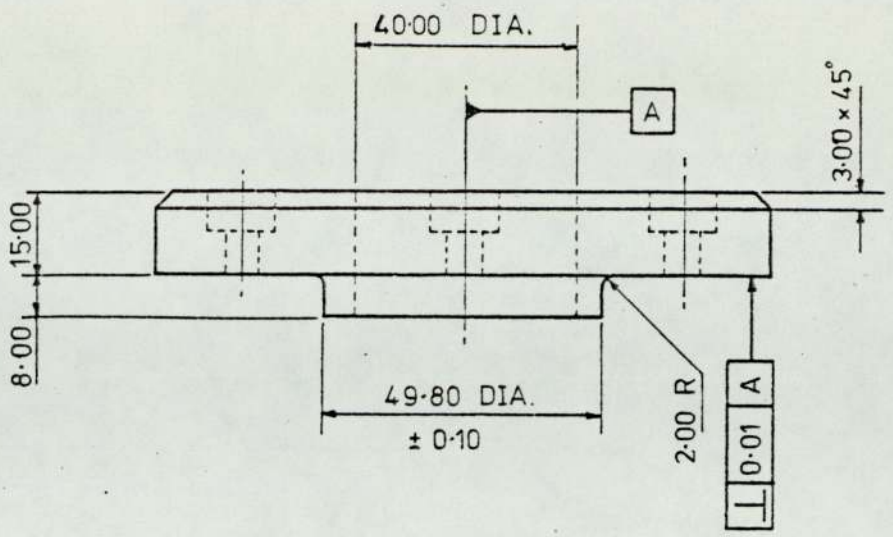

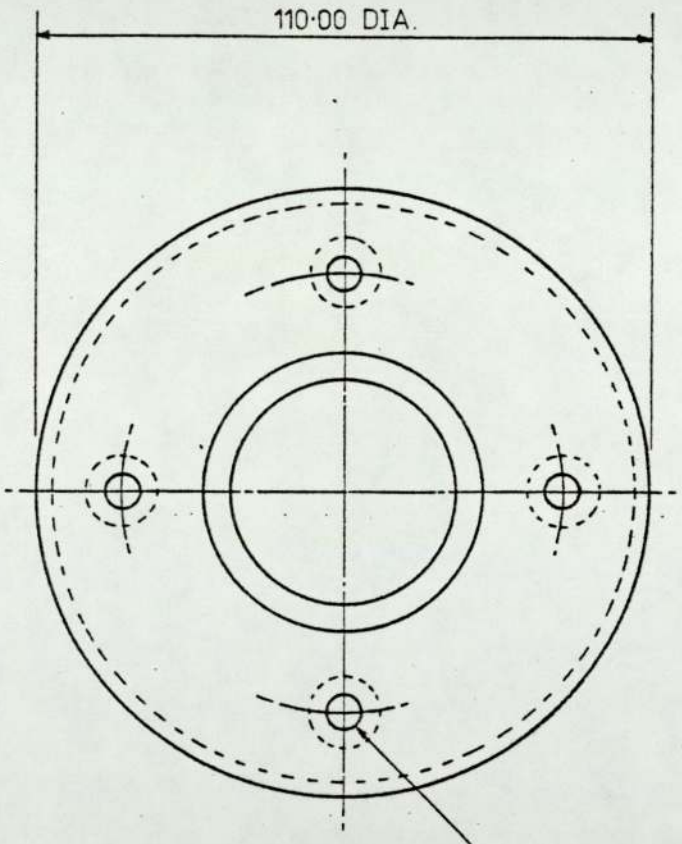

4 HOLES 6·40 DIA. C'BORE
12·00 DIA. × 7·00 DEEP. SPACED
AS SHOWN ON 80·00 P.C.D.

MATERIAL.
EN 26.
HARDENING 820 - 850°C OIL QUENCH.
TEMPERING 650°C AIR COOL.
TO GIVE HARDNESS 33 HRC ± 2.

2 OFF.

TOLERANCE EXCEPT WHERE OTHERWISE STATED ± 0·20.

ALL DIMENSIONS ARE IN mm. UNLESS OTHERWISE STATED.

IMPACT PAD.	DRG. No. 103.
THE UNIVERSITY OF ASTON IN BIRMINGHAM.	SCALE: FULL SIZE.
DEPARTMENT OF PRODUCTION ENGINEERING.	P.J. LEAVESLEY.

DO NOT SCALE.

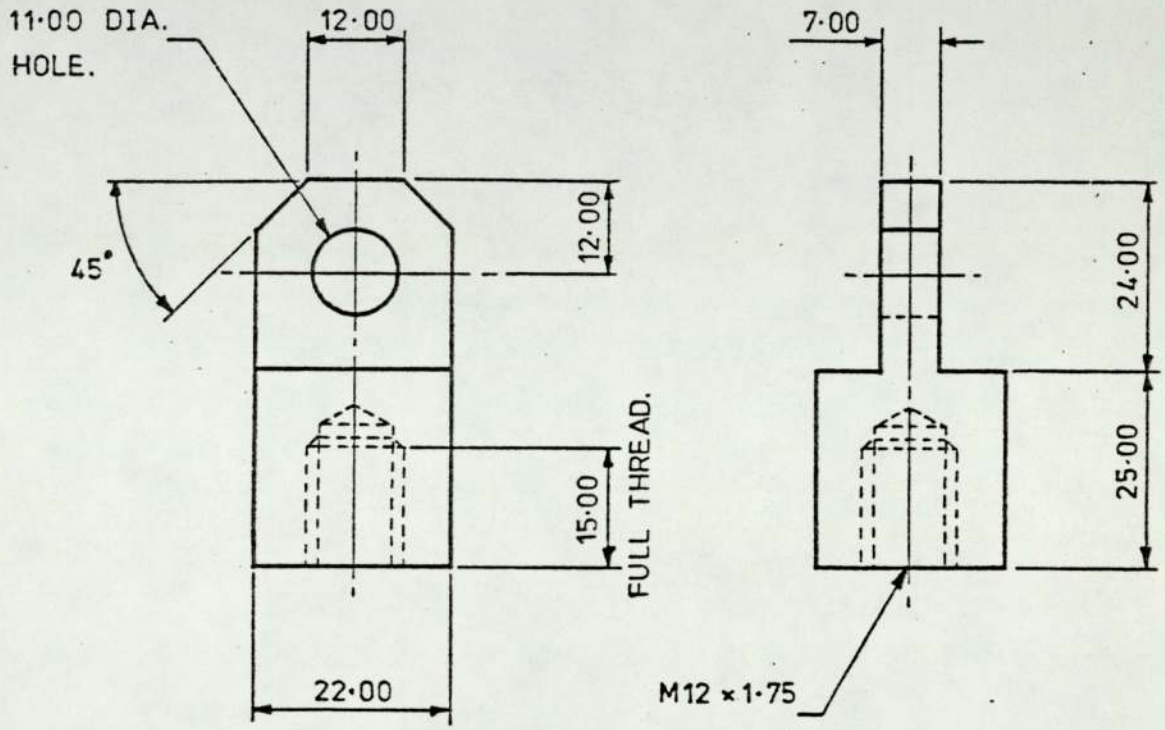

MATERIAL. MILD STEEL.

2 OFF

TOLERANCE EXCEPT WHERE OTHERWISE STATED ± 0·20.

ALL DIMENSIONS ARE IN mm. UNLESS OTHERWISE STATED.

LIFTING RING.	DRG. No. 106
THE UNIVERSITY OF ASTON IN BIRMINGHAM.	SCALE: FULL SIZE.
DEPARTMENT OF PRODUCTION ENGINEERING.	P.J. LEAVESLEY.

DO NOT SCALE.

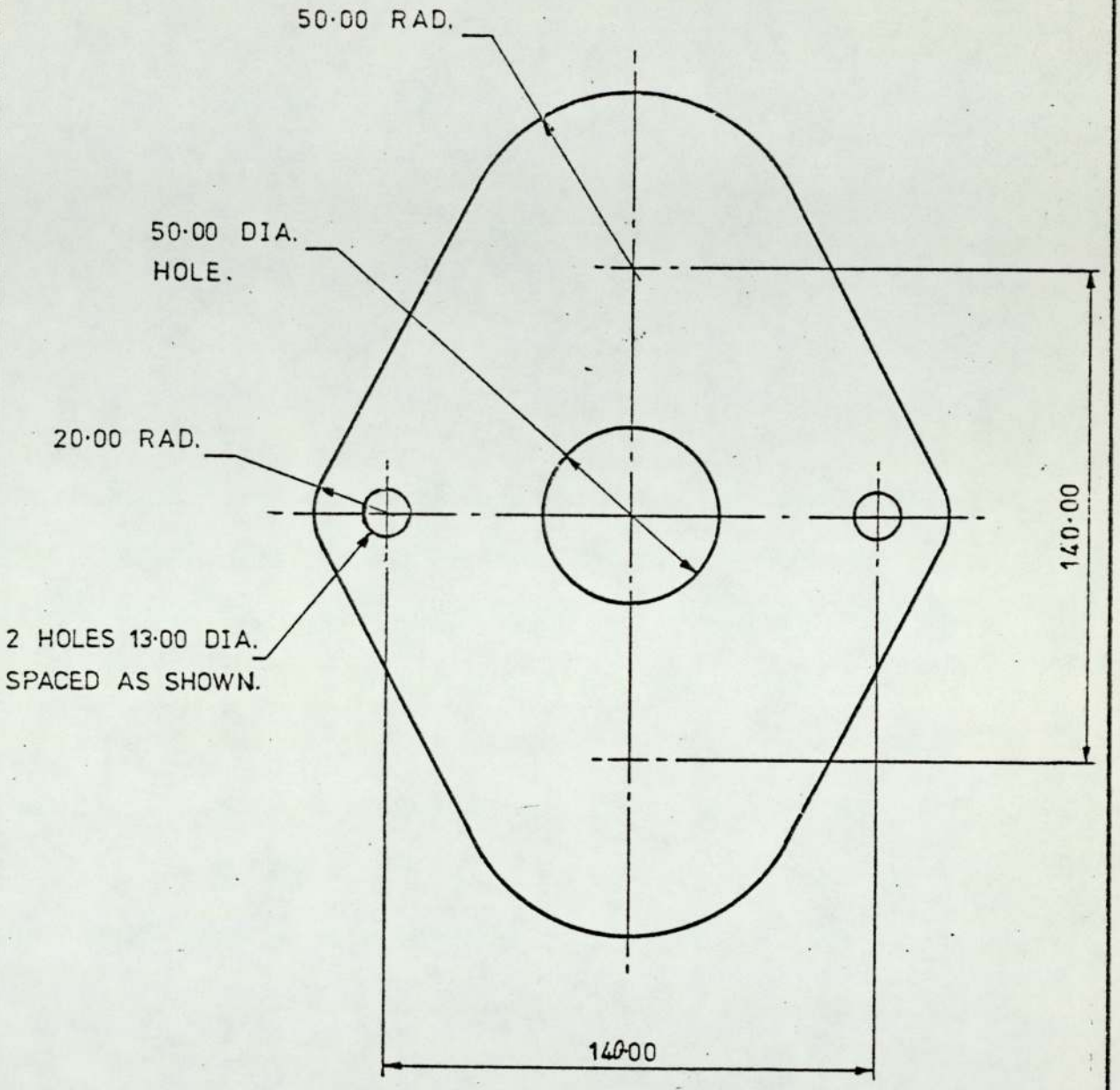

MATERIAL. MILD STEEL. PLATE. 3/8 in. 1 OFF.

TOLERANCE EXCEPT WHERE OTHERWISE STATED ± 0·20.

ALL DIMENSIONS ARE IN mm. UNLESS OTHERWISE STATED.

LIFTING PLATE.	DRG. No. 113.
THE UNIVERSITY OF ASTON IN BIRMINGHAM.	SCALE 1:2
DEPARTMENT OF PRODUCTION ENGINEERING.	P.J. LEAVESLEY.

HOIST MECHANISM ASSEMBLY.

DRG. 200 PART LIST.

PART No.	No. OFF.	DESCRIPTION.	MATERIAL.
201	1	ELECTRIC MOTOR.	$\frac{1}{4}$ h.p.
202	1	GEAR BOX.	40:1
203	1	FLEXIBLE COUPLING.	FENNER. 65F. H.R.C.
204	1	FLEXIBLE COUPLING.	FENNER. 85F. H.R.C.
205	1	DRUM SHAFT.	MILD STEEL.
206	1	DRUM.	WOOD.
207	1	PRE-STRETCHED TERYLENE ROPE.	100 METRES.
208	1	MOUNTING PLATE.	MILD STEEL.
209	2	GEAR BOX SPACER.	MILD STEEL.
210	1	SPACER.	MILD STEEL.
211	3	ANGLE BRACKETS.	$1\frac{1}{2}$"x$1\frac{1}{2}$"x$\frac{1}{4}$" L-CHANNEL.
212	1	CONTROL BOX.	B.O.F.
213	1	SPACING PULLEY.	B.O.F.
214	1	TOP PULLEY.	B.O.F.
215	1	BOTTOM PULLEY.	B.O.F.
216	4	SET SCREW.	M8x25-6g.
217	4	NUT.	M8-6H.
218	8	WASHER.	17 O/D-8.4 I/D -1.6
219	8	SET SCREW.	M10x100-6g.
220	8	NUT.	M10-6H.
221	16	WASHER.	20 O/D-10.6 I/D-2

GUIDE TUBE ASSEMBLY.

DRG. 300 PART LIST.			
PART No.	No. OFF.	DESCRIPTION.	MATERIAL.
301	2	GUIDE TUBE.	MILD STEEL.
302	8	GUIDE LUG.	MILD STEEL.
303	4	GUIDE TUBE ADAPTOR.	MILD STEEL.
304	4	FLANGE.	MILD STEEL.
305	4	GUIDE TUBE PIN.	MILD STEEL.
306	2	FLANGE SUPPORT.	4"x2"x$\frac{3}{8}$" U-CHANNEL.
307	16	SOCKET SCREW.	M6x25-6g.
308	16	SET SCREW.	M12x35-6g.
309	20	NUT.	M12-6H.
310	32	WASHER.	24 O/D-13 I/D-2.5
311	8	SET SCREW.	M8x60-6g.
312	16	NUT.	M8-6H.
313	16	WASHER.	17 O/D-8.4 I/D-1.6
314	4	T-NUT.	MILD STEEL.
315	4	BOLT.	M12x75-6g.

DO NOT SCALE.

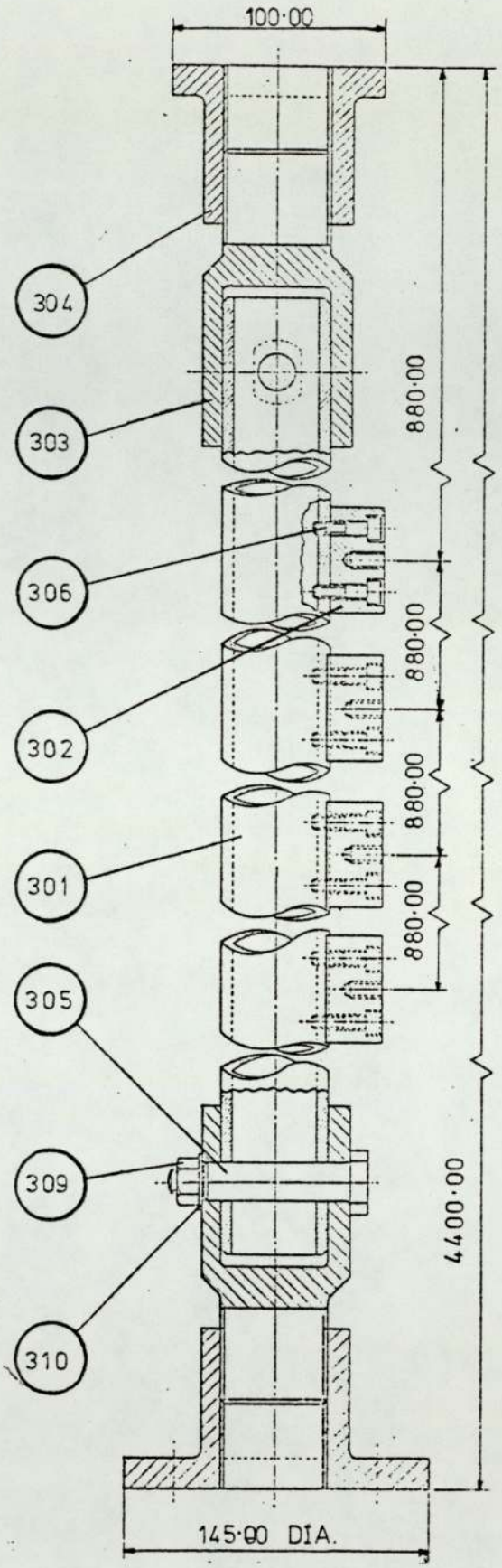

TOLERANCE EXCEPT WHERE OTHERWISE STATED ± 0·20.

ALL DIMENSIONS ARE IN mm. UNLESS OTHERWISE STATED.

GUIDE TUBE ASSEMBLY.	DRG. No. 300
THE UNIVERSITY OF ASTON IN BIRMINGHAM.	SCALE 1:20
DEPARTMENT OF PRODUCTION ENGINEERING.	P.J. LEAVESLEY.

DO NOT SCALE.

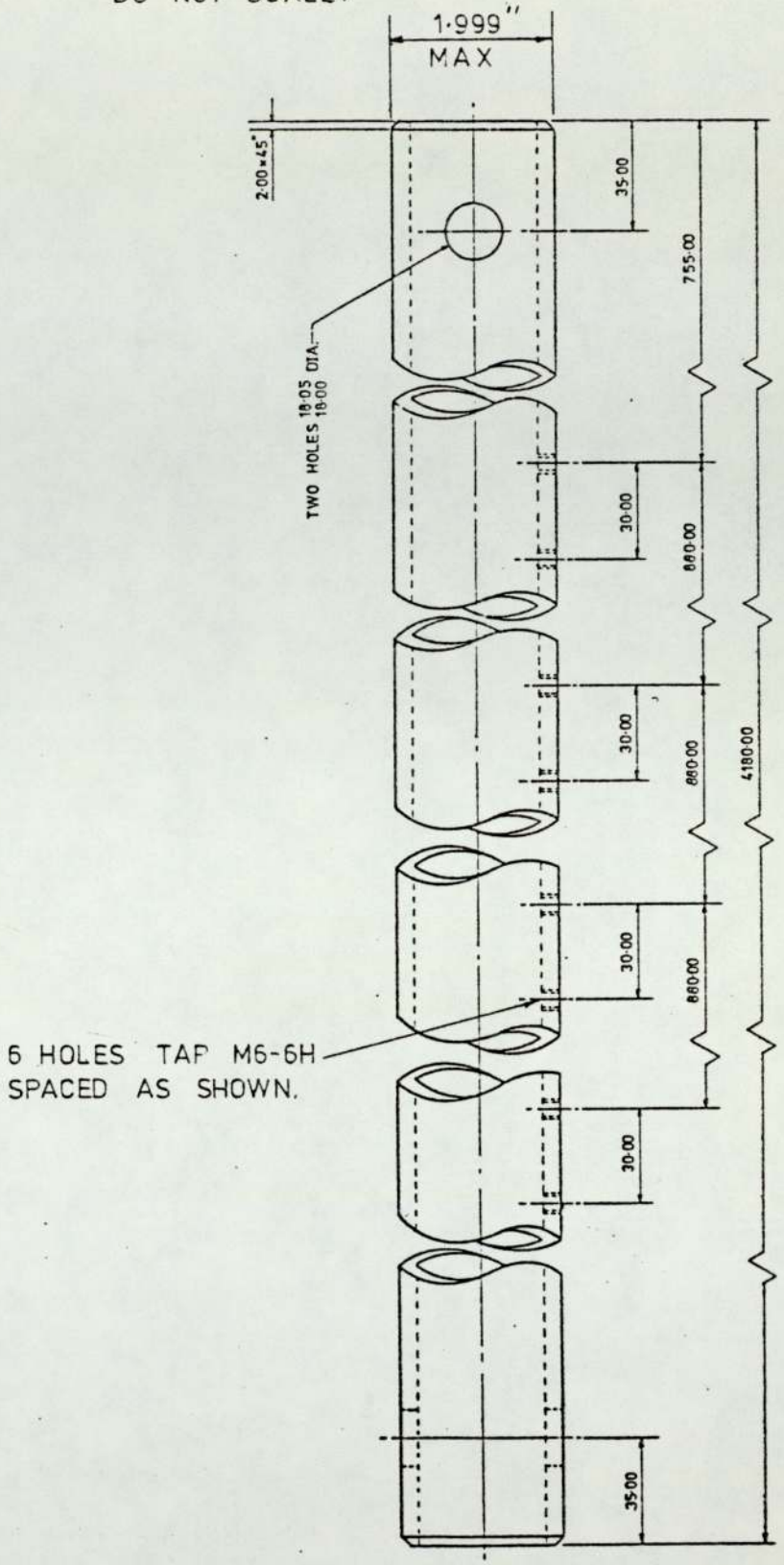

MATERIAL. MILD STEEL.

TOLERANCE EXCEPT WHERE OTHERWISE STATED ± 0·20.

ALL DIMENSIONS ARE IN mm. UNLESS OTHERWISE STATED.

GUIDE TUBE.	DRG. No. 301.
THE UNIVERSITY OF ASTON IN BIRMINGHAM.	SCALE. 1:4
DEPARTMENT OF PRODUCTION ENGINEERING.	P.J. LEAVESLEY.

DO NOT SCALE.

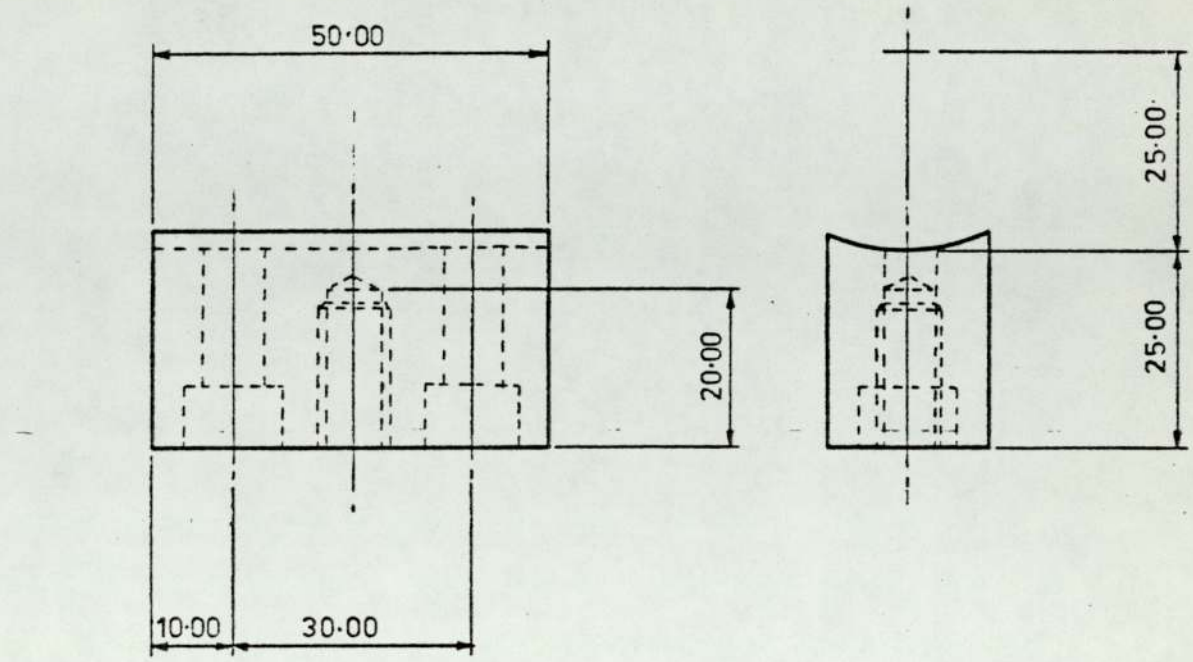

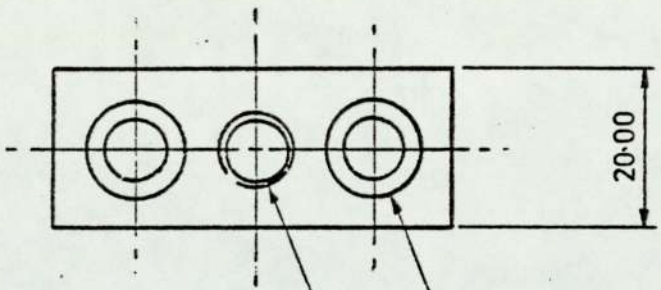

M8 × 1·25 × 16·00 DEEP.

TWO HOLES 7·00 DIA. C'BORE
12·00 DIA. × 8·00 DEEP.

MATERIAL. MILD STEEL.

8 OFF.

TOLERANCE EXCEPT WHERE OTHERWISE STATED ± 0·20.

ALL DIMENSIONS ARE IN mm. UNLESS OTHERWISE STATED.

GUIDE LUG.	DRG. No. 302
THE UNIVERSITY OF ASTON IN BIRMINGHAM.	SCALE: FULL SIZE.
DEPARTMENT OF PRODUCTION ENGINEERING.	P.J. LEAVESLEY.

DO NOT SCALE.

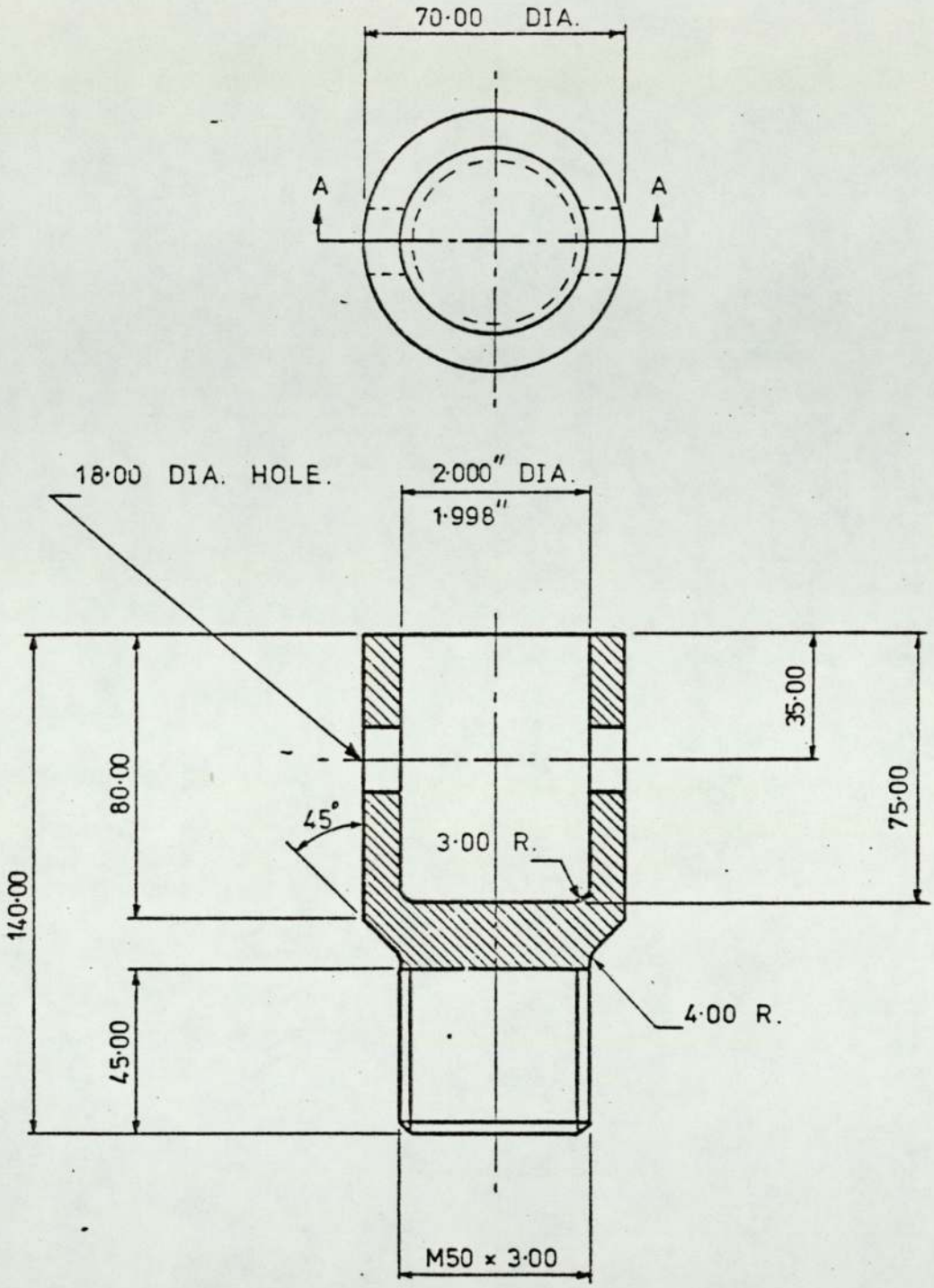

SECTION ON AA.

MATERIAL. MILD STEEL.

4 OFF.

TOLERANCE EXCEPT WHERE OTHERWISE STATED ± 0·20.

ALL DIMENSIONS ARE IN mm. UNLESS OTHERWISE STATED.

GUIDE TUBE ADAPTOR.	DRG. No. 303
THE UNIVERSITY OF ASTON IN BIRMINGHAM.	SCALE 1:2
DEPARTMENT OF PRODUCTION ENGINEERING.	P.J. LEAVESLEY.

DO NOT SCALE.

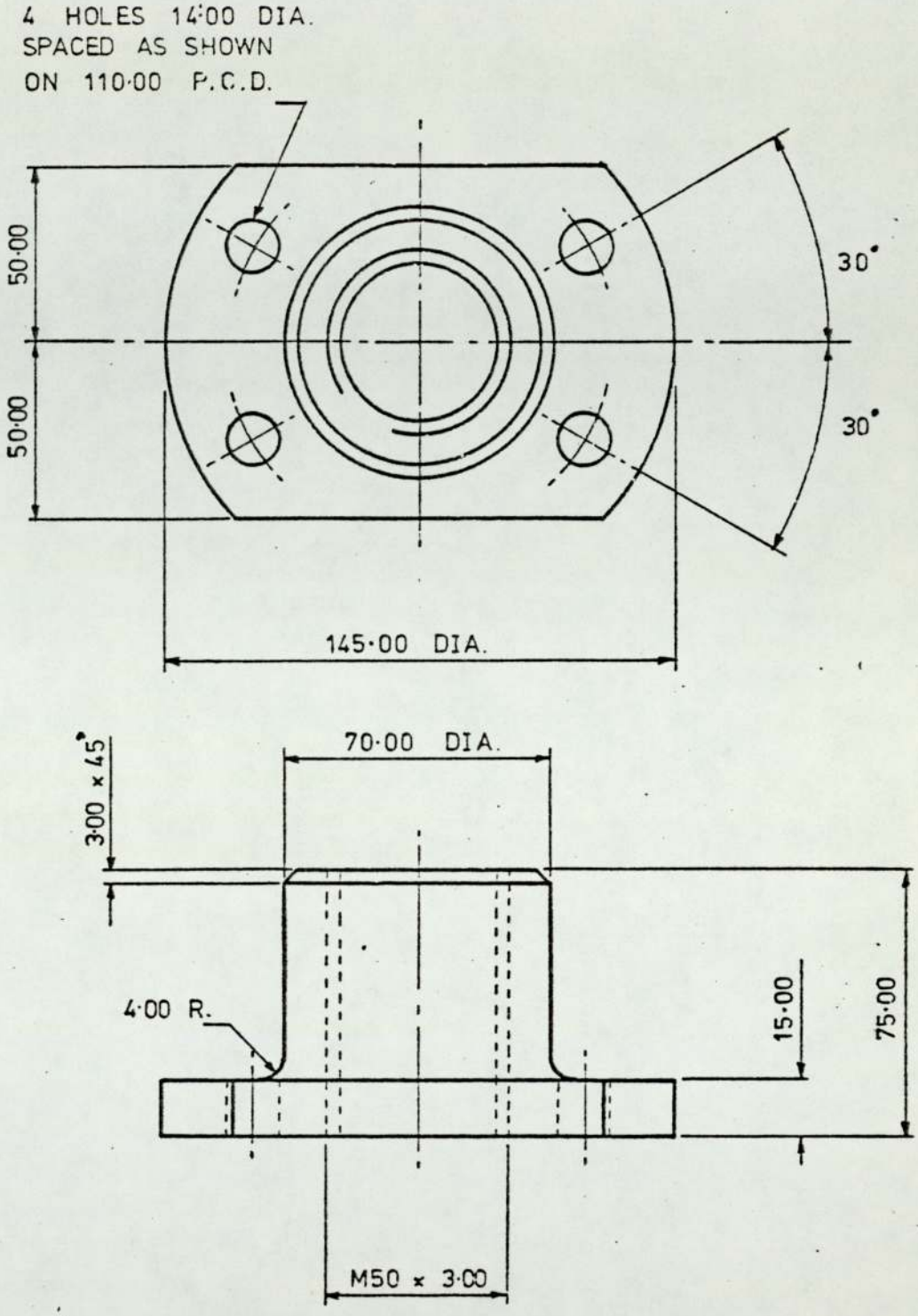

MATERIAL. MILD STEEL.

4 OFF.

TOLERANCE EXCEPT WHERE OTHERWISE STATED ± 0·20.

ALL DIMENSIONS ARE IN mm. UNLESS OTHERWISE STATED.

FLANGE.	DRG. No. 304
THE UNIVERSITY OF ASTON IN BIRMINGHAM.	SCALE 1:2
DEPARTMENT OF PRODUCTION ENGINEERING.	P.J. LEAVESLEY.

DO NOT SCALE.

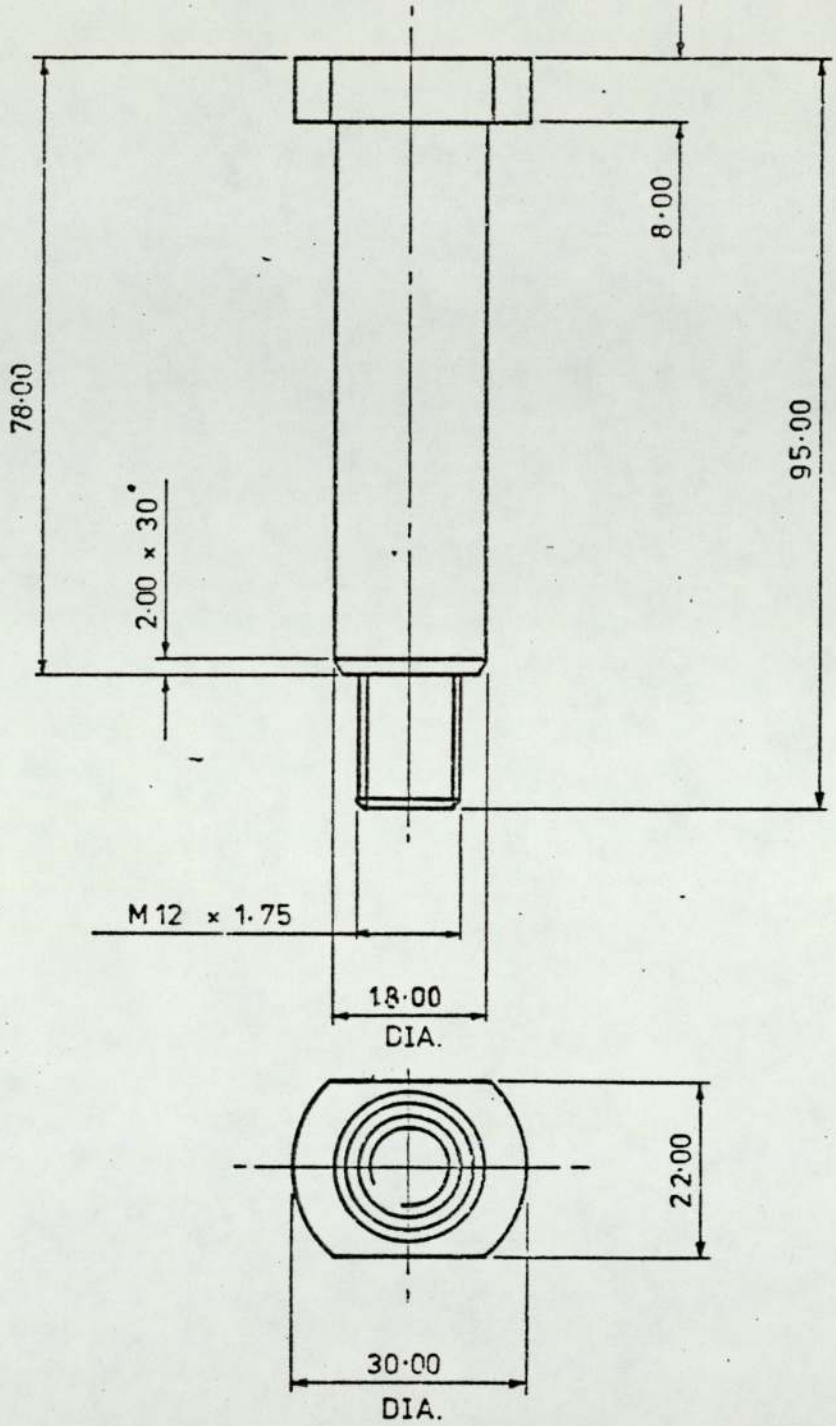

MATERIAL. MILD STEEL.

4 OFF.

TOLERANCE EXCEPT WHERE OTHERWISE STATED ± 0·20.

ALL DIMENSIONS ARE IN mm. UNLESS OTHERWISE STATED.

GUIDE TUBE PIN.	DRG. No. 305
THE UNIVERSITY OF ASTON IN BIRMINGHAM.	SCALE: FULL SIZE.
DEPARTMENT OF PRODUCTION ENGINEERING.	P.J. LEAVESLEY.

RELEASE MECHANISM ASSEMBLY.

DRG. 400 PART LIST.

PART No.	No. OFF.	DESCRIPTION.	MATERIAL.
401	2	SQUARE BEARING HOUSING.	MILD STEEL.
402	2	BRONZE BEARING.	BRONZE.
403	1	LIFTING BAR.	MILD STEEL.
404	1	LIFTING HEAD.	MILD STEEL.
405	2	LIFTING ADAPTOR.	MILD STEEL.
406	1	SOLENOID CONNECTER.	MILD STEEL.
407	1	SOLENOID BRACKET.	MILD STEEL.
408	2	PIVOT BRACKET.	MILD STEEL.
409	1	ACTUATER PIN.	MILD STEEL.
410	2	ELECTRO-MAGNET SPACER.	MILD STEEL.
411	1	ELECTRO-MAGNET SUPPORT.	MILD STEEL.
412	1	SOLENOID.	B.O.F.
413	2	ELECTRO-MAGNET.	B.O.F.
414	2	LIFTING PIN.	MILD STEEL.
415	2	LEVER.	MILD STEEL.
416	6	SET SCREW.	M8x60-6g.
417	12	NUT.	M8-6H.
418	38	WASHER.	17 o/D-8-4 I/D-1.6
419	6	SET SCREW.	M8x35-6g.
420	8	SET SCREW.	M8x25-6g.
421	2	SHOULDER SOCKET SCREW.	10x20-M8-6g.
422	2	SHOULDER SOCKET SCREW.	10x25-M8-6g.
423	2	SET SCREW.	M10x35-6g.

RELEASE MECHANISM ASSEMBLY.

DRG. 400 PART LIST. CONTINUED.

PART No.	No. OFF.	DESCRIPTION.	MATERIAL.
424	2	WASHER.	20 O/D-10.6 I/D-2
425	3	SET SCREW.	2 B.A. x 10 - 6g.
426	4	SOCKET SCREW.	M6 x15 - 6g.
427	1	BOLT (HIGH TENSILE).	M12 x 70 - 6g.
428	1	NUT.	M12 - 6H.
429	2	WASHER.	24 O/D - 13 I/D -2.5

DO NOT SCALE.

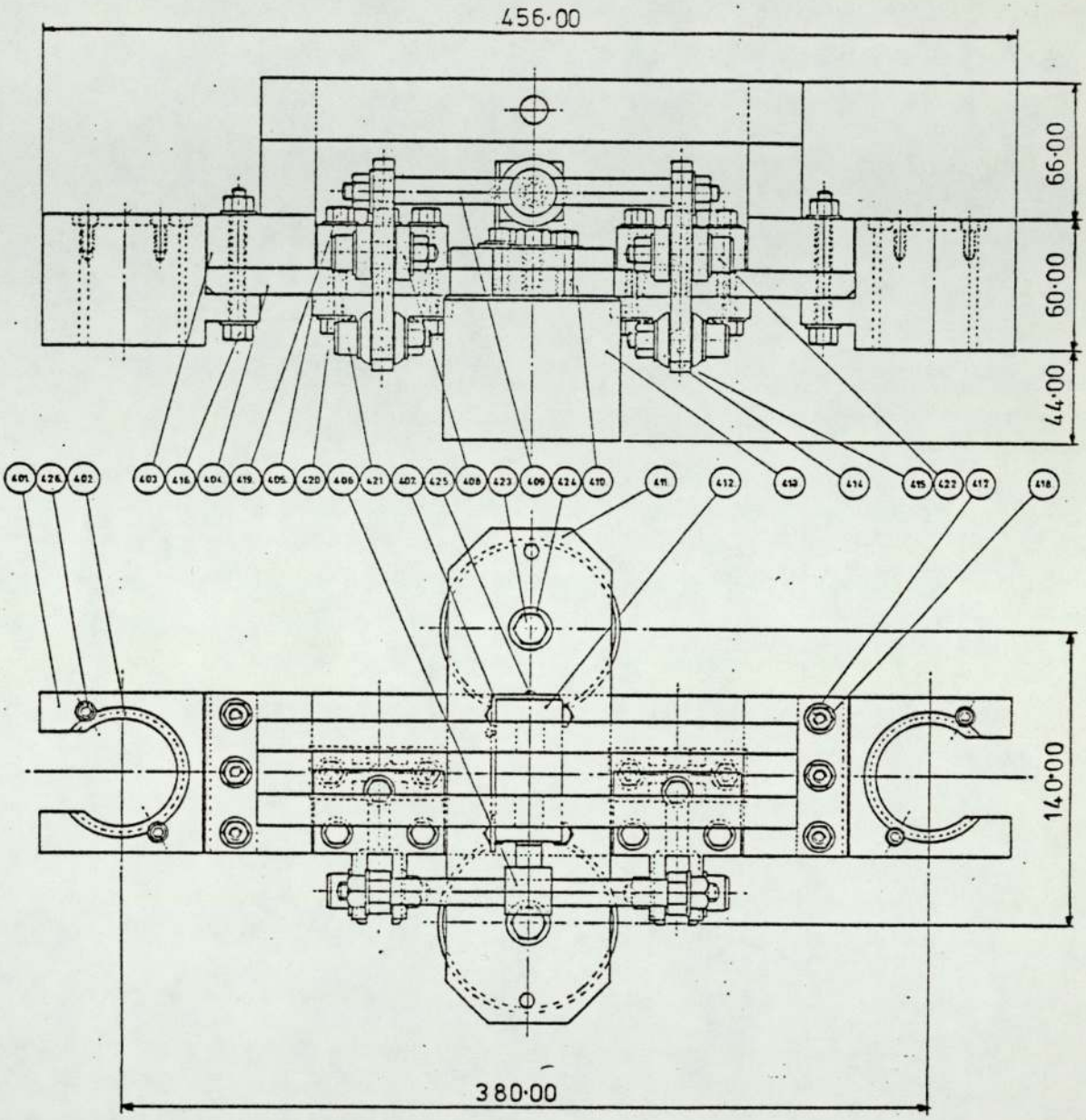

TOLERANCE EXCEPT WHERE OTHERWISE STATED ± 0·20.

ALL DIMENSIONS ARE IN mm. UNLESS OTHERWISE STATED.

RELEASE MECHANISM ASSEMBLY.	DRG. No. 400
THE UNIVERSITY OF ASTON IN BIRMINGHAM.	SCALE 1:3
DEPARTMENT OF PRODUCTION ENGINEERING.	P.J. LEAVESLEY.

DO NOT SCALE.

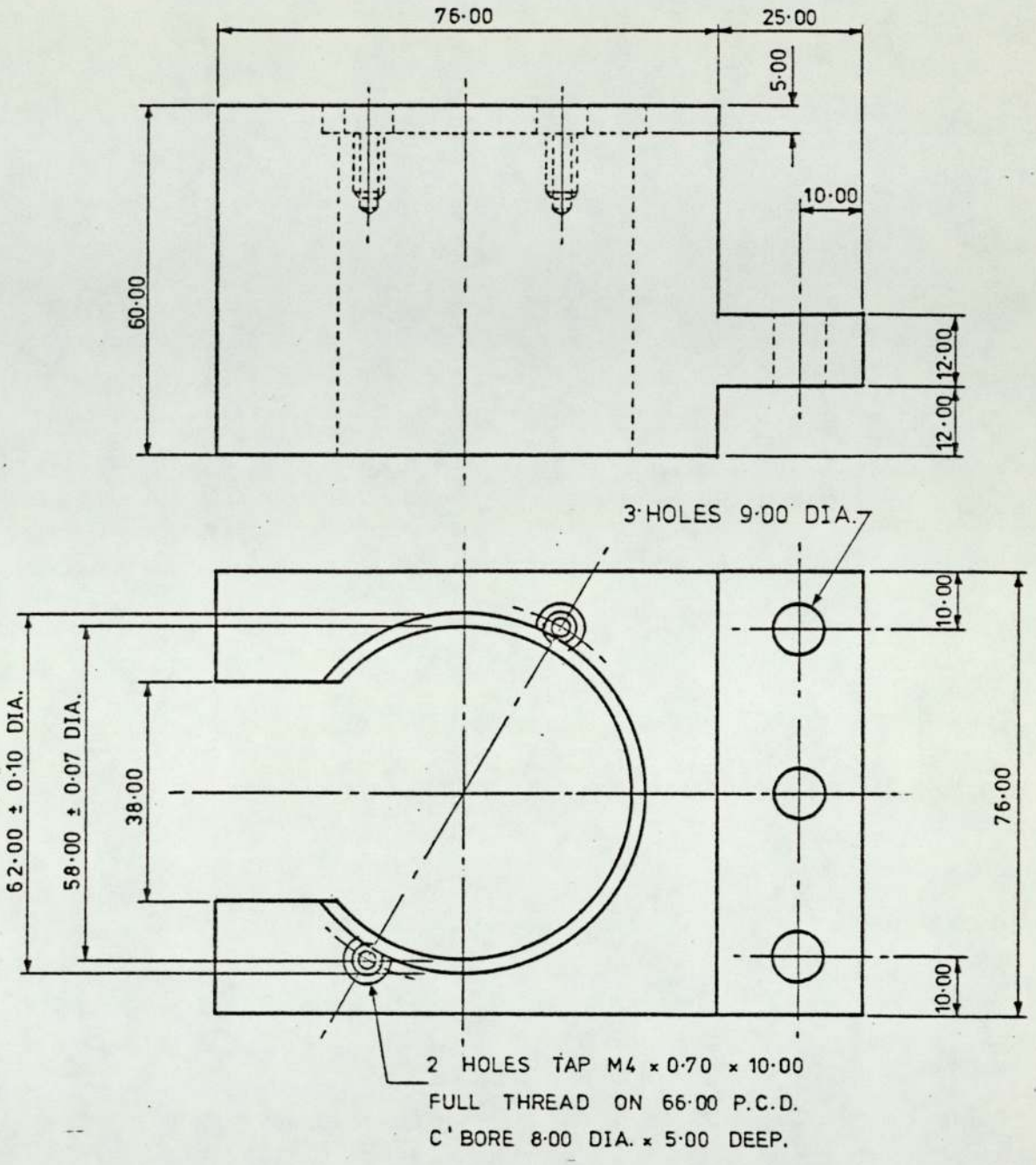

MATERIAL. MILD STEEL.

2 OFF.

TOLERANCE EXCEPT WHERE OTHERWISE STATED ± 0·20.

ALL DIMENSIONS ARE IN mm. UNLESS OTHERWISE STATED.

SQUARE BEARING HOUSING.	DRG. No. 401
THE UNIVERSITY OF ASTON IN BIRMINGHAM.	SCALE: FULL SIZE.
DEPARTMENT OF PRODUCTION ENGINEERING.	P.J. LEAVESLEY.

DO NOT SCALE.

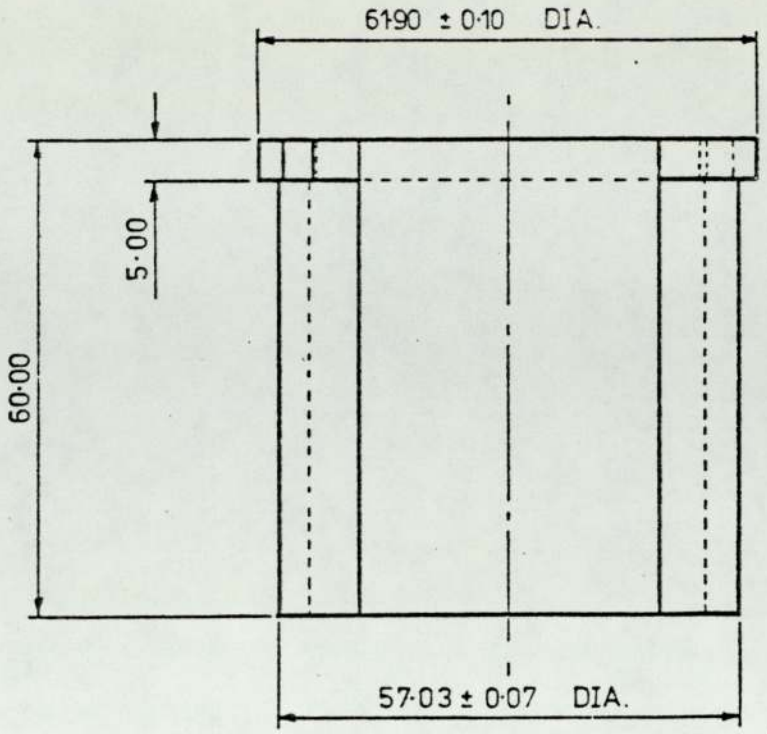

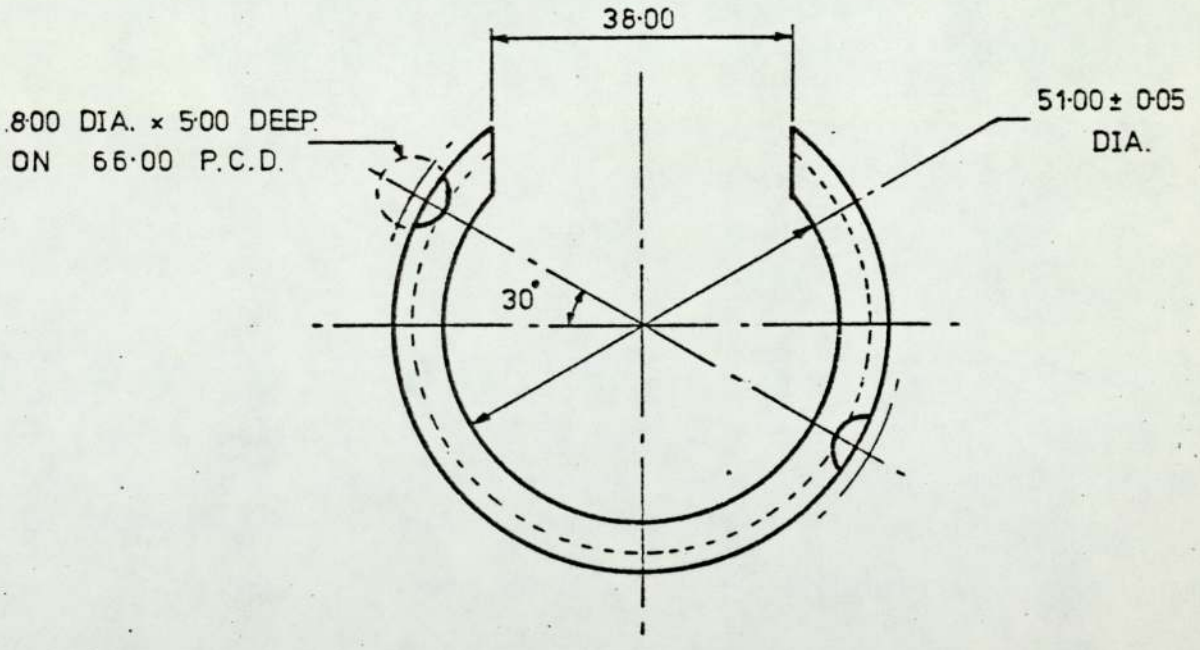

MATERIAL. BRONZE.

2 OFF

TOLERANCE EXCEPT WHERE OTHERWISE STATED ± 0·20.

ALL DIMENSIONS ARE IN mm. UNLESS OTHERWISE STATED.

BRONZE BEARING.	DRG. No. 402
THE UNIVERSITY OF ASTON IN BIRMINGHAM.	SCALE: FULL SIZE
DEPARTMENT OF PRODUCTION ENGINEERING.	P.J. LEAVESLEY.

DO NOT SCALE.

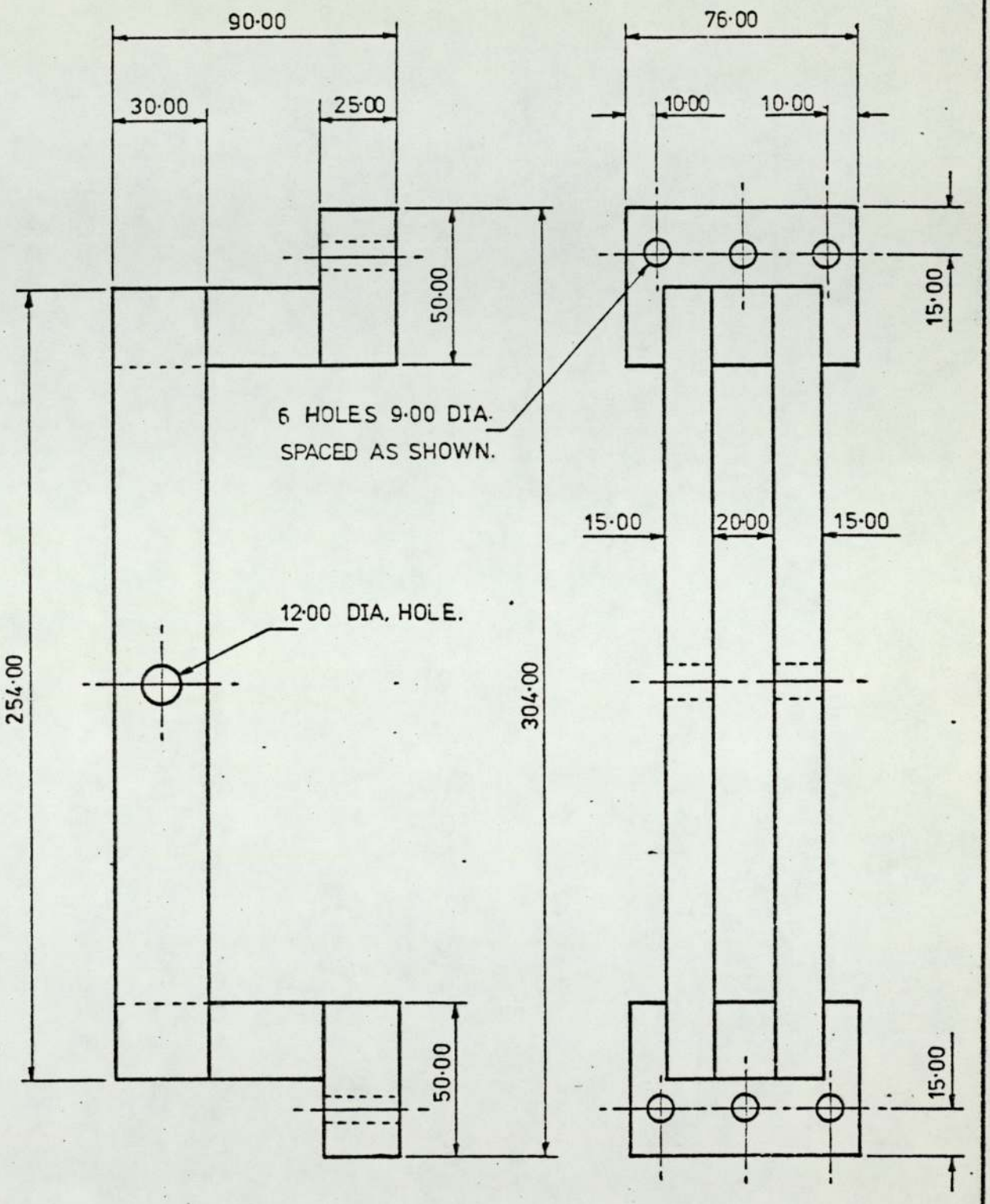

MATERIAL. MILD STEEL.

1 OFF

TOLERANCE EXCEPT WHERE OTHERWISE STATED ± 0·20.

ALL DIMENSIONS ARE IN mm. UNLESS OTHERWISE STATED.

LIFTING BAR.	DRG. No. 403
THE UNIVERSITY OF ASTON IN BIRMINGHAM.	SCALE 1:2
DEPARTMENT OF PRODUCTION ENGINEERING.	P.J. LEAVESLEY.

DO NOT SCALE.

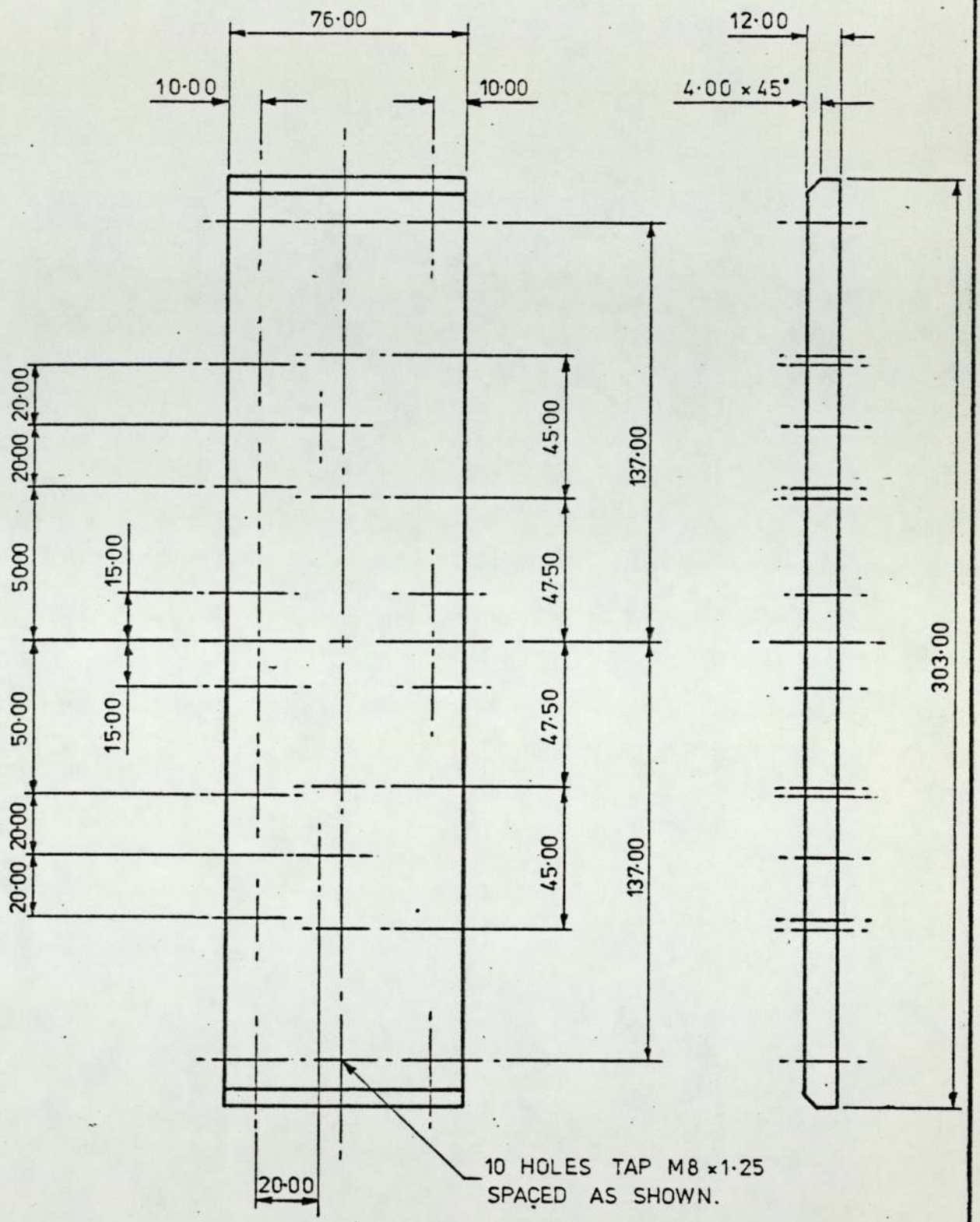

MATERIAL. MILD STEEL.

1 OFF

TOLERANCE EXCEPT WHERE OTHERWISE STATED ± 0·20.

ALL DIMENSIONS ARE IN mm. UNLESS OTHERWISE STATED.

LIFTING HEAD.	DRG. No. 404
THE UNIVERSITY OF ASTON IN BIRMINGHAM.	SCALE 1:2
DEPARTMENT OF PRODUCTION ENGINEERING.	P.J.LEAVESLEY.

DO NOT SCALE.

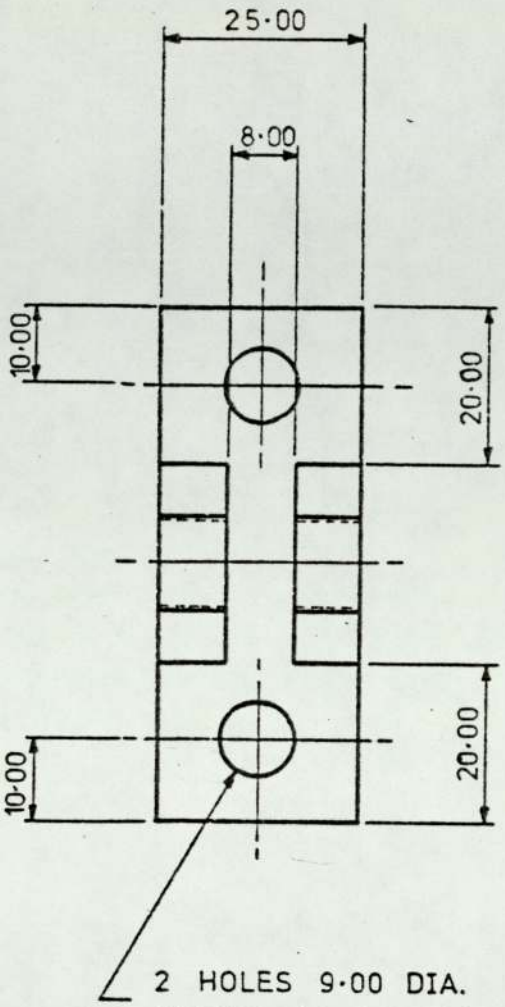

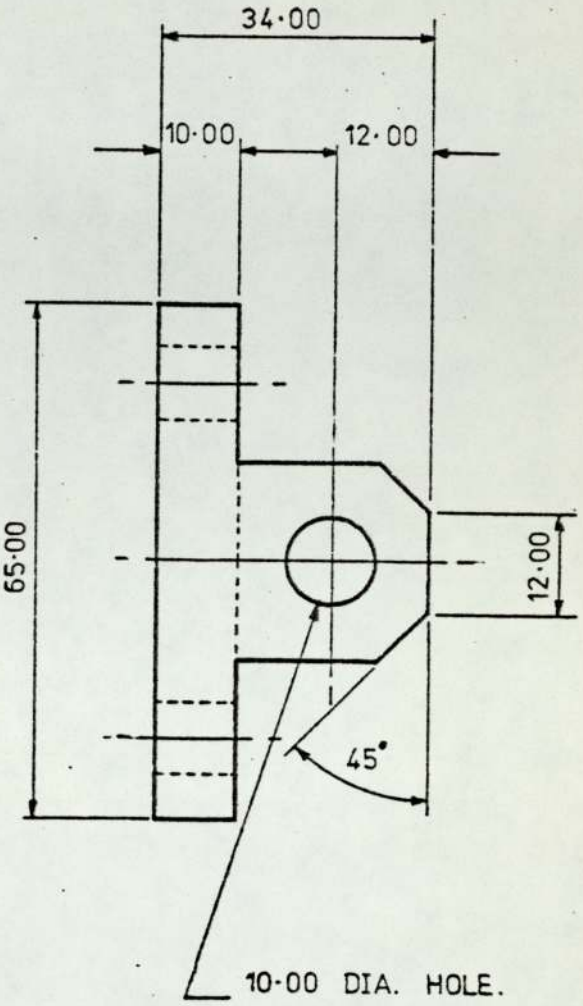

MATERIAL. MILD STEEL.

2 OFF.

TOLERANCE EXCEPT WHERE OTHERWISE STATED ± 0·20.

ALL DIMENSIONS ARE IN mm. UNLESS OTHERWISE STATED.

LIFTING ADAPTOR.	DRG. No. 405
THE UNIVERSITY OF ASTON IN BIRMINGHAM.	SCALE : FULL SIZE.
DEPARTMENT OF PRODUCTION ENGINEERING.	P.J. LEAVESLEY.

DO NOT SCALE.

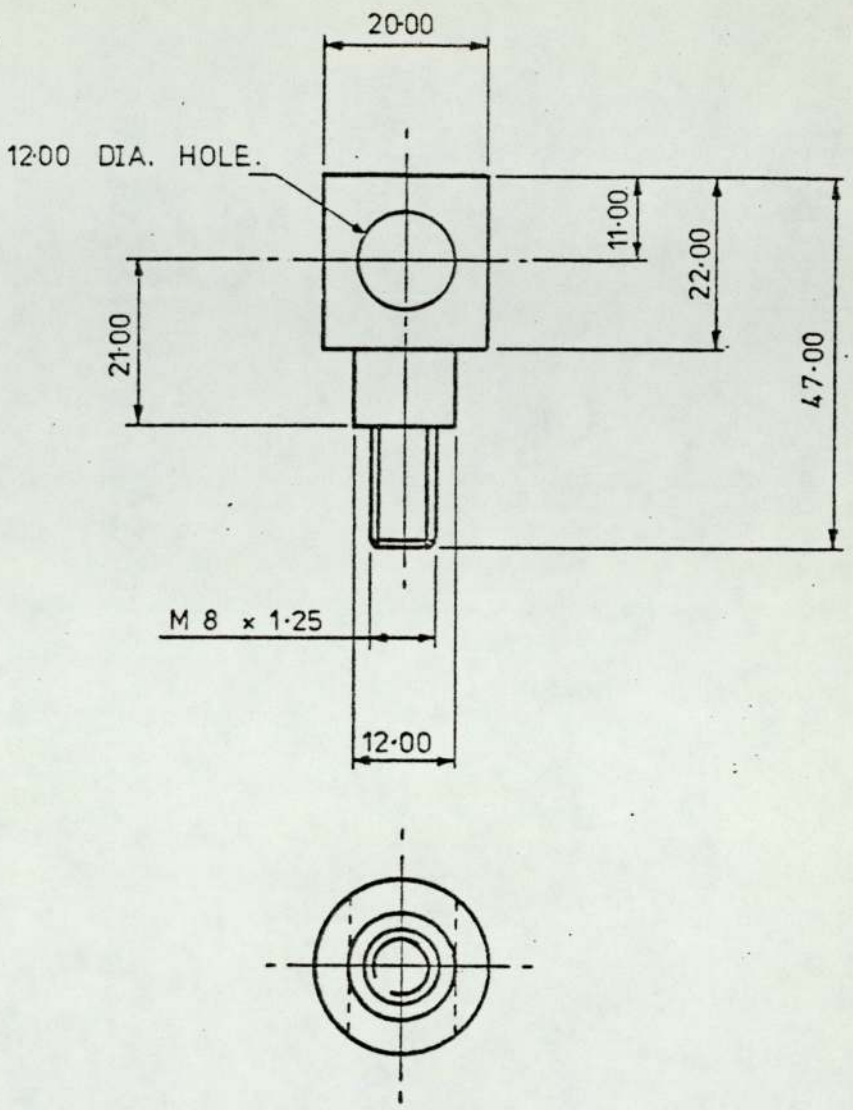

MATERIAL. MILD STEEL.

1 OFF.

TOLERANCE EXCEPT WHERE OTHERWISE STATED ± 0·20.

ALL DIMENSIONS ARE IN mm. UNLESS OTHERWISE STATED.

SOLENOID CONNECTER.	DRG. No. 406
THE UNIVERSITY OF ASTON IN BIRMINGHAM.	SCALE : FULL SIZE.
DEPARTMENT OF PRODUCTION ENGINEERING.	P.J. LEAVESLEY.

DO NOT SCALE.

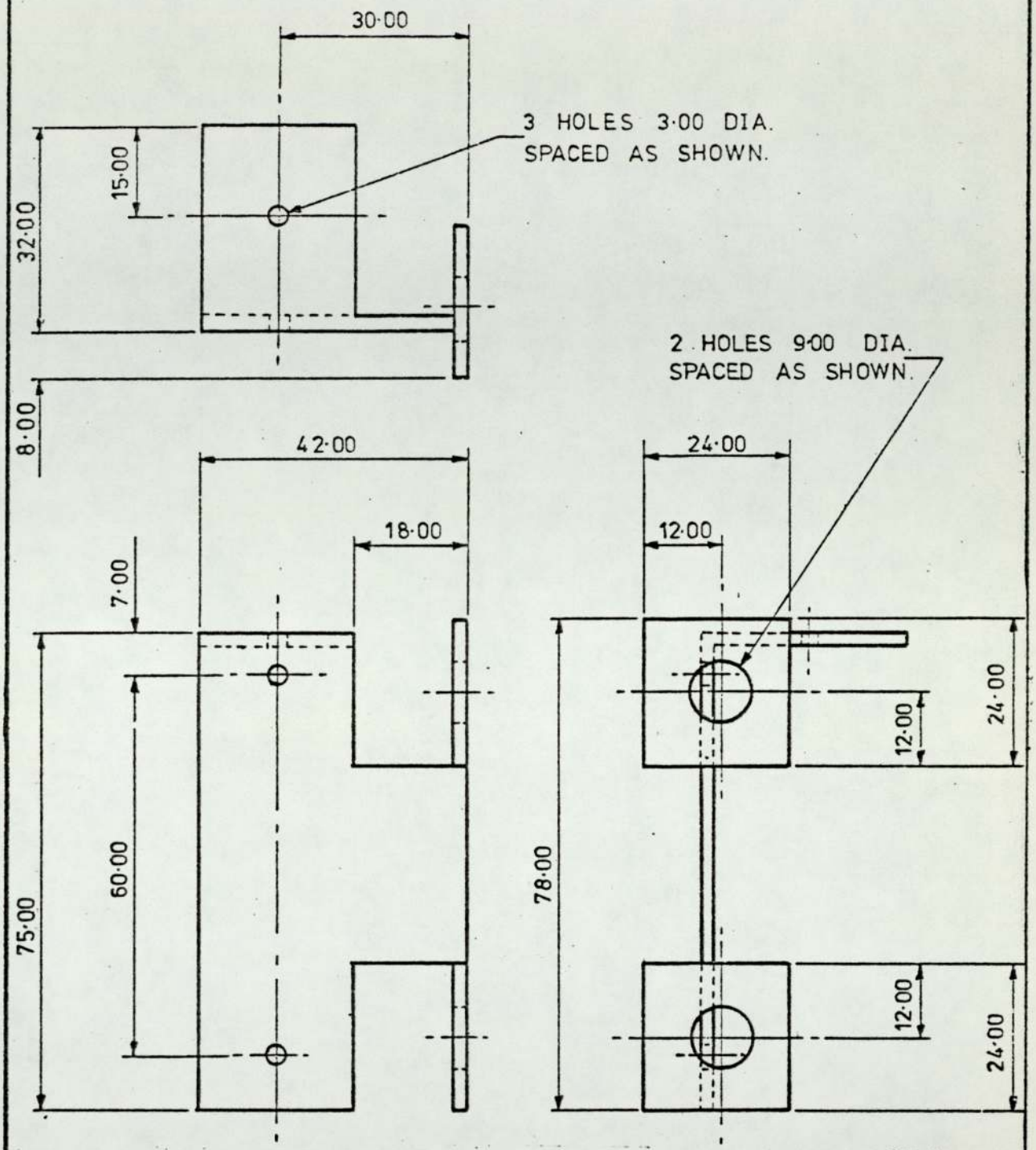

MATERIAL. MILD STEEL.

1 OFF.

TOLERANCE EXCEPT WHERE OTHERWISE STATED ± 0·20.

ALL DIMENSIONS ARE IN mm. UNLESS OTHERWISE STATED.

SOLENOID BRACKET.	DRG. No. 407
THE UNIVERSITY OF ASTON IN BIRMINGHAM.	SCALE: FULL SIZE.
DEPARTMENT OF PRODUCTION ENGINEERING.	P.J. LEAVESLEY.

DO NOT SCALE.

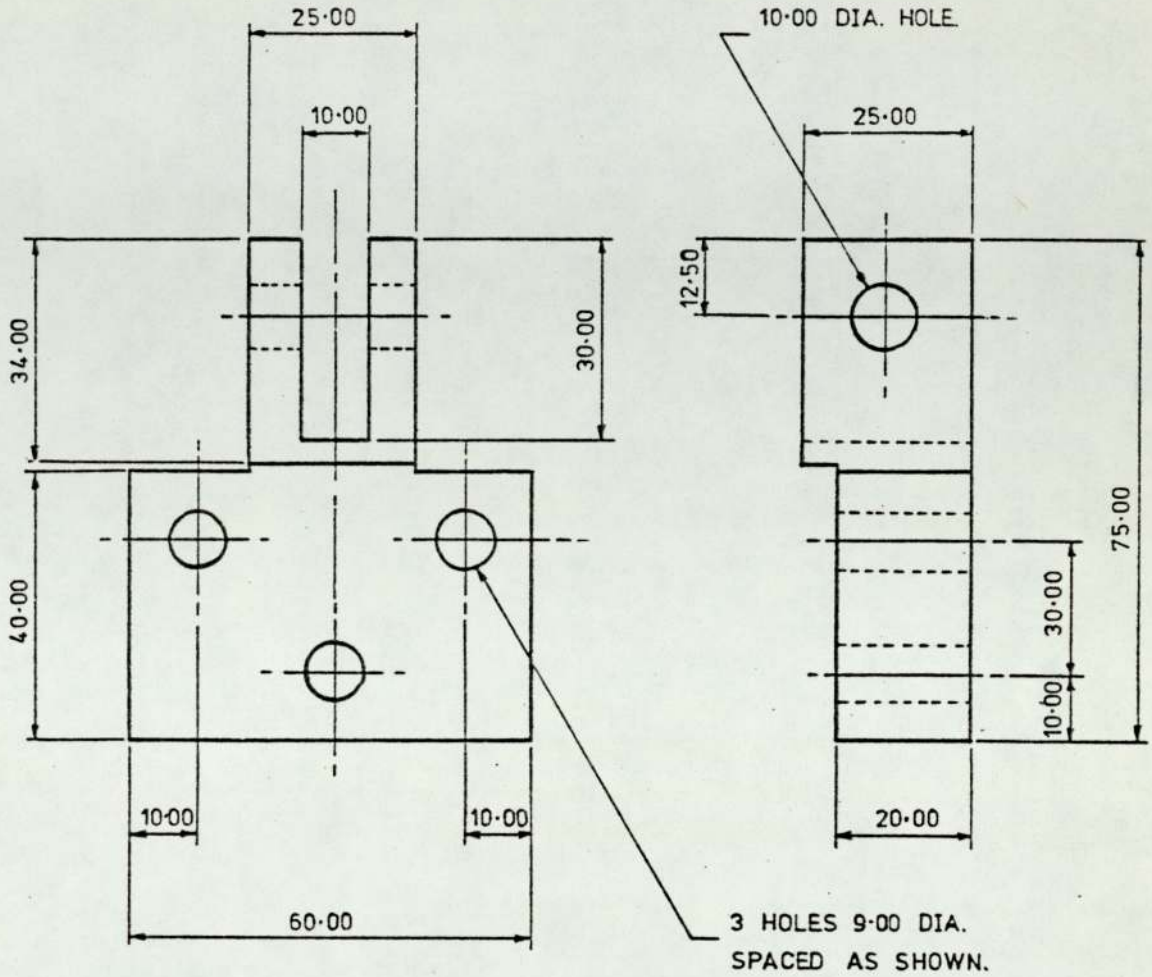

MATERIAL. MILD STEEL.

2 OFE.

TOLERANCE EXCEPT WHERE OTHERWISE STATED ± 0·20.

ALL DIMENSIONS ARE IN mm. UNLESS OTHERWISE STATED.

PIVOT BRACKET.	DRG. No. 408
THE UNIVERSITY OF ASTON IN BIRMINGHAM.	SCALE: FULL SIZE.
DEPARTMENT OF PRODUCTION ENGINEERING.	P.J. LEAVESLEY.

DO NOT. SCALE.

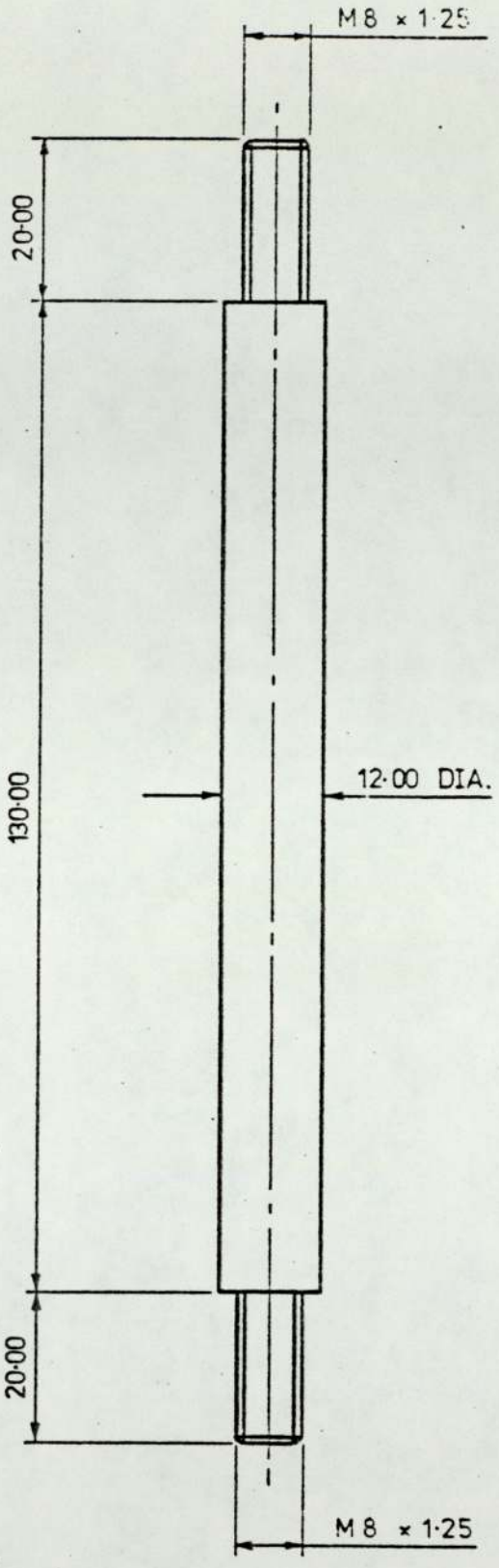

MATERIAL. MILD STEEL.

1 OFF

TOLERANCE EXCEPT WHERE OTHERWISE STATED ± 0·20.

ALL DIMENSIONS ARE IN mm. UNLESS OTHERWISE STATED.

ACTUATER PIN.	DRG. No. 409
THE UNIVERSITY OF ASTON IN BIRMINGHAM.	SCALE: FULL SIZE.
DEPARTMENT OF PRODUCTION ENGINEERING.	P.J. LEAVESLEY.

DO NOT. SCALE.

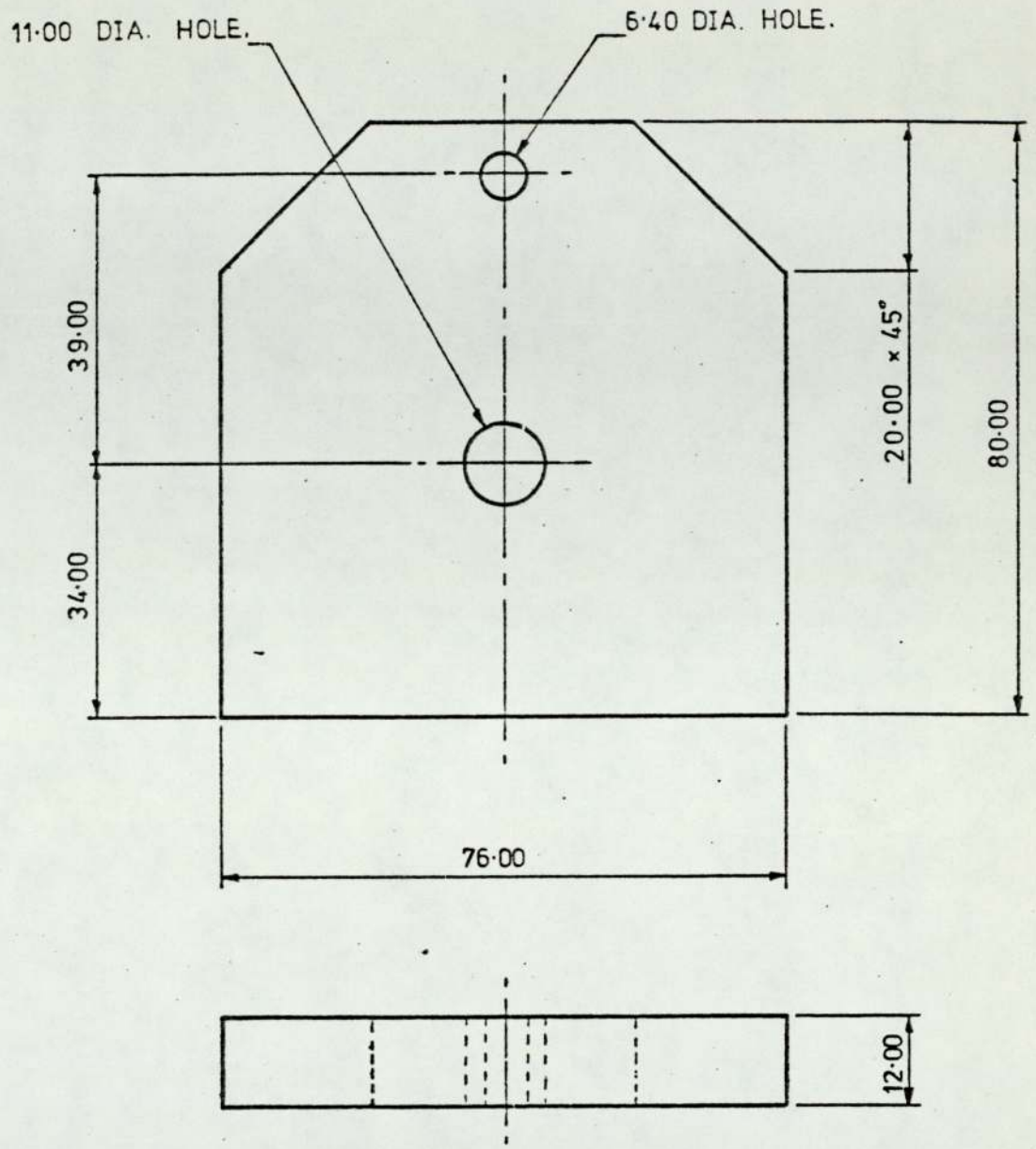

MATERIAL. MILD STEEL.

2 OFF

TOLERANCE EXCEPT WHERE OTHERWISE STATED ± 0·20.

ALL DIMENSIONS ARE IN mm. UNLESS OTHERWISE STATED.

ELECTRO-MAGNET SPACER.	DRG. No. 410
THE UNIVERSITY OF ASTON IN BIRMINGHAM.	SCALE : FULL SIZE
DEPARTMENT OF PRODUCTION ENGINEERING.	P.J. LEAVESLEY.

DO NOT SCALE.

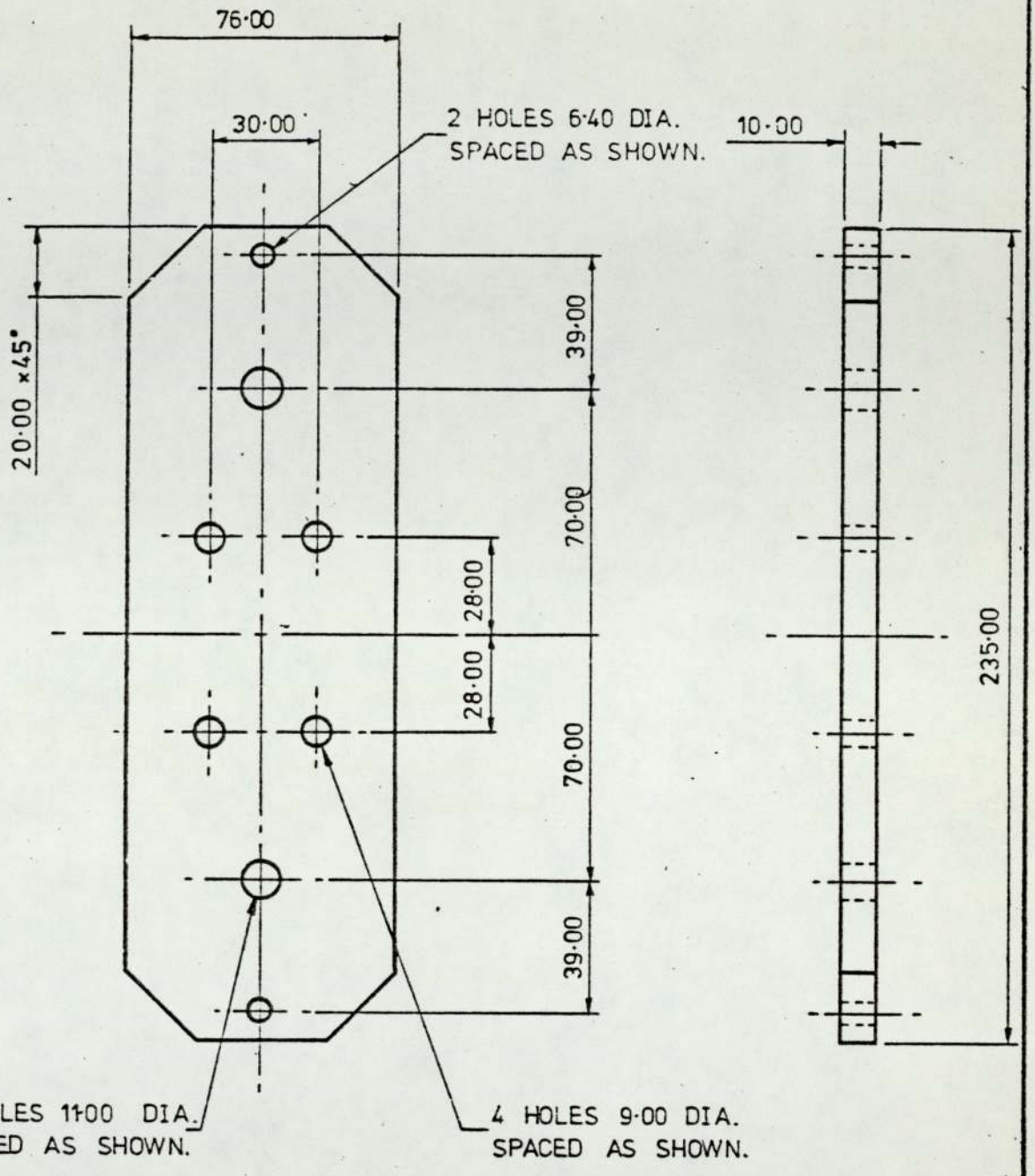

MATERIAL. MILD STEEL.

1 OFF

TOLERANCE EXCEPT WHERE OTHERWISE STATED ± 0·20.

ALL DIMENSIONS ARE IN mm. UNLESS OTHERWISE STATED.

ELECTRO-MAGNET SUPPORT.	DRG. No. 411
THE UNIVERSITY OF ASTON IN BIRMINGHAM.	SCALE 1:2
DEPARTMENT OF PRODUCTION ENGINEERING.	P.J.LEAVESLEY.

DO NOT SCALE.

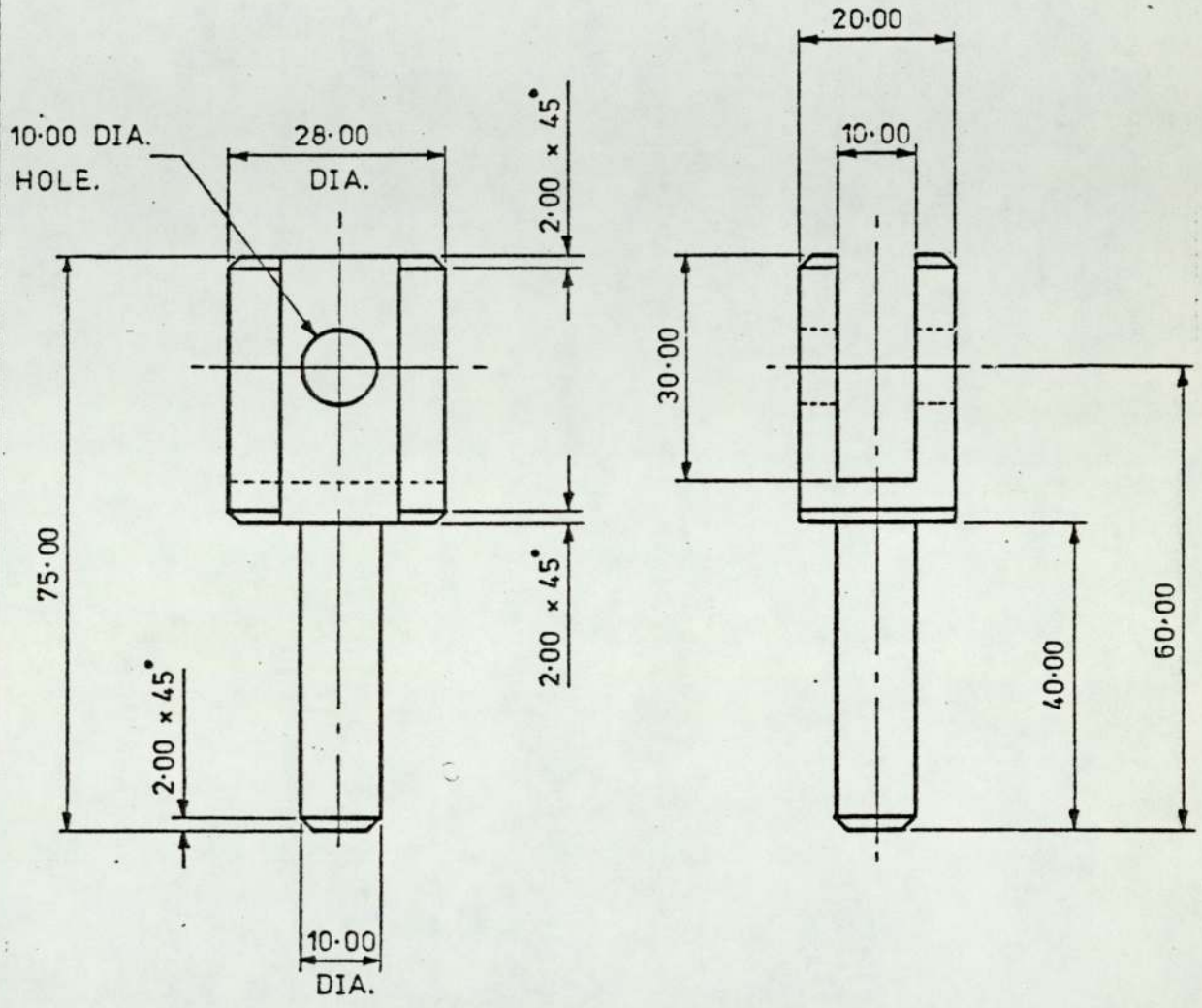

MATERIAL. MILD STEEL.

2 OFF

TOLERANCE EXCEPT WHERE OTHERWISE STATED ± 0·20.

ALL DIMENSIONS ARE IN mm. UNLESS OTHERWISE STATED.

LIFTING PIN.	DRG. No. 414
THE UNIVERSITY OF ASTON IN BIRMINGHAM.	SCALE: FULL SIZE
DEPARTMENT OF PRODUCTION ENGINEERING.	P.J. LEAVESLEY.

DO NOT . SCALE.

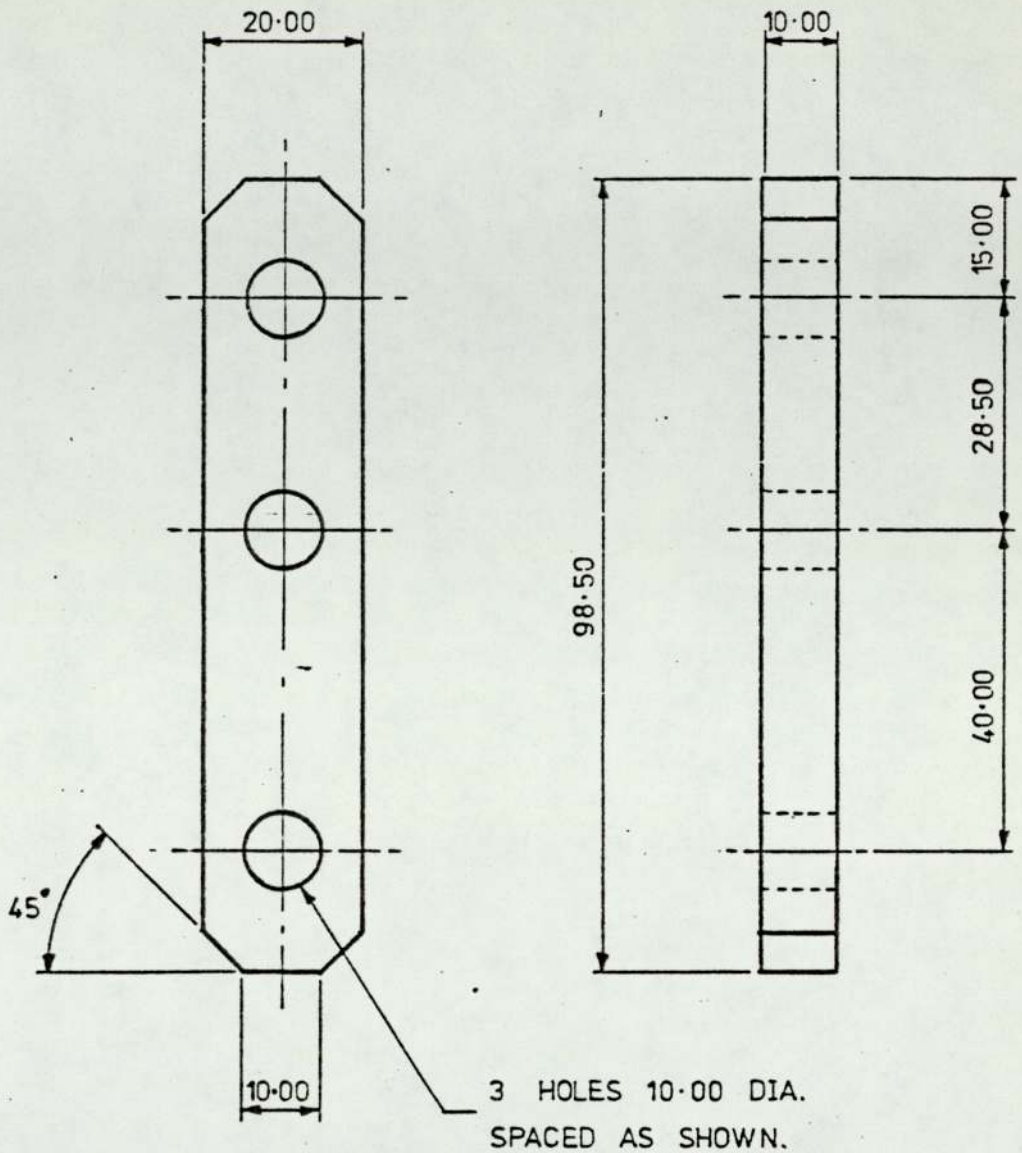

MATERIAL. MILD STEEL.

2 OFF

TOLERANCE EXCEPT WHERE OTHERWISE STATED ± 0·20.

ALL DIMENSIONS ARE IN mm. UNLESS OTHERWISE STATED.

LEVER.	DRG. No. 415
THE UNIVERSITY OF ASTON IN BIRMINGHAM.	SCALE: FULL SIZE
DEPARTMENT OF PRODUCTION ENGINEERING.	P.J. LEAVESLEY.

MAIN FRAME ASSEMBLY.

DRG. 500 PART LIST.

PART No.	No. OFF.	DESCRIPTION.	MATERIAL.
501	2	BASE SUPPORT.	4"x2"x$\frac{3}{8}$" U-CHANNEL.
502	4	BASE SUPPORT BLOCK.	MILD STEEL.
503	2	SIDE SUPPORT LEFT.	1$\frac{1}{2}$"x1$\frac{1}{2}$"x$\frac{1}{4}$" L-CHANNEL.
504	2	SIDE SUPPORT RIGHT.	1$\frac{1}{2}$"x1$\frac{1}{2}$"x$\frac{1}{4}$" L-CHANNEL.
505	8	CROSS BRACE.	1$\frac{1}{2}$"x1$\frac{1}{2}$"x$\frac{1}{4}$" L-CHANNEL.
506	2	MAIN UP-RIGHT.	4"x2"x$\frac{3}{8}$" U-CHANNEL.
507	4	TOP SUPPORT BLOCK.	MILD STEEL.
508	1	UPPER SUPPORT.	4"x2"x$\frac{3}{8}$" U-CHANNEL.
509	1	HOIST SPACER.	1$\frac{1}{2}$"x1$\frac{1}{2}$"x$\frac{1}{4}$" L-CHANNEL.
510	4	TOP SUPPORT BRACE.	MILD STEEL.
511	1	TOP SUPPORT.	4"x2"x$\frac{3}{8}$" U-CHANNEL.
512	1	PULLEY BRACKET.	MILD STEEL.
513	2	SPRING.	RUBBER.
514	2	SAFETY BAR.	MILD STEEL.
515	1	SAFETY BAR SUPPORT.	1$\frac{1}{2}$"x1$\frac{1}{2}$"x$\frac{1}{4}$" L-CHANNEL.
516	4	T-NUT.	MILD STEEL.
517	4	BOLT.	M12x75-6g.
518	16	SET SCREW.	M12x50-6g.
519	38	NUT.	M12-6H.
520	58	WASHER.	24 O/D-13 I/D -2.5
521	26	SET SCREW.	M12x25-6g.
522	2	SET SCREW.	M8x30-6g.
523	5	NUT.	M8-6H.
524	7	WASHER.	17 O/D-8.4 I/D -1.6

MAIN FRAME ASSEMBLY.

DRG. 500 PART LIST CONTINUED.			
PART No.	No. OFF.	DESCRIPTION.	MATERIAL.
525	1	SET SCREW.	M8-50-6g.

DO NOT SCALE.

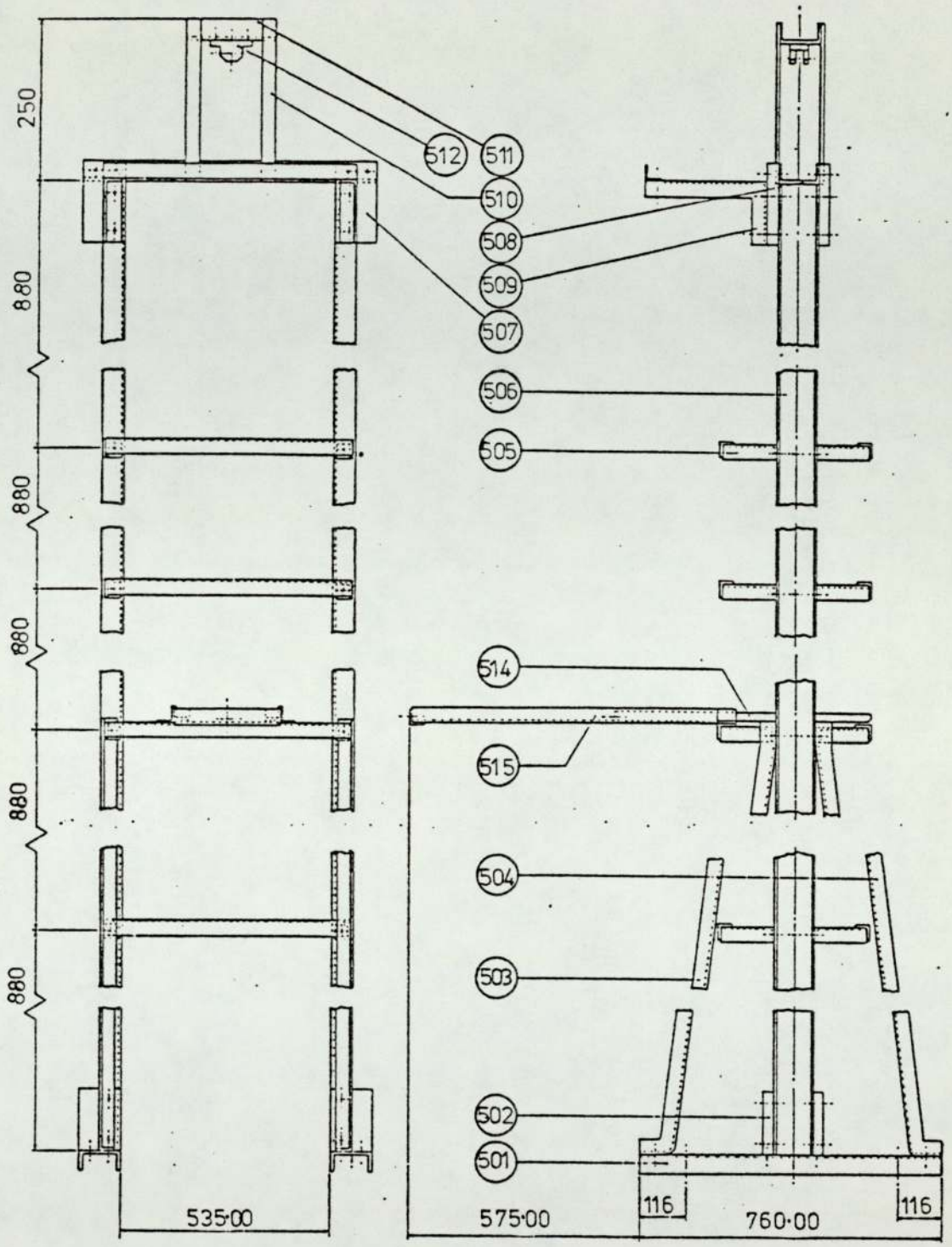

MATERIAL. MILD STEEL.

TOLERANCE EXCEPT WHERE OTHERWISE STATED ± 0·20.

ALL DIMENSIONS ARE IN mm. UNLESS OTHERWISE STATED.

MAIN FRAME ASSEMBLY.	DRG. No. 500
THE UNIVERSITY OF ASTON IN BIRMINGHAM.	SCALE 1:5
DEPARTMENT OF PRODUCTION ENGINEERING.	P.J.LEAVESLEY.

SAFETY CAGE ASSEMBLY.

DRG. 600 PART LIST.

PART No.	No. OFF.	DESCRIPTION.	MATERIAL.
601	-	SUPPORT FRAME.	100ft of 1" SQUARE TUBING.
602	-	ANGLE CONNECTER.	ASSORTED TYPES.
603	-	WIRE MESH.	1" SQUARE WIRE MESH 5'x16'.
604	100	SELF TAPPING SCREW.	No.6.
605	2	HINGE.	3".
606	6	BOLT.	M4x35-6g.
607	6	NUT.	M4-6H.
608	12	WASHER.	9 O/D-4.4 I/D - 1.0
609	100	MESH CLIP.	MILD STEEL.
610	2	SET SCREW.	M8x50-6g.
611	4	NUT.	M8-6H.
612	4	WASHER.	17 O/D-8.4 I/D -1.4
613	1	DOOR ROPE.	10' of $\frac{3}{8}$" ROPE.
614	2	PULLEY 2".	ALUMINIUM.
615	2	SET SCREW.	M12x50-6g.
616	4	NUT.	M12-6H.
617	6	WASHER.	24 O/D-13 I/D -2.5

APPENDIX L

This is a reprint of an Imperial Metal Industries Ltd., publication.

IMI ENERGY-ABSORBING BUMPER SYSTEMS FOR ROAD VEHICLES

It is not surprising that the novel method of absorbing the kinetic energy of vehicle impact by means of extrusion should emanate from Imperial Metal Industries Ltd. of Birmingham, a company with long experience in the shaping, deformation, and extrusion of metals. In the extrusion manufacturing process, very large amounts of energy are needed to force the billet through the extrusion die. In the same way, if a plastic cartridge is squeezed by collision impact through a suitable aperture, large amounts of kinetic energy can be dissipated in a controlled manner.

The basic features of the IMI energy-absorbing mounting for a vehicle bumper are shown in Figure 1, which illustrates the initial movement of the device after impact. The ram (whose left-hand end is attached to the bumper) has started to move to the right, and plastic material has begun to be extruded from the annular die forming the mouth of the container.

Figure 2 illustrates a more advanced version, designed to meet legislative requirements such as those which have recently come into force in the United States. These require that after low speed impacts, the system shall be recoverable; that is, that the bumper shall return to it's normal position. In the IMI design, the recovery and extrusion phases follow in sequence.

During a low speed impact up to 5 m.p.h., the plastic cartridge on the right deforms in a barrelling mode and subsequently recovers it's shape. At higher impact speeds, the left-hand cartridge is extruded through the mouth of the container to absorb large amounts of kinetic energy by deformation and displacement. Typical energy-absorption characteristics for a device of this nature are illustrated in Figures 3 and 4. Figure 3 shows the force-displacement curve, while Figure 4 gives an indication of the amount of energy absorbed at any point of the stroke.

During the design stage, it is possible to tailor impact-absorption devices to suit the specific impact levels, decelerations, and displacements which may be specified by vehicle designers of road safety legislators. Performance variations, based on technical data already amassed, are achieved by the alteration of various parameters including component design, cartridge formulation and pre-treatment, and the judicious choice of extrusion ratio and die geometry.

Once the design of an energy-absorbing bumper mounting has been optimised for a particular vehicle, it is important to ensure that the associated bumper assembly is efficiently designed. A strong bumper bar is essential in order to transmit the impact forces via the energy-absorption devices to the vehicle structure. Some soft facing may also be added to provide partial recovery of the system, as well as some protection for pedestrians. Figure 5 shows a typical arrangement of such a system, in which the mountings are angled to provide improved performance in oblique collisions.

Development work on energy-absorption devices was started at IMI some two years ago, and success with this work led to the recent award of a jointly financed development contract by the Department of the Environment's Transport and Road Research Laboratory.

Findings to date suggest that extrusion may well prove to be the most cost-effective method of energy-absorption, largely because of the simplicity of the hardware, which also ensures a high degree of reliability in service.

In addition to bumper mountings, simple devices based on the extrusion prinicple can be made for use in crash barriers, seat-belt linkages and other safety devices in transport, marine, military, and industrial applications.

IMI, who already have patent coverage for their designs, are now in a position to undertake design and development of energy-absorbing bumper systems in collaboration with vehicle manufacturers.

Further enquiries to:
K.Deutsch, Technical Manager,
New Ventures Department,
Imperial Metal Industries Ltd.,
Birmingham B6 7BA
Telephone: 021-356 4848 Ext. 2680

October, 1973.

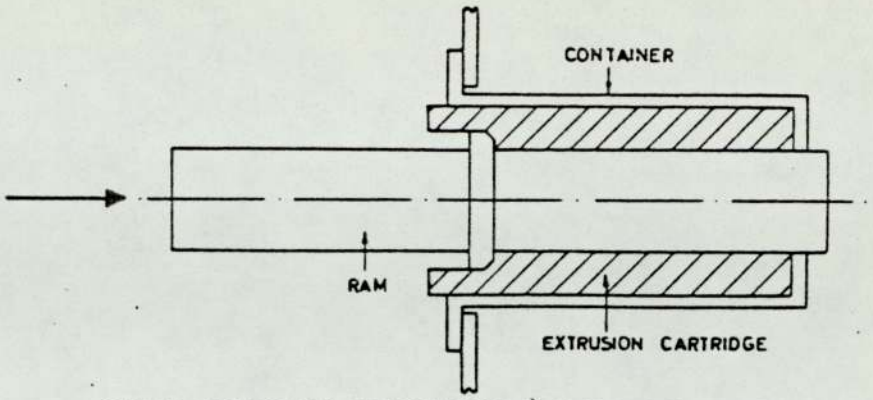

FIG.1 ENERGY ABSORBING DEVICE SHOWING PARTIALLY EXTRUDED MATERIAL

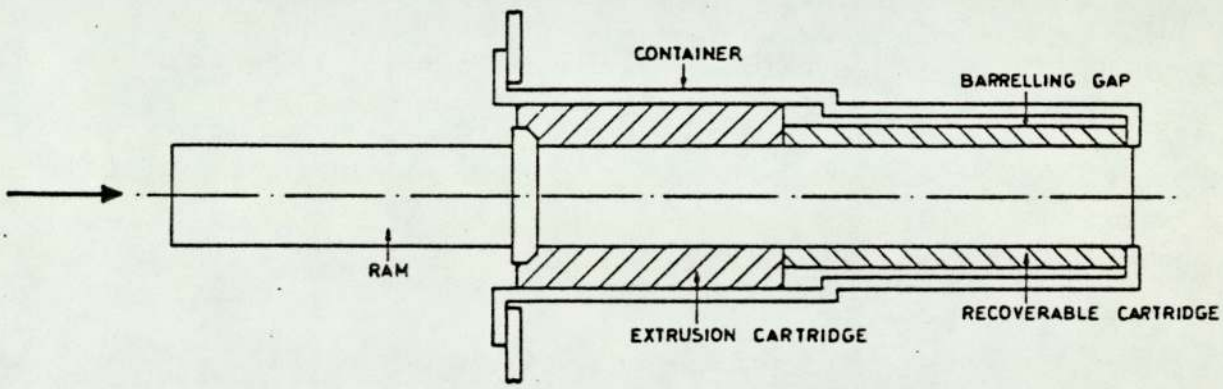

FIG.2 ENERGY ABSORBING DEVICE INCORPORATING EXTRUSION AND RECOVERABLE FEATURES

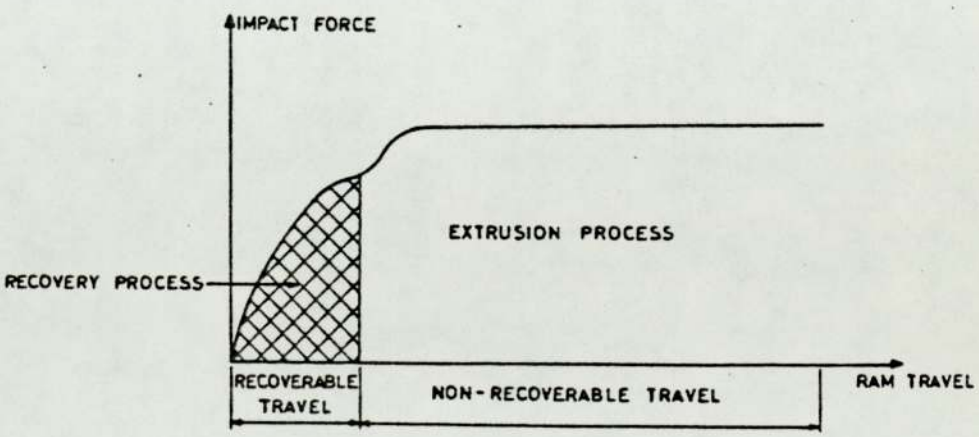

FIG.3 FORCE - DISPLACEMENT CHARACTERISTIC OF ENERGY ABSORBING DEVICE

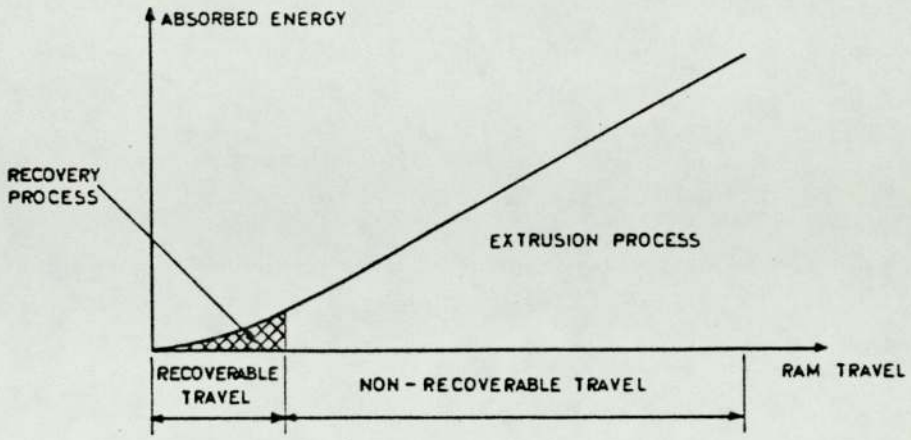

FIG. 4 ENERGY - DISPLACEMENT CHARACTERISTIC OF ENERGY ABSORBING DEVICE

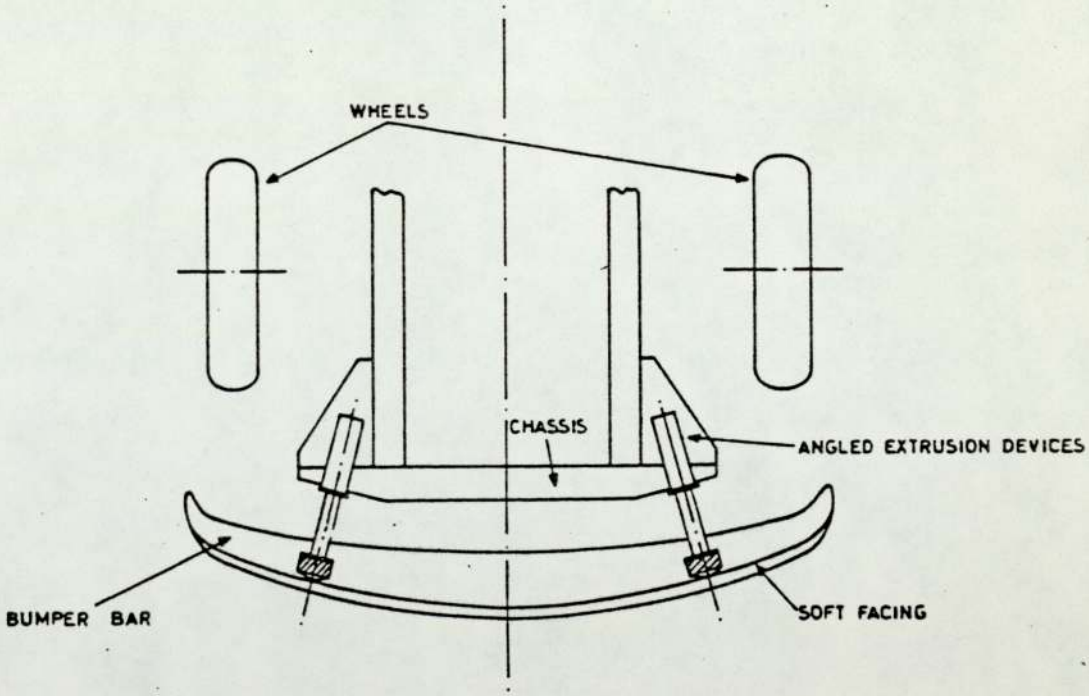

FIG. 5 ENERGY ABSORBING BUMPER SYSTEM

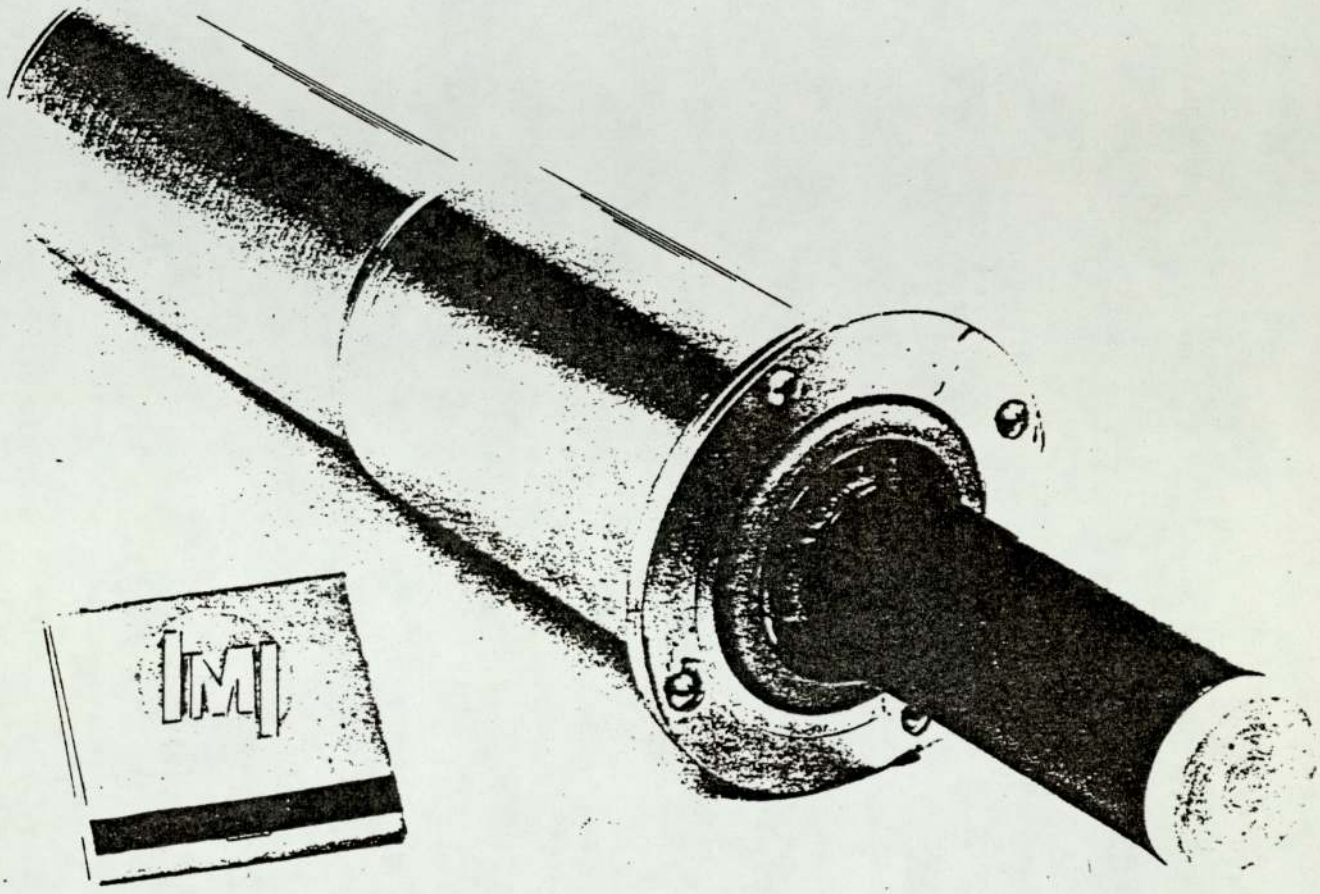

Extrusion of a plastic cartridge is used for energy absorption in this IMI bumper mounting.